

Durham E-Theses

The petrology and structure of the Motzfeldt centre, Igaliko, south Greenland.

Jones, A.P.

How to cite:

Jones, A.P. (1980) *The petrology and structure of the Motzfeldt centre, Igaliko, south Greenland.*, Durham theses, Durham University. Available at Durham E-Theses Online:
<http://etheses.dur.ac.uk/7491/>

Use policy

The full-text may be used and/or reproduced, and given to third parties in any format or medium, without prior permission or charge, for personal research or study, educational, or not-for-profit purposes provided that:

- a full bibliographic reference is made to the original source
- a [link](#) is made to the metadata record in Durham E-Theses
- the full-text is not changed in any way

The full-text must not be sold in any format or medium without the formal permission of the copyright holders.

Please consult the [full Durham E-Theses policy](#) for further details.

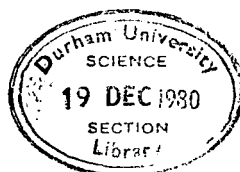
THE PETROLOGY AND STRUCTURE
OF THE MOTZFELDT CENTRE,
IGALIKO,
SOUTH GREENLAND.

A.P.JONES, BSc.

The copyright of this thesis rests with the author.
No quotation from it should be published without
his prior written consent and information derived
from it should be acknowledged.

A thesis submitted for the degree of
Doctor of Philosophy at
The Geology Department,
University of Durham.

1980



The Motzfeldt Centre is the second of four centres of alkaline igneous activity which form the Igaliko Complex. A vertical exposure of 1700m shows several overlapping intrusive units of syenite and nepheline syenite (units SM1 to SM5), which bear mantle Sr isotope ratios and were emplaced by a combination of 5-10km radius ring fractures and block subsidence. The larvikitic parent to SM5 and the presence of a late alkali gabbro dyke, must attest to the availability of more basic magma at depth.

Xenoliths from an earlier supracrustal sequence dominated by lavas, form rafts up to 200-300m thick and several square kilometres in area. Marginal phonolites of the nepheline syenites (SM2, 3 and 4 in particular), which are thought to represent liquid compositions, bear a strong resemblance to phonolites from these lavas and they are quite possibly genetically related. A late sill-like body of lujavrite (eudialyte-nepheline microsyenite = SM6) rich in volatiles and "incompatible" elements, formed beneath some of these rafts.

In general, phonolitic magmas were emplaced at temperatures of approximately 1000° C to form the larger units and were substantially solidified probably within 0.1-0.2 Ma. The considerable variation in rock types found in each major intrusion, is thought to be attributable to varying degrees of crystal fractionation in-situ and differential accumulation (by a variety of mechanisms) from an initially homogeneous magma. Of the extensive mineralogical variations which necessarily occurred, crystallisation of zirconium-rich aegirine depended on low oxygen fugacity, high peralkalinity and the absence of eudialyte. Electron probe microanalysis has shown that REE-bearing minerals are common accessories and may or may not have a negative Eu-anomaly; these may be LREE- or HREE-enriched.

Both fractionation of phonolite magma and recycling of stopped nepheline syenites by partial re-melting could give rise to magma of lujavritic composition.

CONTENTS

	<u>Page</u>
<u>CHAPTER ONE. Introduction.</u>	
<u>1.1. Setting</u>	1
1.2.A. Gardar Setting	2
1.2.B. Gardar igneous activity; The Igaliko Complex	2
<u>1.3. History of previous research</u>	4
<u>1.4. Geography</u>	8
<u>1.5. Fieldwork and sampling</u>	8
<u>1.6. Maps</u>	10
 <u>CHAPTER TWO. Field Description and Petrography.</u>	
<u>2.1. Introduction</u>	11
<u>2.2. Unit SM1</u>	
2.2.A. General	11
2.2.B. Marginal facies	12
2.2.C. Petrography	12
<u>2.3. Unit SM2</u>	
2.3.A. General	13
2.3.B. Petrography	13
<u>2.4. Unit SM3</u>	
2.4.A. General	16
2.4.B. Petrography	17
<u>2.5. Unit SM4</u>	
2.5.A. General	19
2.5.B. Flink's Dal area	19
2.5.C. Petrography	22
2.5.D. Recrystallised SM4	26
<u>2.6. Unit HY: Heterogenous syenites</u>	
2.6.A. General	26
2.6.B. Petrography	27
2.6.C. Additional	29
<u>2.7. Unit SM5</u>	
2.7.A. General	29
2.7.B. SM5* Larvikite	31
2.7.C. Marginal SM5	31
2.7.D. Nepheline syenite	32

2.7.E. Rheomorphism	33
<u>2.8. Unit SM6</u>	
2.8.A. General	35
2.8.B. Dark lujavrite	40
2.8.C. White lujavrite	41
2.8.D. Green lujavrite	42
2.8.E. General	42
<u>2.9. Alkali Gabbro dyke</u>	
2.9.A. General	43
2.9.B. Petrography	43
<u>2.10. Satellitic syenites</u>	44
2.10.A. Unit EM: East Motzfeldt Syenite	45
2.10.B. Unit NM: North Motzfeldt Syenite	45
<u>2.11. Gardar supracrustal rocks: Eriksfjord</u>	
Formation	46
2.11.A. General	46
2.11.B. Agglomerates	48
2.11.C. ?Sediments	48
2.11.D. Aphyric lavas	49
2.11.E. Porphyritic lavas	50
<u>2.12. Volcanic (Ultrabasic/Carbonated) Breccia</u>	
2.12.A. General	52
2.12.B. Petrography	53
 <u>CHAPTER THREE. Structure.</u>	
<u>3.1. Introduction</u>	55
<u>3.2. The relative age of the Motzfeldt Centre</u>	55
<u>3.3. General Comments</u>	55
<u>3.4. Supracrustal xenoliths</u>	56
<u>3.5. Structures in Central Motzfeldt south of</u> <u>the Flink's Dal fault</u>	57
<u>3.6. Structures in Central Motzfeldt north of</u> <u>the Flink's Dal fault</u>	61
3.6.A. Xenoliths	61
3.6.B. Unit SM5*:Larvikite ring dyke	63
3.6.C. Alkali Gabbro dyke	63
<u>3.7. Further structures of the syenite units</u>	64

<u>3.8. Qualitative interpretation</u>	
3.8.A. Mechanisms of intrusion	66
3.8.B. Exposure level	68
3.8.C. Flink's Dal fault: effects on exposure	71
3.8.D. Overlap of intrusions	72
3.8.E. Reconstruction	75
3.8.F. Phonolite magma	75
3.8.G. Density and viscosity	76
<u>3.9. Cooling period</u>	
3.9.A. First approximation	78
3.9.B. Ambient temperature	79
3.9.C. Temperature variations	80
<u>3.10. Settling</u>	81
<u>3.11. Water</u>	83
3.11.A. Water and a silicate melt	83
3.11.B. Water, phase relations and crystallisation	85
<u>3.12. Structures postdating the Motzfeldt Centre</u>	86
3.12.A. Gardar dykes	86
3.12.B. Faulting	87
3.12.C. Ellipticity	88
 <u>CHAPTER FOUR. Mineralogy</u>	
<u>Introduction</u>	90
<u>4.1. Pyroxenes</u>	
4.1.A. General	90
4.1.B. Recalculation and nomenclature	92
4.1.C. Pyroxene substitution	98
4.1.D. Al and Ti and sector zoning	99
4.1.E. Zirconium substitution	101
<u>4.2. Olivine</u>	
4.2.A. General	106
4.2.B. Compositional variation	106
<u>4.3. Amphiboles</u>	
4.3.A. General	110
4.3.B. Classification	111
4.3.C. Amphibole chemistry	114

<u>4.4. Biotite</u>	
4.4.A. General	118
4.4.B. Chemical variation	120
<u>4.5. Feldspar</u>	
4.5.A. General	121
4.5.B. Compositional variation and zoning	122
4.5.C. Subsolidus unmixing	125
4.5.D. Conditions of T and P_{H_2O}	126
<u>4.6. Nepheline</u>	
4.6.A. General	128
4.6.B. Compositional variation	128
4.6.C. Additional	131
<u>4.7. Aenigmatite</u>	
4.7.A. General	132
4.7.B. Chemical variation	132
4.7.C. Conditions of formation	134
<u>4.8. Fe-Ti oxides</u>	135
<u>4.9. Geothermometers</u>	135
<u>4.10. Rare earth mineral analyses</u>	
4.10.A. General	138
4.10.B. Discussion of results	142
<u>4.11. Additional</u>	142

CHAPTER FIVE. Geochemistry

<u>5.1. Introduction</u>	145
<u>5.2. Units SM1, 2 and 3</u>	147
<u>5.3. Unit SM4</u>	150
<u>5.4. The Heterogenous Syenite-unit HY</u>	154
<u>5.5. Unit SM5</u>	155
<u>5.6. Summary of the variation between units</u>	157
<u>5.7. Triangular variation diagrams</u>	163
<u>5.8. Lavas from the Motzfeldt Centre</u>	
5.8.A. The local stratigraphic base	165
5.8.B. Representative analyses and comparisons	165
<u>5.9. Unit SM6: Analyses and comparisons</u>	169
<u>5.10. Normative mineralogy</u>	
5.10.A. The Residua System	171

5.10.B. The Residua System and phase tie lines	174
<u>5.11. Liquid lines of descent</u>	
5.11.A. Summary	176
5.11.B. Unit SM6 and the system $\text{Al}_2\text{O}_3\text{-Na}_2\text{O-Fe}_2\text{O}_3\text{-SiO}_2$	179
 <u>CHAPTER SIX. Conclusions and Petrogenesis</u>	
<u>Introduction</u>	184
6.1.A. Evolution at the current exposure level	184
6.1.B. Evolution of the lujavrites	188
<u>6.2. Partial melting of existing syenites</u>	190
<u>6.3. Association of the Motzfeldt Centre to an earlier sequence of lavas</u>	192
<u>6.4. Magma compositions</u>	193
<u>6.5. Comparison with the Kenya Rift</u>	196
<u>6.6. Evidence for a mantle source region</u>	196
<u>6.7. Derivation of the primary magmas</u>	
6.7.A. Partial melting	198
6.7.B. Fractional crystallisation	199
<u>6.8. Saturation with respect to silica</u>	200
<u>6.9. Assimilation</u>	201
 <u>APPENDIX I. Geochemistry</u>	
<u>I.1. X-Ray fluorescence techniques</u>	
I.1.A. Sample preparation	203
I.1.B. Major element analysis	203
I.1.C. Trace elements analysis	204
<u>I.2. Oxidation state</u>	204
<u>I.3. H₂O Determinations</u>	210
<u>I.4. Sample locations and collection</u>	210
<u>I.5. Additional analyses</u>	210
<u>I.6. Data tables of major element (ox.wt%), trace elements (ppm) and Norms for whole rock samples</u>	211-244
 <u>APPENDIX II. Mineralogy</u>	
<u>II.1. Electron probe microanalysis</u>	245

<u>II.2. Note on REE-mineral analysis</u>	247
<u>II.3. Pyroxene recalculation of end-members</u>	248
Mineral analyses, tabulated	250 - 288
<u>REFERENCES</u>	289 - 302

TABLES

<u>Table no.</u>	<u>Subject.</u>	<u>Page.</u>
(3) 1	Extent and overlap of units, pre Flink's Dal fault	75
(4) 1	Geotemperatures	137
(4) 2	Rare earth mineral analyses	139
(4) 3	Selected mineral analyses	144
(5) 1	Lujavrites of SMG compared	170
(5) 2	Lavas from the Motzfeldt Centre (compared)	182
(5) 3	Compositions of intrusive phonolites	183
(I) 2	List of standards used for XRF major element analysis	207
(I) 2	Sample collection data	208
	Fe ³ /Fe ² and H ₂ O determinations	209
	Whole rock analyses, with Norms	211-244
(II) 1	Electron probe operating conditions and standards	

ILLUSTRATIONS

<u>Figure no.</u>	<u>Subject.</u>	<u>Page</u>
1,1	Sketch geology	6
1,2	Sketch geographical locations	7
2,1	Perspective view of geology in Flink's Dal	21
2,2	Summary of supracrustal succession around the Motzfeldt Centre	47
3,1	Map of S.W. Central Motzfeldt, Flink's Dal	58
3,2	Detail of geology in Flink's Dal	59
3,3	Disposition of supracrustal rocks	62
3,4	Prehnite-pumpellyite stability	70
3,5	Overlap of intrusions	73
3,6	Reconstruction	74
4,1	Pyroxene trends compared	91
4,2	Pyroxene nomenclature	94
4,3	Pyroxene representation	95
4,4	Pyroxene trends and zonation	96
4,5	Pyroxene chemical variation	97
4,6	Variation of ZrO_2 in pyroxenes from SM4 and SM5 compared	102
4,7	Olivine trends compared	107
4,8	Olivine CaO variation	108
4,9	Amphiboles in Phillips (1966) compositional space	112
4,10	Amphibole chemical variation	115
4,11	Generalised amphibole trends	116
4,12	Biotite- chemical variation	119
4,13	Feldspars in the system Ne-Ks-Qz	124
4,14	Nepheline in the system Ne-Ks-Qz	130
4,15	Aenigmatites.	133
4,16	Chondrite normalised REE mineral analyses	141
5,1	Units SM2, 3 and SM4, variation in selected elements	148

5,2	Comparison of syenites cutting the N. Qôroq Centre with SM4	149
5,3	Pressure dependence of phases for phonolitic compositions in the system Ne-Ks-Qz	152
5,4	HY and SM4 compared; TiO ₂ vs FI for unit SM5	153
5,5	Trace element variation in SM5; feldspar control?	156
5,6	SiO ₂ vs FI to summarise the variations between units.	158
5,7	(a) Nb vs Y (b) Zr vs FI	160
5,8	Y vs Zr	161
5,9	Log K(%) vs Log Rb(ppm)	162
5,10	(a & b) AFM diagrams (c)(Na+K)-Fe-Mg (d) Na ₂ O-K ₂ O-CaO	164
5,11	Two basalts from Motzfeldt compared to data from the IVM	166
5,12	Trace elements from Motzfeldt phonolite lavas and intrusive phonolites compared	168
5,13	Ne-Ks-Qz, whole rock and phase tie lines	172
5,14	Ne-Ks-Qz, cumulate/liquid relations and lines of mixing in unit HY	177
5,15	Summary of liquid lines of descent	178
5,16	Lujavrites of SM6 in the system Na ₂ O-Al ₂ O ₃ -Fe ₂ O ₃ -SiO ₂ -(H ₂ O)	180
I,1	X.R.F. Sample density	206

PLATES

<u>Plate*</u>	<u>Subject</u>	<u>Page.</u>
1*	Feldspar exsolution in P.Phonolite	14
2*	Ne-Cpx feather intergrowth in lardalite	14
3*	AM9. P. Phonolite of SM4(margin)	25
4*	AM7. P. ne-microsyenite of SM4(margin)	25
5	Banded dark lujavrites (SM6)	36
6	Xenoliths of SM4 in SM6	36

7	Xenolithic raft of lavas in syenites in Flink's Dal	38
8	Dark lujavrite cutting SM4	38
9	Complex folding of dark lujavrite	39
10	Typical white lujavrite of SM6	39

*photomicrograph

Copyright.

The copyright of this thesis rests with the author. No quotation from it should be published without his prior written consent and information derived from it should be acknowledged.

ACKNOWLEDGEMENTS

My thanks go firstly to the Natural Environment Research Council for the provision of both a research grant and additional support for fieldwork and to the Director of the Greenland Geological Survey (GGU) for providing much of the necessary logistic support.

I am grateful to Professors G.M.Brown and M.H.P.Bott for making available to me the facilities of the Geology Department and to all of the technical staff who have given friendly and efficient support.

My sincere thanks go to Dr.C.H.Emeleus for introducing me to Greenland geology and for his continuous advice, friendship and supervision throughout the past three years. I have greatly benefitted from the assistance of Dr.A.Peckett and Mr.R.Phillips with a number of mineralogical complexities. Detailed discussions with Dr.A.D.Chambers, Dr.M.Powell and Dr.D.Stephenson have proved to be extremely useful and are greatly appreciated. I also wish to thank the several members of GGU for their comforting support in the field and for discussions of a more general nature, including Dr.A.Brown, Dr.L.M.Larsen, Dr.B.L.Nielsen, Mr.P.Nygaard, Dr.A.Steenfelt and Mr.T.Tukiainen.

My warm thanks go to the families of Dr.R.Wilson and Dr.J.Petersen in Århus, to Dr.H.Johanesson and family in Reykjavik and to the Olsen family in Oslo, for their generous hospitality.

Dr.J.G.Holland and Mr.R.Hardy provided much welcomed assistance in obtaining results from the XRF and Dr.B.Beddoe-Stephens instructed me in the use of the electron probe. I am also grateful to Mr.M.Poulter, Dr.M.Reeves and Mr.R.Westerman for their help with computing.

Many and varied discussions with further friends and colleagues of the department, Dr.R.M.Forster, Dr.D.M.Hirst, Mr.R.H.Hunter, Dr.G.A.L.Johnson, Dr.G.Larwood and Mrs.L.Mines amongst them, have been enjoyed over the years. Alternative suggestions which may or may not have proved useful, but were none the less savoured, have come from C.Christodolou, D.P.Mithen, Miss G.R.Moore, M.Ozcelik, M.J.Park, D.Schofield

R. Taylor and many other friends, all of whom I would like to thank.

Lastly, I would like to express my dearest thanks to Nancy Baldwin and especially my parents, for their endless encouragement and moral support.



Frontispiece. View of Igdlarfigssalik from Flink's Dal. The outer contact of the Motzfeldt Centre runs diagonally across the picture, with coarse-grained brown syenite in the foreground and angular weathering gneiss just beyond.

CHAPTER ONE

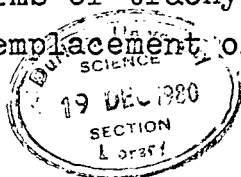
INTRODUCTION

1.1. Setting

Situated in the south of Greenland at approximately $61^{\circ}\text{N } 45^{\circ}\text{W}$, the Igaliko Complex is comprised of four centres of alkaline igneous activity. Of these, the Motzfeldt Centre of nepheline syenites was the second to be emplaced and represents one of the earliest magmatic events in the evolution of the Gardar igneous province. The centre derives its name from the inland lake "Motzfeldt Sø" around which it is located, and has been dated by Blaxland et al (1978) at $1310 \pm 31 \text{ Ma}$.

Three principal episodes of faulting and associated alkaline magmatism are recognised in the evolution of the Gardar province (Emeleus and Upton 1976). Rb/Sr age dating by Blaxland et al (1978) has shown that there is no consistent relationship between emplacement age, geographical location and degree of silica saturation of the intrusive centres. Thus, for example, the major nepheline syenite intrusive complexes of Grønnedal-Ika (Emeleus 1964) and the two oldest centres of the Igaliko Complex (Emeleus and Harry 1970) were both emplaced during the Early Gardar, yet are situated 150 km apart at opposite ends of the province. Furthermore, cross-cutting centres within the Igaliko Complex are petrologically very similar, but span the entire duration of the Gardar province.

In brief, the Gardar province yields evidence for the following episodes; (1) Early accumulations of terrestrial sediments and lavas in fault bounded troughs at about 1300 Ma, were accompanied by the emplacement of large undersaturated volcanic centres; (2) A period of rifting at about 1250 Ma associated with the intrusion of alkaline basic dykes and late injections of silica oversaturated complexes; (3) The widespread intrusion of ENE and NE trending swarms of trachytic dykes at about 1170 Ma and the late stage emplacement of a number of alkaline



complexes. This Late Gardar event also involved the rejuvenation of old transcurrent faults and entailed a 3 km extension across a 70 km wide ENE trending rift zone, the central part of which is associated with a gravity 'high' (Upton and Blundell 1978).

The repeated faulting and intrusion of varied alkaline magmas constitute evidence for magmatism associated with Proterozoic continental rifting. It is probably no coincidence that the magmatic association of alkali basalts, phonolites and trachytes, with sporadic carbonatitic and ultrabasic activity is broadly similar to the comparatively recently developed rift systems in East Africa.

1.2.A. Gardar Setting

Metamorphic basement extending from the Ivigtut area to the south of the Gardar province, consists of metasediments and metavolcanics belonging to the Ketilidian Era. Southwards from Ivigtut towards the Ketilidian mobile belt, these rocks show progressive deformation and plutonism, such that the centre of the belt consists of orogenic granitic and sometimes dioritic rocks, known collectively as "Julianehåb Granite". For a review of the basement geology, the reader is referred to Allart (1964). The Gardar province developed over approximately 150 million years, from about 1300 Ma to 1160 Ma (Blaxland et al 1978) with three major periods of activity, the Early, Middle and Late Gardar, corresponding to the 1300 Ma, the 1250 Ma and the 1170 Ma events of Upton and Blundell (1978). For a general account of the Gardar geology see Emeleus and Upton (1976).

The province has been unaffected by any younger orogenic activity, such that the intrusive and associated rocks of Gardar ages are preserved without regional deformation.

1.2.B. Gardar igneous activity; The Igaliko Complex

Situated approximately 15 km east and southeast

of Narssarssuaq airport, the Igaliko Complex of nepheline syenites occupies at least 500 km² of ground between Tunugdliarfik and Igaliko fjords and the inland ice.

The Igaliko Complex (for general description see Emeleus and Harry 1970) consists of four centres of alkaline igneous activity, with several satellitic intrusions, whose relative ages have been ascertained by a combination of field relations and age dating (Blaxland et al 1978). These four centres are now known to have been emplaced in the order North Qôroq, Motzfeldt, South Qôroq, Igdlerfigssalik. The order of emplacement of the two early centres was originally reversed by Emeleus and Harry (1970) as it was not until the summer of 1977 that further field evidence came to light. Rb/Sr ages for the centres obtained by Blaxland et al (1978), are 1295 ± 61 , 1310 ± 31 , 1185 ± 8 and 1167 ± 15 , in the order of emplacement, revealing a significant delay prior to the intrusion of the South Qôroq and Igdlerfigssalik centres.

Continental sediments and lavas of the Eriksfjord Formation (Poulsen 1964; Stewart 1964, 1970; Larsen 1973, 1977) are both cut by, and preserved as xenoliths within, the Motzfeldt Centre. It is likely that the lavas were erupted shortly before the emplacement of the North Qôroq and Motzfeldt centres and that the petrogenesis of the lavas and intrusions is closely related (Upton and Blundell 1978).

Each centre is comprised of multiple intrusions of undersaturated, nepheline bearing rocks, except perhaps where contamination with siliceous country rocks has occurred. The commonest rock type is foyaitic nepheline syenite, with lesser amounts of more basic augite syenites, which may resemble the larvikites from the Oslo region. Their mode of emplacement was evidently passive and mainly accomplished by a combination of ring fracture and block stoping (Emeleus and Harry 1970). Concentric inward dipping structures, defined by igneous layering and mineral lamination are quite common within certain units. The steep dip of the feldspar laminations may represent

original angles of rest, or perhaps some form of over-steepening in response to further igneous deformation.

In general, the Motzfeldt Centre shows a tendency for successive intrusions to become more basic with time and for each intrusion to display mineralogical and geochemical trends towards peralkaline undersaturated residua. Similarly, units of the South Qôroq Centre become increasingly basic with time (Stephenson 1973, 1976), placing certain constraints on any petrogenetic model invoked for explanation of these two centres. That crystal fractionation has occurred after emplacement, is suggested by accumulations of minerals in the form of layering and cumulus textures, visible in each centre. Igneous layering is best developed in the South Qôroq and Igdlérfigssalik centres, and its modes of origin are considered in Chapter 6.

The North Qôroq and Motzfeldt centres display the most felsic and fractionated rocks, with the appearance of lujavrites in the Motzfeldt Centre.

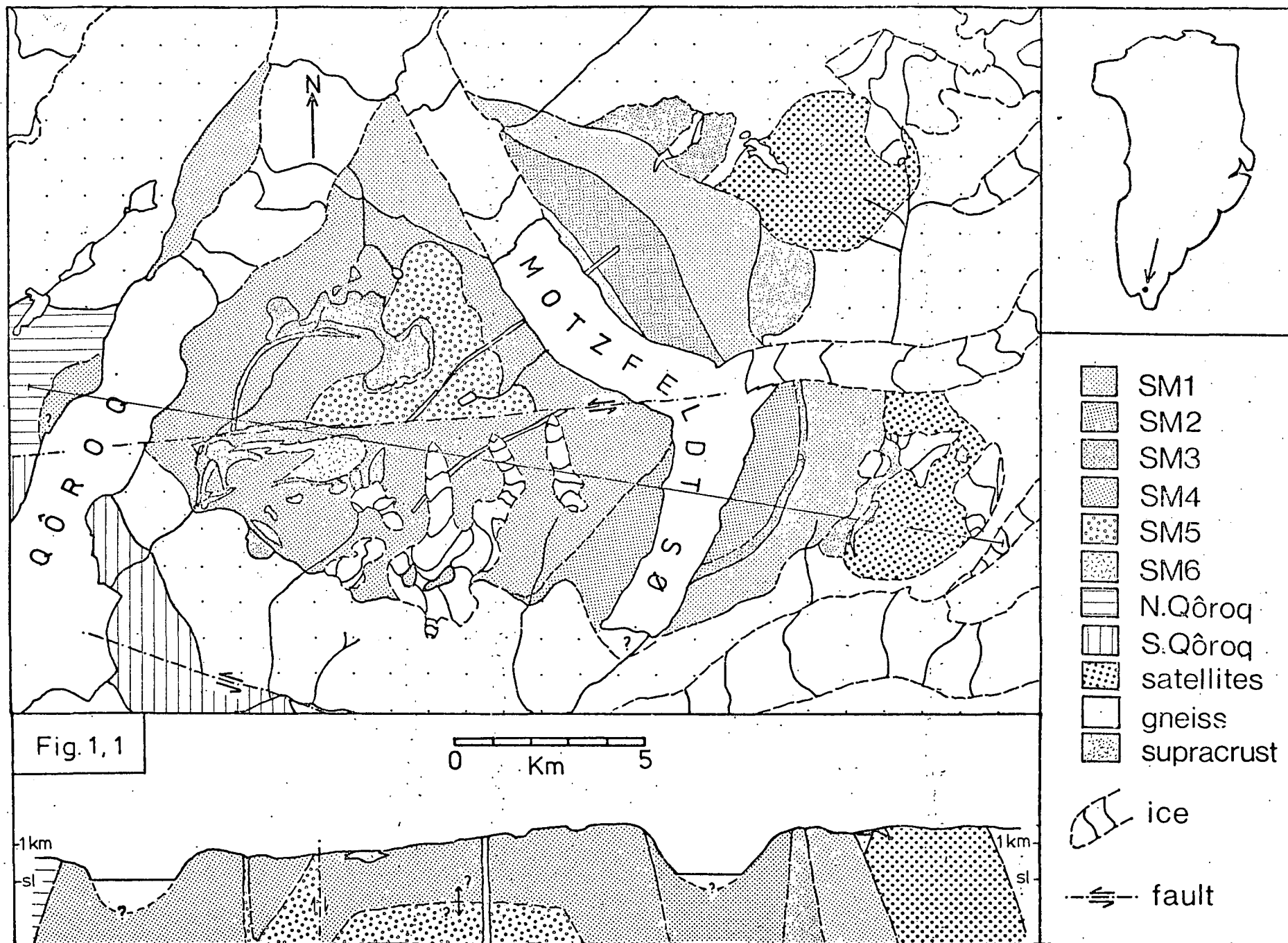
1.3. History of previous research

A more extensive summary of previous investigations in the Igaliko area, can be found in Emeleus and Harry (1970 pp 14-16).

The Igaliko area was first visited by Giesecke in the early part of the nineteenth century, who recorded a "granite" at Qôroq (Giesecke 1910 pp 36-37, 216-218). Subsequent geological and mineralogical investigations (Steenstrup & Kornerup 1881; Flink 1898) revealed the presence of a large area of nepheline syenite, and this was followed by work around the South Qôroq Centre by Ussing and Bøggild (Ussing 1884, 1912). Ussing visited Flink's Dal, to examine a part of the South Qôroq Centre very close to Motzfeldt. However, despite further visits to the area by Wegmann (1938) and Ødum (1927), the Motzfeldt Centre in particular, appears to have escaped attention, possibly due to its more difficult access and somewhat daunting topography. Eventually, in 1970, a detailed map of the whole of the Igaliko Complex, with a general

description of the petrography and field relations was given by Emeleus and Harry. The mapping had been conducted jointly for the Greenland Geological Survey (GGU) in 1961, 1962, and 1963, with additional visits by C.H. Emeleus in 1966 and 1969 following the death of W.T. Harry in 1964. Their original field diaries have been available for consultation throughout the present work and their original map remains substantially unchanged. The majority of the Motzfeldt Centre was mapped and sampled by C.H. Emeleus, although certain areas in the southeastern part of Central Motzfeldt and the area southeast of Motzfeldt Sø were mapped by W.T. Harry.

Since 1970, the individual centres of the Igaliko Complex have been studied in great detail by postgraduate research workers, primarily at the University of Durham, but also at the University of Leeds. Initially the South Qôroq Centre was studied by D. Stephenson (1973) to be followed by the study of A.D. Chambers on the North Qôroq Centre (1976) and later by the work of M. Powell on the Igdlerfigssalik Centre (1976). This investigation of the Motzfeldt Centre thus completes the initial study of the Igaliko Complex as four separate centres of igneous activity. The abundant contributions of the earlier workers cannot, in all fairness, be summarised, although for the sake of completeness an attempt will be made. The first study was made by D. Stephenson (1972, 1973, 1976) who pioneered the way for future work by completing a classical investigation of the South Qôroq Centre, indicating the mineralogical trends likely to be found in these alkaline centres. In the more evolved North Qôroq Centre, the petrogenetic story of fractionation from basic magmas, appeared to be broadly similar although complicated by the effects of late stage fluids, which provided more work and more results for a comprehensive account by A.D. Chambers (1976). With the petrogenesis now somewhat understood, M. Powell (1976, 1978) assessed her mineralogical data in terms of ^{phase} equilibria and demonstrated just how inter-element dispersion continued throughout a long cooling history of the well-layered Igdlerfigssalik



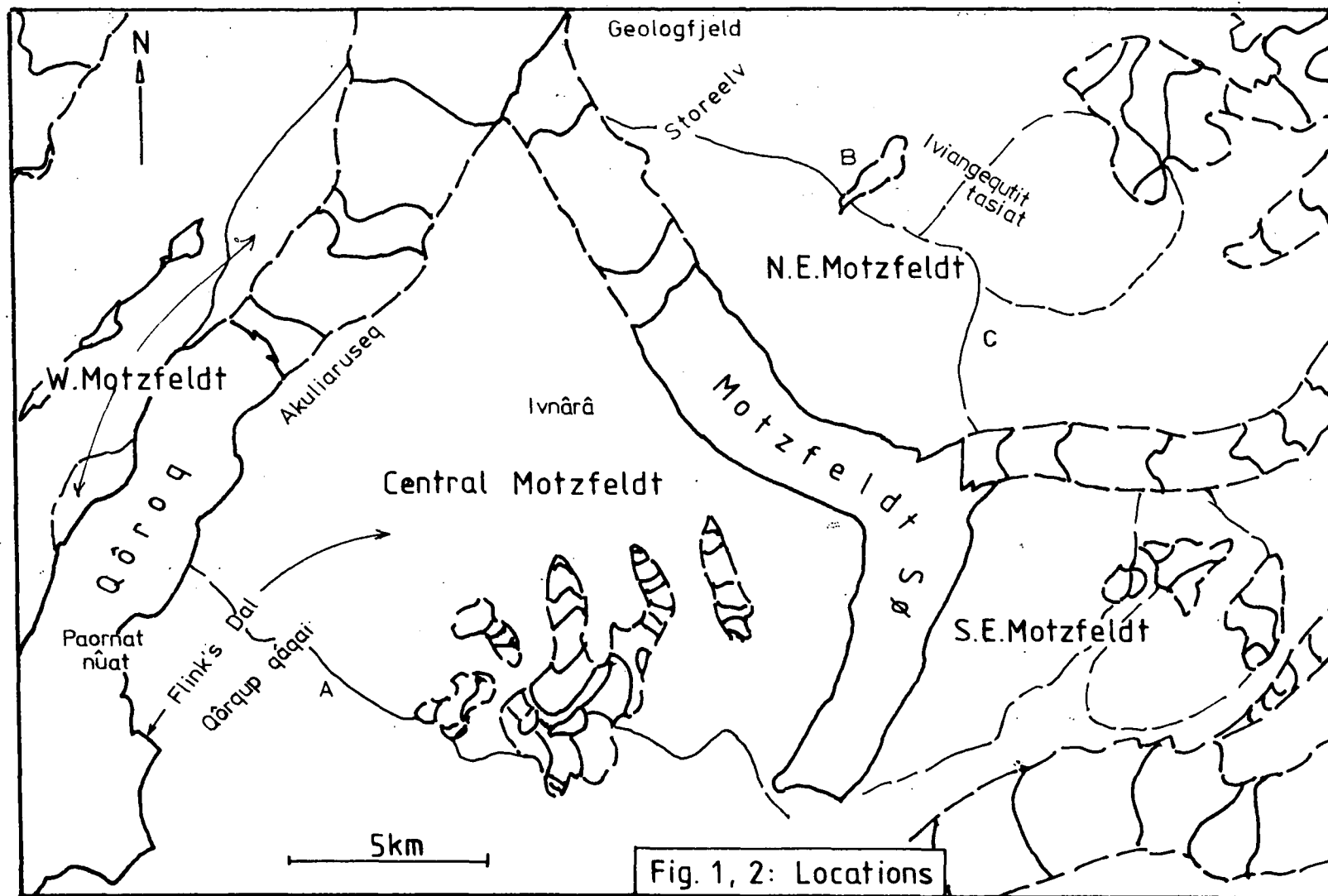


Fig. 1, 2: Locations

Centre.

Each successive author has praised the efforts of his or her predecessor, and in this respect the current author soundly complies. The overall results have quite obviously been continually accumulative and scientifically complementary.

1.4. Geography

The Motzfeldt Centre is deeply dissected by glaciers and glaciated valleys and is in part concealed by the inland lake of Motzfeldt Sø (170 m a.s.l.) and Qôroq fjord (s.l.). The topography is in places severe, due to its relatively recent emergence from beneath the inland ice, rising from sea level (s.l.) to over 1700 m, with several permanent snow fields and retreating glaciers in the higher areas. Vast curtains of scree form the lower slopes to many of the crags, and may account for up to one half of the 1500 m cliffs around Motzfeldt Sø.

The Motzfeldt Centre is naturally divided into four major geographical areas, which may be abbreviated in the thesis as follows; The large northward pointing triangle of ground separating Qôroq fjord from Motzfeldt Sø will be referred to as Central Motzfeldt; two portions lying to the west of Qôroq fjord will be known as West Motzfeldt; two segments of ground to the northeast and southeast of Motzfeldt Sø, separated by a westward flowing glacier, will be known as Northeast (NE) Motzfeldt and Southeast (SE) Motzfeldt respectively. These areas, and further locations referred to are shown in figure 1.2.

1.5. Fieldwork and sampling

Samples in addition to those already available from the collecting of C.H.Emeleus and W.T.Harry were obtained by the author, with the assistance of A.D.Chambers, in the summer of 1977. During this time, certain parts of the centre were mapped in greater detail, using 1:20,000 aerial photographs. Motzfeldt syenites were found to truncate units of the North Qôroq Centre, thus making

the North Qôroq Centre the oldest in the Igaliko Complex. Much of the interpretation of the interaction between xenolithic lavas and the nepheline syenites, has greatly benefitted from the examination of similar relationships in the Oslo province, carried out in the summer of 1978. During the summer of 1979, the Motzfeldt Centre was revisited for the specific purpose of remapping the lujavrites of the newly erected SM6. Mapping was conducted at a scale of about 1:5,000 by the author and N.Baldwin. Certain complex areas were mapped at four times this scale.

Excluding much of the xenolithic material, the exposure on the Motzfeldt Centre is excellent, and the samples collected are generally very fresh. As a result of all the collecting carried out in the centre, samples are now available from all representative areas, except for the steep crags and high ground immediately to the west of Motzfeldt Sô and also from the fjord slopes along the eastern side of Qôroq.

In general, the sample size was estimated according to the grain size of the rock. The samples collected in 1977 and 1979 by the author, have the prefix "AM". The GGU samples are listed as sequences of 5 digit numbers in Appendix I, together with their respective collector, allowing correlation with the GGU field diaries (C.H. Emeleus and W.T.Harry).

1.6. Maps

Two maps are provided in a flap at the rear of this volume, entitled Map 1 and Map 2.

Map 1 is of the entire Motzfeldt Centre and is based on the field mapping of C.H.Emeleus, W.T.Harry and the author. The information, originally in the form of aerial photographs at 1:20,000, was transcribed onto a new base map at a scale of 1:50,000. This base topographic map was a direct enlargement of the relatively new 1:100,000 topographic map of southwest Greenland. The map should ideally be compared to the original map of Emeleus and Harry (1970), from which the major differences are outlined

in an inset on the lower left hand side of the Map 1.

Map 2 is a copy of the map produced by the author as a result of further fieldwork in the Flink's Dal area in 1979 and is at a scale of approximately 1:10,000 . Scale bars of 1000m length along the grid lines indicate the approximate distortions inherited from the aerial photographs, from which it was compiled. Many of the field notes are illegible, but the main units can be distinguished with the aid of the key provided on the Map 2.

A summary sketch map of the geology is given in figure 1.1 .

FIELD DESCRIPTION AND PETROGRAPHY

2.1. Introduction

This chapter describes the basis for classification of the discrete mappable units which are found in the Motzfeldt Centre. A summarised field description of each unit is provided with petrographic and pertinent mineralogical information for direct comparison.

The major intrusive units of the Motzfeldt Centre are given the prefix SM and numbered from 1 to 5 inclusive in order of intrusion, as originally set out in Emeleus and Harry (1970). Unit SM6 is a newly defined unit and does not appear in their original work. The satellitic syenites to the east and northeast of Motzfeldt SØ are given the prefixes EM and NM respectively. Further modifications have been made as additional evidence required. These are principally due to several local variations occurring in the large unit SM4 south of the Flink's Dal fault and to areas of heterogeneous syenite, designated as "unit" HY, in the southern part of Central Motzfeldt. The geological structure of individual units can be found in chapter (3).

In the petrographic descriptions, hyphens which separate different colours indicate pleochroism. Details of the mineralogy should be sought in Chapter 4.

2.2. Unit SM1.2.2.A. General

SM1 is typically a coarse-grained syenite composed predominantly of randomly orientated pink or brown alkali feldspars, 5-10mm in length and 4-5mm broad. Mafic areas are restricted to anhedral and interstitial areas. Nepheline, usually recognised by its white weathering and negative relief, is notably absent from much of SM1 in northeast and west Motzfeldt although red pseudomorphs after nepheline are reasonably common in samples taken from close to the northeast shore of Motzfeldt SØ. One locality in Central

Motzfeldt shows mafic banding developed on a 5cm scale and extending for a few tens of metres laterally. These structures are associated with parallel coarser-grained bands dipping at moderate angles to the south.

2.2.B. Marginal facies

SM1 may become heterogeneous with streaky banding developed roughly parallel to the strike of its external contacts. This occurs just west of the glacier feeding Qoroq fjord, where fine and coarse-grained syenites of similar composition are closely associated. Frequently, the outer parts of SM1 are entirely nepheline free and leucocratic. This is probably due to assimilation of silica saturated material derived either from sedimentary quartzites of the Eriksfjord Formation or from the Julianehab Granite and is discussed further in Chapter 5.

2.2.C. Petrography

80-90 % of the mode consists of coarsely perthitic alkali feldspar, often with Carlsbad twinning and usually with albitic rims. Mafic minerals are characteristically pale olive-deep brown amphibole with variable amounts of green pleochroic aegirine. In several samples, pale grey clinopyroxene cores (salite) sometimes containing apatite needles, are rapidly zoned to dense green rims (aegirine-augite) enclosing small rounded "euhedra" of exsolved Fe-Ti oxides. A second generation of aegirine may occur both as rims to the amphiboles and as separate small euhedra in interstitial positions, often associated with analcite. Where nepheline is comparatively common (> 5 % mode) Fe-Ti oxides tend not to be overgrown by the usual plates of red-brown biotite, but are instead rimmed directly by blue-green amphibole or red-brown aenigmatite (eg: sample AM4). Where nepheline is prominent (> 10-15 % mode), pale red-brown amphibole directly rims green clinopyroxene (now ferrosalite-hedenbergite). Tiny microlites of aegirine are quite common within the nephelines of these more evolved samples.

Samples of SM1 from the marginal facies lacking in nepheline, commonly display very coarsely exsolved perthites. Here, the mafic minerals become aggregates of arfvedsonitic/riebeckitic amphibole (x=grey y=blue z=lilac) intergrown or rimmed by pale brown-orange biotite, or less frequently by golden yellow astrophyllite.

2.3. Unit SM2

2.3.A. General

SM2 forms an arcuate outcrop in the steep cliffs which margin either side of the southern half of Motzfeldt SØ. Usually a rather massive dark grey rock, with tabular feldspars and interstitial mafic minerals, it coarsens from a porphyritic phonolite in the east to a medium-grained nepheline syenite in the west, the latter being still somewhat porphyritic in parts. It is truncated in the west by SM4 and in the east by the ring dyke (incomplete) SM3. Xenoliths of SM1 occur in SM2 in east Motzfeldt and veins of SM3 cutting SM2 show no feldspar deformation or significant recrystallisation of SM2.

2.3.B. Petrography

(a) Porphyritic phonolite

The easterly margin of SM2 is a phonolite, bearing phenocrysts of feldspar, nepheline, clinopyroxene (with amphibole rims) and a fine-grained phonolitic groundmass which includes poikilitic mafic minerals.

Most of the tabular feldspar phenocrysts (c. 5-10mm in length) are apparently unexsolved and yield quite low 2V's of around 40° . Many of the feldspars show a slight optical zonation, recognised by variation in the extinction angle to Carlsbad twinning where present, or to the long edge of the crystal, which is often developed rather abruptly over the outer 5-10 % of the crystal. Analysis has shown this to correspond with increasing K/Na towards the rim. This zonation from relatively Na-rich cores to sanidine-rich margins is similar to that observed in phonolites from the Kenya Rift (Lippard 1973) and is

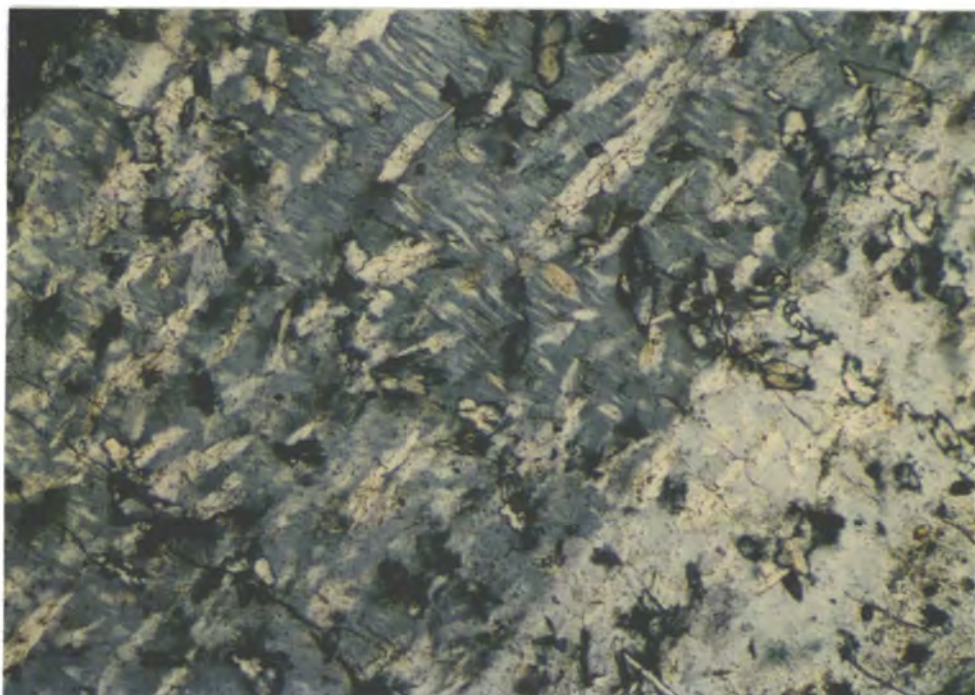


Plate 1. Sample 54142. Complex exsolution (?) in an alkali feldspar phenocryst from the phonolite margin to SM2. Carlsbad twin plane and length of crystal run diagonally across the photograph. x63

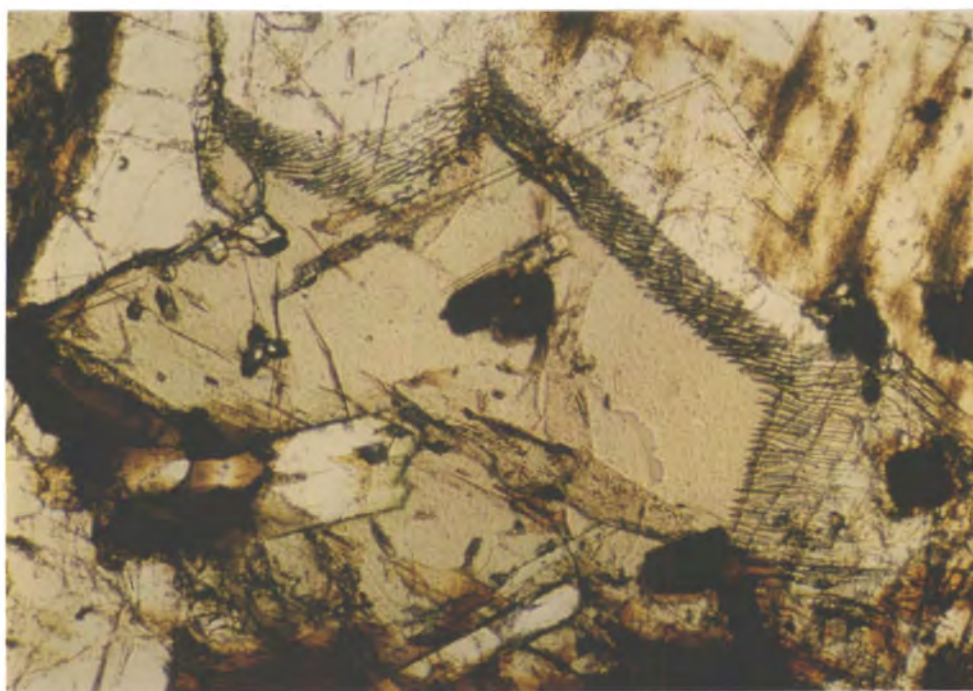


Plate 2. Sample AM39. Pale brown clinopyroxene (salite) showing feather-like intergrowth with colourless nepheline in the lardalitic margin to unit SM5. (Also turbid alkali feldspar, clear needles and stout prisms of apatite, and Fe-Ti oxides often rimmed by dense brown biotite.) x63

known quite frequently from trachytic-phonolitic lavas (eg: Nash et al 1969). There appears to be a direct overgrowth of feldspar into the groundmass, usually enclosing many of the tiny crystals. One or two of the feldspars appear to be partly exsolved, with the development of lenticular prisms of albitic feldspar which may be superimposed on (?) earlier exsolution lamellae (see Plate 1.). The nepheline phenocrysts (1-2mm) may also display slight optical zonation and are usually separated from a rim of additional nepheline by a zone of fine-grained mafic inclusions, thought to mark the initial outline of the crystals, in a manner reminiscent of adcumulus growth. Occasionally, aggregates of up to about 12 crystals can be seen. These are individually unzoned, but grow into the groundmass at their extremities. The same phenomenon has been observed by Lippard in phonolite lavas from Kenya, where aggregates of up to 40 nepheline crystals amass to approximately the same size as the average feldspar phenocryst from the same lava (pers.comm. 1980).

Mafic minerals fall into two categories; early formed relics of zoned clinopyroxene (ferrosalite-hedenbergite) and less common olivines ($\text{Fe}_{69}\text{Tp}_{6.4}$), both of which are overgrown by later amphibole; poikilitic to interstitial crystals of green-brown amphibole and red-brown aenigmatite, both enclosing tiny euhedra of groundmass nepheline and feldspar. Fe-Ti oxides sometimes occur as rounded euhedra within early formed mafic minerals, or as anhedral cores to the larger grains of aenigmatite. Late stage aegirine occurs interstitially and contains up to 4.2 wt% ZrO_2 (54142) being the only major zirconium-bearing phase in this particular rock.

(b) Nepheline syenite (porphyritic)

With increasing distance from the outer contact, SM2 becomes coarser-grained, although two generations of feldspar and nepheline can be discerned in some of the samples. The feldspars become more perthitic, yet may still retain a slight zonation of increasing K/Na from core to rim. In the vicinity of SM4 in southern Central

Motzfeldt and furthest from the contact of SM2 with SM3, unit SM2 varies between a porphyritic microsyenite and a slightly porphyritic syenite, always rich in nepheline (c. 20 % mode). For the first time, Fe-Ti oxides become the stable phase, with a complete loss of the aenigmatite found elsewhere in the unit. The poikilitic mafic minerals now include some biotite and interstitial sodalite is not uncommon. A few substantial crystals of pale grey clinopyroxene (c. 5mm, salite) are zoned through green clinopyroxene (aegrine-augite) and blue-grey arfvedsonitic amphibole to a bluish-green-brown amphibole (also arfvedsonitic) and orange biotite. In these coarser-grained rocks, the zirconium bearing phase becomes eudialyte, lavenite or zircon. Rinkite is locally common.

2.4. Unit SM3

2.4.A. General

This zirconium-rich syenite outcrops in a curve which spans the eastern half of the Motzfeldt Centre. To the north of the Flink's Dal fault it is at its widest and is medium-grained with little nepheline. To the south it is much narrower in outcrop, finer-grained and contains abundant nepheline, often of two generations. Here it is correctly termed a porphyritic nepheline microsyenite and is very similar to the porphyritic phonolite of SM2. It includes xenoliths of SM1 and sends veins into SM3, situated as it is between the latter two units for its southern half. The alignment of abundant tabular feldspars may impart a lamination to the rock. This lamination is usually steeply inclined towards the focus of the arcuate outcrops, although it can be swirled and distorted. Fine-grained syenites with structures simulating gravity stratification occur near to the alkali gabbro dyke in northeast Motzfeldt. Here, mafic bands rich in amphibole and opaques with concordant feldspar lamination show cross cutting relationships on a 10cm scale.

The numerous sheets of microsyenite found in the cliffs of SM1 bordering the northeastern shore of Motzfeldt SØ are possibly related to SM3. These are peralkaline with

bluish amphibole, aligned feldspar laths and plentiful aenigmatite, but show no sign of nepheline. A 50m wide sheet of eudialyte-microsyenite cutting SM3 southeast of Motzfeldt SØ (54157) is somewhat porphyritic and almost certainly related to SM3 itself.

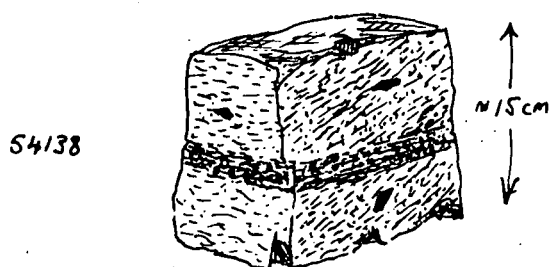
2.4.B. Petrography

(a) South of the Flink's Dal fault

(i) Porphyritic nepheline microsyenite

Composed predominantly of tabular alkali feldspars (c. 10 x 3 x 2mm) and euhedral nephelines (c. 0.5-1.0mm) with interstitial to anhedral mafic minerals, the rock is sometimes dark coloured due to the presence of fine-grained material. The most common mafic mineral is pink brown-greenish brown amphibole (ferro-edenitic) rimmed by blue-green amphibole (magnesio-arfvedsonite), usually as irregular area, but also present in hand specimen as occasional rhombic euhedra to 20mm in length. The alkali feldspars are perthitic and the nephelines may form bands several crystals long in between the feldspars. Aegirine (x=green y=yellow green z=greenish yellow) is a common interstitial phase (c. 5 % mode), often forming semi-radiating clusters of prismatic crystals. These aegirines contain up to 6.96 wt% ZrO_2 (54138) where no other Zr-bearing phase is present. Fe-Ti oxides and olivine are apparently absent, whilst aenigmatite is present in accessory proportions.

Cm-scale "mafic" banding in which mafic minerals and dark fine-grained material enhance the white weathering nepheline euhedra (c. 1mm) may be discordant by 10-15° to the feldspar lamination (54138), as shown in the sketch below:-



(ii) Late sheet, (eudialyte)-nepheline microsyenite

This microsyenite sheet (54157) is aphyric at its margins, but elsewhere contains perhaps 10-15 % phenocrysts (Fsp, Ne, Cpx). The tabular alkali feldspars (to c. 5mm long) show the same blebby exsolution and slight optical zonation so typical of SM2. Smaller feldspars in the groundmass are normally perthitic. Nepheline is present both as optically zoned euhedral phenocrysts and in the groundmass. Mafic minerals are euhedral and consist of many pale green clinopyroxene crystals (hedenbergitic) zoned to dark green rims (aegirine-augite), and similar quantities of blue-greenish grey amphibole (arfvedsonitic). Interstitial sodalite (c. 10 % mode) and cancrinite (c. 5 % mode) are notably common. Moderate relief colourless eudialyte, with typical anomalous birefringence, occurs as occasional net-like poikilitic crystals to 2cm across and less commonly as rather distorted euhedra (3-5mm). Lavenite may occur as an accessory phase.

(b) North of the Flink's Dal fault

Thin sections examined from this area of SM3 are highly feldspathic medium to fine-grained syenites, all apparently devoid of nepheline. Typically, euhedral alkali feldspars 5-10mm in length are microperthitic, sometimes with Manebach twins preserved as "herring bones", and Carlsbad twins. Samples from the south of this outcrop may preserve high temperature anorthoclase (2V c. 45°) in its optically unexsolved state, as cores to microperthites (58400). Mafic minerals consist of olive green-greenish brown anhedral amphibole, enclosing smaller tablets of alkali feldspar (c. 0.5mm) and relic cores of apple green clinopyroxene (ferrosalite-hedenbergite). Pale green clinopyroxene may also occur as discrete euhedra (c. 0.5mm ferrosalite) within the larger perthitic feldspars. Apatite needles (to 0.4mm long) and Fe-Ti oxides are common accessories. Zircon is common, either as early formed euhedra or as anhedral areas (0.3-10mm maximum dimension) sometimes overgrown on smaller euhedra, and can constitute up to about 3-5 % of the mode.

The mafic bands developed within this unit, near to

(c. 0.5 km) the alkali gabbro dyke, typically consist of, in order of decreasing modal proportions (63721C), amphibole, alkali feldspar, Fe-Ti oxides, apatite, and zircon. In addition there is a second generation of the green-brown amphibole (ferro-edenite) and zircon may also be overgrown on early formed euhedra. Green clinopyroxene (hedenbergitic) may form quite frequent relic cores to the amphiboles (63721B) and pale yellowish brown euhedra (c. 0.3mm) of melanite garnet are locally common (63717).

2.5. Unit SM4

2.5.A. General

This unit occupies most of Central Motzfeldt and also occurs west of Qôroq fjord, where it cuts across units of the North Qôroq Centre. On the latter evidence, the Motzfeldt Centre postdates that of North Qôroq, contrary to the earlier beliefs of Emeleus and Harry (1970) though still in agreement with Rb/Sr age dates obtained for these two centres by Blaxland et al (1978). This part of SM4 corresponds to unit ?SN3 in the work of Chambers (1976) on the North Qôroq Centre, and substantiates his original suggestion that ?SN3 did in fact emanate from the younger Motzfeldt Centre.

Within SM4 there are several distinct facies, possibly representing separate intrusive or cooling events, although this has not always been demonstrable in the field, owing partly to their complexity and partly to ambiguous field relations. However, detailed mapping in Flink's Dal has shown there to be three distinct mappable members of syenite, collectively known as SM4, prior to the emplacement of the lujavrites (SM6). SM4 contains large amounts of xenolithic material derived from the supracrustal rocks of the Eriksfjord Formation. These are preserved in all sizes from 5cm diameter inclusions to huge rafts measuring up to 5 kilometres in length. The large rafts, composed mostly of lavas, may have promoted complexity in SM4.

2.5.B. Flink's Dal area

In general, the syenites are variable in character,

possibly due to their proximity to the original roof region of the centre. Large xenolithic rafts appear to have acted as barriers to uniform fractionation within unit SM4, having a profound effect upon the syenites beneath and appearing to act as temporary floors to the syenites crystallising above. One raft in particular, appears to have sunk into the syenite as a massive slab, 1-200 m thick, which has broken up at its edges, where smaller blocks have been spalled off. Syenites beneath the slabs are usually less well laminated and often depleted in mafic minerals, with euhedral nepheline constituting up to 50 % of the mode. Immediately above the rafts, the syenite may be well banded for about 10-20m (see Chapter 3, fig. 3,2). Here, the feldspar has a platey habit and is laminated parallel to the mafic bands. The latter become less mafic and thinner upwards, often commencing with a basal layer practically devoid of nepheline.

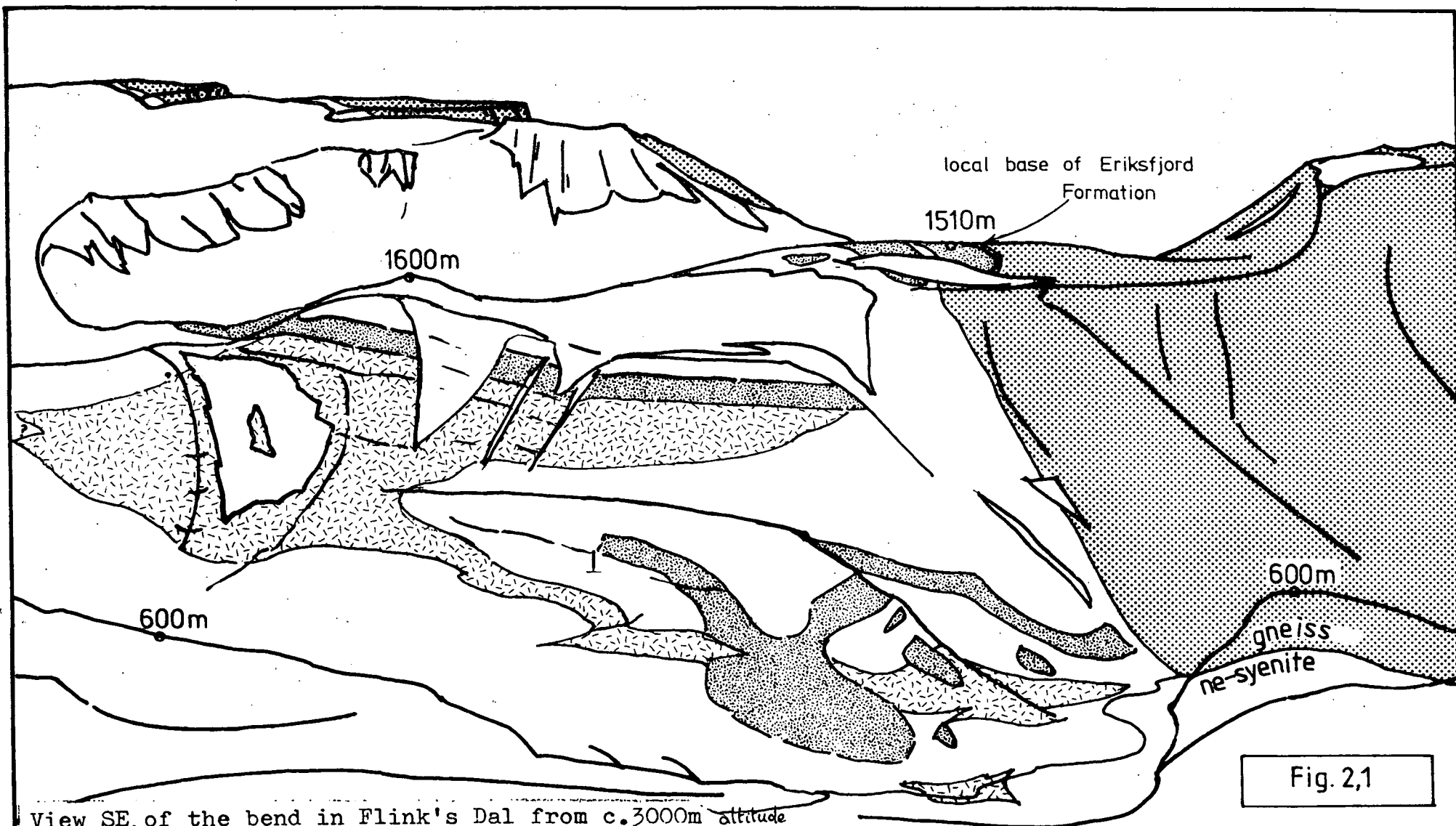
Foyaite

Distinctive because of its platey alkali feldspar, this syenite frequently shows a lamination dipping at moderate to high angles to the NE and presumably towards the original focus of SM4. Immediately above the rafts of supracrustal rock, the lamination is often at low angles, apparently reflecting the topography of the raft. Rare mafic bands beneath the rafts are frequently distorted and discontinuous, suggesting deformation caused by the sinking raft upon a crystalline mush.

Heterogeneous Syenite

Fine to medium-grained syenites and microsyenites, these are normally well laminated and often banded. The alignment of small ubiquitous feldspar phenocrysts may be semi-parallel to the rafts, or distorted with steep and variable angles of lamination.

Xenoliths of Foyaite within the Heterogeneous Syenite and xenoliths of Heterogeneous Syenite within the lujavrites, indicates that the Heterogeneous Syenite postdates the Foyaite and predates SM6, the lujavrites. The Heterogeneous



View SE, of the bend in Flink's Dal from c.3000m altitude showing disposition of lujavrites (light cross hatching) and rafts of supracrustal rocks (denser fine stipple). Clear areas are all ne-syenites of SM4, with some snow fields, and the large regular stipple is country rock gneiss (Julianehåb Granite). After air photo. (oblique)

Syenite found in Flink's Dal is rather discontinuous, although based on field evidence and petrography alone, it appears to be very similar to unit HY, which lies 2-3km to the east of Flink's Dal. Thus, it is likely that these heterogeneous syenites have a similar mode of origin, as a natural consequence of multiple intrusion.

Brown Syenite

A coarse-grained syenite with distictively randomly oriented brown alkali feldspar and small amounts (5-10 % mode) of orange nepheline, forms a narrow outer zone to the southwest part of the Motzfeldt Centre in Flink's Dal. This syenite appears to cut earlier members of unit SM4 as outlined above.

SM4: Summary for the Flink's Dal area

The variability of the syenites in this area can probably be attributed to the proximity of the original roof of the centre. The rafts of supracrustal rock, which have clearly sunk into the syenites and were presumably derived from the roof region, have acted as physical barriers, preventing uniform cooling and solidification of the syenites into which they sank. In detail, the syenites can be very complex. Thus, given the large overall area of outcrop of unit SM4 (c. 170 km²), it is convenient to view these members described above as variants of SM4, at least for the time being.

2.5.C. Unit SM4: Petrography

Foyaite

Foyaite syenite occurs within SM4 mostly in the west and south of Central Motzfeldt and it is this variety which occurs to the west of Qôroq fjord. Consisting of tabular to elongate perthitic alkali feldspar (c. 20 x 5 x 10mm), euhedral nepheline (c. 2-3mm) and interstitial bright green clinopyroxene (hedenbergite-aegirine), it is usually just peralkaline, although (Na+K)/Al is a little less than one for mafic varieties. The feldspar lamination can be extremely well developed (eg: 63754), with rather

small nephelines (c. 1mm) tending to occur as layers in between the feldspars. Nepheline constitutes about 20-30 % of the mode with clinopyroxene and minor Fe-Ti oxides generally accounting for about 10 %. The role of sphene appears to have been taken over by rinkite-type minerals (Na,Ca,Ti,Ce silicates) several different phases contain varying amounts of zirconium (eg; lāvenite, eudialyte). Small amounts of apatite and red-brown biotite may also be present.

Within the more mafic foyaites (eg:54241), pale green clinopyroxene (hedenbergite) zoned towards dark green margins (increasing Na) is poorly rimmed by strongly coloured amphibole (x=olive green y=green z=brown). Together with Fe-Ti oxides and apatite, these mafic minerals comprise up to about 40 % of the mode. Here, nepheline may occur both as euhedra and as optically continuous blebs in the feldspars, the latter being finely perthitic and irregular in outline. Interstitial pale brown sphene may occur as an accessory.

Cumulus horizons

Limited amounts of mafic banding occur in SM4, as for example just to the east of the larvikite ring dyke (SM5*), where individual 5cm scale mafic bands can be traced through crumbly medium-grained pale syenites for 10 or 20m and much less precisely for perhaps 300m along strike. In thin section, cumulus textures are common. These usually involve tabular microperthitic feldspars and smallish nepheline euhedra, set in large continuous areas of dark amphibole, zoned only slightly at its edges. Inclusions of relic clinopyroxene (salite-ferrosalite) and apatite (0.5-1.0mm) are also common within this amphibole and a second generation of green aegirine-rich clinopyroxene occurs as an interstitial phase. The texture would suggest that at least some of the amphibole (x=green y=pale brown z=dark brown) has undergone adcumulus growth.

The mafic minerals in the layered rocks above the xenolithic rafts in Flink's Dal (near to SM6) have

been (?) altered to felted masses of pale green clinopyroxene (aegirine-augite). The microperthitic alkali feldspars are little altered and the original outlines of the clinopyroxenes and apatites are still clear. Small amounts of interstitial nepheline have been altered to gieseckite, cancrinite or sometimes to sodalite.

Porphyritic microsyenite and porphyritic phonolite

Porphyritic microsyenite forms part of the marginal facies of SM4 near to its contact with the older SM1 in northern Central Motzfeldt, whilst porphyritic phonolite may be found to the north and east of the xenolithic rafts around Ivnârâ.

(i) Porphyritic microsyenite (eg: AM7)

Phenocrysts of aligned perthitic alkali feldspar, well zoned nepheline euhedra and several pale brown-red brown amphiboles (edenitic) account for about 80 % of the rock (see Plate 3). The remainder consists of further felsic minerals with interstitial green clinopyroxene (aegirine), arfvedsonitic amphibole and aenigmatite. Relics of pale grey clinopyroxene (salite-ferrosalite) and iron-rich olivine (fayalite) are sometimes found within the amphiboles. In addition, Fe-Ti oxides may be preserved as corroded cores to aenigmatite and rinkite may occur as a few relatively large, twinned (lamellar) crystals (c. 1mm).

(ii) porphyritic phonolite (eg: AM9)

This phonolitic rock is similar to those described from units SM2 and SM3 and is illustrated in Plate 4. Apparently little-altered anorthoclase may be preserved as phenocrysts (c. 5mm), although there has often been a limited amount of blebby exsolution. Both fayalitic olivine and pale green clinopyroxene (ferrosalite) are present as discrete crystals (c. 0.5-1.0mm) generally having a thin rim of dense green amphibole. Nepheline is less common than in either SM2 or SM3, amounting to about 5-10 % of the phenocrysts. Reddish brown-olive green amphibole and lesser amounts of dark red-brown aenigmatite are poikilitic in the medium-grained groundmass. The

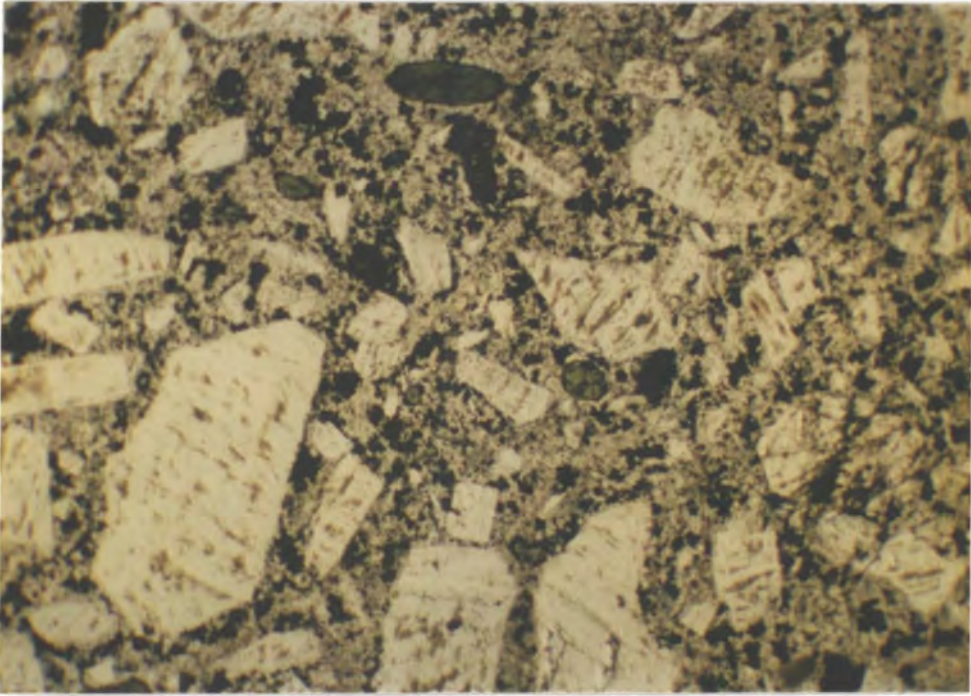


Plate 3. Sample AM9. Porphyritic phonolite of unit SM4, with euhedra of alkali feldspar, green pyroxene, clear nepheline and some olivine (not shown). Dark amphibole and aenigmatite in the groundmass may enclose small euhedra of felsic minerals. x10

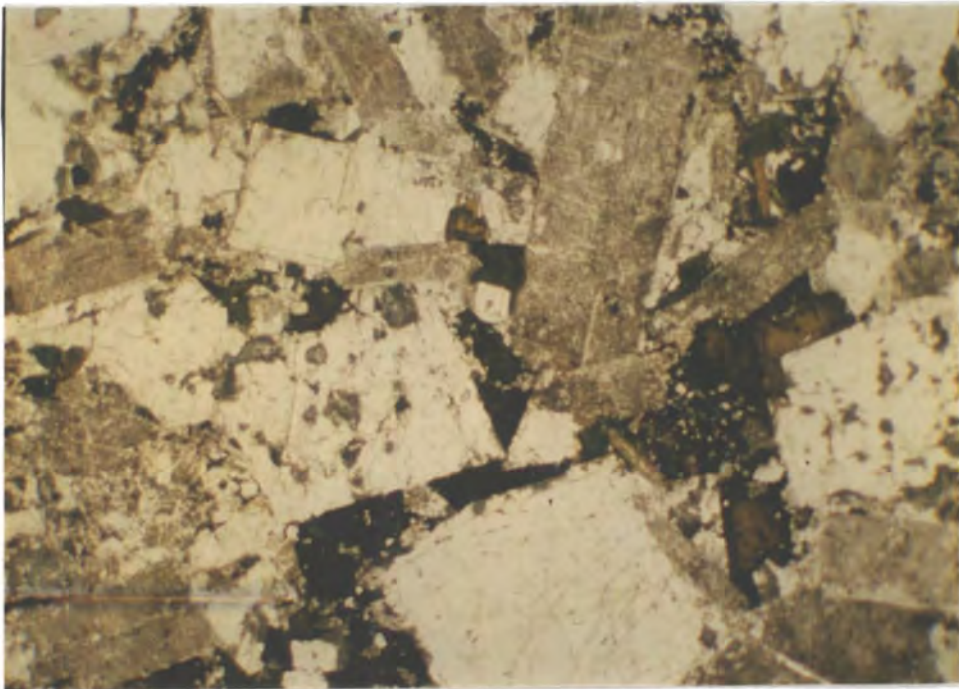


Plate 4. Sample AM7. Porphyritic microsyenite of similar phonolitic composition to the above. More prominent clear nepheline euhedra. Interstitial mafic minerals include dark amphibole, aenigmatite and green aegirine. x10

phenocrysts amount to about 40 % of the rock and are mostly feldspars.

2.5.D. Recrystallised SM4

Where SM4 has been recrystallised by SM5 and SM6, Na-metasomatism can be seen in thin section, where original mafic minerals have been replaced by aggregates of rather pale green aegirine-rich clinopyroxene, orange-brown biotite and small Fe-Ti oxide^{grains}, with or without greenish blue arfvedsonitic amphibole. Albitic rims to the feldspars are often enhanced and interstitial albite may be present.

Near to and directly above the larvikite ring dyke (SM5*), SM4 becomes hardened and the feldspars have often begun to lose their identity. In thin section, the original mafic minerals have often been replaced by optically continuous anhedral areas of pale green clinopyroxene (hedenbergite-aegirine) and nepheline has frequently been extensively altered to natrolite, lending the rock a characteristic reddish colour. Occasionally, magnetite appears to have segregated and forms lenses up to 2m in length. The magnetites have perfect crystal outlines in reflected light (c. 1mm) with triple junctions and are similar to normal low temperature deposits of magnetite.

2.6. Unit HY: Heterogenous syenites

2.6.A. General

Situated south of upper Flink's Dal and forming a northward facing spur, this area consists of mafic and leucocratic fine-grained syenites, porphyritic syenites and microsyenites. Some of the porphyritic microsyenites are similar to the Heterogenous Syenite in Flink's Dal, although the two are not necessarily related. These hybrid (=HY) syenites are not strictly speaking an intrusive unit so much as a mappable member. They appear to be gradational to the surrounding SM4 and within themselves. They are cut by SM4 in the east and by a dyke-like body of SM4 in the west, where they are exposed on glaciated slabs at the toe of a retreating glacier. Within this "dyke" of SM4,

the different varieties of HY can be recognised as angular to rounded blocks (up to about 0.5m) apparently undergoing various stages of assimilation with their host. A sheet of xenolithic microsyenite similar to HY cuts SM1 in southeast Motzfeldt (54135) and also forms a 1-500m² area in the north of Central Motzfeldt. An area of porphyritic microsyenite in SM5 in upper Flink's Dal, is possibly a sunken relic of HY.

HY usually develops a streaky banding, usually in a sub-horizontal attitude and often with quite sharp though discontinuous boundaries, which can be traced for several tens of metres in units from 10cm to 5m wide. Petrographic examination of HY and the adjacent SM4 reveals that much of HY consists of microsyenite mixed in varying proportions with older medium-grained syenite. Xenocrysts and aggregates of ^{crystals from} nepheline syenite appear to be 'tumbled' in a matrix of nepheline microsyenite, which itself shows very well developed flow structures. Sodalite and cancrinite are locally very common. From the recrystallised nature of the relic syenite and the total and intimate variation in proportions of xenolithic syenite and microsyenite, it is thought that much of the microsyenite has been derived in-situ, by remobilisation of the old syenite. It is also apparent that SM4 has become patchily contaminated within a zone up to 0.5km distant from HY. In these syenites, amphibole may be unusually dominant over sodic pyroxene. The overall impression is of an area of nepheline syenite which has been reheated and remobilised, apparently in response to the intrusion of SM4. This is elaborated further in chapters 3 and 5.

2.6.B. Petrography

(i) Porphyritic microsyenite

Varying between a fine-grained syenite and microsyenite, this is the most characteristic variant of HY. Xenocrysts and aggregates of several crystals of nepheline syenite vary in modal amount from about 15 to 50 %. Typically, large slightly zoned nepheline euhedra (c. 1-2mm) and oblong perthitic alkali feldspars (c. 5mm) deflect the

groundmass minerals (the microsyenite). Both pale green clinopyroxene (hedenbergite) and amphibole (x=greenish brown y=pale brown z=brown) exist as xenocrysts, still attached to their original syenite matrix. The xenocrysts of clinopyroxene may show continuous green sodic rims developed irrespective of their original optical orientation or fragmentary nature. The microsyenite consists mostly of elongate K-rich feldspar, abundant nepheline euhedra (c. 0.2mm) which are characteristically zoned and anhedral mafic minerals (c. 0.1mm). The latter consist of dark coloured amphibole (dark green-brown) and dark green clinopyroxene (hedenbergite). Dark orange brown biotite is notably common (c. 1 % mode) and tiny apatite needles are locally abundant.

(ii) Nepheline syenite

Quite frequently the alkali feldspars may show Manebach twins, preserved as "herring bones" within the perthites. The colouration of the feldspars is distinctly patchy, with clear areas coinciding with crenulate crystal boundaries. Very occasionally, one or two feldspars show deformation in that they are bent. Nepheline constitutes about 20-30 % of the rock and may be partly replaced by cancrinite, natrolite or sodalite. Almost all of the nephelines are zoned, yet are effectively of constant composition (see Chapter 4). A particularly dark amphibole (x=dark green y=z=dark brown) is the dominant mafic phase, whose ragged outlines often give the rock a spotted appearance in hand specimen. Throughout a typical thin section, there is a notable amount of small blebs of felsic minerals. The latter (Ne, Ab, K-fsp and cancrinite) have a vague preferential alignment running across an otherwise equigranular medium-grained nepheline syenite (eg: AM119).

(iii) Supplementary

The xenocrysts and aggregates of nepheline syenite within their microsyenite host show recrystallisation, in the form of small crystals (Ne, Fsp, Amph) developed in the relic crystals. The alkali feldspars often show a considerable

range in exsolution types, cryptoperthite, perthite, braid perthite and even apparently homogenous feldspar ($2V \approx 50^\circ$) being present. This presumably attests, at least in part, to their xenocrystic origin. In some of the feldspar it appears that the sodium-rich portions have "annealed", by linking of perthitic blebs into semi-continuous canals. With regard to the patchy pink colour and 'dusting' of the feldspar in the "old" syenite, it is interesting that pink alkali feldspars from the Shap Granite, Cumbria, may turn white upon heating (G.M. Brown pers.comm. 1979). This bleaching is seen again in SM5 remobilised by the alkali gabbro dyke (see following section 2.7.E.). Rinkite is a common accessory phase throughout HY.

2.6.C. Additional

Unit HY has an unusually variable peralkalinity ratio ($(Na+K)/Al=0.9-1.1$) and $Na/(Na+K)$ ratio, more so in fact than any other single unit from the Motzfeldt Centre, although units from North Qôroq are similarly variable (Chambers 1976, Vol.2). Sodalite, cancrinite and hydrated minerals are all rather common, suggesting relatively high concentrations of volatiles (Cl, CO_2, H_2O).

2.7. Unit SM5

2.7.A. General

SM5 is the last major intrusive unit north of the Flink's Dal fault, except for the alkali gabbro dyke. It consists for the most part, of coarse-grained, pale weathering syenite which is often rich in euhedral nepheline. However, along its west and northwest margins it becomes a darker, more basic syenite, which is in fact very reminiscent of the lardalites from southern Norway. A partial ring dyke of larvikite, outcropping as the northwest quadrant of a circle in western Central Motzfeldt appears to be an early, yet more basic intrusion just predating SM5 and is referred to as SM5*.

The ring dyke SM5* was originally termed a syeno-

-gabbro by Emeleus and Harry (1970) yet, in view of its strong similarities to material from the Permian graben of Oslo in S. Norway, it is the preference of this author to call SM5* a larvikite. Similarly, the more nepheline-rich relative of SM5 is called a lardalite (strictly speaking, an olivine lardalite). There is a complete gradation from the most basic members of SM5* through the lardalites to basic syenite, also found near the margin of SM5. This is accompanied by a textural variation, with a progressive change in nepheline habit (see below) and a continual mineralogical and geochemical variation.

SM5 typically contains large rectangular alkali feldspars (3-5cm). prominent white weathering nepheline euhedra (1-3cm) and anhedral areas of mafic minerals. Where the syenite becomes finer-grained towards its western margin, poikilitic coppery coloured biotite becomes a prominent constituent. In this region, three varieties of xenolith may be encountered; (i) Large areas (c 1-500m²) of trachytic and microsyenitic material, often with complex edge effects towards SM5, manifested by streaky and rapidly varying syenites, over 1m or so. These are probably derived from the supracrustal rafts, and may be reworked from rafts in SM4; (ii) Subangular to rounded xenoliths of pale foyaite (c. 0.5m), although not common, these are presumably derived from the adjacent SM4, clearly indicating the younger nature of SM5; (iii) Areas of fine-grained basic syenite, which appears to be the chill of SM5 itself (autoliths), found adjacent to a large raft.

The boundary of SM5 in the eastern end of upper Flink's Dal is somewhat more complicated. Here, close inspection reveals a slight decrease in grain size of SM5 towards SM4. In thin section, SM4 often shows signs of recrystallisation. Some samples of SM5 are again of lardalitic type. It appears that although SM5 is younger than SM4, the original boundary has been effected by later faulting and the present day contact is, at least in part, tectonic.

Mafic banding can be seen at a few localities

within SM5, notably at about 1250m 2-3km east of Ivnârâ, where mafic bands about 2-3cm thick occur over a 30m width and along strike for about 70m, with a lamination of elongated feldspars running parallel to the bands. Textural evidence suggests that accumulation of early formed and dense phases was quite an active process in SM5.

2.7.B. SM5*; Larvikite

Weathering to a dark brown colour along the dyke, this rock is a dark variety of larvikite, with olivines and poorly schillerised feldspars visible in hand specimen. Alkali feldspar forms the bulk of the mode (c. 40-60 %) and is cryptoperthitic, sometimes (58037) enclosing rare xenocrystic cores of plagioclase (c. $\text{An}_{28}\text{Or}_3$) which shows subdued lamellar twinning. In the most mafic representative (58062), the typical lilac clinopyroxene (salite) forms 20-25 % of the mode as large subhedral crystals (c. 3-5mm), with smaller pale yellow olivine euhedra ($\text{Fa}_{57-64}\text{Tp}_{2.5-2.6}$; where $\text{Tp}=\text{tephroite}=\text{Mn}_2\text{SiO}_4$) also being quite common (c. 5-10 % mode). Irregular areas of strongly pleochroic amphibole (dark brown-pale brown-reddish brown) are often optically continuous and very similar in colour to the red-brown biotite plates. Somewhat darker biotite is also very common as enveloping sheaves to rounded and exsolved Fe-Ti oxides and olivines. Elongated apatite needles are abundant throughout the larvikite. Nepheline, quite commonly pseudomorphed by pale brown clay-like minerals (cf. gieseckite) is present (3-5 %) in the most basic members as optically continuous blebs within the feldspar. In more evolved samples (olivines $\text{Fa}_{70-83}\text{Tp}_{3.2-5.7}$ as in AM55) nepheline is also present as an interstitial phase and can form perhaps 10 % of the mode in more leucocratic varieties.

2.7.C. Marginal SM5

(i) Lardalite

In this olivine lardalite, cryptoperthitic alkali

feldspar is a little more common (50-65 % mode) but the most notable change from the larvikite, is the increase in nepheline. This now exists, not only as blebs in feldspar and as interstitial 'stringers', but also as discrete anhedral areas, totalling up to about 15-20 % of the mode. Colourless to pale green olivine ($\text{Fa}_{63-85}\text{Tp}_{3.8-7.2}$) forms common euhedra (c. 10 % mode), once more rimmed by biotite. Subhedral clinopyroxene (c. $\text{Di}_{50}\text{Hb}_{35}\text{Ac}_5$) is now slightly zoned to pale green clinopyroxene at its edges. Nepheline may be intimately associated with the clinopyroxene, and may be intergrown on a $1/100^{\text{th}}$ mm scale (Plate 2), where it is also associated with very fine apatite needles. Nepheline would thus appear to be a high temperature phase, whose nucleation has been more or less simultaneous with clinopyroxene in this instance.

(ii) Mafic nepheline syenite

A mafic syenite may be found at the extreme northwest contact of SM5 with earlier SM4, and is unusual for the amount of nepheline which it contains in excess of feldspar. Perthitic alkali feldspar, often exhibiting Carlsbad twinning, is apparently entirely restricted to interstitial positions and comprises 15-20 % of the mode. The dominant minerals are euhedral nepheline (c. 50 % mode) and slightly zoned subhedral to euhedral amphibole (x=red y z=dark brown) with interstitial amphibole of the same composition. Lilac clinopyroxene and olivine ($\text{Fa}_{74-80}\text{Tp}_{4.8-5.7}$) is much less common, whilst apatite and Fe-Ti oxides are more common than in the lardalites.

2.7.D. Nepheline syenite

Typically, felsic minerals compose 80-85 % of the syenite, of which 20-30 % is nepheline. Subhedral to euhedral perthitic alkali feldspar forms large crystals (c. 10 x 5 x 5mm to 20 x 10 x 10mm) with nepheline occurring as euhedra (c. 5 to 10mm) and as blebs within feldspar. Mafic minerals are distinctly localised anhedral areas in hand specimen and consist of early formed pale lilac

coloured clinopyroxene (salite) zoned to greenish margins (increasing Na) and surrounded for the most part by large anhedral areas of distinctively coloured (x=orangey brown y=pale brown z=bluish green) amphibole (ferro-edenitic). This amphibole may show anomalous extinction across its breadth and especially towards its darker coloured rims (arfvedsonitic). Occasionally, the amphibole may be intergrown with bright green clinopyroxene (cf. AM82, aegirine-augite) but is quite often intergrown with small amounts of orange-brown biotite. Blebby Fe-Ti oxides, apatite and sphene are usually present as accessories. Towards the interstitial positions (generally one or two per slide) the mafic minerals show slight Na-enrichment, blood red-black aenigmatite overgrows Fe-Ti oxides and small crystals of nepheline, alkali feldspar and sodalite may be present.

Very occasionally, euhedra of red eudialyte (c. 2-5 mm) are found (eg: AM82), sometimes partly pseudomorphed by pale micaceous-type minerals and catapleite. In these samples, nepheline appears to be randomly replaced by sodalite and natrolite, or less commonly, by cancrinite. Pinkish to purple coloured fluorite is often present in accessory proportions.

Samples which display cumulus textures (sensu stricto Wager and Brown 1968) often have (eg: AM43) euhedral nepheline (2-3mm) and alkali feldspar (c. 5mm) emphasised by large anhedral areas of optically continuous amphibole (pale orange-dark brown) which may comprise 30 % of the mode and include smaller euhedra of felsic minerals. Early formed lilac or pale green clinopyroxene (salite) is sometimes separated from this amphibole by a feathery reaction rim, up to 0.5mm wide, in which are found (~~microprobe~~) aegirine (Ac₉₅), Mg-arfvedsonite and calcite. Orange coloured biotite is a minor phase, whilst late stage interstitial green aegirine, red aenigmatite, blue green arfvedsonite and twinned albite are common accessories.

2.7.E. Rheomorphism

Within about 1-3m of its contact with the younger alkali gabbro dyke, SM5 has undergone rheomorphism and

has back-veined the dyke. Samples collected at 3m, 1m and 0.5m from this contact (AM109, 108 and 107 respectively) show increasing degrees of melting of the original coarse-grained nepheline syenite. The salient points will be outlined in the following petrographic descriptions, given in the order of increasing melting. Naturally, no glass is preserved, because the melt still cooled at depth and thus relatively slowly, although the syenite which has been re-melted is distinctly finer-grained.

(a) AM109; 3m from contact

1. Consisting of coarse-grained nepheline syenite for the most part, thin sections are characterised by perfectly rounded to oval areas of completely bleached feldspar, in contrast to its normal pale pink/brown colour.

2. Recrystallisation has occurred along the grain boundaries, with fine grained intergrowths of rather granular crystals (Mt, Ne, Fsp, Bi). These are almost exclusively concentrated in the bleached areas and occur prominently at multi-phase boundaries. The latter is in agreement with theoretical predictions of partial melting, which indicate that melting is favoured in proportion to the number of components available at any particular site (S. Maaløe pers. comm. 1980).

(b) AM108; 1m from contact

1. Subordinate areas of coarse-grained nepheline syenite are still recognisable in a fine-grained syenitic matrix.

2. The matrix is characterised by fine-grained crystals of nepheline euhedra or blebs, rounded grains of Fe-Ti oxides, elongate laths of biotite in random orientation and feldspar grains and laths.

3. The elongated crystals of biotite may be bent or curved perhaps indicative of rapid growth. The relic feldspars are also frequently bent and distorted.

4. Patches of abundant granular opaques and small biotite crystals show the vague outlines of original mafic

minerals, such as amphibole from the original syenite SM5.

(c) AM107; 0.5m from contact

1. The rock is of a variable grain size, with no large crystals remaining. The felsic minerals now have angular or crenulate boundaries and are generally anhedral.

2. Needles and elongated crystals of biotite are prominent, and fine needles of apatite are locally prolific.

3. The small feldspars show a variation in their exsolution from cryptoperthites to regularly exsolved little micropertthites and perthites.

4. Some of the feldspars show a patchy colouration (very pale pink) or "dusting" of fine-grained particles, slightly enhancing their relief.

5. There is a suggestion that mafic phases, excluding the larger biotite crystals, are localised in relatively few areas across the slide.

2.8. Unit SM6

2.8.A. General

The Motzfeldt lujavrites consist for the most part of similar portions of dark lujavrite and white lujavrite, with very subordinate or rare amounts of green lujavrite. They are approximately of microsyenite grain size (c. 1mm), with a coarse-grained lujavrite equivalent to about a medium-grained syenite (c. 4-5mm).

Representing the last visible intrusive phase south of the Flink's Dal fault (except perhaps for the alkali gabbro dyke), the lujavrites show excellent flow banding between mafic and leucocratic layers on a 1cm to 10cm scale (Plate 5) which can be seen to swerve around incorporated xenoliths (Plate 6). Large scale banding, on the scale of several metres or several tens of metres can be seen in the vicinity of a large corrie situated at the northern end of Qôrqup qâqai (see Chapter 3, fig. 3,1). On the basis of this layering and the presence of flat-lying fold structures coupled with the rapid fluctuations in composition,



Plate 5. Fallen block of dark lujavrites (SM6) in Flink's Dal. The paler bands are caused by higher proportions of perfect nepheline euhedra. Highly contorted banding occurs just out of view (right). (Hammer 35cm).



Plate 6. Xenoliths of foyaitic syenite in dark lujavrite, whose "contaminated" appearance here resembles heterogenous syenites of unit HY. The foyaite is presumably from the nearby unit SM4.

these lujavrites were originally regarded by Emeleus and Harry (1970) as raft-like inclusions of gneiss that had been thoroughly soaked by and recrystallised in the syenite SM4. Further detailed mapping in the Flink's Dal area has shown this not to be so. The lujavrites behave as a large sill-like intrusion situated beneath large rafts of xenolithic lavas, and are irregular in detail. Their disposition is shown diagrammatically in figure 2,1. Plate 7 illustrates a major raft (also the centre foreground of figure 2,1) which directly overlies the westward part of the lujavrites.

The lujavrites display excellent cross-cutting relationships to both the Foyaite and the Heterogenous Syenite of SM4 in the Flink's Dal area (see Plate 8). They become finer-grained towards contacts, although coarser and finer bands almost immediately away from their margins means that any "chilled" zone is necessarily very thin. The nepheline euhedra, so characteristic of the dark lujavrites in particular, are remarkably constant in size within any given band, yet can vary greatly between adjacent bands (ie: c. 1 to 10mm). Small folds are common within the banding and become more complex (Plate 9) near to xenoliths and contacts, where fine and coarse-grained lujavrite or even pegmatitic lujavrite have been formed simultaneously. At one contact, a mafic band of lujavrite is seen to tear off individual feldspars from the older foyaite (Plate 8). This shows the direction of flow to be consistent with the mapped direction of thinning towards the west, and away from the thickest part in the east.

Eudialyte appears to be very sparse in some of the lujavrites, although this is probably a field recognition problem, since eudialyte from Motzfeldt can be cream coloured (eg: 46261, AM159) as well as the more usual pink colour, both of which can be euhedral and possibly mistaken for nepheline.

Division of the lujavrites into three types, using colour and grain size, with further characteristics as outlined below, has been done in the field. Where two



Plate 7. Dark xenolithic raft of lavas in ne-syenites of unit SM4 in 650m cliff in Flink's Dal. Nearby base of the Eriksfjord Formation from which these lavas were probably derived is at about 1500m, some 600m above the 900m summit in view.



Plate 8. Dark lujavrites (SM6) cutting medium-grained foyaite of SM4 in Flink's Dal (base of cliff in plate 7). Possible additional growth of feldspar on the xenocrysts. Banding of the lujavrite is parallel to the contact.



Plate 9. Complex folding of dark lujavrite (SM6).
Camera lens cap (c. 5cm) for scale.



Plate 10. Typical white lujavrite of SM6 with pencil
for scale. Prisms of black aegirine are prominent against
dull grey nepheline euhedra and white alkali feldspars.
Rose-pink mineral is eudialyte.

or more types of lujavrite occur together, the dark segregations seem to be the last to have solidified, yet there is frequent evidence for both mafic and leucocratic variants to ^{have} been emplaced simultaneously (eg: Plate 9).

2.8.B. Dark Lujavrite

Typically, this is a dark rock with prominent negative-weathering nepheline euhedra which act as "eyes" to a flow aligned matrix of dense black aegirine needles and interstitial white feldspar (eg: AM164). Coarser varieties may be rich in the yellow mineral manganoan pectolite, and in yellowish eudialyte or its alteration products. The eudialyte is usually well formed and can be identified as rose pink, cream or brown euhedra, although it is more difficult to distinguish in the coarser-grained samples.

In thin section (AM164), a dramatic flow structure is portrayed by elongated green~~y~~yellow-green aegirine laths (3-5mm long), and separate albite and microcline laths. This flow structure is deflected and turned by numerous nepheline (2-3mm) and eudialyte (1-3mm) euhedra. The eudialytes are often fractured and show low or anomalous birefringence, sometimes with nicely developed concentric zonation. One tumbled phenocryst of eudialyte, directly abutts a nepheline crystal, the two behaving as a single entity, suggesting that the two crystals had similar temperatures of formation. The eudialyte is frequently altered to a stronger pink coloured material along its cleavage cracks. Further stages of alteration, seen in a few euhedra, indicate eventual complete replacement by colourless intergrowths of catapleite and a brownish mineral similar to pectolite. In the coarser varieties, the eudialyte may appear to have been a little crushed (eg: AM165).

There are two separate feldspars, albite ($\text{Ab}_{97}\text{Or}_3$) and microcline ($\text{Or}_{96}\text{Ab}_4$), both of which are present as Albite twinned laths (c. 1-2mm). The albite has higher birefringence, reaching 1st order whites and yellows,

whereas the microcline has subdued grey birefringence and less brightly defined Albite twins. Distinction between the two feldspars is a simple task in the somewhat thicker probe sections.

Isotropic sodalite and lesser amounts of faintly cross-hatch twinned analcite are often present in varying amounts, sometimes after nepheline. Occasionally, the lujavrites contain excellent evidence of autobrecciation. In one sample (AM155a), angular and abruptly terminated fragments of dark lujavrite act as physical obstacles to flow of the host, which is also dark lujavrite.

2.8.C. White Lujavrite

Essentially richer in felsic minerals, this variety bears now prominent mafic needles and prisms of densely coloured aegirine. Nepheline euhedra with aegirine microclites and tiny twinned albite laths may be seen in hand specimen with the aid of a hand lens. Eudialyte is usually recognisable by its rose-pink colour and is now interstitial or poikilitic (Plate 10).

In thin section the dominance of feldspars and euhedral nephelines is instantly apparent. The feldspars, although now composed of near end-member compositions, appear to have crystallised as one feldspar in many of the samples of white lujavrite, and are now very coarse patch perthites (as used by Parsons 1978) which may indicate feldspar-fluid interactions at temperatures below 400°C. The areas of microcline are more common towards the centres of these crystals, and separate microcline and albite can both be found in the same slide. Perhaps more striking is the subtle change in habit of the aegirines, particularly in samples from the west of SM6. The pyroxenes are now sub-ophitic to the feldspars and have grown relatively late, such that the flow structure delineated by the feldspars (c. 1 x 3 x 0.1mm) warping around nepheline euhedra (2-3mm) is entirely uninterrupted and was clearly present to a large extent, before growth of many of the pyroxenes. Aegirine is also present as prismatic microlites

scattered throughout the felsic minerals. Eudialyte, whether cream or pink coloured, may form perhaps 5 % of the rock (eg: AM157) and is sometimes altered to dark coloured minerals along its cleavage (eg: ?zirconite)^{see Vlasov et al 1966}. Amphibole is locally common (x=pale green y=greenish blue z=greyish blue) though nowhere forms more than about 5 % of the mode. This amphibole is arfvedsonitic yet may contain up to 7 wt% MgO.

2.8.D. Green Lujavrite

This variety of lujavrite is severely limited in outcrop to segregations and veins up to about 1 metre or so wide and is altogether uncommon. Nevertheless, it is a distinctive fissile green rock extremely reminiscent of green lujavrite from the Ilímaussaq Intrusion (Ferguson 1964, 1970). It is composed almost entirely of green aegirine needles, with locally common pinkish nepheline euhedra and red eudialyte.

In thin section, the aegirine needles (c. 0.1 x 2-3mm) are pleochroic in greens and yellowish greens and are very strongly aligned. The nepheline euhedra (c. 1mm) are often extensively replaced by reddish natrolite, and may be locally common, with elongated stringers of a dozen or so crystals. Microcline feldspar is present in small interstitial areas along with small amounts of albite. Eudialyte does not appear to be present, but appears to have been totally replaced by reddish brown rather amorphous-looking material and micaceous aggregates (AM152).

2.8.E. General

Representative analyses of the lujavrites are tabulated in Chapter 5 (Table (5) 1). In addition to the major phases mentioned (Aeg, Alb, Mic, Ne, Eud) the lujavrites contain several less common minerals, of which perhaps the most frequently encountered are pectolite, manganoan-pectolite, pyrochlore and a whole host of alteration products after eudialyte, such as catapleite. Many of

these are dealt with in Chapter 4 (Mineralogy).

Geochemically, the lujavrites are unusually enriched in "residual" elements, and in particular, Zr, Nb, Ce, Rb, La, Y and Th. In this, they are very similar to lujavrites described from other agpaitic alkaline centres (see Table (5) 1). However, one striking difference between the lujavrites at Motzfeldt and their counterparts at Ilímaussaq, is the paucity of amphibole at Motzfeldt, whose role instead seems to have been adopted by aegirine.

2.9. Alkali Gabbro Dyke

2.9.A. General

A large vertical dyke of alkali gabbro (c. 200m wide) trending ENE cuts SM5 north of the Flink's Dal fault and units SM4 and HY to the south, placing sinistral movement on this fault at a little under 4km. The dyke is headed in the south, where it appears to narrow upwards. A continuation of the same dyke cuts units SM1 and SM3 in northeast Motzfeldt, where it may again be headed. The dyke is at its widest in Central Motzfeldt, where it weathers symmetrically about a 15m core of possibly unrelated phonolitic trachyte.

Some facies of the alkali gabbro are porphyritic, with phenocrysts and blocks of plagioclase to 10 or even 25cm in length. These are most abundant towards the south wall of the dyke. Each euhedral to rounded block of plagioclase is often encrusted with small granular opaques and olivines. In thin section, quenched elongate olivines (Fo_{63}) and small dendritic clinopyroxenes (salite) are found within cracks in some of the blocks (eg: AM113). South of the Flink's Dal fault, small pale blocks xenolithic nepheline syenite (c. 5-10cm scale) become quite common in the upper part of the dyke and are petrographically very similar to the surrounding host syenite.

2.9.B. Petrography

The alkali gabbro is a dark weathering rock. In

hand specimen, brownish green or white plagioclase feldspars appear to form the bulk of the mode with small granular olivines and sometimes notable copper coloured biotite. In thin section, the plagioclase crystals are strongly zoned from cores of labradorite to rims of oligoclase, which are themselves often mantled by rather interstitial alkali feldspar. Pale green olivine euhedra and often well formed Fe-Ti oxides are both plentiful and frequently rimmed by dark red-pale brown biotite. Fairly large areas of sub-ophitic lilac coloured clinopyroxene (salite) are common throughout. Apatite is common both as stubby prisms (2-5mm) and as smaller needle-like crystals (to 10mm). Interstitial nepheline is present in rather small amounts (<1 % mode).

The chilled marginal rocks are doleritic and sometimes quite fine-grained. Where SM5 has suffered rheomorphism, it is perhaps to be expected that the gabbro does not become very fine-grained. The clinopyroxene in these rocks tends to be elongated (// to the c-axis), and red biotite is always present, as is alkali feldspar, in varying amounts. Occasionally, the doleritic facies contain blocky plagioclase (c. 5mm) which seems to be xenocrystic in origin. The latter are overgrown by further plagioclase, which often terminates the well defined lamellar twinning of the original crystal (eg: 58017). Occasionally, there is an almost abrupt zonation to alkali feldspar which may be intergrown on a fine scale with nepheline (58017).

2.10. Satellitic syenites

Two separate areas of syenite predating the major units of the Motzfeldt Centre are found to the east and northeast of Motzfeldt SØ. These are called the East Motzfeldt and North Motzfeldt Centres and have prefixes EM and NM respectively (Emeleus and Harry 1970). Both EM and NM contain recognisable xenoliths of breccias, lavas and porphyritic lavas which have presumably been derived from the supracrustal Eriksfjord Formation.

2.10.A. Unit EM: East Motzfeldt Syenite

(a) Syenite

Covering about 10 km², this intrusion has neither been examined nor sampled in great detail. The typical syenite consists of rectangular perthitic alkali feldspar (c. 10 x 3 x 5mm) with interstitial albite and alkali amphibole. The amphibole is pleochroic in shades of brown and often poikilitic, enclosing small plates of albite (c. 0.1mm) and less common original K-rich feldspar (c. 0.1mm). Nepheline appears to be totally absent, although several irregular areas of apatite may bear a close resemblance at first sight. Where the amphibole becomes pleochroic in shades of blue, quartz appears in the norms at about 3-5 %. Occasionally, the original mafic minerals (?amphibole) may be replaced by a mosaic of aegirine, red biotite and blebby Fe-Ti oxides.

(b) Poikilitic microsyenite

Forming a sill-like body, this syenite occupies about 1-2km² in the west of EM. Geochemically, this rock is peralkaline. A fine-grained groundmass of alkali feldspar is characterised by irregular or semi-regular areas (c. 3-5 mm) of poikilitic amphibole (pleochroic from brownish green to blue green) and roughly equal proportions of similarly disposed reddish brown-dense brown aenigmatite. These mafic minerals comprise about 20-35 % of the mode. One or two phenocrysts of poorly exsolved alkali feldspar (c. 0.5-1.5 mm) are almost always present and have resorbed or recrystallised margins. No quartz or nepheline has been observed by the author.

2.10.B. Units NM: North Motzfeldt Syenites

Situated near the northeast margin of the Motzfeldt Centre, an early outer unit, NM1, is more or less cored out by a younger and more nepheline-rich unit NM2. Both of the syenites are fairly rich in clinopyroxene and are rather basic in appearance. Mapping shows that NM2 must be truncated by unit SM1 of the Motzfeldt Centre.

(a) Unit NM1. (augite syenite)

This rather equigranular syenite bears blocky perthites and small amounts of interstitial nepheline (< 5 % mode) which is often altered. Frequent pale apple green clinopyroxene (ferrosalite) is rimmed by olive green-chestnut brown amphibole, which is subhedral and zoned to bluish green rims. Fe-Ti oxides and apatite are common in the somewhat localised mafic areas. Interstitial albite is quite common and also occurs along feldspar grain boundaries.

(b) Unit NM2. (nepheline syenite)

In the field, this unit is notable for its variation in grain size, often bearing patches of coarse-grained material in a finer grained matrix of the same composition (Emeleus and Harry 1970). Feldspars up to 5cm in length may be developed in the coarser-grained areas. A prominent hill of dark brown weathering rocks occurs near to the centre of these pale grey syenites. These dark rocks are xenoliths derived from the Eriksfjord Formation and include breccias, porphyries and lavas.

In thin section, green clinopyroxene is more prominent than in NM1 though is rimmed by a similarly coloured amphibole. Nepheline occurs in the interstices and as discrete anhedral areas, forming about 10 % of the mode. Rather dark green pleochroic clinopyroxene (aegirine-augite) is a common interstitial phase, along with analcite and some natrolite. Needle-like apatites are locally common.

2.11. Gardar supracrustal rocks: Eriksfjord Formation

2.11.A. General

Terrestrial sediments and volcanic rocks directly overlying the granitic Ketilidian basement, are found at several localities around the Igaliko Complex in general, and around the Motzfeldt Centre in particular. In addition, large masses are preserved as rafts within the Motzfeldt syenites. These rocks form the eastward extension of the Eriksfjord Formation, a known sequence of about 3500m of

Figure.2,2. Summary of supracrustal rocks at localities* adjacent to the Motzfeldt Centre (data from Emeleus and Harry 1970).

<u>Thickness (m)</u>	<u>Rock type</u>	<u>Notes.</u>
A* 1510m above Qorqup qaai. Dip 5°N		
10	Basaltic sheets	Thin. Vesicles & brecciated tops and bases.
	Volcanic breccia	Layered. Angular quartzite & rounded basic fragments (3-5cm max.).
30	Agglomerate	Coarse, fines upwards with quartzite & basic fragments to 30cm then 1cm.
15	Quartzite	
4	Basalt	Thin ledge.
80	Quartzite (basal)	Pink & grey, bedded.
<hr/> 140m		
B* 1530m near Iviangequtit tasiat. Dip 15° SW		
80	Basalt, agglomerates and quartzites.	Thin quartzites, coarse agglomerates (to 20cm Δ's).
100	Quartzite	Grey & pink with two 5m basalt sheets (mid & top)
10	Mudstone	Ripple marks, sun cracks.
3-10	Basal quartzite	Grey
<hr/> 200m		
C* 1600m NE of Motzfeldt SØ. Dip 15° W		
20	Basalt flows	Aphyric, green/grey.
60	Agglomerate	Coarse, fragments of basalt & quartzite to 20cm.
125	Tuffs	Flinty, grey, bedded (1-2cm)
400	Quartzite	Pale grey, ripple marks & false bedding.
20	Basal quartzite	Massive red/grey, grades into the above.
<hr/> 605m		

*localities A, B and C are located on key map (fig. 1,2: see page 7).

Proterozoic supracrustal rocks which occupy much of the ground between Tunugdliarfik and Sermilik fjords (Poulsen 1964; J.Larsen 1974, 1977). They probably accumulated shortly before 1310 ma, over a short period of time, since no major unconformities exist which would indicate substantial erosion of the sequence or a change in tectonic regime. The lower 2300m of the formation is composed largely of uniform continental sandstones, a few conglomerates, alkaline ultramafic and carbonatitic volcanics, basalt lavas and sills (Poulsen 1964; Stewart 1964, 1970). The upper 750-1300m of the formation, the Ilímaussaq Volcanic Member (Larsen 1974, 1977), is almost entirely composed of lavas. These lavas comprise a series of basalts, hawaiites, trachybasalts and trachyandesites, with subordinate trachytes and phonolites.

The location of three main successions around the Motzfeldt Centre is given in figure 1,2 and these are summarised ("A", "B" and "C") in figure 2,2. Despite their variability, it is just about possible to characterise these sequences in the following manner; (i) A basal sequence of sediments, often with quartzites and a few thin basalt flows; (ii) Tuffs and agglomerates. In addition, lava flows tend to become more numerous upwards. A thin succession from about 1500m near Qôrqup qáqai (A in figure 2,2) shows horizontally bedded sediments, volcanoclastics and thin basalt flows, directly overlying the Julianehåb Granite. These are truncated a few hundred metres to the north by unit SM4 of the Motzfeldt Centre. Within the syenites, large masses of vesicular basalt show flow structures which dip steeply to the north. Tracing these lavas further into the syenites, it becomes apparent that huge masses have subsided and broken up in the syenites. This can be seen rather nicely in cliffs about 2km to the north of the original succession and is illustrated in figure 2,1.

Thus, large areas of xenolithic supracrustal material exist as raft-like bodies both north and south of the Flink's Dal fault in Central Motzfeldt and in units SM2, SM5, EM and NM2. In detail, the edges of the rafts are often less precise than the map might suggest (Map 1), with the

proportions of included material to host syenite diminishing to a negligible amount often over several tens of metres. Field mapping of internal variations within these rafts proved to be impossible, especially in the time available. Their characteristic preservation is in a frost shattered state, where they have weathered largely in-situ. The collection of fresh material was limited to relatively few sites and for this reason, the various types described below, do not necessarily refer to mappable units but serve as an indication to the variety and predominant ^{type} of xenolithic material present.

2.11.B. Agglomerates

Small amounts of recognisable coarse agglomerate occur near to the base of the major raft north of the Flink's Dal fault in Central Motzfeldt. About 1km north-west of the ring dyke (SM5*) this consists of angular to rounded fragments on a 10cm scale, closely packed into a fine-grained chloritised and carbonated matrix. Another exposure, in a stream at the eastward limit of SM5*, is of toughened agglomerate. In thin section (AM62) this is composed of angular fragments of altered basalt, trachyte and medium-grained feldspathic rock (syenitic) bearing pseudomorphs after nepheline. The heavily altered and often streaky matrix, contains a little fresh nepheline and small perthitic alkali feldspars in otherwise rather amorphous masses of pale green chlorite, brownish calcite and granular opaques.

2.11.C. (?) Sediments

Based on their high Al-contents, mafic, fine-grained and bedded nature, these rocks give the impression of an originally sedimentary origin. In thin section, the rock is roughly equigranular, with about 30 % of dull brown-green biotite and small granular or poorly formed alkali feldspar which is colourless and untwinned. A few large relic feldspars may be totally recrystallised into aggregates of smaller crystals, whose original ghostly outlines can still be discerned. Very dark varieties in the

west, near Akuliaruseq, occasionally contain (eg: AM21) small garnets ($\text{Alm}_{72}\text{Spes}_{17}\text{Pyr}_9\text{Gros}_2$) in a fine-grained rock composed of similar biotite and alkali feldspar with a few altered stubby apatite crystals. The latter outcrops are distinctly bedded and were initially thought by the author to be lavas, but their precise origin remains in doubt. Further work on the origin of the garnets could prove useful in this respect. Occasionally, otherwise similar samples contain vague relic fragments of basaltic rocks (eg: AM57) which might suggest a volcanoclastic origin.

2.11.D. Aphyric lavas

(a) Basalts and basic lavas

Quite fresh basalts of possible alkali affinities are found at about 1500m just to the southwest of, and abutting the Motzfeldt Centre. These are aphyric and composed of basaltic plagioclase with sub-ophitic lilac clinopyroxene (?salite) as the mafic mineral. Slight alteration has taken the form of a little pale green amphibole around some of the pyroxenes, and some sericitisation of the plagioclase. Opaques and apatite are quite common but no olivine is present. Geochemically, these conform in almost every detail to the lowest part of the lava sequence examined by Larsen (1977), the Ilímaussaq Volcanic Member (see Chapter 5).

Within unit SM4, the most recognisable basaltic rocks come from the agglomerates, where the plagioclase texture is still evident. One or two small rafts from the Flink's Dal area are of dense, fine-grained hornfelses with abundant green clinopyroxene, small dark green amphibole, alkali feldspar and a few apatites. Occasionally, the outlines of original mafic minerals are replaced by concentrically zoned clusters of mafic and opaque minerals. The original composition of these rather small (c. 100m long) rafts, must have been very basic.

Altered rocks of definite basaltic parentage are rare inside the Motzfeldt Centre. Several areas which were thought in the field to be basaltic, on the basis of their

colour index, density and grain size, were apparently much more differentiated in composition, since they may contain relic alkali feldspar phenocrysts and pseudomorphs after nepheline phenocrysts.

(b) Trachyte and trachyphonolite

Generally a dark weathering rock with a rather flinty fracture, these lavas may contain one or two small phenocrysts, but are for the most part aphyric. The types described here, come from the lower parts of the large raft referred to previously, in the western part of Central Motzfeldt, near to SM5*. In thin section, fine-grained lath-like alkali feldspar shows two preferred orientations at right angles to each other. With higher magnification it is possible to identify many tiny granular crystals of green amphibole, green clinopyroxene and opaque minerals, "floating" in a sea of colourless felsic minerals. A few small clusters of granular opaques may represent the original positions of microphenocrysts of mafic minerals (c. 0.2-0.3mm).

2.11.E. Porphyritic lavas

Porphyritic lavas are almost certainly the most commonly encountered type of xenolith, both within the larger rafts and the smaller scale inclusions in the syenites. Many of the feldspar phenocrysts are relics, quite often recrystallised and altered, but in some of the inclusions, the feldspars appear quite fresh and may have grown after their incorporation into the syenites.

(a) Trachyandesite

Typically a rather mafic rock composed mainly of alkali feldspar and mafic minerals such as biotite or amphibole, there are usually several larger feldspar phenocrysts in various states of preservation. The latter are often rather spikey or even rhombic in outline and can be up to about 3cm in length. In thin section, they are often very clouded and sometimes largely recrystallised, being replaced by aggregates of small felsic minerals

and having rather poorly defined margins. Occasionally, relic plagioclase twinning can be seen in one or two of the phenocrysts (eg: AM18). Where this variety of lava is found near Akuliaruseq, groundmass feldspar is clearly flow aligned around the felsic phenocrysts, which do not include nepheline. Denser clots of amphibole, biotite, chlorite and opaque minerals are presumably after the original mafic minerals of the lava (eg: AM21). Small amounts of calcite are also quite common in these mafic patches. The proportion of feldspar phenocrysts to groundmass is usually about 10-15 % and the rhombic outline to some of the feldspars, coupled with the more mafic nature of the rock, bear certain similarities to trachyandesite lavas described by Larsen (1977) from the Narssaq peninsula.

In terms of bulk chemical composition, many of the small rounded inclusion, so typical of unit SM4 in Central Motzfeldt, north of the Flink's Dal fault, fall into this category, although their original nature is difficult to ascertain. For example, in some of the small inclusions, elongate and perfectly fresh alkali feldspar (Or_{75+}) may well have grown metasomatically.

(b) Phonolite

This appears to be a common category of lavas in the Motzfeldt Centre, existing both north and south of the Flink's Dal fault. It differs from the above category of lavas in that nepheline phenocrysts are necessarily present. The rock is usually dark weathering and fine to medium-grained.

In thin section, the alkali feldspar phenocrysts are often totally clouded and altered (eg: AM24) and are sometimes perthitic, with Carlsbad twins (AM37b). Less commonly, relic anorthoclase with a relatively low 2V, can be found in partly recrystallised and patchily exsolved phenocrysts (eg: AM70a). Nepheline may still exist as a few euhedra (typically c. 1mm) but is more usually pseudomorphed by pale brownish coloured clay-like minerals. Smaller euhedra of grey clinopyroxene (?salite) may be preserved within green amphibole rims (AM70) but

are more frequently totally replaced by concentric aggregates of green-yellow biotites, green amphiboles and opaque minerals. The groundmass typically consists of alkali feldspar, biotite, amphibole and somewhat altered apatite. The norms suggest that further nepheline is present in the groundmass, since there may be insufficient nepheline in the form of phenocrysts to satisfy the amounts predicted (c. 3-10 %). The olivine predicted in the norms has not been observed.

2.12. Volcanic (Ultrabasic/Carbonated) Breccia

2.12.A. General

An ochre weathering plug of volcanic breccia cuts SM4 just north of the lujavrites in Central Motzfeldt. This measures about 100m by 40m and causes hardening and recrystallisation of the syenites for about 10m away from this more or less vertical body. Angular to rounded fragments from a 1mm scale to around 25cm stand proud of a dark grey fine-grained matrix. The matrix contains several clots of botryoidal iron oxides (c. 5-10mm) and occasional rounded books of dark mica, and is rich in carbonate since it "fizzes" with acid. A slight streaming of the smaller fragments, steeply up to the west, is in agreement with the oval plan of the outcrop, although some of this is obscured by scree and moraine deposits. The readily identifiable fragments include: medium-grained foyaite, mafic foyaite, fine-grained syenite with prominently bent feldspar, microsyenite, medium-grained gneiss and various dark fine-grained trachytic rocks.

The plug appears to have been emplaced with considerable force and at a rather high temperature, bearing in mind the plastic deformation shown by some of the fragments and the extent of the recrystallised zone in the surrounding syenite. Fragments incorporated early in the upward passage of the plug material are generally mafic, rounded and plastically deformed, whereas those more locally derived are angular with signs of brittle failure. The incorporation of much trachytic material might at first suggest emplacement postdating the regional

Mid Gardar dyke swarm. However, the trachytic material could have been derived from xenolithic supracrustal lavas. Intersection of the vertical plane of the plug with sub-horizontal trachyte lavas would favour the varied abundance, precisely as observed. The absence of any lujavrite fragments, despite their proximity (the plug is topographically about one or two hundred metres below the lujavrites) would tend to support a high level of formation of the lujavrites.

2.12.B. Petrography

The plug has suffered extensive carbonate metasomatism and for this reason, most of the phenocrysts are identifiable as pseudomorphs only. Similarly carbonated and indeed very similar rock types have been described by Stewart (1964) from the Qagssiarssuk area, some 25km to the west of the Motzfeldt Centre. Additional carbonate-rich plugs cut rocks in northeast Motzfeldt (Emeleus and Harry 1970), where they are associated with basic material, and a carbonatitic plug also cuts the North Qôroq Centre (Chambers 1976).

The included fragments of rounded, resorbed, shattered and angular fragments, occur on all scales and fall into the following categories as a result of a fairly rapid examination of just three thin sections.

(a) Fine-grained feldspathic basalt, showing areas of distinct recrystallisation. Only the texture is properly preserved, with original mafic minerals totally absent, but possibly partly represented by aggregates of carbonate, opaques and some chlorite.

(b) Medium-grained dolerite. Some of the sub-hedral opaques may be relics from the original rock. Occasionally preserved twinning in the relic plagioclase suggests a composition close to oligoclase.

(c) Several small aggregates of alkali feldspar, individually often rounded and crushed or fractured. Any original mafic minerals seem to have been swamped by the abundant carbonates of the host matrix.

(d) One or two Carlsbad twinned rounded xenocrysts of alkali feldspar are still discernible, with a thin

mantle of granular opaques.

(e) A multitude of crystalline outlines in the fine-grained matrix are of imprecisely known origin. Many appear to be feldspathic, with basaltic-looking textures, and many are composed of abundant small lath-like (?) alkali feldspar, presumably of more trachytic origin. It is not clear whether or not any of this fine-grained crystalline material is from the original matrix of the plug.

(f) Tiny elongate laths of colourless minerals, now replaced by carbonates, are often well developed as abundant tangentially aligned sheaves surrounding the botryoidal opaques. These are very similar to relic melilite described by Stewart (1964), and to this mineral, they are tentatively ascribed.

(g) Pale orange-dark orange mica is locally common as small platelets and their sometimes rounded outline may suggest a xenolithic origin.

(h) Several areas of chlorite/calcite/opaque aggregates have almost euhedral outlines and are thus after mafic minerals (to about 5mm) of uncertain parentage.

CHAPTER THREE

STRUCTURE

3.1. Introduction

This chapter describes the geological structure of the Motzfeldt Centre and is devoted primarily to the igneous events which occurred at and around 1310 ma. This will hopefully act as a background for the following chapters and sections by clarifying the disposition of the various units and rock types.

Firstly, the igneous structure of the centre and its Early Gardar setting are described in some detail. In later sections, likely origins and modes of formation of these igneous structures are considered in the light of quantitative and semi-qualitative mathematical treatment. Lastly, geological structures postdating the formation of the Motzfeldt Centre and constituting events in the Mid and Late Gardar periods are considered.

3.2. The relative age of the Motzfeldt Centre

The strike of several semi-circular units in the North Qôroq Centre are truncated by syenite now thought to belong to unit SM4 of the Motzfeldt Centre. This syenite was mapped by Chambers as ?SN3 (1976) who recognised its similarities to syenites from the Motzfeldt Centre. As a result of further work, its similarity to almost identical nepheline syenite of SM4, some 2km to the east on the opposite side of Qôroq fjord, has been substantiated. Thus, the North Qôroq Centre predates formation of the Motzfeldt Centre. This revision of the order of emplacement from that proposed by Emeleus and Harry (1970) is in agreement with the range of uncertainty associated with the Rb/Sr ages obtained by Blaxland et al (1978: N.Qôroq = 1295±61 ma, Motzfeldt = 1310±31 ma).

3.3. General Comments

The Motzfeldt Centre is in many ways similar to other igneous centres, both in the Igaliko Complex and

elsewhere in the Gardar province. However, perhaps the two most obvious features which set Motzfeldt apart from almost all other centres are, firstly, the incorporation of large quantities of lavas as raft-like xenoliths and secondly, the presence of a late stage body of lujavrites. Incorporation of country rock xenoliths is not particularly uncommon. Rafts of gneiss are, for example, found in the Kûngnât Centre (Upton 1960) where they are exposed in the Roverborg cliff face. However, perhaps nowhere else in the Gardar province is there such a clear suggestion of a genetic link between intrusion of an igneous centre, and the semi-contemporaneous extrusion of surface lavas (see Chapter 5).

Lujavrites are also found in the Ilímaussaq Intrusion, situated about 40km to the southwest of Igaliko and have received considerable attention (Ussing 1912; Sørensen 1962, 1966; Sørensen et al 1969; Ferguson 1964, 1970; Engell 1973: and many others). The relatively high level disposition of the lujavrites beneath large masses of lavas, both at Motzfeldt and at their only other known occurrence in the Gardar, at Ilímaussaq, may be for similar reasons.

3.4. Supracrustal xenoliths

A zone of dark weathering xenoliths occurs in an arcuate belt nearly 5km long in Central Motzfeldt, to the north of the Flink's Dal fault and as several kilometre scale rafts to the south. The derivation of numerous smaller xenoliths, which are often rounded in outline and feldspar-porphyrific, is almost certainly from the break up of similar lavas to those preserved as rafts.

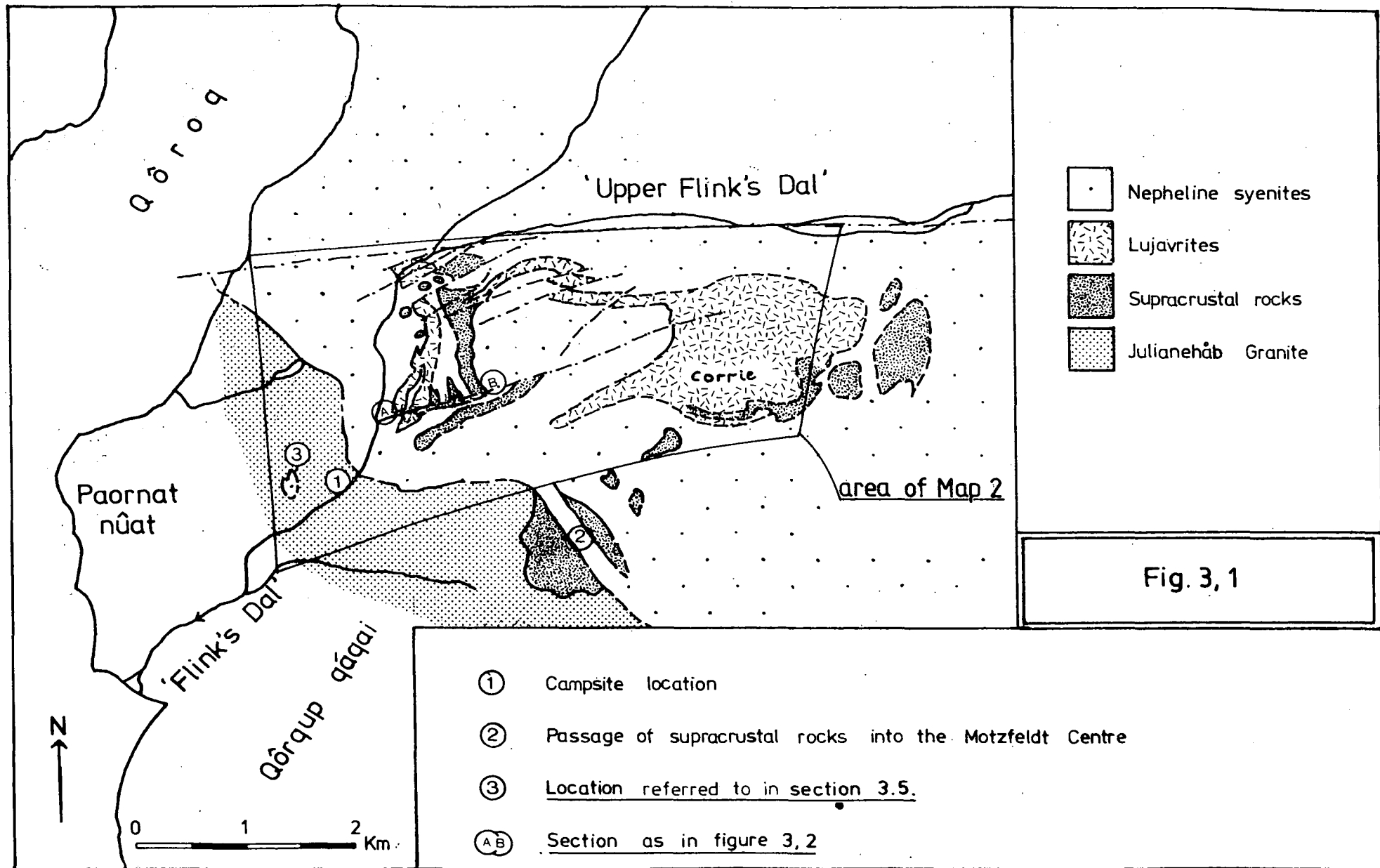
Above the slopes of Qôrqup qâqai, near to a 1410m peak, several raft-like inclusions, just within the Motzfeldt Centre, can be traced from comparable bedded lavas in the supracrustal succession at its margin (Emeleus and Harry 1970). These supracrustal rocks form part of the Eriksfjord Formation, and their unconformable base upon the Julianehåb Granite, is at about 14-1500m in the south of Central Motzfeldt. Further sequences of sediments and

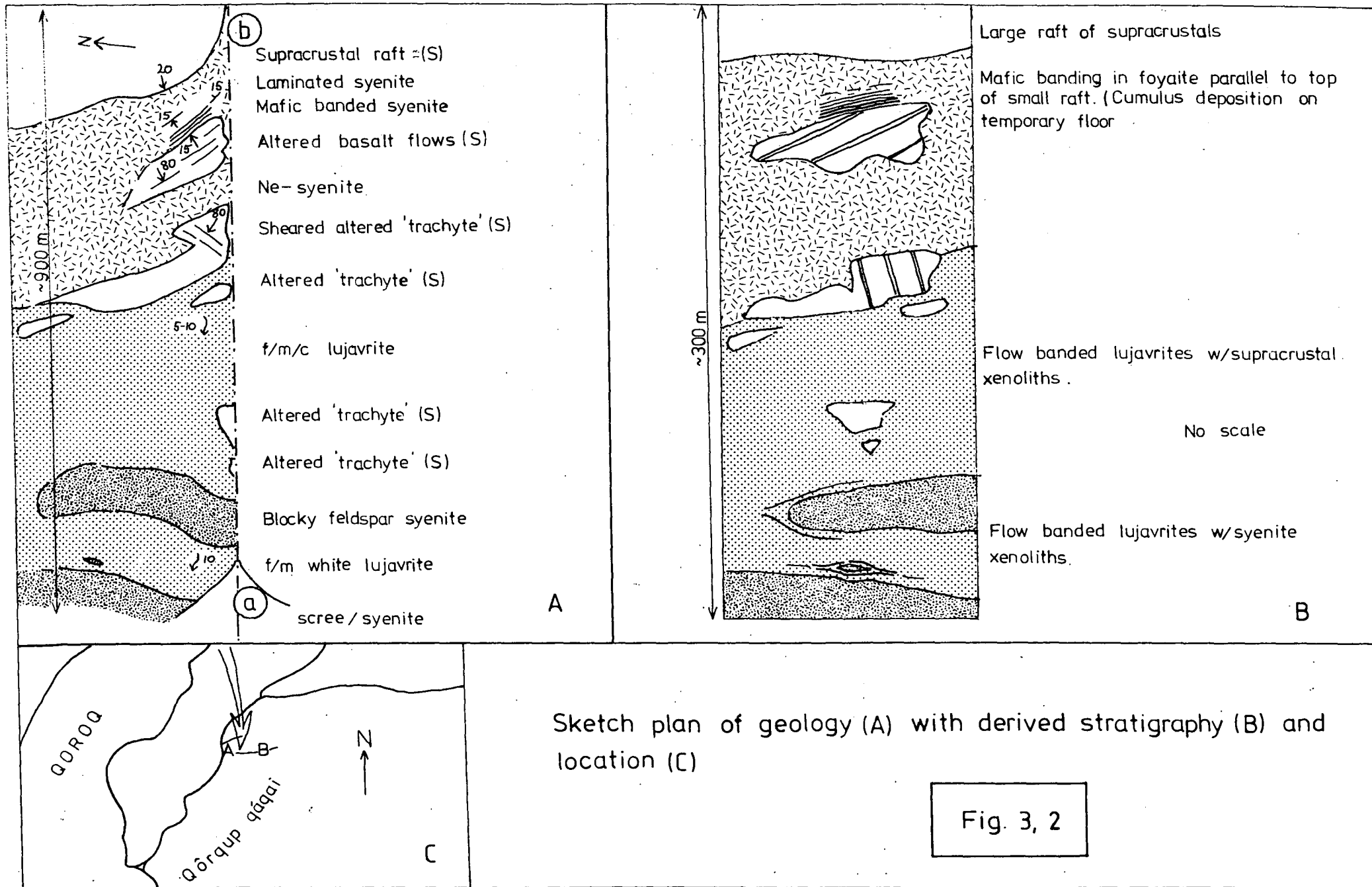
lavas are found around the eastern parts of the centre, although the various sequences have not been correlated. They appear at varying geographical levels and are often inclined at low to moderate angles of dip (usually 15°) in towards the centre. Comparable lavas and sediments of the Eriksfjord Formation are seen to downwarp considerably near to the southwest margin of the Igdlarfigssalik Centre (Emeleus and Harry 1970).

3.5. Structures in Central Motzfeldt south of the Flink's Dal fault

Steep cliff sides (c. 1000m) at the northern end of Flink's Dal, afford a fine three dimensional view of a number of large xenolithic rafts, and reveal their influence on the surrounding syenites. A general illustration has been given in chapter 2 (fig. 2,1). Examination of the igneous stratigraphy in this particular area reveals several processes which must have occurred within the Motzfeldt magma chambers at around 1310 ma.

Figure 3,1 shows the disposition of the supracrustal rocks around Flink's Dal. In several places the geology has been complicated by the late arrival of the lujavrites, which have cut back through the earlier syenites and xenoliths. However, the salient points are still quite clear. A large raft of lavas, at least 100m thick, can be traced around the hillside (near B in fig. 3,1) for almost 2km and is illustrated in Plate 7. This raft dips radially to the west and northwest from B (fig. 3,1) at between 15° and 25° and is completely engulfed in nepheline syenite. The raft has broken up into smaller blocks, shown rather diagrammatically in figure 3,1, which rest at unpredictable angles. An enlargement of the gulley (A-B in fig. 3,1) shows (fig. 3,2) the typically disrupted nature of these smaller included blocks. The upper surface to a black weathering raft of lavas, dips at a shallow angle (c. 15° NW) into the hillside, in contrast to the very steep attitude (c. 80°) of 1-10m flows within the block. The syenite immediately above the raft contains platy feldspar in a series of mafic bands, which reflect the underlying





topography of the raft. In contrast to these layered syenites, and as described previously (section 2.5.B.) the syenite beneath the rafts is often very leucocratic and rich in nepheline, with euhedral crystals of the latter forming up to 50 % of the rock. Occasionally, thin mafic bands and feldspar lamination may be distorted beneath the rafts, as if compressed in response to its sinking upon a crystalline mush.

A coarse-grained brown syenite forms the marginal part of the Motzfeldt Centre in this area, and dips outwards at about 50-60°. This is fairly representative of the syenite contacts with country rock of the Motzfeldt Centre in general.

On the eastern slopes of Paornat nûat, in small cliffs which form the western edge of the lower Flink's Dal valley, a "blister" of syenite emerges over some 3-400m distance and some 50-70m height. Here (location 3 in figure 3,1), the "chilled" variant is a mafic micro-syenite with phenocrysts (c. 15-20 %) of tabular feldspar. The contact with the country rock gneiss is easily accessible at the top of loose scree and is very well preserved. Fairly thin mafic bands within the syenite, steepen and fade over the last 10m or so, where they pass into a 10cm wide zone of pegmatitic syenite. This in turn passes into between 1cm and 1m of leucocratic gneiss sheared parallel to the contact (c. 30°S), and then through 1-2m of recrystallised gneiss giving way to normal Julianehåb Granite within about 3m of the contact. The syenite exposed in the cliff face is strongly layered, with genuine mafic bands, graded variations of mafic minerals (including zircon) and rapid alternations of grain size. Pegmatites, more or less parallel to the other banding, form fairly continuous layers parallel to the roof. Pendants of gneiss, 20-30m long 'tongue' down into the syenite, but were not examined in detail. There appears to be no outward expression of the blister above the cliffs. This syenite bears many similarities to marginal variants of SM4 seen in one or two places elsewhere in the Motzfeldt Centre. Thus, it is thought to belong to the Motzfeldt

rather than to the South Qôroq Centre.

3.6. Structures in Central Notzfeldt north of the Flink's Dal fault

3.6.A. Xenoliths

A dark, often reddened and splintery weathering belt of inclusions occurs in a 4-5km long arc from Akuliaruseq in the west to Ivnârâ in the east (see fig. 3,3). This large, almost continuous area is composed mostly of lavas, with subordinate volcanoclastics, derived from the supracrustal Eriksfjord Formation (see section 2.11.). The overall attitude of the raft is sub-horizontal and it has been surrounded and invaded by syenite to varying degrees. An area of agglomerate occurs near the base of the raft in the west and again near to the eastward extent of the ring dyke SM5*. The majority of the raft is composed of porphyritic phonolites, porphyritic trachyandesites and sparsely phyrlic trachytic lavas. In the extreme southwest of this raft, the underlying syenite (SM4) shows increasing amounts of xenolithic material upwards, with a mixture of associated coarse and fine-grained syenites and microsyenites. In detail, the raft is not a single entity, nor is it uniformly inclined, especially at its margins.

In certain areas, flinty weathering trachytic lavas form a sharp boundary with the underlying syenites. At locality 2 in figure 3,3, the transition occurs over 1-2m, with syenite veins penetrating the trachyte and splitting off angular blocks on a 0.5m scale. Here, as at all syenite/xenolith contacts, the syenite becomes patchily pegmatitic, often visibly coinciding with three dimensional pockets and irregularities in the raft. These are again developed at locality 3 in figure 3,3, where pink syenite (SM4) abuts an area of grey weathering xenoliths.

Many smaller rafts and inclusions on all scales occur within SM4, and less frequently within the north-western part of SM5. The latter ^{xen} may have been reworked

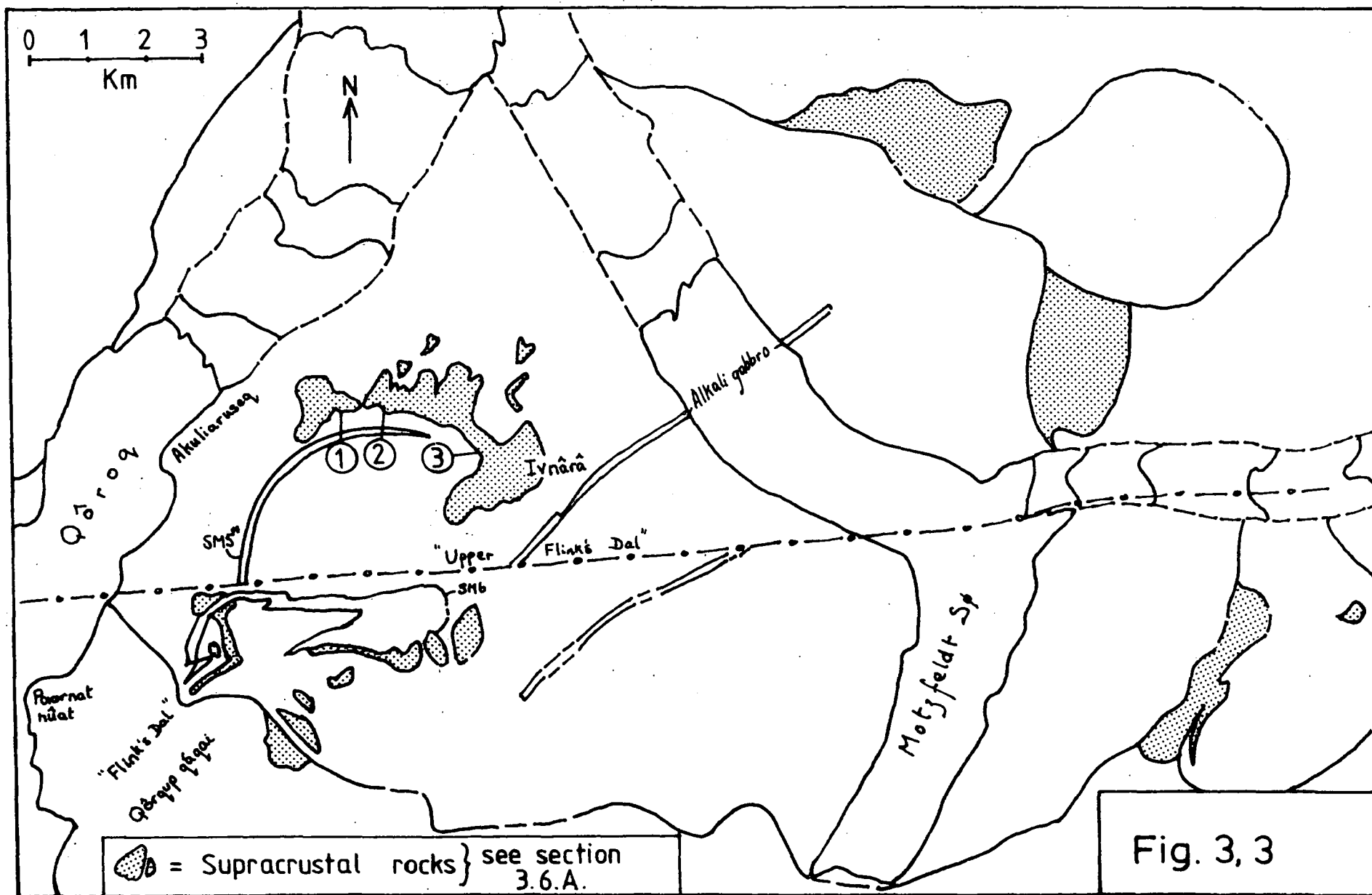


Fig. 3, 3

from within SM4.

3.6.B. Unit SM5*: Larvikite ring dyke

Forming the northwest quadrant of an arc focussed on SM5, both inner and outer contacts of this partial ring dyke appear to be very steep. The dyke causes some recrystallisation of the surrounding syenites for up to about 100m, and disappears beneath syenites and inclusions in the northeast. Here, a zone of rather intense recrystallisation probably marks its near-surface outcrop for a further 0.5km or so. Thus, since there is no reason to doubt that unit SM5 should have normally outward sloping margins, this ring dyke SM5* must intersect SM5 at depth, from which it is thought to emanate.

It is uncertain whether or not several N/S shear zones in the syenites immediately adjacent to the west of the dyke are directly associated with its emplacement. The contrast in weathering of syenites east and west of the dyke is striking, and a variation in rock types may suggest that some differential (vertical) movement has taken place. To the west of the dyke, SM4 is a laminated foyaite, whereas to the east it is coarser-grained and displays mafic banding, with a total lack of xenoliths. This could also be a result of the different levels of exposure, such that the low topography to the east of the dyke would be below the level of the xenoliths and expose deeper level syenites. Any vertical movement along the ring dyke would have to be hinged around Ivnârâ, since the major raft of supracrustal rocks crosses the projected path of the ring dyke with no measurable disturbance.

3.6.C. Alkali gabbro dyke

Striking between ENE and NE, a large vertical dyke of alkali gabbro cuts both SM5 and SM4 north of a lake at 700m in upper Flink's Dal. This dyke is about 200m wide, with coarse and fine-grained facies symmetrically disposed about a core of (?) later phonolitic trachyte. South of the Flink's Dal fault the dyke is narrower (c. 100m) and is

visibly roofed in a syenite cliff. In this portion, small syenite blocks of similar appearance to the surrounding syenite are locally very common. The upper termination of the dyke seems to be wedge-shaped and the syenite immediately above the dyke appears to have been vertically sheared or faulted, although this was not examined at first hand. The roofing of this dyke seems to behave exactly as predicted by Anderson (1942). In advance of the upper wedge-shape at the time of intrusion, must have been an area of tensile stress (Anderson 1942) which may be manifested by the small faults directly above the dyke. This can be modelled using mathematical approximations based on the Griffiths Crack Theory, wherein the advancing crack approximates to a parabola (extensively developed in Lawn and Wilshaw 1975). Any vertical variation in thickness of the dyke could be simply explained in terms of dyke emplacement into a tensional fault, whose undulose surfaces have undergone vertical displacement. The same dyke is found in northeast Motzfeldt, where it is again thinner and cuts units SM1 and SM3. It may be headed there also, since it was not found above the cliff in which it is exposed (Emeleus and Harry 1970).

Rheomorphism of coarse-grained nepheline syenite SM5, in the form of back-veining, can be seen on the north edge of the dyke about 0.5km west of the lake at 700m in upper Flink's Dal. Lobate margins of syenite and gabbro interfinger, with occasional large (c. 10cm) plagioclase xenocrysts, clearly derived from the gabbro, now surrounded by the remobilised syenite host. Samples of syenite collected at spaced intervals away from the gabbro, show progressively decreasing amounts of partial melting and recrystallisation (see section 2.7.E.).

3.7. Further structures of the syenite units

In general, each unit of syenite has steeply outward sloping contacts, whether against earlier syenite or country rock and there is little if any sign of violent emplacement. Pegmatites and veins of syenite are frequently developed at contacts and may be associated with either the older or the

younger unit, or both.

Unit SM3 is a partial ring dyke which has steep contacts. It is notably narrow in southeast Motzfeldt and consistently broader in northeast Motzfeldt, north of the Flink's Dal fault. The corresponding variations in lithologies are given in chapter 2 (section 2.4.).

The form of the lujavrites, SM6, is quite different. These occur as a sub-horizontal shelf-like mass and are probably a sort of sandwich horizon. They are a high level sill-like body within the Motzfeldt Centre and are at their thickest in a corrie illustrated in chapter 2 (fig. 2,1). Small scale structures in their flow banding suggest that they flowed away from this thick (c. 4-500m) region and cut back through the earlier syenites and xenoliths in the Flink's Dal area. In detail, they are quite irregular and may form smaller peripheral sheets or sill-like bodies. The lujavrites occur beneath large rafts of lavas, which may well have been more extensive at the time of their formation. The different varieties of lujavrite are largely the result of varying proportions and habits of the five major phases and support an initial temperature of around 850-900°C with a long cooling interval (see sections 4.5., 4.6., 6.1.B.).

Summary of igneous structures

(a) General

(i) The individual syenite units have outward sloping external contacts which may be steep, except for SM6 and SM5, the latter of which may be partly roofed by SM4.

(ii) External contacts of the syenites are invariably passive.

(iii) The lujavrites of SM6 are a high level feature, of sub-horizontal nature, formed relatively late in the history of the Motzfeldt Centre.

(iv) The partial ring dykes SM3 and SM5* have very steep contacts, probably near-vertical.

(v) Contacts of syenite/syenite, syenite/xenolith and syenite/country rock almost always display pegmatites and are frequently associated with both coarse and fine-

-grained syenites.

(b) Structures associated with the xenoliths

(i) The rafts may be large, measuring up to about 2 x 2 x 0.2 km south of Flink's Dal and perhaps 4-5 x 2 x 0.4 km in the north of Central Motzfeldt

(ii) The large rafts are sub-horizontal, becoming randomly oriented with decreasing size.

(iii) The xenoliths have sunk at least 1000m (1km) in Flink's Dal to reach their present position, and possibly much more than this in total.

(iv) Some of the rafts have acted as temporary floors above which layered syenite has accumulated.

(v) Several rafts appear to have acted as roof-zones to underlying nepheline-rich syenite.

(vi) In one or two instances, the rafts appear to have caused plastic deformation to the underlying syenite.

(vii) Syenites of variable grain size and especially pegmatites, are practically ubiquitous at every contact of syenite with a large xenolith. The obvious explanation here would be "sweating out" of volatiles (H_2O) from relatively wet xenoliths into the surrounding syenite magmas.

3.8. Qualitative interpretation

3.8.A. Mechanisms of intrusion

The most common shape of each syenite unit is based on a circular plan, with a kilometre scale radius and moderate to steeply outward sloping margins. Less common, although equally important, are the semi-circular near vertical ring dykes. It is clear from the large rafts of supracrustal rocks that large quantities of material once overlying the Motzfeldt Centre have been stoped and subsided into the underlying syenites. In this way, the creation of space for each successive intrusion probably occurred by a combination of ring fracture and block subsidence (Emeleus and Harry 1970). The amount of syenite or other rock displaced in this way is indeed voluminous, as can be seen from the overlap of each unit (see fig. 3,5).

Furthermore, this process must have been cumulative, with for example, SM1 of some 10km radius being stopped by at least three subsequent intrusions of syenite. Assuming that the minimum vertical displacement associated with each intrusion is 3km, then at least a part of SM1 must have been displaced to 9km ($= 3 \times 3\text{km}$) beneath its current exposure level.

Several mechanisms of intrusion of magma via ring dyke and ring intrusion have been investigated theoretically by Roberts (1970). Making the reasonable assumption that the intruded rocks behave initially as elastic solids which undergo brittle failure, he has shown that shear failures developed at the surface of a magma chamber can be predicted for several chamber types. One fundamental implication he derives from this, is that the form and distribution of dilational intrusions, just such as ring intrusions and certain ring dykes, may be a direct result of the generation of magma in the upper mantle. He also demonstrates that for ring dykes and ring intrusions which are .."dilational intrusions occupying shear fractures formed under conditions of reduced magma pressure.", such as volume contraction upon crystallisation then (i) if such fractures reach the surface, caldera formation might occur in association with the eruption of lava (not ignimbrite) and (ii) if such fractures intersect each other below the surface, the characteristic form of a bell jar intrusion will result.

Taken one stage deeper, Roberts has shown (1970) that the internal pressure within regions of partial melting and within discrete magma chambers, is controlled by the maximum and minimum pressures which such cavities can sustain without failure under specified boundary conditions. To a large measure, such pressures are controlled by the shape of the cavity. Important here, is that very small amounts of partial melting (eg: as little as 1 %) are required to cause tensile failure, by creating excess pressure in response to the volume expansion on melting, of even the most stable shape, that of a sphere. It could well be volume expansion on melting, for example, which is the primary mechanism whereby intrusions in the crust

are fed from a magma source in the mantle. The effect of this mechanism is further enhanced since the excess pressure required to initiate the tensile failure, is greater than that required for their continued propagation. The resulting difference in density between magma and the upper mantle would develop a positive head of hydrostatic pressure above the magma source, favouring its upward intrusion.

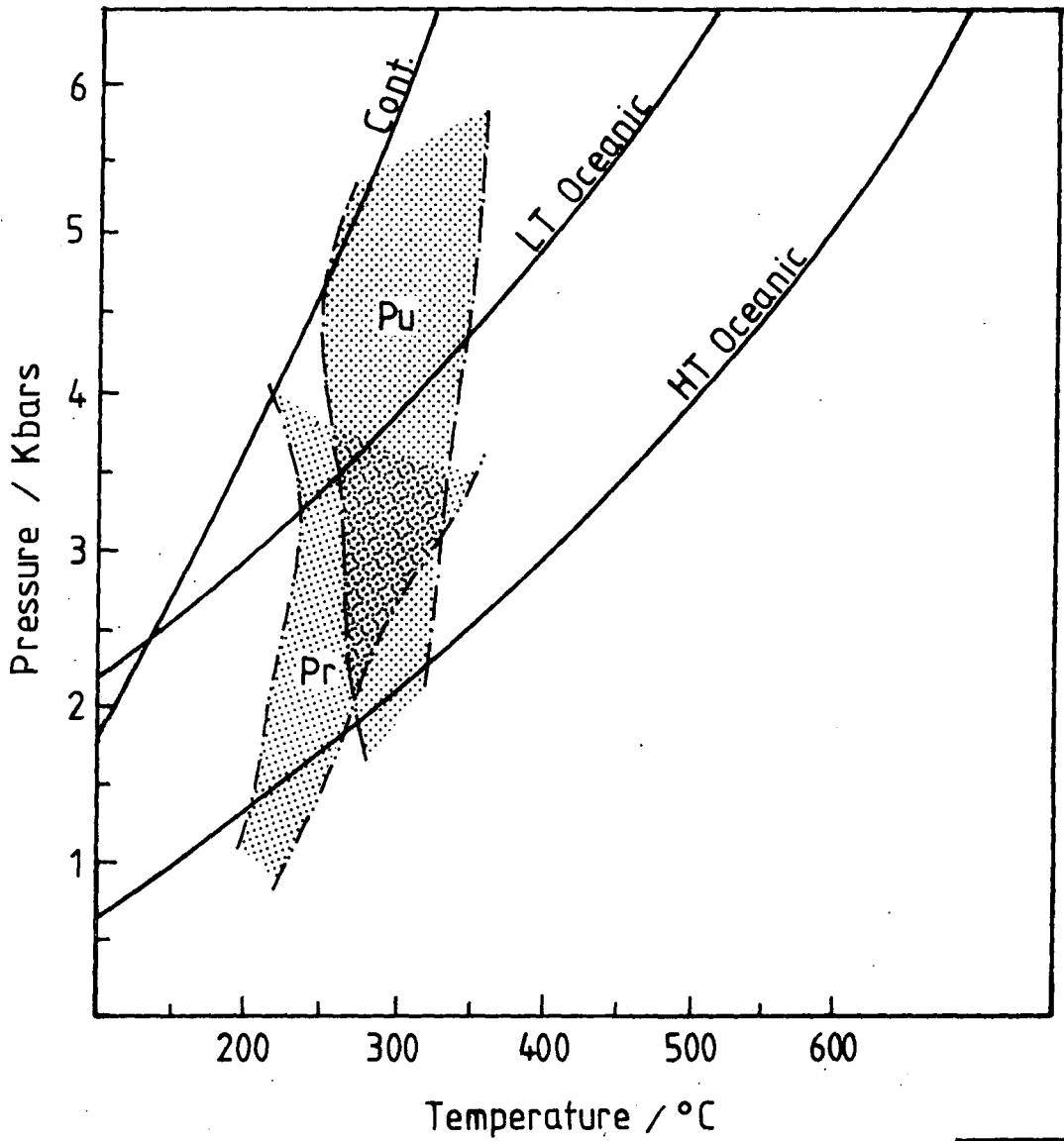
3.8.B. Exposure level

The Motzfeldt Centre is emplaced into basement gneiss, the Julianehåb Granite, and forms a steep topography which rises from sea level to over 1700m. In general, the supracrustal rocks of the Eriksfjord Formation are preserved unconformably upon the gneiss in the higher ground around the centre. Thus, sub-horizontal quartzites and lavas directly overlie Julianehåb Granite at around 1500m near the southwest of the centre (sequence A in fig. 2,2). Two fresh basalt flows from the base of the succession correlate very well with the base of the Ilímaussaq Volcanic Member (IVM) as analysed by Larsen (1977) from the Narssaq peninsula some 40km to the southwest (see section 5.8.A.). At first sight this might suggest that much of the predominantly sedimentary units of the Eriksfjord Formation, so prominent in the Igaliko area and on the Narssaq peninsula, is missing from the Motzfeldt district. At most, about 500m of quartzite and sediments are preserved around the Motzfeldt Centre, mostly on the south facing slopes of northeast Motzfeldt. However, since much of the Eriksfjord Formation has accumulated in fault-bounded troughs (eg: Berthelsen and Noe-Nygaard 1965), with some of the lavas having different sources, lateral variation is to be expected. Lateral variation occurs within the IVM along just a few kilometres of the Narssaq peninsula (Larsen 1977) and certainly there are considerable variations within the successions local to Motzfeldt. That the supracrustal rocks are preserved at all, is almost certainly due to down-faulting, possibly from superposition of the later ENE-WSW rift upon an earlier

E-W tensional regime. A general downward movement of country rock at the very edge of the Motzfeldt Centre, may also have helped to preserve the supracrustal rocks. This has been described for members of the Eriksfjord Formation adjacent to SI4 of the Igdlérfigssalik Centre, to the north and northwest of Igaliiko village (Emeleus and Harry 1970).

It is almost certain that the 3500m of the Eriksfjord Formation was once considerably thicker. Since dykes of the Mid Gardar swarm are equally numerous at different topographic (=stratigraphic) heights throughout the supracrustal pile on the Narssaq peninsula, B.G.J.Upton believes it to have been initially several kilometres thicker (pers.comm. 1980). It is thus possible that the fractionated lavas preserved within the Motzfeldt Centre represent part of a hypothetical unit forming an upward extension to the currently known Eriksfjord Formation, and whose base may be directly comparable to the base of the IVM. Within a vertical 1000m of syenite in the Flink's Dal area, the rafts total about 3-400m. When unexposed rafts and perhaps higher level though now eroded rafts, are taken into consideration, it is easy to accept an original succession of supracrustal rocks several kilometres thick. On the evidence of the currently exposed rafts, these consist mostly of lavas, and it is interesting that the IVM reported by Larsen (1977) consists mostly of lavas (c. 95 %).

From the occurrence of prehnite (pr) with pumpellyite (pu) on the Ilímaussaq (Narssaq) peninsula, Larsen deduces a clear indication of "low pressure" metamorphism (1977). However, the occurrence of pr+pu can be most constructive in support and constraint of a relatively thick lava pile. Extensive work in the zeolite, lawsonite and the lower part of the greenschist facies of metamorphism has been performed by Liou (1971), Thompson (1971) and Surdam (1973) and has been comprehensively summarised by Mueller and Saxena (1977). A diagram of the stability limits for pr and pu (fig. 3,4) compiled from Mueller and Saxena (1977, pp. 183,229) shows three possible geothermal gradients



Pu = approx stability field of pumpellyite
Pr = " " " " prehnite

Fig. 3,4

— = geothermal gradients after Mercier & Carter (1974)

LT = Low Temperature Cont. = Continental

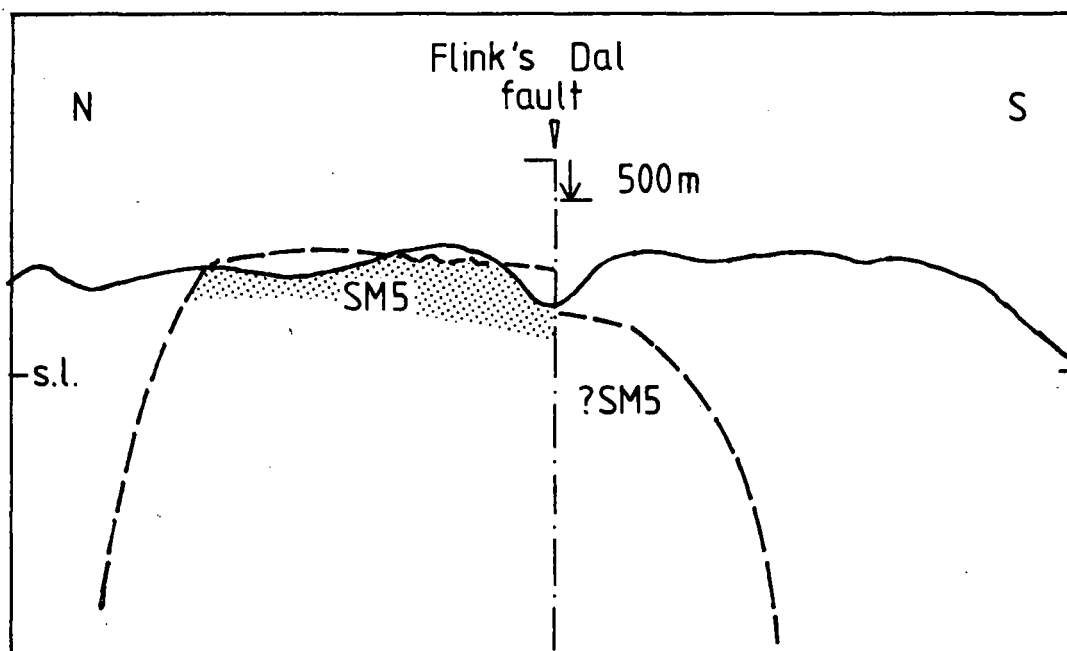
superimposed from the work of Mercier and Carter (1975). Assuming that the geothermal gradient for an active rift system would lie somewhere between the High and Low Oceanic curves, then this would suggest metamorphism of the lavas in the range 2-3 kbar, corresponding to a pile of supracrustals at least 6 and possibly 9 kilometres thick. Thus, given the correct assemblage and bearing in mind that pr and pu are sensitive to a fluid phase, the coexistence of pr+pu could actually be predicted as the product of low grade burial metamorphism. Larsen maintains that contact metamorphism with some hydrothermal activity has been the dominant process which led to alteration of the supracrustals (1977).

3.8.C. Flink's Dal fault: effects on exposure

Lateral movement along this near E/W fault is about 4km, as shown both by the displacement of the alkali gabbro dyke and the outer margins to the centre. From the outcrop of SM5 and the wide nature of the alkali gabbro north of the fault in Central Motzfeldt, vertical movement appears to have downthrown material to the south. Trying to bracket this vertical movement is difficult. Rafts exposed at similar levels are quite different across the fault, although were there any correlation it would at best be very tentative. Unit SM4 occurs both to the south and the north of the fault, making the vertical extent of this unit 1700m plus an amount equivalent to the movement on the fault. To the east of Motzfeldts SØ, unit SM3 is wide to the north of the fault and narrow to the south. This would agree with a downthrow to the south if SM3 narrows upwards. Also in northeast Motzfeldt, the alkali gabbro dyke has not been mapped above the cliff in which it occurs. This could be due to lack of exposure, since there is quite a lot of scree, or alternatively that the dyke is headed.

Returning to Central Motzfeldt, a relatively small downthrow to the south could explain the absence of SM5 south of the fault. It would appear that SM5 is partly roofed by SM4 and supracrustal material, resulting in a flat-topped and steep sided "bell jar" type of chamber.

In this way, completion of the semi-circular plan of SM5 may occur at comparatively shallow depths south of the fault (see sketch below).



3.8.D. Overlap of intrusions

By considering the overall form of each intrusive unit in the Motzfeldt Centre, it is possible to see that substantial overlap has repeatedly occurred. In this way, large amounts of progressively older syenite could have been stoped to ever deeper levels as a result of multiple intrusion. Thus, for example, SM1 may have reached depths of 15km or more below the Early Gardar landsurface prior to the intrusion of SM5. Interpolation between the High and Low Temperature Oceanic geothermal gradients derived by Mercier and Carter (1975) suggests that any material stoped to a depth of 18km and pressures of approximately 6kbar, would encounter temperatures of between 470 and 650°C (see fig. 3,4). Under these conditions, one would expect some degree of partial melting, and since nepheline syenite is a low temperature composition, this would be an ideal candidate for considerable melting.

The overlap of the successive intrusions is shown in figure 3,6 and the areas of the units, with their overlap are listed in Table (3) 1.

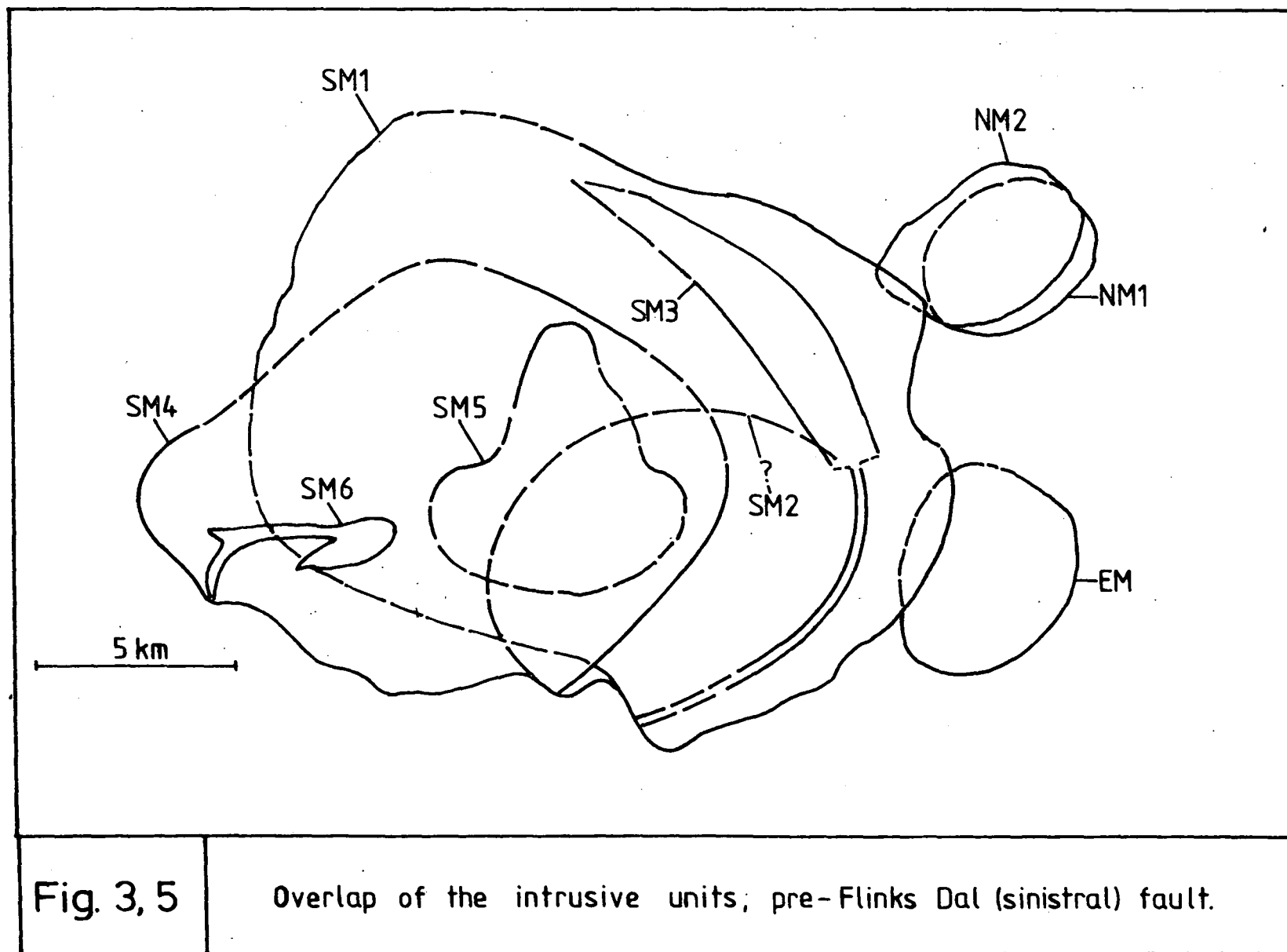


Figure 3,6 : Reconstruction c. 1310 ma.

The reconstruction summarises a number of the major features which contributed to the formation of the Motzfeldt Centre, although it is not drawn accurately to scale.

- (1) The present day topography is indicated by a thin continuous line relative to sea level (S.L.).
- (2) The presence of a thick lava pile, with fictional topography, can be compared with the minimum known* succession of supracrustal rocks (the Eriksfjord Formation) thought to correlate below the Motzfeldt succession. These* are shown by horizontal rows of dots.
- (3) Early units of ne-syenite (eg: SM1) were presumably stopped to considerable depths by virtue of the successive intrusion of overlapping units. Partial melting is sometimes apparent at the current exposure level and may have more readily occurred at greater depths, allowing possible re-working of syenitic material (eg: section 3.8.D.).
- (4) Xenoliths of lavas were actively stopped into the syenites and may themselves have been genetically related to the ne-syenites (section 5.8.).
- (5) A possible general subsidence of the centre may have lead to the downwarping of supracrustal rocks around its periphery, which although not well developed at Motzfeldt, is convincingly displayed around the Igdlarfigssalik Centre (Emeleus and Harry 1970).
- (6) The late stage mobile sandwich horizon of lujavrites (L) are indicated at their high level in the centre, beneath xenolithic lavas.

Additional minor intrusives which postdate the centre have not been indicated.

* If the base of the Motzfeldt succession correlates with the base of the Ilímaussaq Volcanic Member (Larsen 1977), (sections 3.8.B. & 5.8.), these amount to around 2.5km .

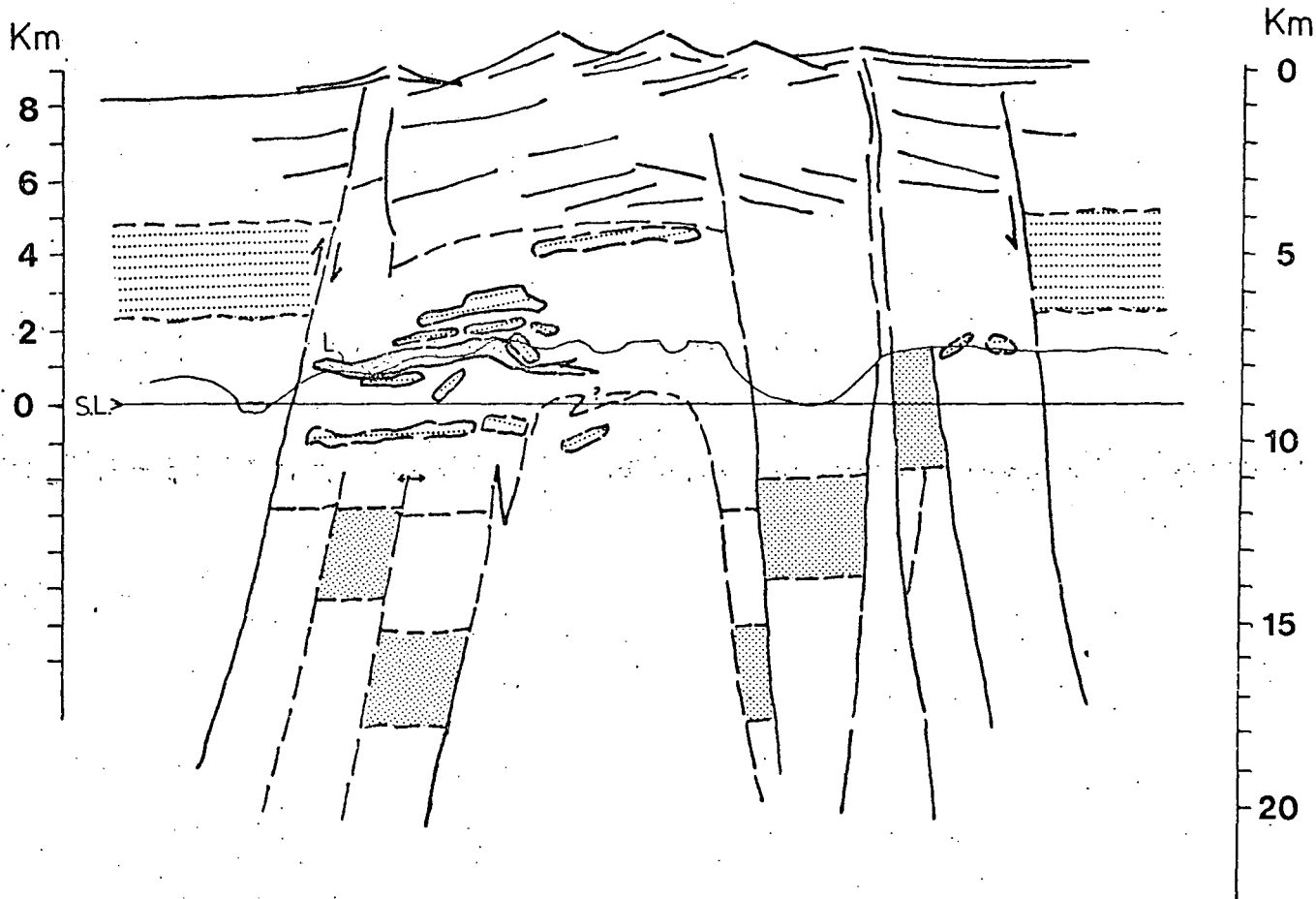
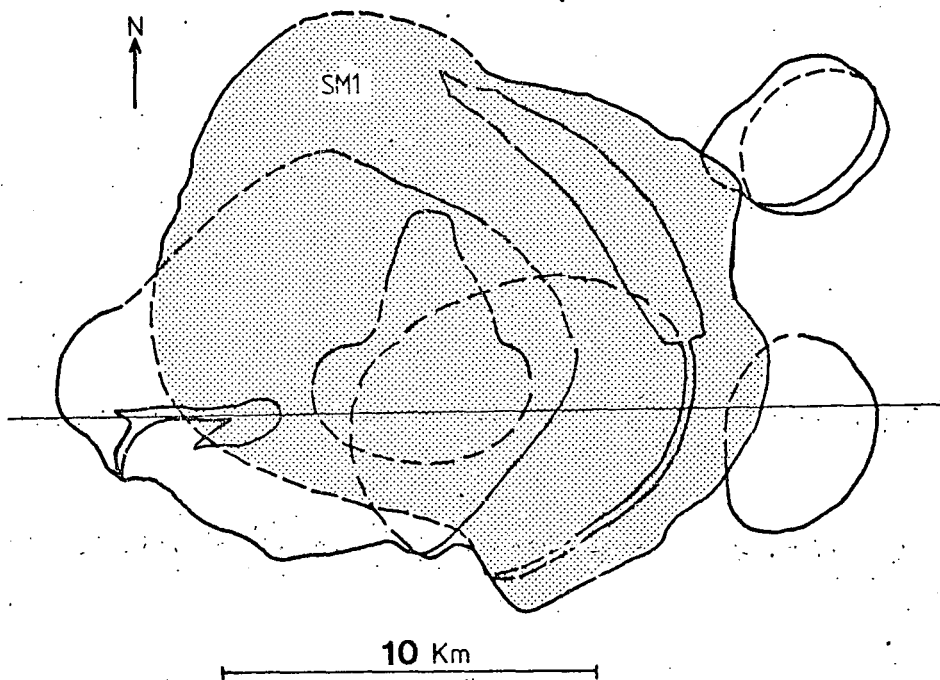


TABLE (3) 1. Extent and overlap of units

Unit	Area exposed (km ²)	Area initial (km ²)	Est. height (km)	Initial volume (km ³)	Overlap (area%)	Volume "missing" (km ³)
SM1	40	180	3.0	540	78	420
SM2	15	?80	3.0	240	80	190
SM3	8	8	3.0	24	0	0
SM4	105	150	3.0	450	30	135
SM5	55	55	1.5	83	0	0
SM6	5	?6	0.5	3	0	0

3.8.E. Reconstruction

A reconstruction shown in figure 3,6 illustrates many of the points covered to date. This is not intended to be an accurate scale drawing, but does represent diagrammatically the processes and conditions which prevailed during the formation of the Motzfeldt Centre.

The main features are, stoping of earlier units to considerable depth (SM1 for example) and, a much thicker supracrustal succession than the 3500m preserved at the present day. The topography of the Early Gardar landsurface is entirely fictional, but may not be unreasonable in the light of the topography associated with, for example, the east African rift in Kenya. In the latter, Mount Kilimanjaro (5200m) rises abruptly from the surrounding countryside, above which it towers an additional four kilometres. The positions of rafts stoped from the roof of chamber SM4 have been projected onto the line of section and an arbitrary vertical movement on the Flink's Dal fault has been set at 1km for this purpose (downthrown to the south).

3.8.F. Phonolite magma

In view of the similarity in composition between the intrusive phonolites of SM2, SM3 and the phonolite lavas (see section 5.8.), it is not inconceivable that magma associated with the ring fracture of SM2/3 might have reached

the surface to allow eruption of similar phonolitic lava. Since the parental magmas to much of the Motzfeldt Centre (SM2, 3 and 4) were phonolitic, a fresh sample of the phonolite margin from SM2 (54139) has been used for consideration of physical properties in the following sections. The analysis, given below, does not differ remarkably from much of the nepheline syenite from the Motzfeldt Centre, and is thus all the more instructive. The major element analysis of 54139 is as follows:-

54139. Porph. Phonolite.

SiO ₂	56.27
TiO ₂	0.49
Al ₂ O ₃	20.60
FeO*	5.15
MnO	0.21
MgO	0.44
CaO	1.21
Na ₂ O	8.84
K ₂ O	5.91
Total	<u>99.12</u>

The intrusive phonolites contain upwards of about 20 % phenocrysts (mostly Fsp, Ne) whereas the porphyritic lavas contain perhaps 10-15 % of similar phenocrysts. The presence of phenocrysts in a magma would serve to increase its viscosity.

3.8.G. Density and Viscosity

Following the method of Bottinga and Weill (1970), the density of a magma can be fairly quickly ascertained to within about 1% relative error. Here, partial molar volumes of the major oxides have been calculated from published measurements in binary and ternary silicate melts. Since these partial molar volumes display little compositional dependence in liquids ranging from 40 to 80 mole% silica, it is possible to calculate the density of most magmatic liquids, whether anhydrous or water bearing, for any given temperature. Because of a small lack of data, it is necessary to estimate the partial molar volume of titanium (\bar{v}_{TiO_2}) and to estimate that of water ($\bar{v}_{\text{H}_2\text{O}}$).

Thus, given the partial molar volumes = v_i , gram

formula weight = M_i and the mole fractions calculated from the analysis = X_i , the density (p) can be calculated from

$$p = \sum_i X_i M_i / X_i \bar{v}_i$$

To compare the effects of water on the magma density (p), phonolite 54139 dry at a temperature of 1250°C yields a density of 2.53 (gm/cm³) compared with the density of 2.47 for the same magma and conditions with the addition of 2.0 wt% H₂O (at a pressure of 2 kbars). The increase of density caused by decreasing temperature is less important than the decrease caused by water. Thus for dry phonolite 54139 at 1000°C, $p = \underline{2.58}$

Viscosity

Using Shaw's refinement (1972) of an empirical method developed by Bottinga and Weill (1972) it is possible to calculate the viscosity of any anhydrous or water-bearing magmatic silicate liquid. The method relies upon empirical values for partial molar coefficients, which require the molecular proportions of a given composition expressed as four equivalent metal oxide-silicate pairs (or five including water). These are then multiplied by empirical values and summed to provide a precise slope (S) for use in the system

$$\ln N = S (10^4/T) - C_{ts} + C_N$$

which is a plot of \ln viscosity ($=N$) versus $1/T$, where T = temperature and C_{ts} and C_N are axis intercepts. The resulting straight lines predict the change of viscosity of a silicate liquid with varying temperature and compare favourably with measured viscosity data from a variety of sources. Ideally, additional data specifically in the phonolite spectrum would allow the empirical values to be further refined. The minimum viscosity values obtained are tabulated below and display a strong dependence on the amount of water present (as wt% H₂O). Values of the viscosity at a temperature of 1000°C have been underlined

since this is probably a fair estimate of typical liquidus temperatures upon intrusion. The presence of phenocrysts, as mentioned earlier, would serve to increase the viscosity of the bulk magma.

The viscosities in poise obtained for each of the following amounts of water present in phonolite 54139 ;

(A) 54139 Dry

(B) 54139 with 1 wt% H₂O

(C) 54139 with 3 wt% H₂O are as follows:-

Temp/°C	(A)	(B)	(C)
1250	3.0×10^3	1.2×10^3	2.2×10^3
1000	1.3×10^5	3.6×10^4	4.4×10^3
750	2.7×10^7	6.0×10^6	3.6×10^5

(viscosities in poise).

3.9. Cooling period

3.9.A. First approximation

Following the mathematical treatment of Jaeger (1968) for basaltic liquids, it is possible to calculate temperatures in cooling bodies of igneous rock. It is assumed in this model that the magma was emplaced instantaneously into country rock having the same thermal properties as the magma. Further assumptions and possible refinements are clarified later.

By selecting a spherical body of syenite (phonolite magma) at depth, which allows no radiative heat loss at the surface, the temperature T at any location within the intrusion at time t after intrusion (t_0) can be expressed as T/T_0 , where T_0 is the initial temperature. This is best modelled for a dimensionless factor r , where $r = kt/\underline{a}$. In this instance, k = thermal diffusivity, t = time in seconds and \underline{a} = the dimension of the body. In this model, k is taken at $0.01 \text{ cm}^2 \text{ sec}^{-1}$, an average suggested by Jaeger (1968) and \underline{a} is the radius of the sphere.

In general, four magnitudes of r are important. For $r < 0.01$ cooling is superficial only; for $r = 0.1$, cooling

will have permeated to the centre of the intrusion; for $r = 1.0$ there is substantial cooling; for $r > 10.0$ cooling is practically complete. Thus, by taking 1000°C as the liquidus temperature and ignoring any superheat, r is selected to represent both the degree of cooling and the proportion of the intrusion which has cooled. This has been carried out for two different intrusions; (a) a sphere of radius 2 km and (b) a sphere of radius 5 km. The results are tabulated below.

Cooling periods:-

	Proportion (volume) below specified temperature	Temp/ $^{\circ}\text{C}$	(r)	Time (yrs) (a)	Time (yrs) (b)
1.	5%	900	0.01	1270	7940
2.	30%	750	0.10	12700	79400
3.	60%	500	0.20	25400	158700
4.	95%	200	1.00	127000	794000

The results fall into the four categories 1 to 4 which can be referred to as ; 1. Superficial cooling; 2. Substantial cooling; 3. Effectively solid; 4. Solid and cold.

Fortunately for the user, the rather complex equations necessary to solve the equations T/T_0 and $r = kt/a$, have been solved graphically (Jaeger 1968) to which intrusions of any size can be applied. Given that the solidus for such a phonolite magma is likely to be around 750°C , since essentially subsolidus reactions occur in the feldspars below this temperature, and certainly below 500°C , then categories 2 and 3 from the above table are the most important. Thus, perhaps 30% of a sphere with 2km radius will have solidified after about 10,000 years. In the same length of time, an intrusion of radius 5km will only be 7-8% solidified.

3.9.B. Ambient temperature

One of the more important potential deviations from the simple model above, is in the assumption that the country rock is cold at t_0 . Using the geothermal gradients of Mercier

and Carter (1975) and taking their High and Low Oceanic gradients as limits for an active rift region, then the temperature predicted for a depth of 9km would be 200 to 400 °C (see fig. 3,4). This would place the country rock within the stable limits of chlorite and perhaps into the lower stability fields of certain amphiboles, which would seem to agree quite well with features seen in the Eriksfjord Formation. Any ambient temperature would serve to extend the cooling interval.

3.9.C. Temperature variations

Superheat

In the simplest case, magma above its melting point may be considered to possess superheat. Hess (1960) speaks strongly for this condition being the norm upon intrusion of most basaltic magmas. In most cases, latent heat will be liberated at a fixed temperature equivalent to the melting point (T_1) for the magma. Modification to the simple cooling model could be made such that superheat (ie: $T_1 = T_0$) is accounted for. The presence of early crystallising phenocrysts in the intrusive phonolite 54139, and in all cases of phonolitic margins to the syenites in Motzfeldt, suggests that the magma was near to the onset of crystallisation upon intrusion.

Temperature irregularities

Irregular temperature distribution may be caused in the magma chamber for a number of reasons. Convection in the simple sense of hot fluid being less dense than cold, is almost certain to occur and is suggested by cross cutting mafic banding in SM3, SM4 and SM5. This may be further complicated by restricted convection cells in the raft-bearing unit SM4.

Where in-situ fractionation occurs, there must be a removal of early-formed crystals, which would in themselves redistribute heat. Since most heat is lost from the top and sides of a magma chamber, and if these crystals accumulated at the floor of a 2km radius chamber, then a pile of cumulates equivalent to 30% by volume might

form within about 10,000 years. Further modifications to the temperature distribution would be necessitated by the vagaries of volatiles.

In view of the uncertainties associated with these modifications, it was considered prudent to leave this model as a first approximation, for which purpose it is probably as good as any.

3.10. Settling

Objects settling in liquids where the Reynolds number is less than 0.05 are found to have settling velocities which can be predicted according to the Stokes Theorem such that

$$\text{settling velocity} = 2/9 \times dp/N \times gr^2 \quad (\text{ms}^{-1})$$

where dp = density contrast, N = viscosity, $g = 9.81 \text{ ms}^{-2}$.

Big or heavy particles settle sufficiently fast that the drag force departs from Stokes Theorem, although this typically only effects the settling velocities by a few %. These refinements and equations for use with settling particles other than spheres, can be found in Lerman (1978).

Given the density contrast ($dp = d_{\text{phonolite}} - d_{\text{xtal}}$) between phonolite magma and early-formed mafic minerals such as olivine ($dp=1.5$), pyroxene ($dp=1.0$) and magnetite ($dp=2.5$), it would appear that settling of such crystals might readily occur. Where the predicted settling velocities are very small, either due to very small dp or small size of the particle concerned, then the velocities associated with convection of the magma might become more important. The settling of the xenolithic blocks of all sizes in excess of about 10cm should, in theory at least, be very rapid in comparison to other processes, even if they are considered as oblate spheroids or flattened discs settling at right angles to their maximum cross sectional area (formulae in Lerman 1978), due to their comparatively huge size. Indeed, the problem here is not to accept their sinking, but rather to understand why they have not disappeared altogether. At this stage, alternative explanations are that either the observed blocks were spalled off very

late in the cooling history of SM4 and were arrested at high levels by cooler magma of high viscosity, or that convection currents were upwelling at similar rates to the settling velocities of the rafts. Taking the latter alternative, for example, and using phonolite magma at the low temperature of 750°C then the resultant viscosity of 6×10^6 poise would require a convection velocity of the order of 200-300 metres per day to arrest a raft of $200\text{m} \times 200\text{m} \times 20\text{m}$.

The rather complicated treatment of the data necessary to maintain rafts of varying sizes at their present level, by changing the viscosity of the magma with lowering temperature, leads one to seek a different and simpler solution. There is no real field evidence to suggest that any of the rafts fell into syenites of different temperatures.

Porosity and effective density

A far more plausible reason for the bouyancy displayed by the rafts, and in particular the very large kilometre-scale rafts, arises from the realisation that any density contrast (dp) is a major factor* which permits or precludes settling. Furthermore, it is clear that dp is critically dependent upon the porosity and thus the water content of any raft at the time of its incorporation into the magma. Assuming that gneiss has a low porosity, as indeed it might, then taking its expected density of 2.66-2.87 (granite-diorite) and phonolite at 2.60, this should sink quite rapidly, dependent on the size of the blocks. In contrast, the addition of just 2.0 wt% H_2O to an andesitic lava ($\text{p} = 2.65$) would reduce its effective density to 2.60, a crucial adjustment! Naturally, sediments and bedded lavas, together with the more stratiform and porous nature of the supracrustal strata in general, would lend these rocks to a relatively high water content. In this way, a sequence of basalts with fractures and other micro-irregularities may retain a porosity of up to 5 or even 10% at depths of 5-6 kilometres (R. Westerman pers. comm. 1980). If this were true, then the addition of 10%

* but see McBirney & Noyes, 1979.

H₂O to even the most basic rock likely to be encountered in the supracrustal lavas, would reduce the density of basalt from 2.87 to 2.58. In this way, it becomes clear that the water content possessed by the rafts, would be crucial in determining their behaviour. The porosity would be less at depth, increasing with height and decreasing pressure of overburden upward through the supracrustal pile. Thus, rafts obtained from progressively higher up in the sequence could be potentially ever greater providers of water.

This feature may also help to explain the field observation that smaller blocks, once parted from their "parental" raft, subside ever more readily into the engulfing syenite. That water was being transferred from the rafts to the syenites is supported by the almost ubiquitous presence of pegmatites and syenites of mixed grain sizes at syenite/xenolith contacts. With decreasing block size, the "drying" effect should become ever more efficient, with the net result that the blocks increase in density. In practice, this whole process would be rather complex, and susceptible to both physical and chemical processes, but the underlying principle is thought to be sound. Mineral reactions involving the fixation of water, such as the formation of biotite and amphibole, so characteristic of the xenolithic rafts, would not hinder this process, since $p_{\text{biotite}} = 2.7-3.3$ and $p_{\text{amphibole}} = 3.0-3.5$, both of which may be a little less than the mafic minerals from which they formed ($p_{\text{pyroxene}} = 3.2-3.6$), but both being greater than the density (ρ) of phonolite magma.

3.11. Water

3.11.A. Water and a silicate melt

From the simple considerations of density and viscosity, it is clear that the addition of as little as 1 wt% H₂O to a relatively anhydrous melt, lowers both of these physical properties significantly. At this point it is worthwhile considering the processes by which water can be accommodated in a silicate melt.

The following summary of silicate melts has been derived largely from the work of Saxena and Mueller (1977). There is much evidence that silicate melts have as their fundamental units the SiO_4^{4-} tetrahedral group and the associated larger cations such as Ca^{2+} and Na^+ . Also, as in the crystalline solids, the SiO_4^{4-} groups will be linked or polymerised to varying degrees into chains, rings, sheets and three dimensional frameworks dependent upon composition and physical environment. Thus, silicate melts are effectively highly disordered versions of the crystalline solids. In the first approximation, an orthosilicate or olivine melt might consist of the units Mg^{2+} , Fe^{2+} and SiO_4^{4-} , a metasilicate or pyroxene-like melt of Mg^{2+} , Fe^{2+} and Si_nO_{3n} chains or rings, whilst feldspar melts might consist of Ca^{2+} , Na^+ and K^+ ions in a fairly continuous but disordered $(\text{Si},\text{Al})\text{O}_2$ framework. In practice, this is far too simple and dissociation would require, for example, that silica and alumina be distributed among a variety of groups, with simpler units being favoured at higher temperatures. In spite of this relative chaos, considerable order might be maintained, with the familiar associations and linkages being supported for short distances.

The distribution of silicate species in the melt is a function of temperature and SiO_2 content (Hess 1971), and the number of SiO_4 monomers at a given temperature decreases with increasing SiO_2 . Upon the introduction of volatiles, the structure of the melt is often radically altered. In particular, water might be expected to react energetically both with larger cations and with the SiO and Al-O chains and frameworks present. Of these, the latter is particularly important since it leads to the rupture of bridging oxygen bonds. In a statistical treatment of water solubility in feldspar melts, Wasserburg (1957) defined the following occurrences of water (as interpreted by Mueller and Saxena 1977); (i) H_2O as molecules segregated in holes or as water of hydration of the large cations; (ii) OH replacement of the bridging oxygen atoms; (iii) OH replacement of nonbridging or

unshared oxygen or as OH in combination with the larger cations.

For simple systems such as the binary H_2O -Albite, the addition of water to melt can be predicted mathematically (Wasserburg 1957). This has been extended to include solubility of water in complex silicate melts (which are still relatively simple) as discussed by Shaw (1964), who tackled the system $\text{CaAl}_2\text{Si}_2\text{O}_8$ - KAlSi_3O_8 - $\text{NaAlSi}_3\text{O}_8$ - SiO_2 - H_2O . In the join SiO_2 - H_2O he found that a negative heat of solution was needed to fit the data. This is important since it would indicate that certain felsic melts, which are at least in the right magma spectrum for phonolite/syenite, have an affinity for water.

3.11.B. Water, phase relations and crystallisation

Although the phase relations will be returned to in later chapters (Chapter 5 in particular), it is as well to outline the salient points here. The addition of water to a feldspar melt or feldspar dominated melt has a well documented effect of lowering the liquidus temperature, whilst having little effect upon the solvus (Yoder et al 1957; Bowen and Tuttle 1950). Thus, the depression of the liquidus temperature is proportional to $P_{\text{H}_2\text{O}}$ in the alkali feldspar system Ab-Or- H_2O . This has led to the popular view that loss of volatiles from such a system as granite, will rapidly raise the liquidus temperature and thereby crystallise the magma. Naturally for a hydrous syenite, the same process might apply although it is worthwhile considering the converse situation.

Typical modal analyses of Motzfeldt syenite suggest that they were not especially hydrous, probably containing less than 1.0 wt% H_2O (eg: 60% Fsp @ 0.25% H_2O = 0.15, 20% Ne @ 0.7-0.9% H_2O = 0.20, 10% Amph @ 2.0% H_2O = 0.20, 0-2% Bi @ 4% H_2O = 0.10, ol,px, etc anhydrous; total = 0.7 wt% H_2O). The upward passage of the Motzfeldt phonolites was through crystalline gneiss, which is thought to have a low porosity. The syenites are exposed at around the level of the base of the supracrustal rocks. The latter are potentially

porous compared with the gneiss and are thought to have been water-bearing. It is conceivable that water was added to the phonolite magmas, both directly from the adjacent Eriksfjord Formation and from the included rafts stoped from the roof region. The abundant evidence of pegmatites associated with the rafts and at contacts within the syenites might support this, as might the abundance of biotite and other hydrous phases in the xenoliths. The relationships of pegmatites near syenite/syenite contacts are often more ambiguous, but in many instances these may also suggest that the older syenite was water-bearing upon intrusion of the younger syenite (view supported by A.D. Chambers pers. comm. 1977).

Since the water is encountered at depth ($P_{H_2O}=2-3$ kbar) and since it is believed that water might be favourably incorporated into a felsic magma (see Water 1 above) one might expect a rather rapid reduction of both density and viscosity of the magma. This would appear to be an eminently reasonable way of accelerating the upward passage of the affected magma, with perhaps increasingly vigorous fracture propagation. However, once such magma has erupted at the surface, the system would then logically be susceptible to degassing of perhaps much of the remaining volatile content of the magma. This lowering of P_{H_2O} would raise the liquidus temperature, followed perhaps by relatively rapid crystallisation of the remaining magma and little additional upward movement.

In detail, one can envisage numerous variables to complicate the process, such as success of mixing, convection, fracturing and so on, but the general concept appears to find support from the similar exposure levels encountered in other of the Igaliko centres and also perhaps throughout the Gardar province.

3.12. Structures postdating the Motzfeldt Centre

3.12.A. Gardar dykes

As recorded by Emeleus and Harry (1970), the number of dykes intruding country around Igaliko and Tunugdliarfik

fjords, is indeed striking. The dykes constitute part of a swarm which occupies a broad zone from Tugtutôq in the west to the country north and west of the Igaliko Complex, a distance of over 100km.

Several generations of dykes are present in the Igaliko Complex and neighbouring rocks, although their close adherence to a parallel ENE strike often makes it difficult to determine their ages. To the northwest of the Motzfeldt Centre, distinct generations of dolerite, Big Feldspar dykes and alkali trachytes have been recognised by Walton (1965) and appear to correlate with similar dykes within the Igaliko Complex (Emeleus and Harry 1970).

It is likely, though as yet unproved, that the majority of dykes cutting the Motzfeldt Centre belong to the Mid Gardar swarm, as defined by those dykes which postdate the early centres and which are in turn cut by the youngest members of the Igdlérfigssalik Centre. An account of the major types is given in Emeléus and Harry (1970) to which the reader is referred. The recognition of petrographic types is, for the present, one of the simpler ways of grouping the dykes and yields a variety of essentially alkali-trachytic rocks. Of these, perhaps the most numerous dykes cutting the Motzfeldt Centre are undersaturated nepheline-bearing phonolites. Some of the spectacular quench textures observed during a rather cursory examination of these dykes, may prove fruitful areas for future experimental work. At least one dyke in Motzfeldt is composed of basic spheres in a "thumbprint" matrix of quenched crystals, which reminded this author of immiscible relationships seen on the Isle of Arran.

3.12.B. Faulting

Two groups of faults effect the Igaliko syenites, a N/S to NE/SW set and a more important E/W set. Of these, the first group is not responsible for major movements, in contrast to the E/W set which is represented by relatively few dykes often with large transcurrent displacements. The lines of many of the faults are marked by a zone of reddened

and sheared rock, which may stand out quite nicely in the otherwise pale weathering syenites.

Flink's Dal fault

This sinistral fault is the northernmost of two major E/W faults which affect the Igaliko Complex. It extends from a steep glacier filled valley east of Motzfeldt SØ westwards across Central Motzfeldt, across Qôroq fjord and then across the peninsula separating Qôroq from Tunugdliarfik fjords. Correlations further to the west as far as Sermilik fjord, have been proposed by Emeleus and Stephenson (1970). Sinistral movement on the fault is placed at about 4km by the displacement of the alkali gabbro dyke in Central Motzfeldt and is consistent with the east and west margins of the Motzfeldt Centre. This movement is greater by a factor of two than that originally proposed by Emeleus and Harry (1970) and may complicate the later work of Stephenson on ductile deformation of the South Qôroq Centre (1976b)

Within Central Motzfeldt, the fault forms the broad valley of upper Flink's Dal and is marked for most of its length by a distinctive zone of reddened and crushed syenite typically 1-200m wide. The vertical movement across this fault has been considered in a previous section (3.8.C.) and suggests a downthrow to the south in the east of the centre of maybe 1km and a downthrow also to the south in Central Motzfeldt of perhaps 500m, although neither amounts are accurately known. Vertical movement in the opposite sense is suggested by internal boundaries in the North Qôroq Centre (Emeleus and Harry 1970). The combined vertical movement could be explained by some form of "hinge" operating around Qôroq fjord, or by separate and additional fault movements occurring along Qôroq fjords and beneath Motzfeldt SØ, neither of which have been substantiated.

3.12.C. Ellipticity

A number of the major ring intrusions in the Gardar province, including major representatives of the Igaliko

Complex, are frequently elliptical in plan and located at the intersections of regional dyke swarms with sinistral wrench fault systems. This is considered by Stephenson (1976b) to be due to fault movement nearly contemporaneous with igneous formation of the centres. In the South Qôroq Centre, he explains the ellipticity by ductile deformation of hot igneous intrusions which have undergone large scale simple-shear. Although possibly applicable to the South Qôroq and perhaps the Igdlérfigssalik Centre, this does not necessarily hold for the somewhat elliptical outline. Rather, the outline of the Motzfeldt Centre is a direct result of the complex overlap of intrusions, which may in themselves have been controlled initially by some fracture. Later brittle fracture has then effected the centre along the Flink's Dal fault, with no large scale rotation of dykes as is seen in the South Qôroq Centre.

CHAPTER FOUR

MINERALOGY

Introduction

This chapter describes and reports analyses of the mineral phases from the different intrusive units SM1 to SM6. The phases are dealt with in no specific order, other than the major mafic phases are considered first and the less abundant phases are reported towards the rear of the chapter. Of the major phases, pyroxene receives the most extensive treatment and the importance of zirconium substitution in particular, is examined and resolved by the institution of a new end-member. Several of the minor phases contain significant quantities of REE elements, and a number of these have been analysed. Full details of the analytical procedures employed with the electron microprobe together with the analytical results and classification systems can be found in Appendix II .

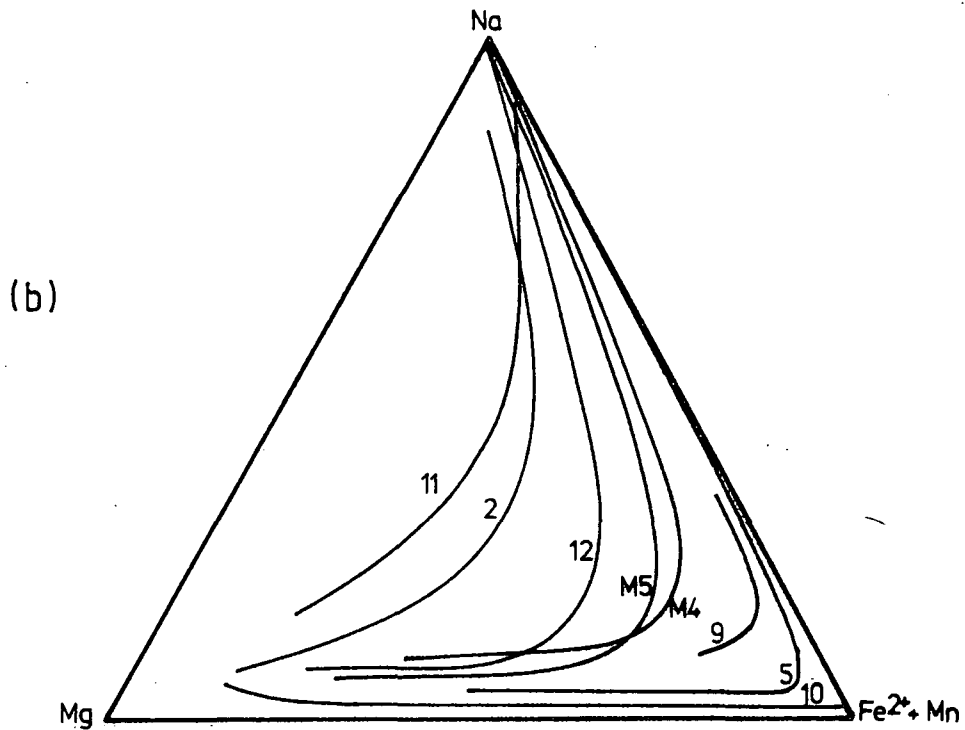
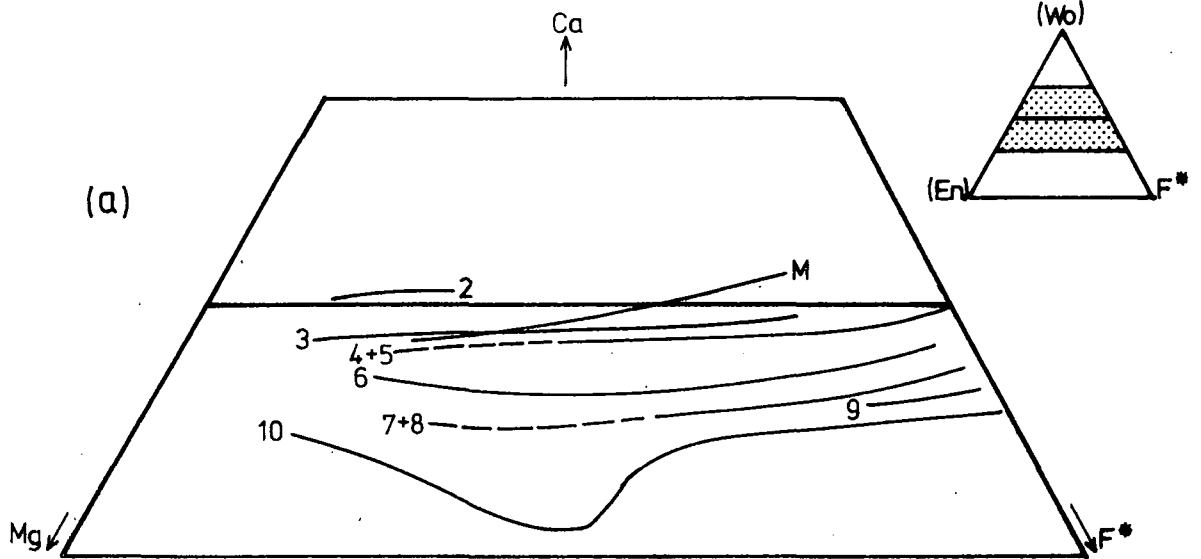
4.1. Pyroxenes4.1.A. General

All of the pyroxenes are monoclinic and lamellar structures have not been observed. Fine scale schiller inclusions are common in the most magnesian pyroxenes, which are characteristically pink-lilac pleochroic salites found in the alkali gabbro dyke and the basic members of unit SM5. One or two pyroxenes from the alkali gabbro are included since they display rather good sector zoning and occasional quench textures, which may be important in understanding some of the minor element variation. Slightly less magnesian and paler coloured pyroxenes are found as somewhat zoned euhedra in the phonolite chills. In general, sector zoning is not apparent, but outward zonation from magnesian and Ca-rich cores to Fe and Na enriched margins is quite usual. In most units, the mafic minerals may be concentrically zoned, with pyroxene often mantled by amphibole and quite commonly by a second generation of

Figure 4,1. Pyroxene trends compared.

- (M) Motzfeldt Centre, general trend (this work)
- (M4) Motzfeldt Centre, unit SM4 (this work)
- (M5) Motzfeldt Centre, unit SM5 (this work)
- (2) Uganda nephelinites (Tyler and King, 1967)
- (3) Shonkin Sag Laccolith main trend (Nash and Wilkinson 1970)
- (4) Tugtutôq giant dykes (Upton, 1964)
- (5) Ilímaussaq Intrusion (Larsen 1976)
- (6) Shiant Isle Sill (Gibb, 1973)
- (7) Nandewar volcano (Abott, 1969)
- (8) Kûngnât Intrusion (Upton, 1960)
- (9) Pantellerites (Nicholls and Carmichael, 1969)
- (10) Skaergaard Intrusion (Brown and Vincent, 1963)
- (11) Itipirapuã, Brazil (Gomes et al, 1970)
- (12) South Qôroq Centre (Stephenson, 1972)

- (a) Note modification to iron-rich corner. Restricted to analyses with $Ac < 15$
- (b) Trend (3) for Shonkin Sag is very similar to that of South Qôroq (12). See also figure 4,4 .



Pyroxene trends compared

(a) Different Ca levels for different associations, after Larsen (1976) whence $F^* = Fe^{2+} + Mn + Fe^{3+} - Na$

(b) Alkali pyroxene plot, (+Skaergaard (10) for comparison)

Na-rich pyroxene.

The Motzfeldt pyroxenes form a trend from salite towards hedenbergite and then towards aegirine and are compared with pyroxene trends from other alkali associations and the Skaergaard Intrusion in figure 4,1 . Pyroxenes from Motzfeldt with intermediate Ac ($\text{Fe}^3 = 0.2-0.5$) do not show quite such extreme Mg-depletion as do otherwise comparable pyroxenes from the Ilímaussaq Intrusion. As will be elaborated below, the display of pyroxene data on the traditional Ac-Di-Hed diagram, where $\text{Ac} = \text{Na} = \text{Fe}^3$, assumes that all of the Na is present as acmite, and is certainly incorrect for the earlier Na-poor and relatively Mg-rich pyroxenes from Motzfeldt. In general, this means that all of the sub-horizontal parts to the trends are displaced incorrectly towards the Ac position and in all probability lie closer to the Di-Hed join.

4.1.B. Recalculation and nomenclature

Approximately 115 point analyses of pyroxenes have been made by electron microprobe, which returns all iron contents as Fe^2 . Estimation of the Fe^3/Fe^2 ratio is very important and is not merely dependent upon $\text{Fe}^3 = \text{Na}$. Fe^3 has been calculated independently by assuming stoichiometry of the pyroxenes, such that 4 cations and 6 oxygens are equivalent to one formula unit. In order that this should not rely entirely upon the completeness of the analysis, small deviations in silica (which constitutes about 50% of a typical pyroxene) have been considered in the computer programme PXPROG8, written by A. Peckett (see Appendix 11) which was used as an additional aid in pyroxene classification. This programme was designed specifically to accommodate the newly postulated zirconian end-members (Jones and Peckett in press). The method of calculation is, in outline;-

1. Divide each analysis weight percent element by its atomic weight to give the cation proportions.
2. Assign cations to the end-member stoichiometric pyroxenes in the order analogous to the CIPW Norm procedure.
3. Group ferric and ferrous iron from the appropriate

pyroxenes.

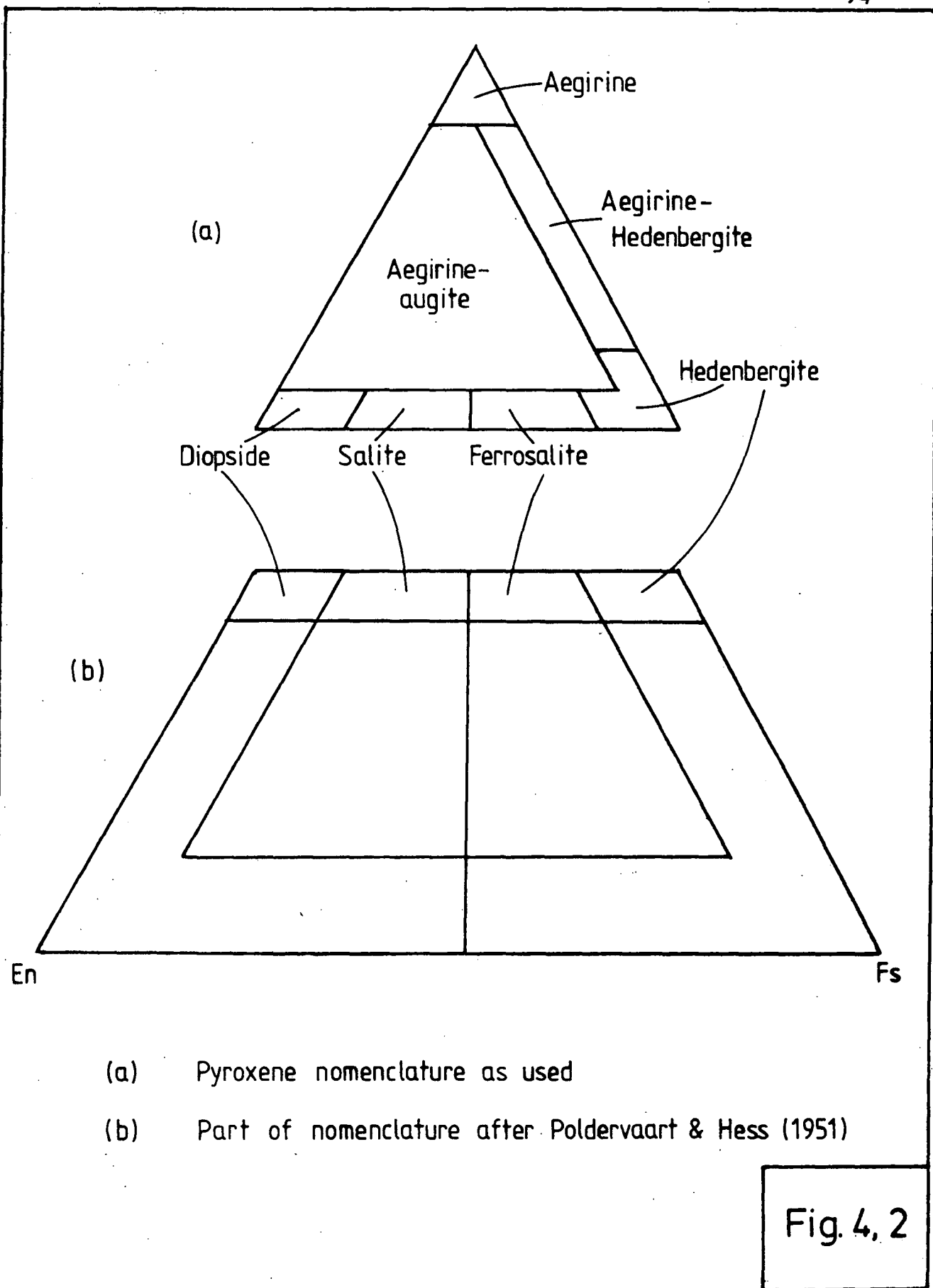
4. Recast the analysis to conventional oxide form and unit formula to the conventional six oxygens form.

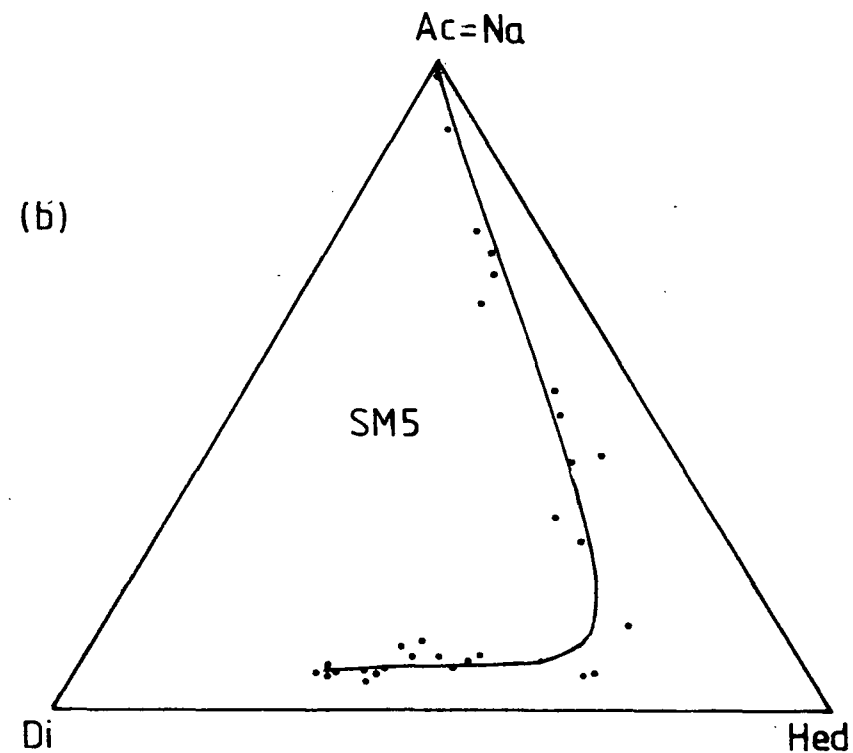
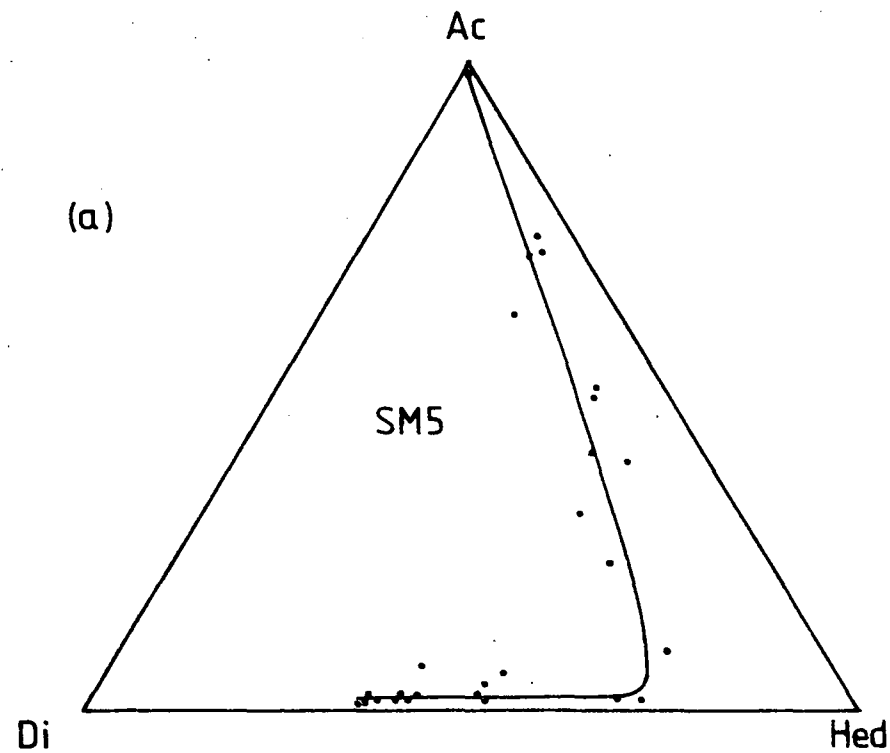
5. Retotal the molecular proportions of the end-member pyroxenes to 100.

An iterative procedure is used, if necessary, to preserve the ferrous iron/magnesium ratio in all ferro-magnesian pyroxene end-members. It has been noticed that where zirconium is prominent, some silicon (c. 1%) may be left over after assigning as much as is needed for the various pyroxene end-members (after step 2.). This feature is not in general true of the analyses of pyroxenes of all types listed in Deer et al (1978) recalculated with this same procedure.

Nomenclature

Alkali pyroxenes involving $\text{NaFe}^{3+} = \text{Ca}(\text{Fe}^{2+}, \text{Mg}^{2+})$ and $\text{CaFe}^{2+} = \text{CaMg}^{2+}$ substitutions are best described with reference to the system Acmite (Ac)-Diopside (Di)-Hedenbergite (Hed). Following the suggestions of Deer et al (1978), the term aegirine has been reserved for pyroxenes where $\text{Fe}^{3+} > 0.8$. All of the early-formed pyroxenes are too calcic to be called augites and are more correctly termed salites and ferrosalites as part of the diopside-hedenbergite series (after Poldervaart and Hess, 1951). It is proposed that the members diopside-salite-ferrosalite are given an upper limit of $\text{Fe}^{3+} = 0.1$, with diopside further restricted to $\text{Mg} > 0.8$. ^{The field of} Hedenbergite has an odd polygonal shape, and is defined by the conditions $\text{Fe}^{2+} > 0.8$ where $\text{Fe}^{3+} < 0.1$, and $\text{Fe}^{2+} > 0.9$ where $0.1 < \text{Fe}^{3+} < 0.2$. The remainder of pyroxenes whose compositions are such that $\text{Fe}^{3+} < 0.8$ and $\text{Mg} > 0.1$ are aegirine augites, whilst pyroxenes with $0.2 < \text{Fe}^{3+} < 0.8$ and $\text{Mg} < 0.1$ are termed aegirine-hedenbergite. Figure 4,2 illustrates the classification used for the Motzfeldt pyroxenes and is partly related to the original classification of Poldervaart and Hess (1951) for the system Wo-En-Fs (Fig. 4,2 (b)). Modification to the latter system such that the iron-rich corner is plotted as $\text{Fe}^{3+} + \text{Fe}^{2+} + \text{Mn} + \text{Na}$, and all of the analyses have $\text{Ac} < 15$, a method employed by Larsen

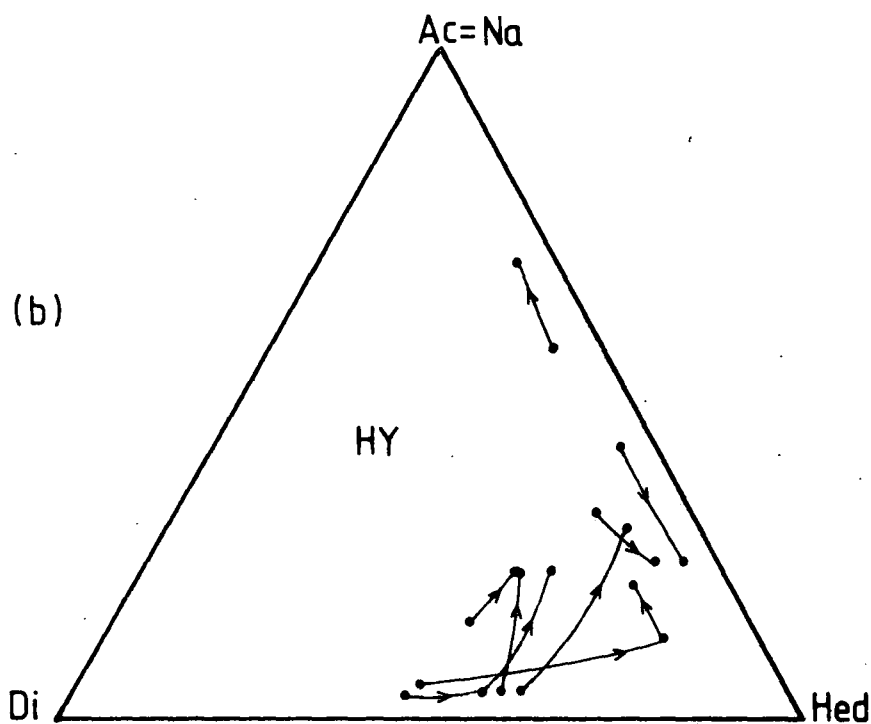
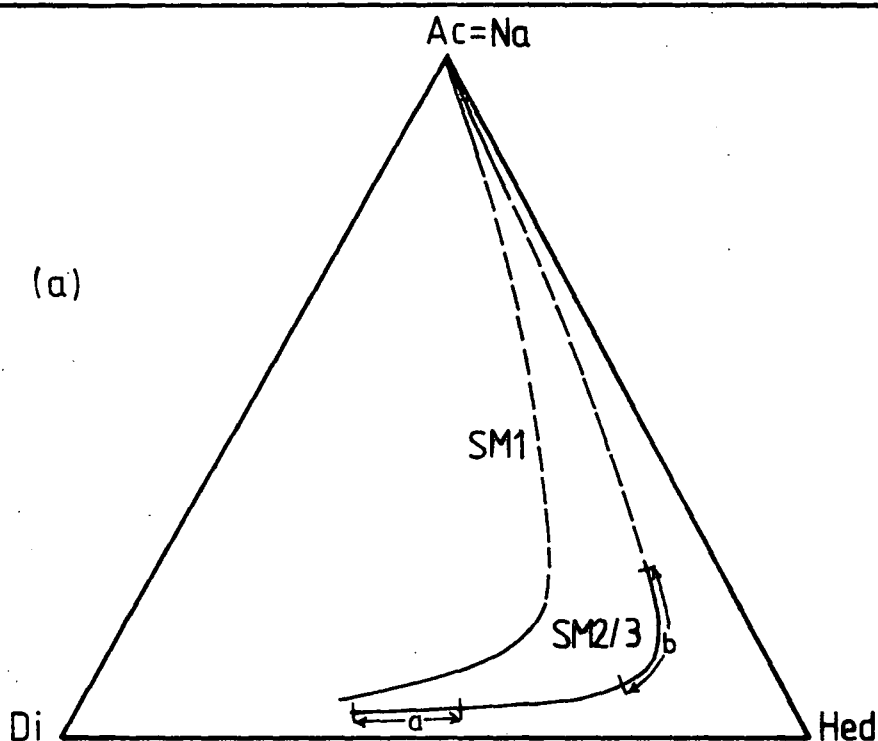




(a) Pyroxene end-members according to PXPROG8

(b) Standard plot, where $Ac=Na$, $Di=Mg$, $Hed=Fe^{2+}+Mn$

Fig. 4, 3



(a) Pyroxene trends for units SM1 & SM2 with SM3

a = range from phonolite margin; b = range from layered rocks N of the Flinks Dal fault.

(b) Zonation from core to rim of pyroxenes from unit HY

Fig. 4, 4

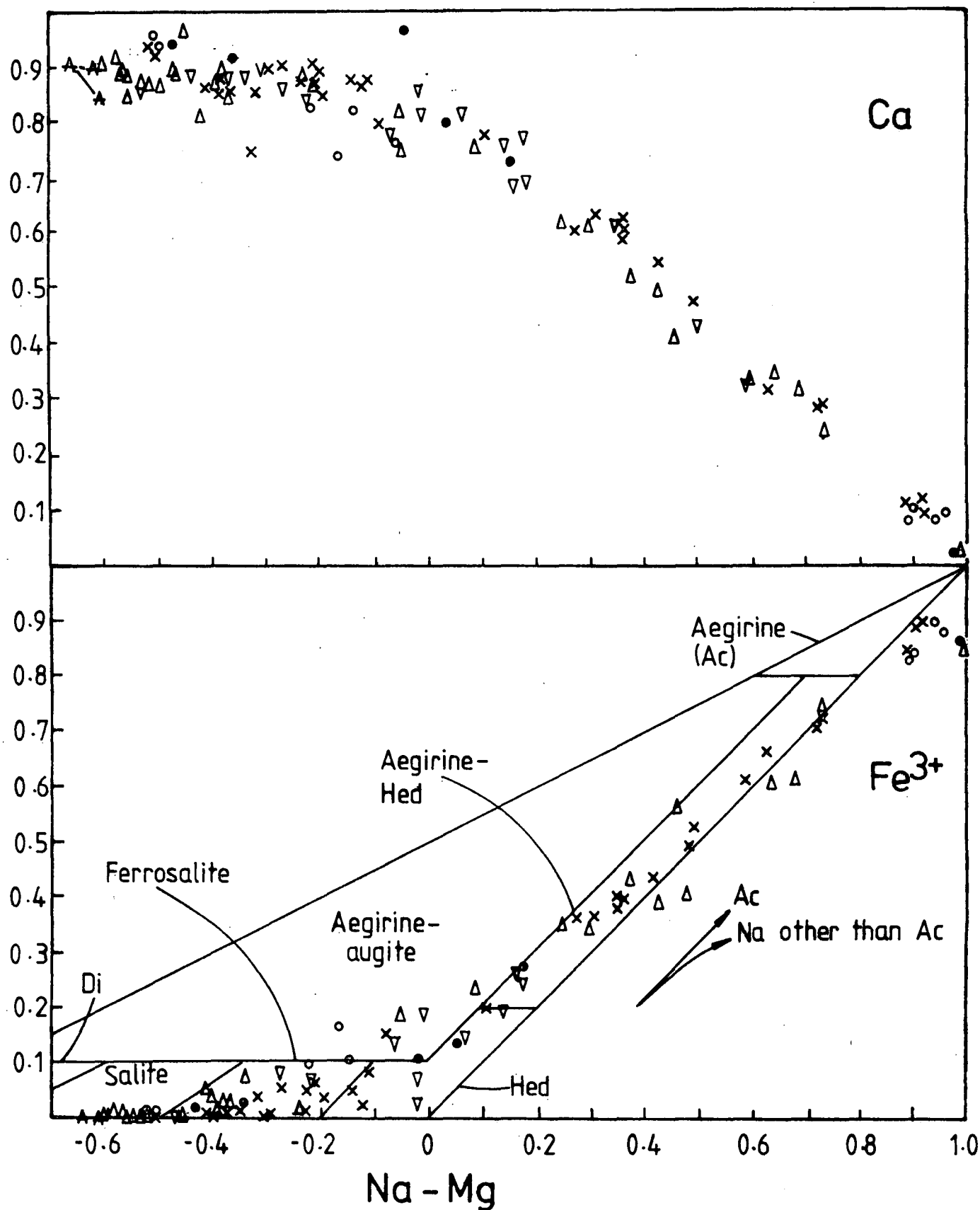
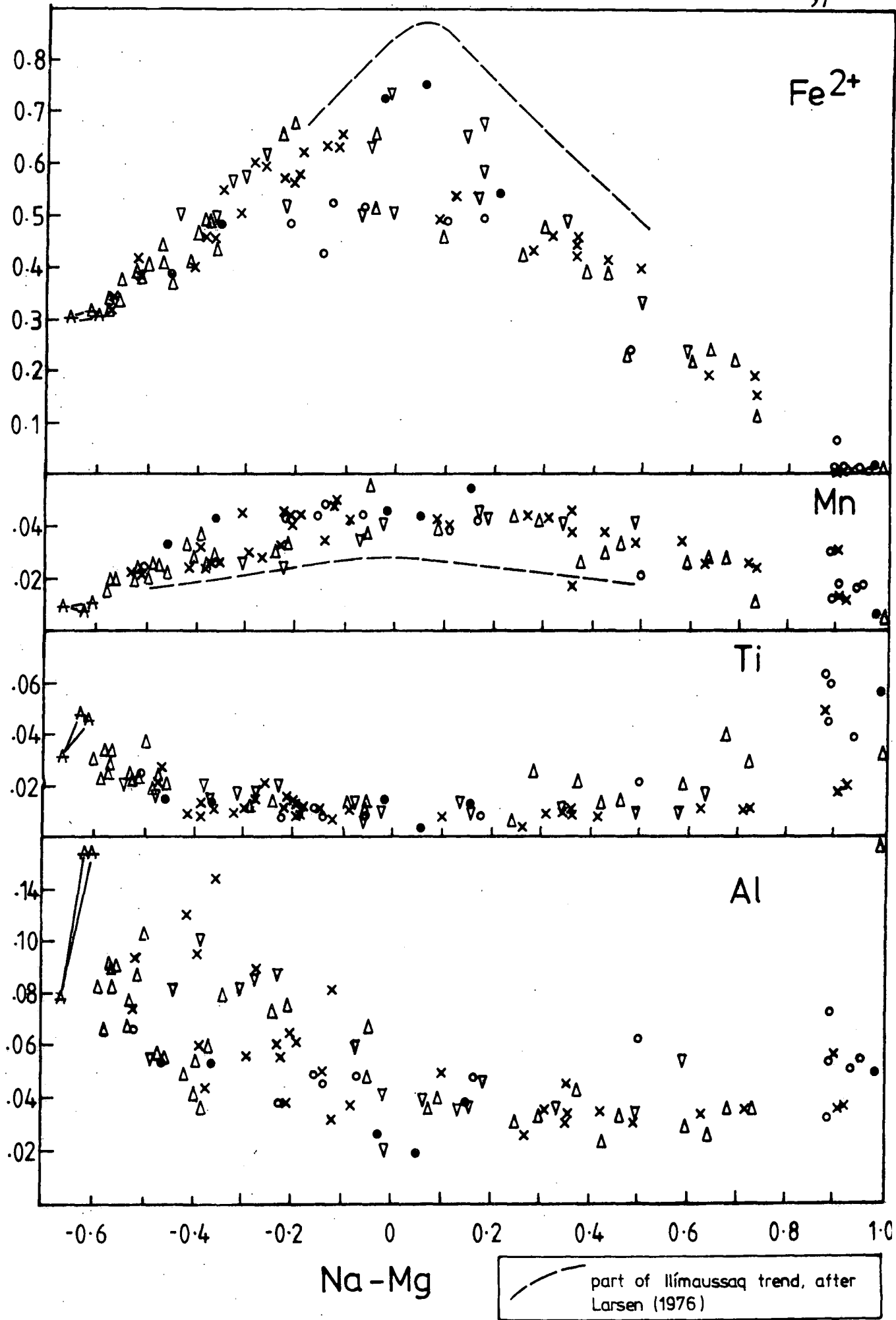


Fig. 4, 5

Pyroxene chemical variation diagrams: figures are in atoms per formula unit.

○ = SM1, ● = SM2/3, × = SM4, ▽ = HY, Δ = SM5

★ = alk. gabbro (tie lines to different sectors)



(1976), allows comparisons to be made with other alkali associations (Fig. 4,1).

Inspection of the trends shown in figures 4,4 and 4,6 with the Fe^3 variation in figure 4,5 and the classification outlined in figure 4,2 indicates that the Motzfeldt pyroxenes are mainly restricted to the fields of salite-ferrosalite-hedenbergite-aegirine-hedenbergite and aegirine.

End-member variation

Previous workers in alkali pyroxenes have usually referred to the diagram Ac-Di-Hed based on $\text{Ac}=\text{Na}=\text{Fe}^3$, $\text{Hed}=\text{Fe}^2+\text{Mn}$ and $\text{Di}=\text{Mg}$. In practice, this procedure must be incorrect, since it does not allow for other Na-rich end-members which may be present, such as, for example, jadeite in the early pyroxenes from Motzfeldt. By recasting the analyses to their correct end-members using PXPROG8 as outlined above, it is possible to see the effects of the approximation $\text{Na}=\text{Fe}^3=\text{Ac}$ by taking unit SM5 as representative of the likely range of pyroxenes and comparing the two methods, side by side (fig. 4,3). Clearly, for Na-rich pyroxenes which are Mg-poor, the approximation $\text{Ac}=\text{Na}=\text{Fe}^3$ holds well. However, bearing this in mind, and the inevitable inaccuracies which must result, the pyroxene trends have been presented in the customary way, for comparative purposes. The trends do not convey any sense of volumetric abundance, though it would be true to say that the more basic pyroxenes were preferentially sought in the probe sections, with the result that aegirine is far more abundant in the Motzfeldt Centre than the variation diagrams might suggest.

4.1.C. Pyroxene substitutions

The general pyroxene formula $\text{X}^{\text{viii}}\text{Y}^{\text{vi}}\text{Z}_2^{\text{iv}}\text{O}_6$ is referred to in the following parts of this section.

Z-position

Essentially occupied by Si and Al, the ratio $\text{Si}/(\text{Si}+\text{Al})$ increases steadily with increasing Na-Mg of the

pyroxene. It has been found that the microprobe determinations of silica may be susceptible to an error of about 2% relative, although this can be allowed for, and estimated by PXPROG8.

X-position

The major elements involved here are Ca and Na. In the salites (Ca+Na) may be as low as 0.90 though is usually around 0.92 to 0.96 and rises through the ferrosalites to around 0.98. This is thought to be a direct result of small amounts of calcium-poor pyroxene in solid solution in the early pyroxenes. Thus up to 10% "opx" exists in salites from the alkali gabbro and up to 8% "opx" in salites from the larvikites of SM5*. With increasing Na, (Ca+Na) closely approximates to 1.0, as is normal for alkali pyroxenes. In the more sodic pyroxenes, K is present in small amounts (typically 0.01-0.05 wt% K₂O) and is thought to reflect minor K-acmite substitution.

Y-Position

This position may involve substitution of many different elements. Initially, Mg, Fe²⁺ and Mn are present as diopside and hedenbergite and related components. The position of hedenbergite is at Na-Mg = 0 in the variation diagrams (fig. 4,5), as indicated by the maximum position of the Fe²⁺_{peak}, and is closely echoed by Mn, both of which features are similarly developed in pyroxenes from Ilímaussaq (Larsen 1976). These divalent ions are progressively replaced by trivalent ferric iron in balance to increasing Na in X, constituting substitution of the acmite molecule (NaFe³Si₂O₆). Further elements to occupy this site are the higher valence Al, Ti and Zr. Occasionally the aegirines contain significant Al, with up to 11 mol% jadeite in aegirine from SM5.

4.1.D. Al and Ti and sector zoning

TiO₂ is apparently present as NaTiSiAlO₆ in the early pyroxenes and thus behaves similarly to Al₂O₃. Both Al₂O₃ and TiO₂ decrease with increasing Na-Mg, with the

irregular resumption of higher levels in the aegirine-hedenbergites and the aegirines. Insufficient sodium in the salites to accomodate all of the Al_2O_3 , indicates that the excess Al_2O_3 is probably present as the calcium Tschermak's molecule (CATs), $\text{CaAl}_2\text{SiO}_6$. Pyroxenes from the early part of SM5 and SM5* contain about 2.0 wt% Al_2O_3 and 2 mol% CATs, whilst salites from the alkali gabbro contain about 3.0 wt% Al_2O_3 and up to 4.5 mol% CATs (see below).

Samples of elongated needle-like pyroxenes found in a vein of alkali gabbro which has penetrated a plagioclase xenocryst, is intergrown with needles of apatite and appears to be a quench texture. A few larger salites are sector zoned, optically in shades of lilac and compositionally in content of TiO_2 and Al_2O_3 . In two zones (sector "A") $\text{Al}_2\text{O}_3 = 3.10$ and $\text{TiO}_2 = 1.75$, whilst in a third zone (sector "B") $\text{Al}_2\text{O}_3 = 1.77$ and $\text{TiO}_2 = 1.10$. The elongate pyroxenes are almost identical in composition to sector "A" and have $\text{Al}_2\text{O}_3 = 3.10$ and $\text{TiO}_2 = 1.65$ (all in wt% oxides). This is the converse of the more commonly observed situation (Deer et al 1978) where rapidly grown pyroxene elongated parallel to the z-axis, is depleted in Al and Ti. Augites from Mt. Etna in Italy, were shown by Downes (1974) to have higher Al and Ti in (100) and (010) sectors, which he related to slow growth compared to the Al- and Ti-poor ($\bar{1}11$) sector. In a study of diopsides and salites from the Narce area in Italy, Hollister and Gancartz (1971) outlined the following four conditions which might influence the variation of Al and Ti between different sectors; (i) The size and composition of the ionic complexes added during crystal growth; (ii) The rate at which material is added; (iii) The rate of re-equilibration with the matrix at surface dislocation steps; (iv) The rate of re-equilibration of surface layers with the matrix by ion exchange at 90° to the crystal faces.

It is notable that the two different sectors analysed from the salite described above, encompass the entire spread of Al and Ti data for the Motzfeldt pyroxenes (see Fig. 4,5).

4.1.E. Zirconium substitution

Zirconium is an important constituent of the more sodic and iron-rich pyroxenes from the Motzfeldt Centre, frequently reaching 1 or 2 wt% ZrO_2 and attaining as much as 6.96 wt% ZrO_2 , with HfO_2 measured up to 1.5 wt%. The Zr:Hf ratio (mass/mass) is fairly constant at 35 over the analysed range of zirconium contents. In general, the zirconium content of the pyroxenes, hereafter referred to as zr/px, increases with fractionation (Na-Mg index). A conventional plot of the compositions of pyroxenes from units SM4 and SM5 is shown in figure 4,6 (a,c and d). Representative trends from the South Qôroq Centre (Stephenson 1972) and the Ilímaussaq Intrusion (Larsen 1976) have been inserted for comparison (Fig. 4,6 (a)). The overall trends are similar, but only in the Motzfeldt pyroxenes is there high zirconium in the more acmitic pyroxenes. This can be seen in figure 4,6 (b), where curves represent the approximate limits of zirconium in pyroxenes both from Motzfeldt and from Ilímaussaq (data from Larsen 1976).

It is apparent that zr/px does not increase smoothly with fractionation, especially in unit SM5. The rate of increase in zr/px is higher in SM5 than SM4. Unit SM4 contains no major zirconium phase and ZrO_2 increases with fractionation to 1.5 wt%. Sporadic crystals of eudialyte ($(\text{Na,Ca})_5\text{ZrSi}_6\text{O}_{16}(\text{O,OH,Cl})_2$) are found in the most evolved samples of SM5 and coincide with relatively low zr/px. It has been found that where a second Zr-bearing phase, such as eudialyte, occurs, the pyroxene in the same thin section contains relatively little zirconium. Thus, typical aegirine from the lujavrites (SM6) contains 0.39 wt% ZrO_2 and eudialyte is common. Point "B" in figure 4,6 (d) coincides with crystallisation of coexisting eudialyte and resumed low levels of zr/px in SM5. Similarly, point "A" (Fig. 4,6 (d)) and minor irregularities in zr/px with fractionation in SM4 (Fig. 4,6 (c)) might coincide with crystallisation of lesser amounts of zr-rich phases.

Variation in zr/px within one particular sample

Sample GGU 54138 is a fine-grained nepheline syenite

Fig 4,6 Pyroxene End-Member Variation Diagrams. zr/px in SM4 and SM5; compared.

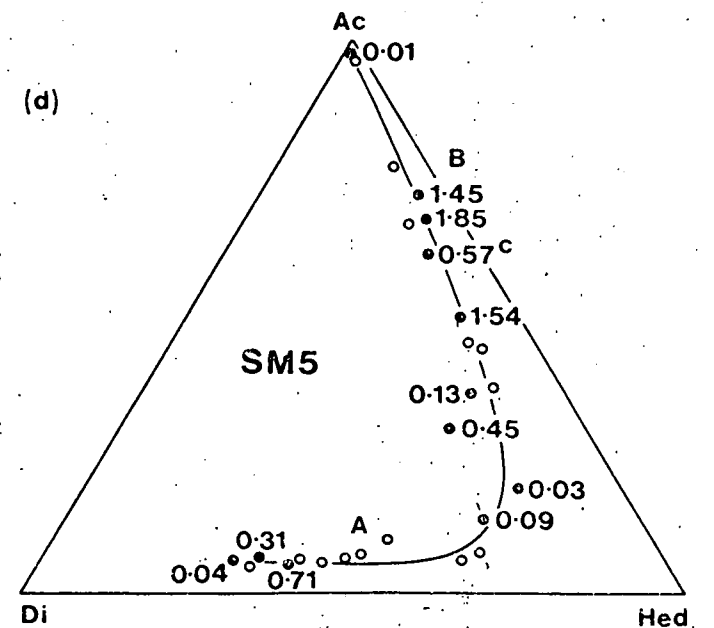
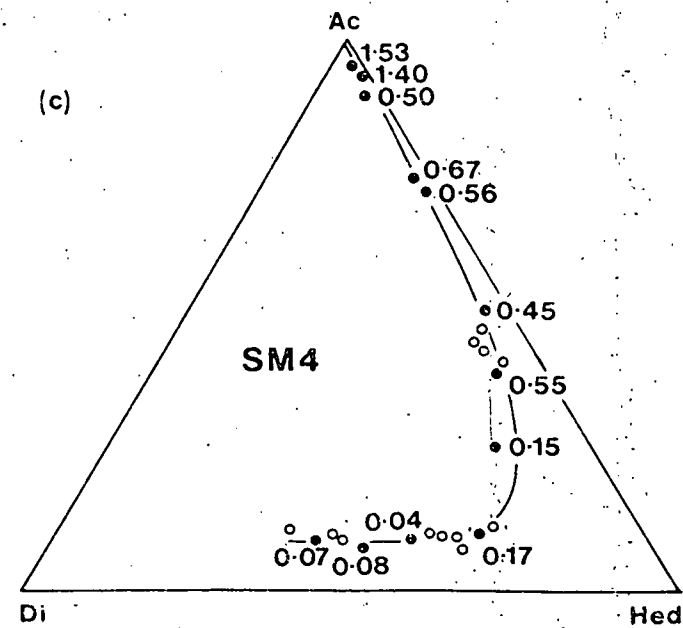
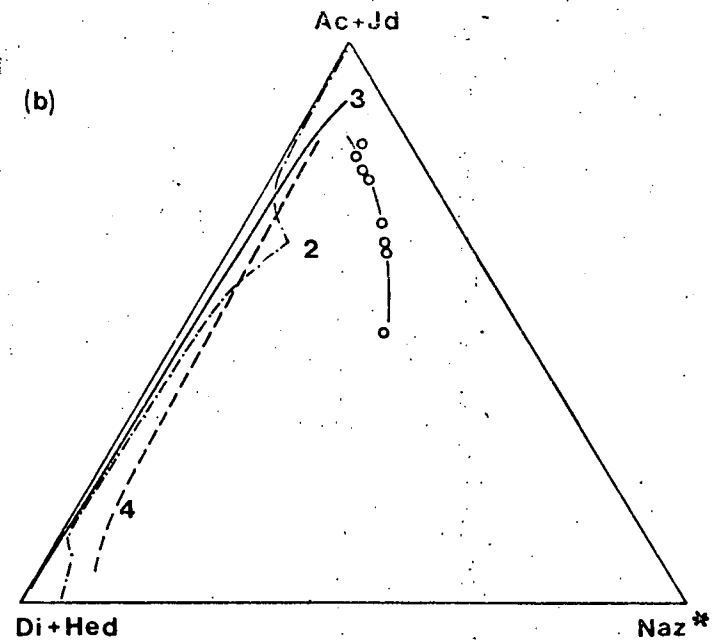
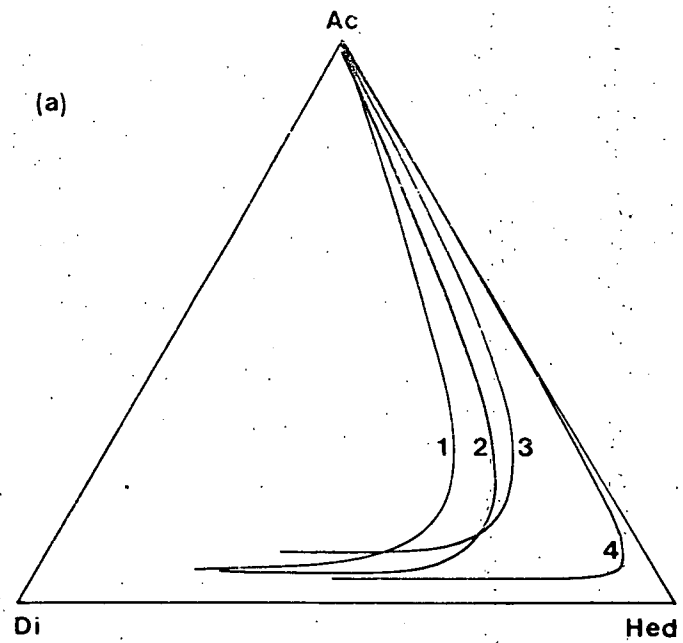
Ac=Acmite, Di=Diopside, Hed=Hedenbergite, $\text{NAZ}^* = \text{FM-NAZ} + \text{NAZAL} + \text{minor (NAT+NATAL)}$. $\text{FM-NAZ} = \text{NaFM}_{0.5}\text{Zr}_{0.5}\text{Si}_2\text{O}_6$, $\text{NAZAL} = \text{NaZrSiAlO}_6$ (see text).

(a) Generalised trends from the Gardar Province, South Greenland. 1 = S.Qôroq (Stephenson 1972), 2 = SM5 Motzfeldt, 3 = unit SM4 Motzfeldt, 4 = Ilímaussaq (Larsen 1976).

(b) Curves represent approximate limits to NAZ substitution in 2,3 and 4. Note the prominent inflexion in curve 2 which may correspond with onset of crystallisation of eudialyte. Open circles represent zirconian pyroxenes from sample GGU 54138.

(c) Filled circles represent pyroxene analyses whose Zr/px values are quoted as wt% ZrO_2 . Thus SM4 (=3) shows gradual increase of Zr/px with fractionation.

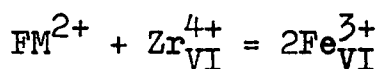
(d) Notation as (c) for unit SM5 (=2). Here Zr/px build up is more rapid with resumed low levels at "A" and "B". Thus "B" and perhaps "A" correspond with onset of crystallisation of eudialyte which preferentially removes Zr from the liquid, and so denies significant entry of Zr into pyroxene (see text). Superscript "c" denotes pyroxene coexisting with eudialyte.



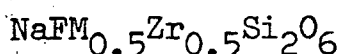
from the topmost part of the ring dyke SM3 and is composed of perthitic alkali feldspars (c. $1.0 \times 0.6 \times 0.1$ cm; bulk compsn Ab_{62}) and smaller euhedral nephelines about 1 mm across. The mafic minerals are restricted almost entirely to interstitial areas, although a few large euhedral amphiboles (up to 2 cm long) are visible in hand specimen. In thin section, the feldspar forms the bulk of the mode (57%) with subordinate nepheline (30%). Mafic minerals consist of pink-brown ferro-edenite (5%) with narrow blue magnesio-arfvedsonite rims and green pleochroic interstitial pyroxene (6%). Optically equivalent to aegirine, these pyroxenes contain from 1.5 to almost 7.0 wt% ZrO_2 . The zr/px contents are rather uniform across each individual grain yet may vary considerably from one cluster to another. Thus a range of zr/px values exists within one thin section, with higher values being progressively less frequent. The radiating texture and variable ZrO_2 contents could be due to rapid crystallisation under highly non-equilibrium conditions, but the perthitic exsolution of alkali feldspar argues against this. The pyroxene has thus, presumably, crystallised from small pockets of residual liquid late in the cooling history of SM3 and is the only Zr-bearing phase present. It would appear that different values of zr/px reflect different concentrations of Zr in the melt, implying that diffusion was severely restricted, even on a mm-scale.

End-member proportions

For aegirines from Motzfeldt with ZrO_2 in excess of about 2.0 wt%, there is insufficient aluminium to account for coupled substitution into the octahedral and tetrahedral sites. Thus, most of the Zr is present in the pyroxene as a result of the coupled substitution in the octahedral sites alone of



where FM denotes divalent ferromagnesian cations, including Mn. This substitution requires the end-member



(Jones and Peckett, in press) and has been given the acronym FM-NAZ.

Physico-chemical conditions

Recent experimental work concerning the solubility and saturation of zirconium in felsic melts (Watson 1979) has shown that, at least over the temperature range 700–800 °C and for $P_{H_2O} = 2$ kbar, the solubility of zirconium in felsic melts is critically dependent upon the peralkalinity index (moles $(K_2O + Na_2O)/Al_2O_3$). The solubility of zirconium appears to be insensitive to temperature, activity of silica, total zirconium or the ratio Na_2O/K_2O . Furthermore, Watson showed that the solubility of zirconium was reduced by the additions of minor quantities (c. 1.0 wt%) of lime and ferric oxide.

The peralkalinity index is high for most of the Motzfeldt syenites, frequently exceeding unity. Assuming that the interstitial phases in 54138 represent locally the last liquids in the solidifying syenite SM3, then these were strongly peralkaline since, excluding minor analcite and sodalite, all of the interstitial phases are rich in alkalis and extremely deficient in both lime and alumina.

The notably higher Fe^2/Fe^3 ratio present in the Zr-rich aegirines, compared with Zr-poor aegirines, suggests a fairly low oxygen fugacity. The absence of Fe-Ti oxides and the presence of aenigmatite from samples with high zr/px (in particular 54138) probably relates to an oxygen fugacity below the FMQ buffer (see Larsen 1977 for discussion). Since the high zr/px requires a Fe^2/Fe^3 charge balance reaction, the precise conditions under which Zr-rich aegirine forms may be very different from those under which Zr-poor aegirine forms.

High peralkalinity, low lime and low oxygen fugacity will cause high solubility of zirconium in the melt, with the last phase to crystallise from the melt being rich in zirconium. In practice, it appears that zirconium is incorporated into the clinopyroxene structure, as FM-NAZ or NAZAL ($NaZrAlSiO_6$, see Larsen 1976), only when no other

zirconium-bearing phase such as eudialyte is formed. Thus, Zr/px may be directly and antithetically related to the different stability relations of eudialyte, the most frequent mineral in Motzfeldt (apart from pyroxene) whose partition coefficient ($\text{Zr}_{\text{min}}/\text{Zr}_{\text{melt}}$) is greater than one. In this way, it is likely that the serious depletion in Zr/px and consequently Zr of the late melt in SM5, is related to the arrival of eudialyte on the liquidus. A similar argument has been presented for the presence or absence of eudialyte from the liquids of different units in the Ilímaussaq "Intrusion" by Larsen (1976).

The antithetic relationship between high Zr/px and other coexisting zirconium-bearing phases is a complex problem and one which can not be fully explored here. However, of undoubted importance is the structure of the silicate melt prior to the crystallisation of any Zr-bearing phase. In this respect it is interesting that Watson (1979) has found that zirconium appears to form complexes in felsic melts, in which $(\text{Na}+\text{K}-\text{Al})/\text{Zr} = 4$, with species such as $\text{Na}_4\text{Zr}(\text{SiO}_4)_2$. The high activity of soda thus presumably prevented the crystallisation of baddelyite, ZrO_2 , and furthermore the low activity of silica has prevented the formation of zircon, ZrSiO_4 .

The observed variability in Zr/px between different interstitial patches in the same sample must reflect a low diffusion rate for Zr. This is reasonable for such a highly charged ion at comparatively low (c. 600 °C) temperatures and this is consistent with the observations of Seitz (1974) for thorium in the system diopside-albite-anorthite.

By considering the end-member proportions of jadeite and zirconian pyroxenes together, a clear antithetic relationship is once again very evident. Since the Al^{3+} content of pyroxene is proportional to the activity of Al_2O_3 in the melt (Campbell and Borley 1974), this reinforces the above conclusions that high Zr/px is favoured by peralkalinity and thus low activity of Al_2O_3 in the melt.

4.2. Olivine

4.2.A. General

Olivine is a common phase only in the alkali gabbro, the larvikite ring dyke SM5* and the lardalitic margin to SM5. Olivine may also be found in the phonolitic margins of SM2/3 and SM4, but elsewhere is almost entirely absent from the syenites. Occasional relics of olivine are sometimes preserved, although ^{they} are often deeply corroded and extensively replaced by opaque iron oxides. The olivines are mostly iron-rich and contain appreciable amounts of manganese and calcium, in line with other of the Igaliko centres (see Stephenson 1974).

4.2.B. Compositional variation

Excluding the alkali gabbro, MnO in the olivines varies from 1.76 to 5.00 wt%, with a related variation in the tephroite (Mn_2SiO_4) end-member from 2.3 to 7.2 mol%. SM5 and SM5* span a similar range in composition, which is quite extensive and is from $\text{Fo}_{39}\text{Fa}_{59}\text{Tp}_{2.5}$ to $\text{Fo}_{11}\text{Fa}_{84}\text{Tp}_{5.2}$ in SM5* and from $\text{Fo}_{31}\text{Fa}_{65}\text{Tp}_{3.9}$ to $\text{Fo}_8\text{Fa}_{85}\text{Tp}_{7.2}$ in SM5. Olivine from the alkali gabbro is predictably more magnesian and is typically around $\text{Fo}_{63}\text{Fa}_{36}\text{Tp}_{0.6}$ in the more rapidly cooled facies. The range in both Ca and Mn is similar to Mn- and Ca-enriched olivines from the other three centres of the Igaliko Complex (Stephenson 1974).

When plotted in the system Mg-Fe-Mn (=Forsterite-Fayalite-Tephroite) and compared to olivines from other intrusions (Fig. 4,7) the olivine trend from Motzfeldt is similar to that from South Qôroq (Stephenson 1974), both of which are more Mn-enriched than trends from the Ilímaussaq Intrusion and from Skaergaard (Larsen 1976 and Deer and Wager 1939 repectively). The relative dispositions of Mn-enrichment in olivine from Motzfeldt, Ilímaussaq and Skaergaard is reminiscent of the corresponding Na-enrichment in pyroxenes from the same intrusions, when plotted in the system Di-Hed-Ac. This has been noted by Larsen (1976) who deduces that the differences in Na in the pyroxene and Mn in the olivine are for the same reason, namely the different oxidation states of these magmas.

• = SM5* (larvikite ring dyke)

◦ = SM5 (Iardalitic margin)

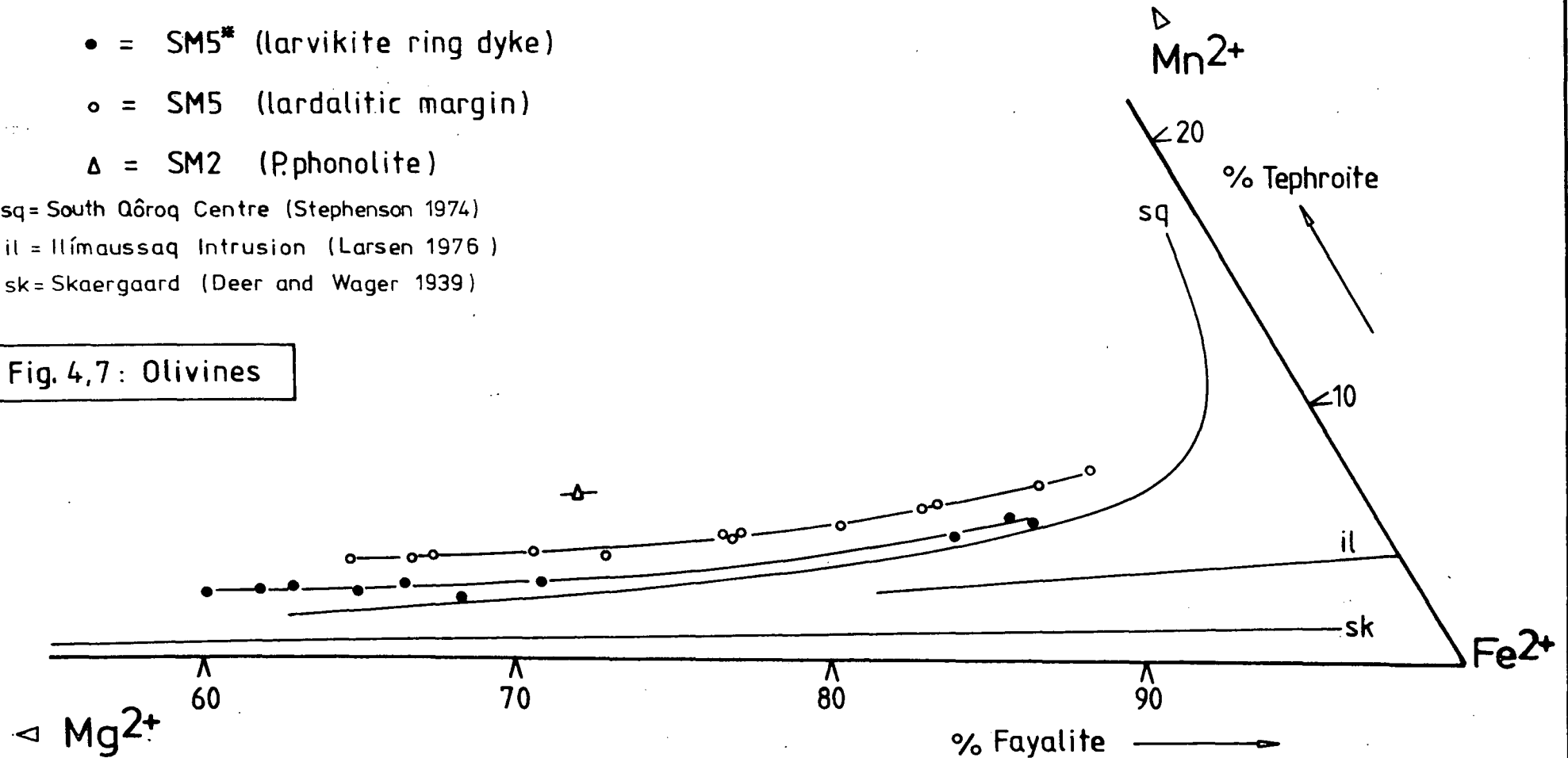
Δ = SM2 (P.phonolite)

sq = South Qôroq Centre (Stephenson 1974)

il = Ilímaussaq Intrusion (Larsen 1976)

sk = Skaergaard (Deer and Wager 1939)

Fig. 4,7: Olivines



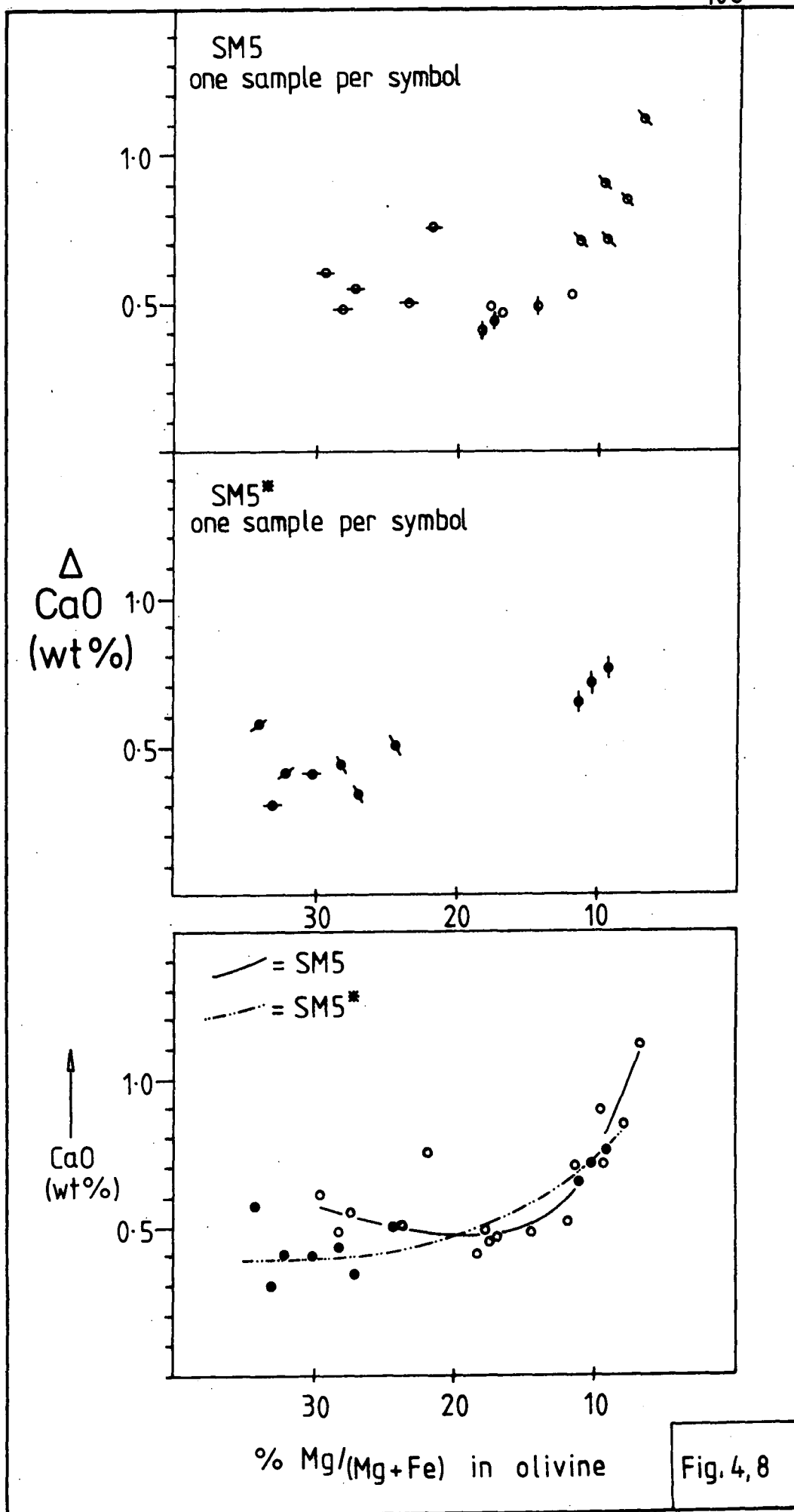
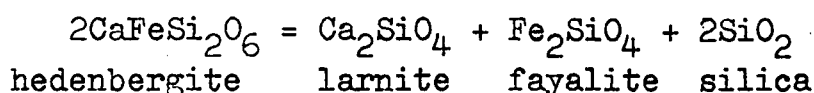


Fig. 4, 8

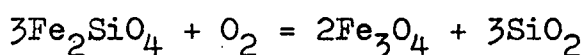
Based on his observations of olivines from re-crystallised syenites, Chambers (1976) suggests that the Mn-content of the olivines is likely to be controlled by solid state diffusion. However, he too suggests that the oxidation state is a primary consideration and decides that a magma with higher fO_2 would give rise to Fe^{3+} and correspondingly earlier enrichment in manganese.

The calcium content of the olivines from Motzfeldt is also similar to that reported from Ilímaussaq (Larsen 1976) and can be related to a larnite (Ca_2SiO_4) component. As can be seen from the reaction



the content of Ca in olivine may be dependent on silica, wherein low activity of silica promotes increased Ca in olivine. Low pressure may have the same effect (Nicholls et al 1971; Stormer 1973). Thus, high level, silica undersaturated magmas such as those at Ilímaussaq and Igaliko may be expected to yield Ca-rich olivines. Such types were not included in the study of plutonic olivines by Simkin and Smith (1970) who none the less still recognised a positive correlation between the Ca content of olivine and the degree of silica undersaturation (normative nepheline). There is a reasonable correlation between CaO content and the index Fe-Mg in the olivines for both SM5* and SM5 (Fig. 4,8) and it can be seen that individual samples possess a range in Fo content of about 5 mol% or so. The level and rate of increase of CaO in SM5* and SM5 is very similar. The Ca contents of the olivines seem to be sensitive to what are presumably small differences existing between separate samples from the same parts of the same units. Perhaps any correlation of CaO with Fe-Mg has been missed by previous workers because of the scale on which the variation occurs.

The departure of olivine from the liquidus is adequately explained by increasing oxygen fugacity (Stephenson 1974) in a reaction such as



although Chambers (1976) points out that decreasing silica activity could have the same effect. In certain instances it is also quite feasible that the reaction is buffered by a new silicate rich in iron, as may be the case where aenigmatite is stable (see section 4.7.).

Of the trace elements, Cr and Ni were not detected and Al and Ti were often present in small amounts, with up to about 0.1 wt% TiO_2 .

4.3. Amphiboles

4.3.A. General

The amphiboles are probably the most abundant mafic mineral in the Motzfeldt Centre. They are usually anhedral in outline and, in accord with the work of Chambers (1976) on the North Qôroq Centre, there is a fairly predictable change in colour with degree of fractionation of the host syenite. The more basic syenites, such as the larvikites and lardalites associated with SM5, are characterised by amphiboles with a dominantly brown pleochroic scheme (typically x=pale brown y=reddish brown z=dense brown). With increasing fractionation the amphiboles take on shades of green (eg: x=olive y=bluish green z=dark greenish brown) whilst the most fractionated syenites are characterised by amphiboles with blue oriented pleochroic schemes. In unit SM1 the latter include pale yellow-indigo blue amphiboles where the syenite is near to the outer contact of the centre.

In addition to this change in amphibole colour with degree of fractionation of the rock, there is often outward zonation of the individual amphiboles through part of the same sequence of colours, indicating zonation to alkali-enriched rims. Most commonly, this zonation is developed rapidly over the outer part of the amphibole. The ~~role~~ of amphibole crystallisation has clearly been associated with the formation of pyroxene. The alternation of growth from early pyroxene cores to amphibole which in turn is rimmed by sodic pyroxene, is frequently observed in the Motzfeldt syenites, as in the North Qoroq Centre.

(Chambers 1976) and is broadly reminiscent of a "discontinuous reaction series" such as that reported from the syenites of Tugtutôq by Upton (1964).

Occasionally, small plates of reddish biotite may be found at the cores to edenitic amphiboles in the porphyritic phonolites. A few large euhedral amphiboles are also present in the phonolitic microsyenite of SM3, and are of ferro-edenitic composition with thin arfvedsonitic rims.

4.3.B. Classification

The amphiboles are the most complex and variable of the major rock-forming minerals studied. This is primarily due to the presence of a wide variety of cation sites in the amphibole structure, enabling ions with a large range in ionic radius to be accommodated (Ernst 1968).

Of the various methods for presentation of the compositional data, that of Phillips and Layton (1964) and Phillips (1966) has been selected. This is a rapid and practical method for processing a large number of amphibole analyses into a manageable array of data, and is by nature of this practicality a little less precise than the more recently propounded method of Leake (1978). The scheme allows direct comparison with the data from earlier workers on amphiboles from the Gardar province, such as Stephenson (1972), Rowbotham (1973) and Chambers (1976).

The Phillips (1966) system of nomenclature is based on the possible substitutions which can effect the tremolite end-member. The basic formula of an amphibole ($AX_2Y_5Z_8O_{22}(OH)_2$) is thus completely defined by stating the number of sodium atoms in the X positions and the number of aluminium atoms in Y and Z. These three numbers are coordinates in a 3-D compositional space that can easily be represented. Alkali amphiboles are defined (Phillips 1966) as having at least one atom of sodium in X in the basic formula unit. Thus by considering the cations as their equivalent Mg, Na or Al, there are nine basic

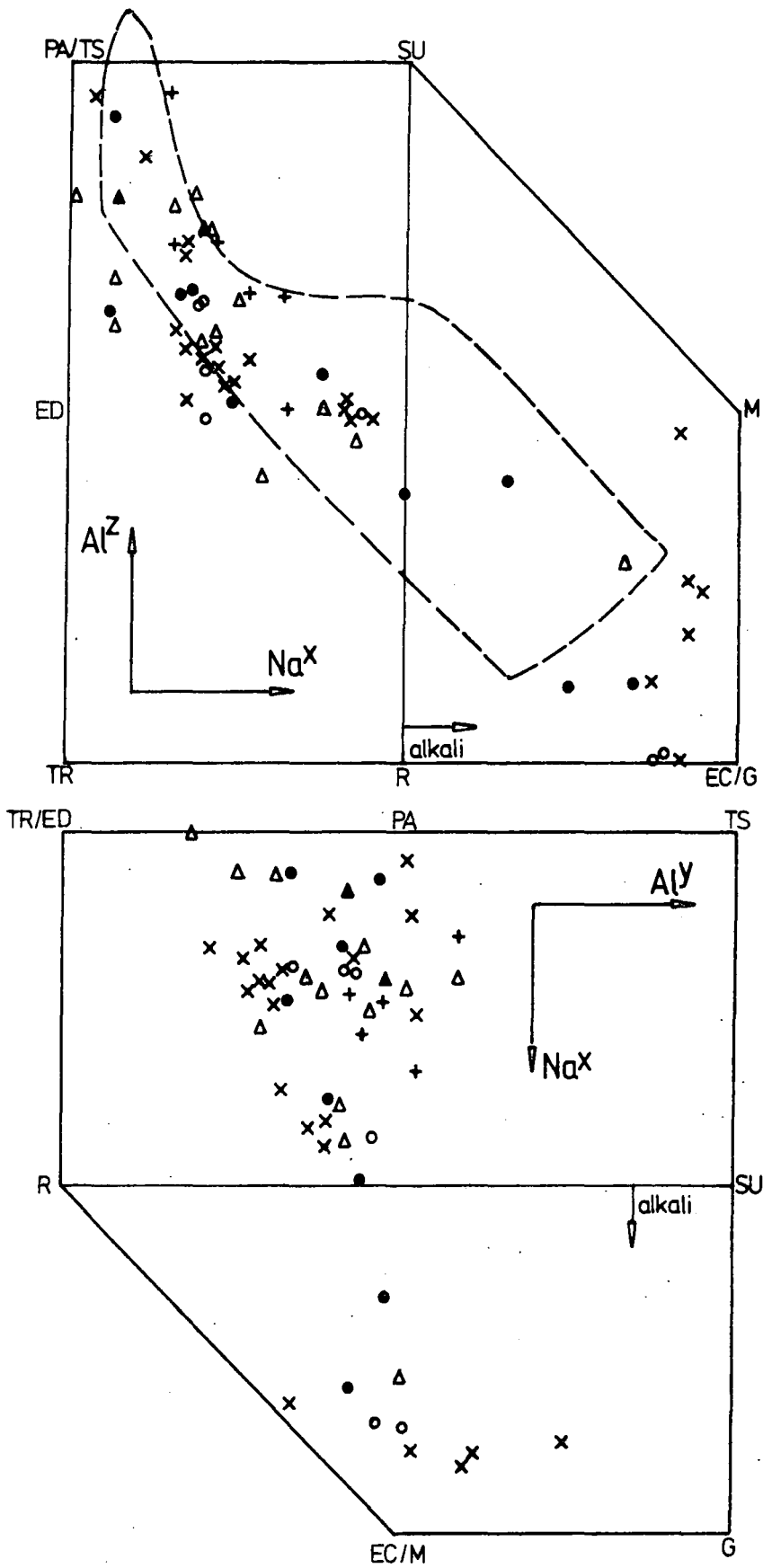
Figure. 4,9. Sections through the amphibole compositional space of Phillips (1966).

Abbreviations for end-members are as follows;

Tr	=	Tremolite
Ed	=	Edenite
Pa	=	Pargasite
Ts	=	Tschermakite
Su	=	Sundiusite
M	=	Miyashiroite
G	=	Glaucophane
Ec	=	Eckermannite
R	=	Richterite

Note that the determination of Al^Y is partly dependent the Fe^3/Fe^2 ratio for these iron-rich amphiboles.

The orientation of these two projections can be seen in figure. 4,11.



- = SM1
- = SM2/3
- x = SM4
- ▲ = SM5*
- Δ = SM5
- + = HY

Fig. 4,9: Amphibole

Tremolite	$\text{Ca}_2\text{Mg}_5\text{Si}_8\text{O}_{22}(\text{OH})_2$	(TR)
Edenite	$\text{NaCa}_2\text{Mg}_5\text{Si}_7\text{AlO}_{22}(\text{OH})_2$	(ED)
Pargasite	$\text{NaCa}_2\text{Mg}_4\text{AlSi}_6\text{Al}_2\text{O}_{22}(\text{OH})_2$	(PA)
Tschermakite	$\text{Ca}_2\text{Mg}_3\text{Al}_2\text{Si}_6\text{Al}_2\text{O}_{22}(\text{OH})_2$	(TS)
Glaucophane	$\text{Na}_2\text{Mg}_3\text{Al}_2\text{Si}_8\text{O}_{22}(\text{OH})_2$	(G)
Richterite	$\text{NaNaCaMg}_5\text{Si}_8\text{O}_{22}(\text{OH})_2$	(R)
Eckermannite	$\text{NaNa}_2\text{Mg}_4\text{AlSi}_8\text{O}_{22}(\text{OH})_2$	(ECK)
Miyashiroite	$\text{NaNa}_2\text{Mg}_3\text{Al}_2\text{Si}_7\text{AlO}_{22}(\text{OH})_2$	(MY)
Sundiusite	$\text{NaNaCaMg}_3\text{Al}_2\text{Si}_6\text{Al}_2\text{O}_{22}(\text{OH})_2$	(SU)

The Motzfeldt amphiboles are shown on two projections through the Phillips compositional space in figure 4,9, one perpendicular to the Al^Z axis and the other perpendicular to Al^Y . The locus of amphiboles from the North Qôroq Centre (Chambers 1976) has been inserted on the plot of Al^Z versus Na^X for comparison. The basic amphiboles found in North Qôroq, such as ferrohastingsites, are considerably less abundant in the Motzfeldt Centre. Amphiboles from the Motzfeldt Centre proceed to further enrichment in Na^X and greater depletion in Al^Z .

The amphibole analyses have been classified using the computer programme MINDATA5 (Knight 1976) based on the Phillips system. MINDATA5 also provides an estimate of the iron oxidation ratio, which appears to increase with fractionation. In view of the acmite ($\text{NaFe}^3\text{Si}_2\text{O}_6$) enrichment exhibited by the pyroxenes, this seems reasonable. In practice, the amphiboles are all iron-rich, with $\text{Fe}/\text{Mg} > 60\%$ and should all be prefixed "ferro". Adopting the procedure of Chambers (1976), pyroxenes classified by MINDATA5 as "pargasite" are actually ferrohastingsites, with less than 0.5 aluminium atoms in the Y site (real Al and not equivalent Al as plotted in the Phillips system). There is therefore a total lack of the ferropargasites from Motzfeldt, which are apparently common in North Qôroq (Chambers 1976) perhaps suggesting the somewhat overall more fractionated nature of the magmas. Furthermore, those amphiboles classified as "eckermannite" are Fe^3 -rich and poor in Al^3 in Y, and represent dominance of the arfvedsonite

end-member ($\text{NaNa}_2\text{Fe}_4\text{Fe}^3\text{Si}_8\text{O}_{22}(\text{OH})_2$ = "A"). Occasionally, the more fractionated pyroxenes possess Fe^3 in Y greater than 1.0, indicating partial presence of the riebeckite end-member, which plots at the glaucophane position in the Phillips system. The resultant classification for the amphiboles from Motzfeldt is outlined below, which if compared to the results of Chambers (1976) reveal the consistent absence of truly pargasitic amphiboles, as mentioned above.

Results of Mindata 5 (with modifications as above)

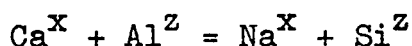
Unit	FHA	FED	FRI	A	Other
SM1	3	4	2	3	MY(1)
SM2/3		4		2	
SM4	5	12	1	4	MY(1)
SM5	6	6	1	1	
HY	6	1			
SM6				1	

FHA=ferrohastingsite, FED=ferroedenite, FRI=ferrorichterite.

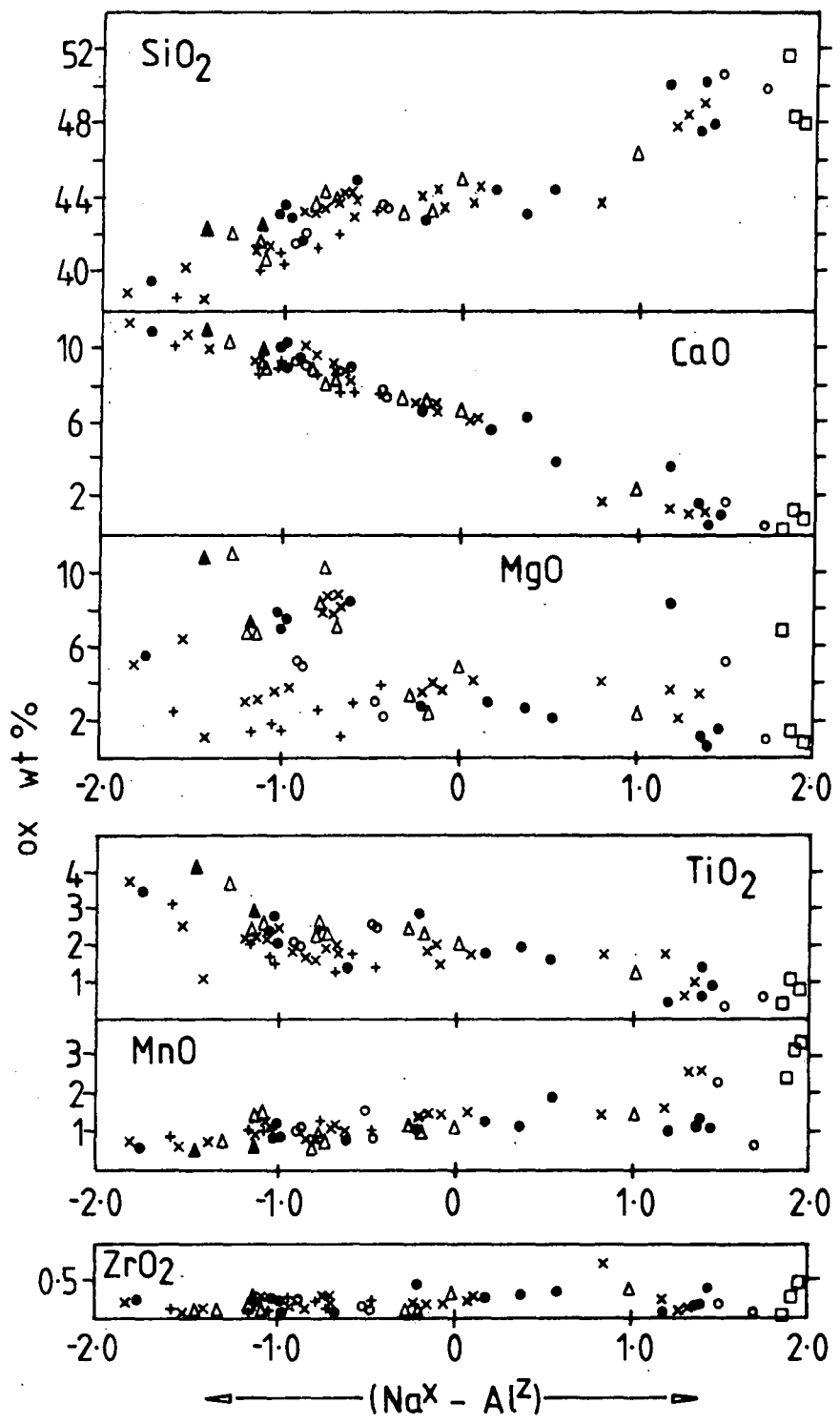
The general trend FH-FE-FR-A, is identical to that seen in the North Qôroq Centre (Chambers 1976) apart from the absence of ferropargasite. The trend is well represented by SM1, which contains fewer basic pyroxenes than other units. This presumably implies conditions of relatively high $P_{\text{H}_2\text{O}}$ such that amphibole adopts the role of pyroxene by removing Ca, Mg and Fe from the melt, in which case the peripheral disposition of much of SM1 may be significant.

4.3.C. Amphibole chemistry

The major substitution occurring in the Motzfeldt amphiboles is



and is identical to that described by Chambers (1976) from North Qôroq and occurs in the other Igaliko centres. It is also the dominant substitution affecting amphiboles from the Ilímaussaq Intrusion (Rowbotham 1973; Larsen 1976) and parts of the Nunarssuit complex (Anderson 1972).



- = SM1
- = SM2/3
- x = SM4
- ▲ = SM5*
- △ = SM5
- + = HY
- = SM6

Fig. 4, 10: Amphibole

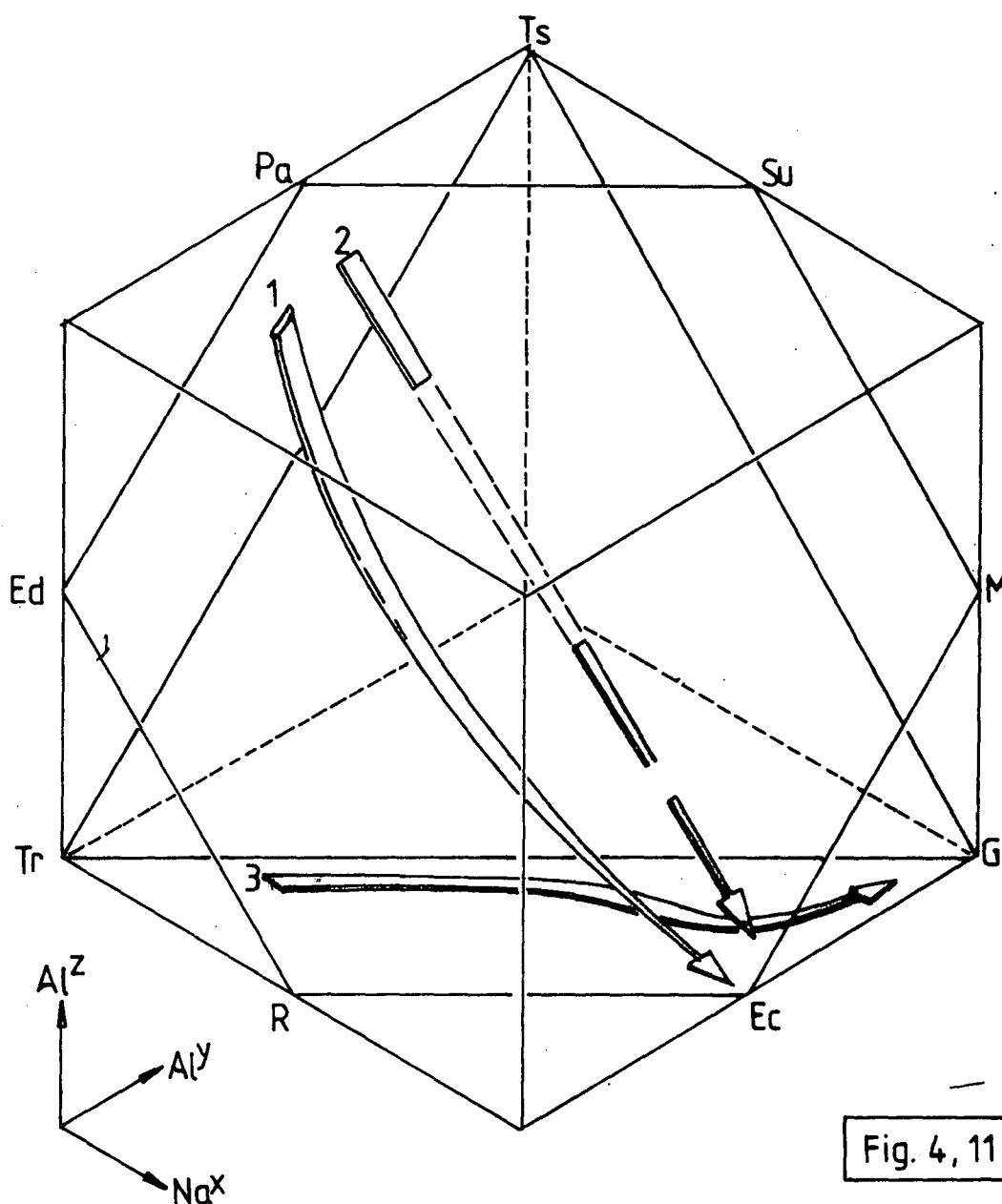


Fig. 4, 11

Generalised trends in amphibole crystallisation.

1 = Motzfeldt (this work); 2 = Ilímaussaq* ;

3 = Tugtutôq*

*Rowbotham (1973)

(for end-member abbreviations see Fig. 4, 9)

Consequently, the variation in amphibole chemistry has been portrayed against the index $\text{Na}^{\text{X}}\text{-Al}^{\text{Z}}$ as used by Chambers (1976) with the result that SiO_2 and CaO show a steady increase and decrease respectively (Fig. 4,10).

In the majority of the early amphiboles, and practically all of the later ones, the A site is full ($\text{Na}^{\text{A}} = 1.0$ in the Phillips system) in accord with the work of Chambers (1976). This is apparently at variance with the observations of Helz (1973) who finds that for a constant composition of host, the A site occupancy decreases with falling temperature. However, both Helz (1973) and Jakes and White (1972) and Wills (1974) have all shown that there is a correlation between A site occupancy and whole rock alkali content.

The systematic trend of falling TiO_2 with falling Al^{Z} content, agrees with the observations of Helz (1973) and suggests falling temperatures of crystallisation with increasing fractionation, although Helz further points out that increasing oxygen fugacity ($f\text{O}_2$) can have similar effects. Beddoe-Stephens (1977) emphasises that this could in part be due to the stabilisation down-temperature of Fe-Ti oxides. Cawthorn (1976) maintains that TiO_2 is also proportional to total pressure.

There is a general decrease in MgO with increasing $\text{Na}^{\text{X}}\text{-Al}^{\text{Z}}$ (Fig. 4,10) and a corresponding increase in total iron. In detail, amphiboles from HY have consistently low MgO contents and amphiboles from SM5 may show a wide range of MgO for similar values of $\text{Na}^{\text{X}}\text{-Al}^{\text{Z}}$. In his study of natural amphiboles, Cawthorn (1976) finds that MgO generally increases with falling temperature and that the ratio MgO/FeO also rises.

Manganese increases gradually with fractionation (Fig. 4,10) and also tends to increase towards the edges of zoned crystals. The most fractionated amphiboles display rather sporadic MnO contents, perhaps reflecting the presence or absence of a discrete Mn-phase on the liquidus prior to crystallisation of the amphibole, or perhaps reflecting variable partition coefficients. Arfvedsonitic amphibole from SM6 is rich in MnO (2.64 wt% MnO) and apparently crystallised before interstitial manganoan-pectolite in

some lujavrites.

Potassium remains more or less constant, and averages around 1.5 wt% K_2O for all of the amphiboles, having a total range from 1.18 to 2.26 wt% K_2O . According to Cawthorn (1976) high Na_2O and high Na_2O/K_2O in amphibole are both signs of relatively low pressure crystallisation.

Zirconium is usually present in small amounts (Fig. 4,10) but varies unpredictably. The amount of zirconium in any amphibole is invariably less than that in the coexisting pyroxene. Similarly, Larsen (1976) found that Zr in amphibole is approximately half the amount found in coexisting pyroxene from the Ilímaussaq Intrusion. The amount of Zr in amphibole from SM6 is below the detection limits of the electron microprobe (at least on the sample analysed), which is perhaps to be expected since this amphibole formed after eudialyte.

A summary of the Motzfeldt amphibole trend in the Phillips (1966) compositional space is shown in figure 4,11 with trends for Tugtutôq and Ilímaussaq inserted for comparison (data from Rowbotham 1973).

4.4. Biotite

4.4.A. General

Biotite is only a minor phase in most of the Motzfeldt syenite and for this reason few analyses have been made. However, these cover a representative range of rock types in Motzfeldt, excluding SM6 which is biotite-free.

Biotite is most prominent in the lardalites of SM5, where its coppery colour is evident in hand specimen. In this unit, which shows strong affinities to augite syenite related magmas described from the other Igaliiko centres (eg: Chambers 1976), biotite (x=straw yellow y=z=dark brownish red) forms large anhedral plates (to 1-2cm) and radiating sheaves which mantle Fe-Ti oxides and olivine. Slightly paler biotite (x=orange brown y=z=red brown) may occur as a minor phase in SM2, 3 and 4. Unit HY contains similarly coloured biotite in rather

Figure. 4,12. Biotites from Motzfeldt.

ng = Locus of biotites from the North Qôroq
Centre (Chambers 1976).
k = trend of biotites from Klokken (Parsons
1979).

x = Alkali gabbro
▲ = Unit SM5*
Δ = Unit SM5
● = Unit SM3
◆ = Unit SM4
○ = Unit HY

$Al^{iv} = (Al + Ti)^{iv}$ from the anhydrous analysis.

Note the trend towards increasing Fe/Fe+Mg, increasing Mn and decreasing Ti and Al^{iv} with increasing FI of the host rock (ie: Alkali gabbro → syenite). Na_2O appears to decrease with decreasing Al^{iv} .

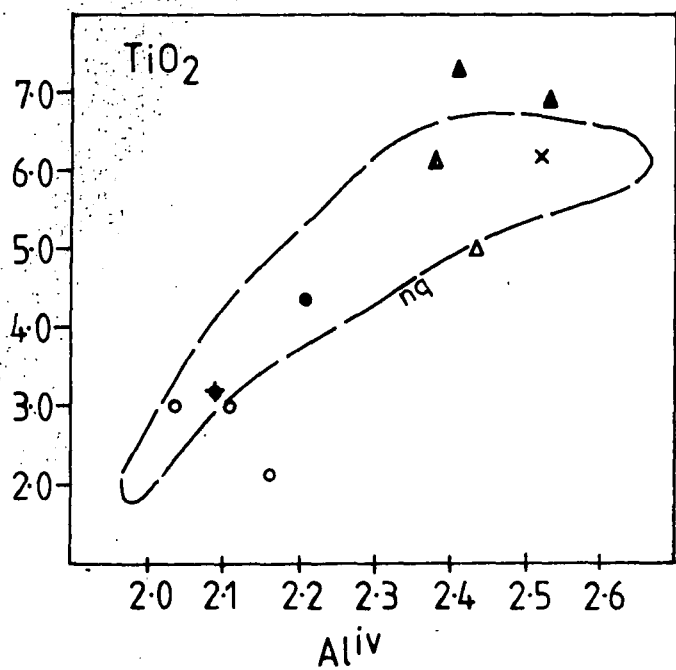
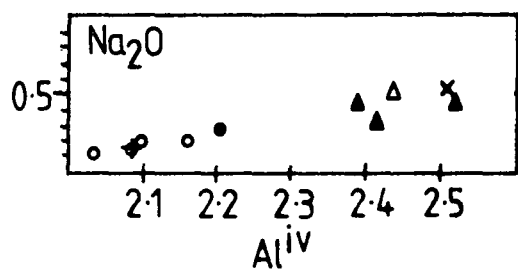
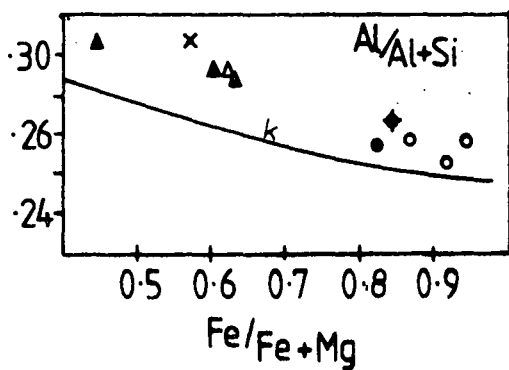
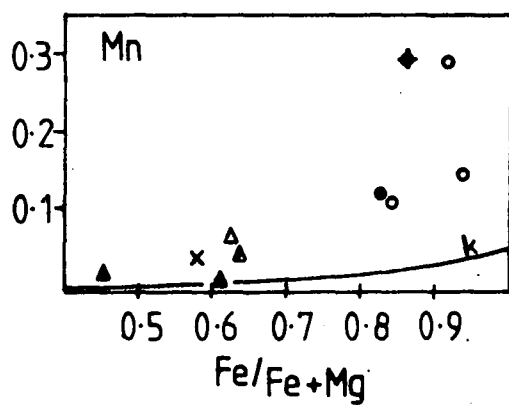
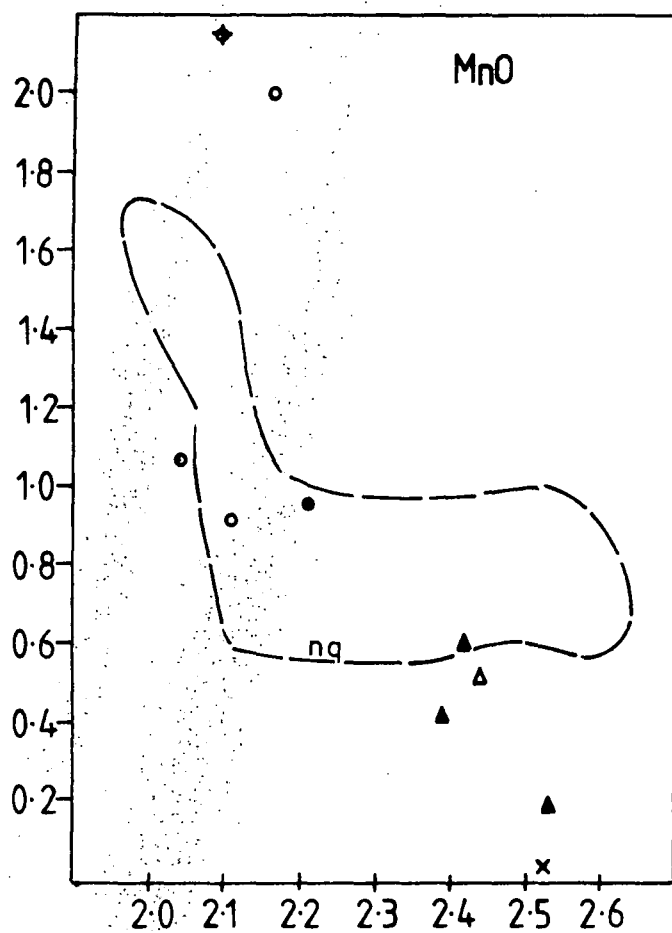
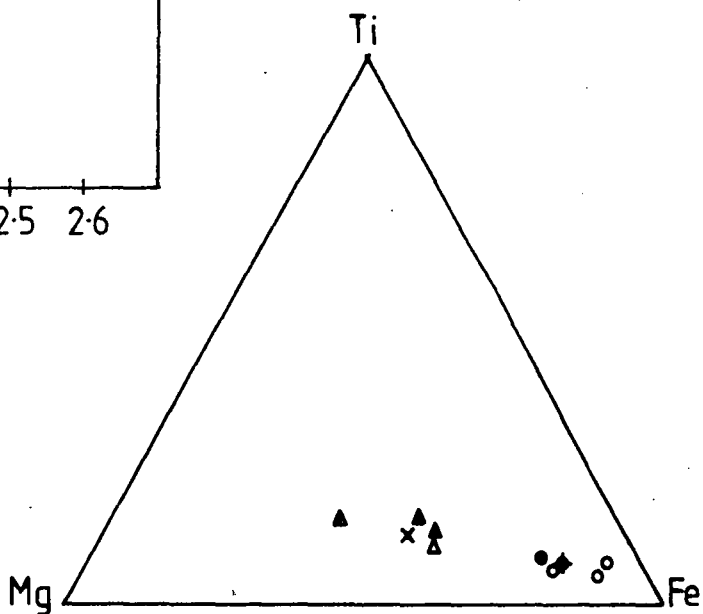


Fig. 4, 12: Biotites



greater abundance, achieving perhaps 2-3 modal% in some samples, with greenish biotite equally common in other rocks of HY (x=pale brown y=green brown z=dense green brown). According to Deer et al (1963) red-brown biotite can be caused by high Ti, whereas green biotite may attest to high Fe^{3+} contents.

4.4.B. Chemical variation

A general formula for biotite is $\text{X}_2\text{Y}_{4-6}\text{Z}_8\text{O}_{22}(\text{OH},\text{F})_4$ and is referred to in the following discussion. Since ferric iron has not been determined, all of the iron is considered as FeO in distributing ions between lattice sites. In accord with the findings of Chambers (1976) for biotites from the North Qôroq Centre, the octahedral Y site has less than 6 cations, which may suggest that the biotites are intermediate between micas with 6 octahedral cations and micas with 4 octahedral cations. There is considerable variation in the Al content of the tetrahedral (=Z) site with a coupled decrease in Al^{Z} and increase in Si^{Z} , as the fractionation index of the parent rock increases (vis; alkali gabbro-larvikite-lardalite-syenite-nepheline syenite).

$\text{Fe}/(\text{Fe}+\text{Mg})$ decreases uniformly with decreasing Al^{Z} such that $\text{Al}/(\text{Al}+\text{Si})$ decreases with increasing $\text{Fe}/(\text{Fe}+\text{Mg})$ in figure 4,12 . The trend for biotites from the Klokken Gabbro-Syenite Complex has been inserted for comparison (Parsons 1979).

Both Ti and Mn vary systematically with Al^{Z} and $\text{Fe}/(\text{Fe}+\text{Mg})$, TiO_2 decreasing and MnO increasing with increasing fractionation. TiO_2 descends from a maximum of 7.3 wt% to 2.1 wt%, whilst MnO increases from 0.2 wt% to a maximum value of 2.7 wt% in unit HY, representing 7.0 mole% of the manganophyllite (Mang) end-member compared with $\text{Mang}_{1.0}$ from Klokken (Parsons 1979) and $\text{Mang}_{4.5}$ from the soda syenites of Shonkin Sag (Nash and Wilkinson 1970). The corresponding loci of data from the North Qôroq Centre have also been superimposed for comparison (Chambers 1976).

Of the minor elements, sodium (Na^{X}) appears to decrease uniformly from 0.51 to 0.14 wt% Na_2O with decreasing

Al^Z , although there are barely sufficient analyses to justify this observation (see fig. 4,12). CaO is low, and generally less than 0.1 wt%. Zr was detected only in one sample, which at 0.008 wt% ZrO_2 can be considered to be effectively absent.

4.5. Feldspar

4.5.A. General

A considerable variety of feldspar types can be found in the Motzfeldt Centre. The bulk of these are "hypersolvus" alkali feldspars, which crystallised from syenite magmas whose temperature upon intrusion was above the feldspar solvus. These show a diversity of subsolidus unmixing and are often flattened parallel to (010). Plagioclase feldspar is found in the alkali gabbro, where it is an early crystallising phase and is also present as rare cores to cryptoperthitic alkali feldspar in the larvikite SM5*. The latter dark coloured feldspar may show an iridescent schiller in hand specimen in SM5* and are reminiscent of feldspars in rocks from the type locality to the southeast of Oslo (Smith and Muir 1958).

In general, the feldspars have been analysed for their average bulk composition. This was achieved by oscillating the beam of the electron microprobe in either a vertical or horizontal plane, depending on the orientation of the crystal under study. Since the "line scan" is infinitely variable from a few microns to several millimetres in width, all but the coarsest of perthites could be analysed. Usually each analysis represents an average for a particular crystal which has been checked at one or two positions along or across its length. Variations in composition between different feldspars within the same probe section were examined a few times, and were found to be relatively small (c. \pm 2-3 mole%). Samples showing a considerable range in composition were found in the porphyritic marginal variants of SM2, 3 and 4 and also in unit HY and are described below.

Strictly speaking, most of the alkali feldspars

from the Motzfeldt Centre are "mesoperthites" according to the nomenclature of Smith (1974, vol.2). However, it is more convenient to use the terms micro- and cryptoperthite for optically visible and sub-optical intergrowths respectively, as advocated by Parsons (1978) and implicit in many of the earlier accounts from the Gardar province. The white lujavrites from SM6 contain the coarsest perthites with each original crystal now consisting of two or three broad areas of nearly pure microcline and albite, the microcline tending to be situated towards the cores. These, and coarse perthites found near the external margins of unit SM1 are similar to "patch perthites" described by Parsons (1978).

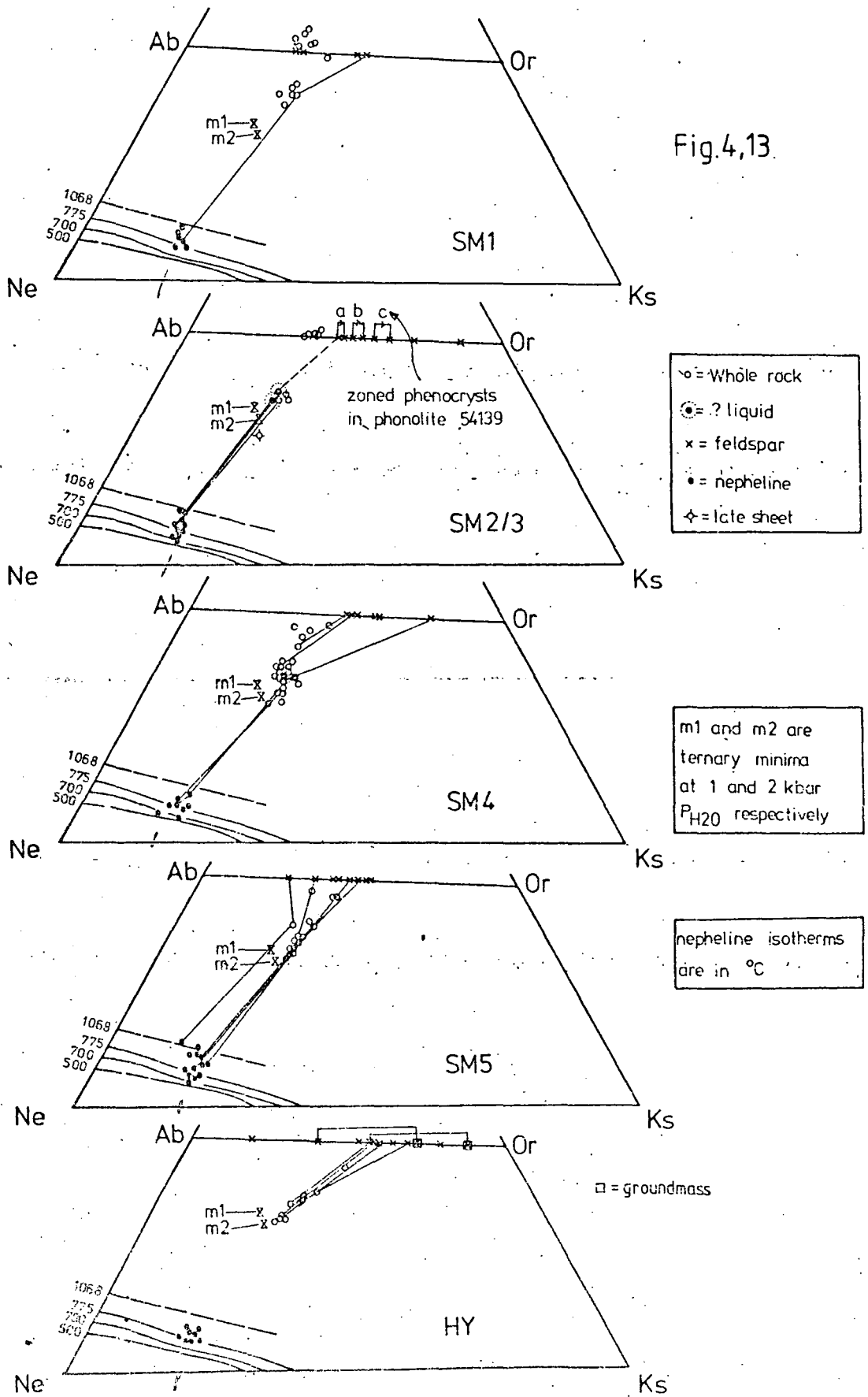
4.5.B. Compositional variation and zoning

Samples showing a considerable range in orthoclase (Or) content are found in the phonolitic margins and in unit HY. The analyses of three separate phenocrysts from the marginal phonolite of SM2 (sample 54139) are plotted in terms of Ab-Or-An in figure 4,13 as "A", "B" and "C" indicating the direction of zonation from core to rim. The feldspars from this sample vary from apparently homogenous crystals to those which show what appear to be two generations of exsolution (see plate 2, chapter 2) and several have rather lobate margins, which appear to grow directly into the groundmass. With increasing distance from the margin, SM2 becomes coarser-grained and the feldspar resembles more normal microperthitic types, although slight optical zonation may still be apparent. This zonation towards K-rich rims is reminiscent of anorthoclase cores zoned to sanidine-rich rims observed by Lippard in phonolites from the Kenya Rift (1973) and can be seen in other trachyte-phonolite lavas (eg: Nash et al 1969). The variety of initial compositions in sample 54139 may suggest an originally heterogeneous source.

Discontinuous zoning from plagioclase cores to increasingly K-rich feldspar rims is sometimes shown by SM5*. In SM5 in general, there is a reduction in CaAl (the

anorthite component) and a straightforward increase in K/Na of the feldspar. The anorthite content is consistently a little higher in feldspars from SM5* and SM5, than from any other of the intrusive "SM" units. This is in agreement with the experimental predictions of Bowen and Tuttle (1950) and Schairer and Bowen (1947) in the system $\text{CaAl}_2\text{Si}_2\text{O}_8$ - $\text{NaAlSi}_3\text{O}_8$ - KAlSi_3O_8 as summarised by Carmichael et al (1974), in that sanidine (K-fsp) coexisting with plagioclase, will contain more $\text{CaAl}_2\text{Si}_2\text{O}_8$ (An) than a sanidine of otherwise similar composition crystallising by itself. The rapid or discontinuous zonation from plagioclase cores to K-rich rims is rather typical of fractionating augite syenite and related magmas found throughout the Gardar province and in other of the Igaliko centres in particular (eg: South Qôroq, Stephenson 1974; North Qôroq, Chambers 1976). Feldspars from oversaturated alkaline magmas where there is no feldspathoid, and from augite syenites where only small amounts of interstitial nepheline are found, tend not to cross the plagioclase/alkali feldspar field boundary at 5 kbar (Yoder et al 1957). However, they frequently move down the cotectic towards the minimum-melt composition on the Ab-Or join (Kûngnât, Upton 1960; Tugtutôq Central Complex, Upton 1964; Loch Ailsh, Parsons 1965; Klokken, Parsons 1979). SM5* and SM5 cross this cotectic. Two reasons for this may be related to nepheline crystallisation. Firstly, co-precipitation of nepheline with alkali feldspar may cause an increase in the K/Na ratio for subsequent feldspar. Since nepheline is clearly an early-formed phase, as witnessed by its occasional intergrowth with clinopyroxene (see plate 1, chapter 2) and its existence as phenocrysts, this seems quite feasible. Secondly, nepheline may be exsolved from the feldspar and is seen as rounded blebs in optical continuity. Widenfalk (1972) suggests that this is due to an initial SiO_2 deficiency in the feldspar. Whatever the reason, this exsolution probably takes place quite early in the subsolidus history of the feldspar (cryptoperthitic) and must presumably increase the K/Na ratio of the remaining feldspar. Alternatively, as pointed out by Chambers (1976), the position of

Fig.4,13



plagioclase-alkali feldspar cotectic may be irrelevant for magma which has undergone feldspar fractionation in the absence of a plagioclase^(Anorthite) component, and is perhaps indicated by the xenocrystic appearance^(i.e. totally unrelated origin) of any plagioclase cores.

The contrast between phenocryst and groundmass feldspar composition in unit HY is perhaps to be expected, given their different modes of origin. The K-rich nature of feldspar from the groundmass (microsyenite) is consistent with a residual composition for that liquid and with an origin by partial melting in-situ of the earlier nepheline syenite, and concides with high concentrations of Rb in samples consisting predominantly of the microsyenite host (see section 5.10.). The striking absence of any sodic feldspar in certain samples, yet which still contain plentiful nepheline, could be consistent with removal of some Na, perhaps as a Na-rich fluid phase, as perhaps suggested by the sporadic and locally common late stage occurrence and replacement textures of volatile-rich phases in HY.

Similar overall K-enrichment of the alkali feldspars has been demonstrated for foyaites from the South Qôroq Centre by Stephenson (1976), who favours a process of depletion of the liquid in Na/K by early co-precipitation of nepheline, causing a complementary late build up of K in feldspar.

4.5.C. Subsolidus unmixing

Following their initial crystallisation, the Motzfeldt feldspars continued to cool relatively slowly under subsolidus conditions. This resulted in the unmixing into separate K- and Na-rich phases, concordant with increased Al-Si ordering and the development of a perthitic texture. The degree of ordering in the feldspar can be considerably influenced by volatile fluxes, as shown by Emeleus and Smith (1959). Ferguson (1970) has shown that marked structural differences between feldspars of the Ilímaussaq augite syenites and agpaites, may be attributable to higher volatile pressures in the latter. Stephenson (1976) draws

the same analogy between augite syenites and foyaites from the South Qôroq Centre and concludes that the lower structural state and coarser perthites of feldspars in the foyaites reflect a higher water/volatile content coupled with lower crystallisation temperatures and slower cooling in the latter. More recently, Parsons (1978) has elaborated upon the role which fluids may play in determining the exsolution textures of plutonic feldspars. Here, he stresses the relationship between increasing feldspar/fluid interaction and increasing Al-Si order. With particular reference to the Klokken intrusion (Parsons 1978, 1979) he concludes that fluids are the primary factor in determining exsolution textures and framework structural state variation, whilst specific thermal events and cooling rate are not necessarily very important.

4.5.D. Conditions of T and P_{H_2O}

The feldspars of the syenites are hypersolvus and consistent data for both the feldspar solvus and the solidus (liquidus) now exist, enabling estimates of the minimum temperature and maximum P_{H_2O} of crystallisation to be made. At lower temperatures or with greater P_{H_2O} , the solidus would intersect the solvus and two separate feldspars would form, as may be the case for the lujavrites. Data for the solvus was obtained from Smith and Parsons (1974) and can be extrapolated from the pressure of 1 kbar at which it was determined, to higher pressures by the application of their recommended factor of 16°C/kbar . A further correction of $33^\circ/\text{mol\% An}$ was applied in accordance with the findings of Bachinski and Muller (1971). Thus, composition-dependent data exist for both the liquidus and the solvus. This enables a minimum temperature of formation (T_{\min}) to be determined from an average bulk feldspar analysis, which in turn allows an estimation of the maximum P_{H_2O} ($P_{H_2O.\max}$). In practice, this was achieved graphically, using a P-T graph contoured for solvus and liquidus at specific compositions. The results for the various units are tabulated below.

<u>Unit</u>	<u>Max value of T_{\min}</u> (°C)	<u>Min value of $P_{H_2O \cdot \max}$</u> (bars)
SM1	705	2950
SM2	650	4200
SM3	665	3950
SM4	675	3600
SM5*	815	1200
SM5	780	1400

Although not really very informative, it is evident that the cryptoperthitic feldspar from units SM5* and the margins of SM5, ^{certainly} crystallised at relatively high temperatures and under conditions of comparatively low P_{H_2O} , and the rest of the syenite units, might have. This is entirely in keeping with the findings of Chambers (1976) for similar augite syenites from the North Qôroq Centre. The single feldspar found in the white lujavrites, now of near end-member Ab and Or exsolution in a coarse "patch" perthite, suggests initial crystallisation at moderately high temperatures, followed by a long cooling interval under conditions of high P_{H_2O} . Crude estimates of the initial cover above the Motzfeldt Centre at the time of its inception, based on normative mineralogy and the existence of an originally thick lava pile, suggest an upper limit of $P_{H_2O} = 2$ kbars. With this in mind, it is unlikely that P_{H_2O} could have exceeded this value, since normally $P_{H_2O} < P_{\text{total}}$, although Chambers expresses his suspicion that P_{total} may be exceeded (1976), but then one might expect to see some visible expression, perhaps in the form of vesiculation (drusy cavities) and these have not been observed. Certainly the two primary feldspars observed in the dark lujavrites would be capable of crystallising under conditions of high P_{H_2O} , perhaps in excess of 3 kbars, and infer low temperatures of crystallisation, possibly around 400 °C. This does not agree with findings of Sood and Edgar (1970), who indicated that feldspar forms at high temperatures from a melt of lujavritic composition, even at pressures of about 2 kbars ($T=880^\circ\text{C}$).

4.6. Nepheline

4.6.A. General

Nepheline is a major phase in the vast majority of the Motzfeldt syenites and may constitute up to about 50 % of the mode. As well as forming euhedral and subhedral crystals, it also occurs as interstitial stringers and as blebs in some of the feldspars. Phenocrysts of nepheline are characteristic of the phonolitic margins to SM2, 3 and 4 and are also recognisable in several of the xenolithic rafts of lavas. Abundant small nepheline euhedra are also prominent in the dark lujavrites and are common throughout SM6. An interesting variation in nepheline habit can be traced with increasing fractionation through the larvikites and lardalites of SM5* and SM5. Firstly, nepheline occupies small interstitial positions and occurs as a few blebs in the cryptoperthitic feldspars. The amount of nepheline exsolved from the feldspars increases and in some cases appears to approach the maximum value of 13-14 mole% Ne reported from the Oslo larvikites by Widenfalk (1973). Finally, the proportions of interstitial nepheline increase and fairly large anhedral areas of nepheline become common in the lardalites. Occasionally, nepheline and clinopyroxene from SM5 display a feather-like intergrowth, developed from interlocking edges of nepheline and clinopyroxene (salite) on a 1/10 to 1/100mm scale (see plate 1, chapter 2) and is consistent with separate geothermometers for each which suggest temperatures of formation of about 1000 °C (using the nepheline geothermometer of Hamilton, 1961; and the olivine-clinopyroxene geothermometer of Powell and Powell, 1974).

4.6.B. Compositional variation

The analysed nephelines are plotted in the customary system Ne-Ks-Qz, where Qz is often referred to as "excess silica" and represents the amount of silica in solid solution which is superfluous to the needs of Na and K in the general formula $(\text{Na},\text{K})\text{AlSiO}_4$. The amount of excess silica is temperature dependent and has been established

as an empirical geothermometer by Hamilton (1961), whose isotherms are included in the diagram Ne-Ks-Qz (Fig. 4,14 and 4,13). This geothermometer relies on an accurate analysis, especially of silica and is also liable to subsolidus re-equilibration of Na, K and Al with feldspar. Stephenson (1973) notes that the geothermometer may be inapplicable where nepheline coexists with sodalite.

Nephelines generally change their compositions in two ways (Tilley 1954); the Si/Al ratio decreases with falling temperature and subsolidus exchange of Na and K may occur. In the latter, nepheline compositions tend towards an ideal ratio of Na/K=3:1 and approach the Buerger theoretical composition of $\text{Na}_3\text{KAl}_4\text{Si}_4\text{O}_{16}$. Most of the Motzfeldt nephelines do not fall between the Morozewicz theoretical rock composition ($\text{Na}_{6.1}\text{K}_{1.52}\text{Al}_{7.62}\text{Si}_{8.38}\text{O}_{32}$) and the Buerger composition, a feature which is seen in nephelines from other plutonic syenites (eg: South Qôroq Centre, Stephenson 1976; North Qôroq Centre, Chambers 1976; Kangerdlugssuaq, Kempe and Deer, 1970). This suggests that subsolidus exchange has been minimal, and therefore the compositions do reflect temperatures of crystallisation.

Upon inspection (Fig. 4,14), it is apparent that the analyses tend to cluster around temperatures of 800 °C or so, comparing favourably with other of the Igaliko centres. Units SM5* and SM5 display a wide range of temperatures, which are more or less consistent with the observed variation in habit and may indicate slight lowering of liquidus temperatures. As mentioned earlier, the nepheline coexisting with clinopyroxene in a lardalite from SM5, suggests temperatures of around 1000 °C. Nepheline phenocrysts from the lujavrites suggest temperatures ranging from around 850 °C to below 500 °C. At these lower temperatures, it is very likely that some re-equilibration of Na and K has occurred, especially since sodalite is a rather common accessory in the lujavrites and can show replacement of nepheline.

Partial hydrous alteration of nepheline to the micaceous or clay-like aggregate gieseckite is locally

Figure. 4,14. Motzfeldt Centre nephelines in the system Ne-Ks-Qz

Isotherms are after the geothermometer of Hamilton (1961) and are in °C.

"M" = the theoretical Morozewicz composition of rock-forming nepheline ($\text{Na}_{6.1}\text{K}_{1.52}\text{O}_{0.38}\text{Si}_{8.38}\text{O}_{32}$). "B" = theoretical Buerger composition ($\text{Na}_3\text{KAl}_4\text{Si}_{16}$).

(---) = locus of majority of nephelines from Motzfeldt

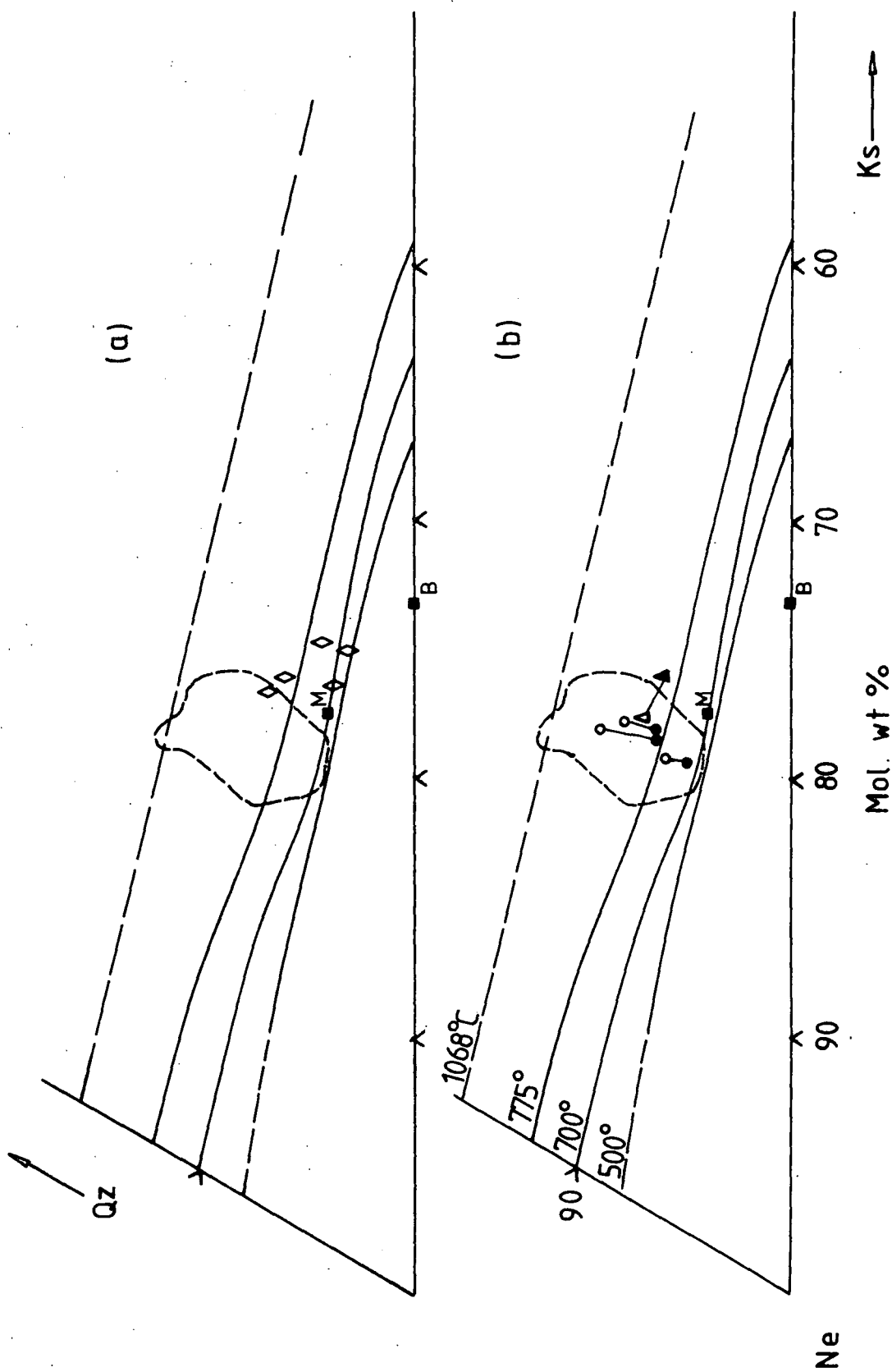
(a) \diamond = SM6 (lujavrites). Note departure from the principle field and trend towards "B".

(b) Zoned nephelines:

• = rim and ◦ = core of nephelines from phonolite margin, SM2.

▲ = rim and Δ = core of zoned crystal from microsyenite, HY

Zonation in HY is particularly common, though not always of significant compositional variation. Nephelines from HY tend to cluster around 775 °C (see Fig. 4,13), perhaps suggesting that they have all been "re-set". Nephelines from recrystallised samples of SN5 in the South Qôroq Centre show similarly uniform and relatively high temperatures to the other units (Stephenson 1976).



common, an analysis of which is given by Chambers (1976). Replacement by natrolite, sodalite and analcite are locally common and particularly in the lujavrites. Cancrinite is a minor phase in unit HY and appears to partly replace nepheline.

Minor elements

Apart from the major elements of Na, K, Al and Si, the nephelines contain small amounts of iron, possibly as Fe^{3+} replacing Al^{3+} , with up to 0.8 wt% Fe_2O_3 being quite common. Calcium is invariably low and usually less than 0.1 wt% CaO, although nephelines from the margin of SM5 contain up to 0.71 wt% CaO (3.5 mole% An). There is no measurable difference in the minor element composition of the nepheline exsolved as blebs from feldspar and interstitial nepheline from the same sample. That the host feldspar is relatively Ca-rich agrees with the observations of Chambers (1976) and supports the conclusions of Widenfalk (1973) that increased Ca in feldspar will inhibit the solid solution of nepheline and so promote its exsolution.

4.6.c. Additional

In unit SM5, nepheline tends to become more abundant away from the margins, though this is not in general true of the other syenite units. However, there is a definite tendency for nepheline to be significantly more abundant where emplacement of a unit has been adjacent to older rocks which are themselves undersaturated. Thus, for example, unit SM4 is particularly rich in nepheline where it cuts nepheline syenites of the North Qôroq Centre. Several reasons for the presence or absence of nepheline in the syenites are considered in section 5.3. This includes a discussion of the variation with structural height and the apparent interaction of rafts of xenolithic lavas with syenite magma.

4.7. Aenigmatite

4.7.A. General

This mineral is perhaps best seen in the porphyritic phonolites of SM2, where dark brown poikilitic crystals enclose tiny euhedral feldspars and nephelines. Rather corroded grains of Fe-Ti oxides can be found at the cores to this aenigmatite. It occurs quite frequently in accessory proportions in the more fractionated nepheline syenites, usually as rather small interstitial or late-formed crystals which may again have cores of corroded Fe-Ti oxides. Certain samples from the more evolved parts of SM5 possess quite large anhedral areas of dark brown-black aenigmatite which may measure several millimetres across, and may enclose smaller crystals of felsic minerals and pyroxene.

Although few analyses have been made, the presence of aenigmatite is instructive in conveying information about the physico-chemical conditions of the magma from which it crystallised.

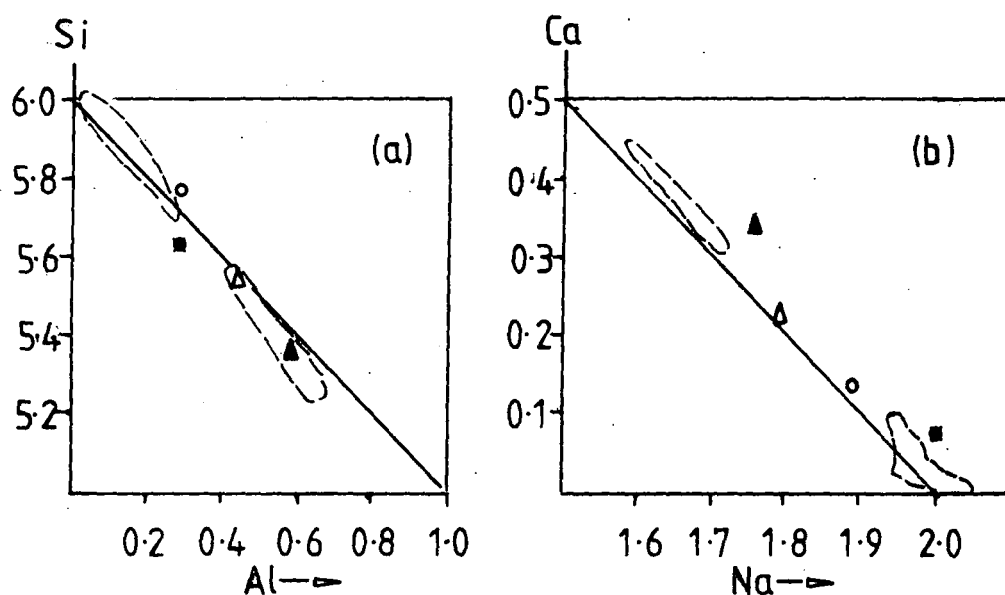
4.7.B. Chemical variation

The theoretical formula for aenigmatite, as used by Larsen (1977) is $X_2Y_6Z_6O_{20}$. In natural aenigmatites, Si+Al usually amount to less than the theoretical 6 atoms in Z and it has been suggested by previous workers that Fe^{3+} may also be in 4-fold coordination (Larsen 1977; Deer et al 1978). The aenigmatites analysed from Motzfeldt are affected by identical substitutions to those described by Larsen from the Ilímaussaq Intrusion (1977). These principally involve Al, Si and Na with Ca in a coupled substitution of the type



in which Ca and Al decrease from core to rim in the zoned aenigmatites from Ilímaussaq. The reader is referred to the work of Larsen (1977) for a more complete appraisal of the naturally occurring substitutions in aenigmatite.

Figure 4,15 shows the variation in Si with Al and in Ca with Na, and outlines the fields of aenigmatite



○ = locus of aenigmatites from Ilímaussaq (Larsen 1977)

(a) atoms/formula unit, line of slope $\text{Si} + \text{Al} = 6.0$

(b) " " " , line of slope $\text{Na} + \text{Ca} = 2.0$

▲ = AM43, large anhedral (SM5)

△ = AM82, late anhedral (SM5)

■ = AM7, late int'stit' (SM4)

○ = 58066, large anhedral (SM4)

Fig. 4,15

Aenigmatites.

from Ilímaussaq. Ca and Al are highest in a large anhedral aenigmatite from a rather basic syenite of SM5 (sample AM 43 with FI=83) which would not disagree with the observation of Larsen (1977) that high Ca^{x} and Al^{z} may be due to the combined effects of low silica activity and relatively high crystallisation temperatures.

Of the minor elements, MgO is higher than recorded at Ilímaussaq (to 0.82 versus 0.03 wt% MgO) and ZrO_2 is at a similar low level of 0.1–0.2 wt%. Manganese increases with fractionation and attains higher values at Motzfeldt (1.75 to 2.72 wt% MnO) than are found in otherwise similar aenigmatites from Ilímaussaq (c. 0.68 to 0.87 wt% MnO). The increase in manganese may be caused by decreasing temperature, as is the case for oxides (Lipman 1971) or by rising $f\text{O}_2$ (Larsen 1977). The higher total MnO contents at Motzfeldt probably reflect higher initial Mn contents of the magmas. Chambers (1976) relates high Mn contents in aenigmatites of recrystallised rocks in the North Qôroq Centre, to initially high Mn in the Fe-Ti oxides which they appear to have replaced.

4.7.C. Conditions of formation

The existence of a "no-oxide" field in $f\text{O}_2$ -T space in phonolitic liquids inferred by Marsh (1975), is readily supported by aenigmatite rimming and replacing titanomagnetite, as seen both at Motzfeldt and North Qôroq (Chambers 1976) and reported at some length from Ilímaussaq by Larsen (1976). In an experimental Ti-free system, Ernst (1962) found that ferri-aenigmatite ($\text{Na}_2\text{Fe}_4\text{Fe}_2^3\text{Si}_6\text{O}_{20}$) was stable only at conditions of very low $f\text{O}_2$. Further experimental work by Lindsley (1971) showed that aenigmatite can crystallise from a peralkaline magma between 900 and 400 °C at low to moderate conditions of $f\text{O}_2$, being stable to the FMQ buffer and metastable to the NNO buffer. Larsen (1977) argues, largely on textural grounds, that Ti-bearing aenigmatite is stable at higher $f\text{O}_2$ for any given temperature than ferri-aenigmatite.

Aenigmatite in the Motzfeldt Centre, and the North Qôroq Centre (Chambers 1976) is almost invariably accompanied

by acmitic pyroxene and sodic amphibole. Both Nicholls and Carmichael (1969) and Hodges and Barker (1973) attribute the formation of aenigmatite to the peralkaline condition, which Nicholls and Carmichael equate with the activity of sodium disilicate ($\text{Na}_2\text{Si}_2\text{O}_5$) in the liquid.

4.8. Fe-Ti oxides

Although Fe-Ti oxides are often quite common, they are not present throughout all of the units in Motzfeldt, being notably absent from parts of SM2, SM3 and all of SM6. Regrettably, this phase has not been studied in detail. Nevertheless, a comprehensive description of Fe-Ti oxides with similar optical properties in reflected light and from units SN1A, SN4B and SN4B of the North Qoroq Centre, which are broadly similar to units SM5* and SM5 from Motzfeldt, has been given by Chambers (1976). The temperatures which Chambers derives for their crystallisation, of 860-880 °C can probably be approximated to the likely crystallisation temperatures in SM5* and the margins of SM5. In addition, calculations on the Fe-Ti oxides from the Igdlarfigssalik Centre by Powell (1978) have revealed that the temperatures for cessation of macroscopic exsolution in the magmatic grains, are comparable to the cessation of exsolution in the alkali feldspars and lie in the range 670-500 °C.

4.9. Geothermometers

A number of geothermometers have been applied to the Motzfeldt syenites and the results are outlined in the following section.

(a) Olivine-clinopyroxene

An indication of the likely liquidus temperatures for one or two of the major intrusive magmas can be made where olivine coexists with clinopyroxene. The geothermometer of Powell and Powell (1974)* is based on a regular solution model of the iron-magnesium exchange reaction between olivine and Ca-rich pyroxene and is also partly dependent

*but see B.T. Wood (Contrib. Mineral. Petrol. 56, 297-303 (1976)), for criticism of this work.

on the content of trivalent cations in the pyroxene analysis. For this reason, the pyroxene should be recalculated in the manner outlined by Powell and Powell.

It has been possible to derive temperatures for coexisting olivine euhedra and clinopyroxene in the phonolitic margin of SM2, the larvikite ring dyke SM5*, the lardalitic margin to SM5, and for the alkali gabbro. A pressure correction of about 5 °/kbar is inherent in the geothermometer, and a pressure of 2kbars was used. Despite a significant range in the olivine and pyroxene compositions, the results indicate that both the phonolitic and the larvikitic magmas had similar liquidus temperatures, assuming that the temperatures obtained (Ol-Cpx) approximate to the initial magmatic temperatures.

<u>Unit</u>	<u>Sample</u> (description)	<u>Temp</u> ^a (°C)
SM2	54139, phonolitic margin	1010
SM5*	58037, larvikite (FI=59)	1015
SM5*	AM55 , larvikite (FI=69)	996
SM5	AM38 , lardalite margin	1010
SM5	AM39b, lardalite margin	997
SM5	AM40 , lardalite margin	1005
Alkali gabbro. AM149, chill.		1025

^atemperatures for Ol-Cpx geothermometer of Powell and Powell (1974).

(b) Nepheline-alkali feldspar

Using the nepheline-alkali feldspar geothermometer derived by Powell and Powell (1977) it appears that nepheline and alkali feldspar continued to equilibrate with falling temperature after their crystallisation from the magma. This appears to have ceased at lower temperatures in units and samples which show coarse perthitic exsolution and further low temperature assemblages such as zeolites or analcite. Thus, given the inherent temperature uncertainty, which can be considerable (typically \pm 70-130 °C, Powell and Powell 1977), the results still appear to be consistent with other geological considerations.

Three phenocrysts cores from the phonolite SM2, in conjunction with the core analysis of nepheline, give

Table (4) 1. Geotemperatures (all in °C)

Unit	P _{H2O} max ^a (bars)	Fsp.cryst. ^a min.	Ne.cryst. ^b	Ne-Fsp ^c	Ol-Cpx ^d	Notes
SM1	2950	705	850-950	600 ±60	-	normal syenite
SM2/3	3950	665	900-1000	820 ±80 850 ±80 875 ±90 700 ±75	1010	phonolitic margin. three high T's (cores) low T is rim of Fsp & Ne
SM4	3600	675	800-900	650 ±75 600 ±70 780 ±75 725 ±70	-	normal syenites/foyaite
SM5*	1200	815	950-1050	-	995- 1015	larvikite ring-dyke
SM5	1400	780	950-1050	775 ±75 850 ±80 870 ±80 825 ±75	995- 1010	lardalite margin
SM6	-	-	750-850	-	-	nepheline phenocryst
HY			750-850	725 ±75 825 ±75		variable, possible xenocrysts.

^a estimates from composition and solvus/liquidus data (see section 4.5.D.).
cryst=crystallisation temperature.

^b estimate from geothermometer of Hamilton (1961)

^c estimates calculated from geothermometer of Powell and Powell (1977)

^d estimates calculated from geothermometer of Powell and Powell (1974), see section 4.9.

equilibration temperatures of 820-875 °C, whereas their respective margins suggest considerably lower temperatures of equilibration, at around 700 °C. By comparison, samples from unit SM1 in the north of Central Motzfeldt, suggest equilibration continued to lower temperatures of around 600 °C.

(c) Additional

The above geothermometers have been used to obtain temperatures for several units and are summarised in table (4) 1, along with estimates for nepheline crystallisation from the geothermometer of Hamilton (1961)(see Fig. 4,14) and the minimum temperatures of feldspar crystallisation deduced from their composition (see section 4.5.D.)

If the initial cumulus temperatures approximate to the liquidus temperatures of the magmas, then this indicates an extended interval between solidus and liquidus of up to 3-400 °C, as suggested by Powell (1978) for the syenites from the Igdlarfigssalik Centre. Further, since the melting interval (liquidus-solidus) appears to be directly related to the peralkalinity of the melt (Sood and Edgar, 1970; Piotrowski and Edgar, 1970; Edgar and Parker, 1974) an even greater interval may have existed in the more evolved and peralkaline syenites of the Motzfeldt Centre. Thus, presumably the lujavrites of SM6 had the lowest liquidus temperatures and the longest melting interval*, perhaps from about 8-850 to 400 °C.

4.10. Rare earth mineral analyses

4.10.A. General

Six minerals containing significant quantities of rare earth elements (REE elements) with Re_2O_3 ranging from 2.16 to 22.89 wt%, have been comprehensively analysed by electron microprobe. The standards and conditions used are given in Appendix II. The minerals comprise the following; Two samples of eudialyte, the first an interstitial phase in laminated foyaite of unit SM4 (AM49) and the second an interstitial eudialyte from white lujavrite of SM6 (AM159);

* Theory predicts that residual liquids of any fractionation process must have progressively narrower melting intervals.

Table (4) 2. Rare earth mineral analyses

	AM49 eudialyte	AM159 eudialyte	AM51 lavenite	AM81 rinkite	AM84 core rink/lav	AM84 rim rink/lav
Y2O3	a	a	a	2.18	2.09	0.98
SiO2	47.33	46.51	30.30	30.46	31.19	30.04
Al2O3	0.18	0.73	0.01	5.03	1.38	0.19
TiO2	0.15	0.11	0.74	10.41	10.34	6.69
FeO	6.97	6.73	1.53	6.63	0.97	0.82
MnO	2.19	4.59	1.37	0.09	0.79	0.91
MgO	n.d.	0.01	0.05	0.03	0.01	n.d.
CaO	10.40	6.25	30.78	10.18	20.30	28.29
Na2O	12.13	10.79	6.49	1.96	3.12	8.12
K2O	0.17	0.12	0.02	0.15	0.21	0.08
ZrO2	12.52	12.21	17.13	1.47	6.26	9.16
Nb2O5	1.74	2.47	2.63	2.66	3.01	1.61
La2O3	0.49	1.40	0.17	3.46	1.53	0.41
Ce2O3	1.29	2.87	0.49	10.94	5.53	1.52
Pr2O3	0.22	0.39	0.09	1.05	0.63	0.29
Nd2O3	0.41	0.76	0.26	4.36	2.20	0.73
(Pm)						
Sm2O3	0.16	0.26	0.18	0.77	0.51	0.24
Eu2O3	0.01	0.02	0.04	0.16	0.13	0.09
Gd2O3	0.10	0.28	0.15	0.68	0.48	0.25
Tb2O3	0.10	0.16	0.04	0.14	0.16	0.11
Dy2O3	0.37	0.66	0.35	0.69	0.63	0.36
Ho2O3	0.08	0.32	0.10	0.17	0.24	0.18
Er2O3	0.12	0.20	0.13	0.27	0.28	0.24
Tm2O3*	0.04	0.16	0.06	0.04	0.07	0.09
Yb2O3*	0.06	0.26	0.07	0.15	0.25	0.21
Lu2O3*	0.01	0.08	0.03	0.04	0.06	0.07
Total	97.24	98.34	93.21	94.17	92.37	91.68
Re2O3	3.36	7.82	2.16	22.89	12.70	4.79

*error becomes serious in the low levels of the HREE elements. ^apresent but not analysed.

One sample of euhedral colourless l⁸avenite with good twinning (lamellar to cruciform) from laminated foyaite of SM4 (AM51); Core and rim analyses of a yellow zoned to colourless margins, interstitial crystal compositionally intermediate between rinkite and l⁸avenite in nepheline syenite of unit SM5 (AM84); An analysis of rinkite, pale yellow in colour and of subhedral form in nepheline syenite of unit SM5 (AM81). The total REE element contents are summarised below, with the principle elements in order of abundance, for each of the analyses.

Mineral	Sample no.	Principle elements (4.5 ox.wt%)	Re ₂ O ₃
Eudialyte	AM49	Si,Zr,Na,Ca,Fe	3.36
Eudialyte	AM159	Si,Zr,Na,Ca,Fe,Mn	7.82
L ⁸ avenite	AM51	Si,Ca,Zr,Na	2.16
Rinkite/L ⁸ av?	AM84core	Si,Ca,Ti,Zr	12.70
Rinkite/L ⁸ av?	AM84rim	Si,Ca,Zr,Na,Ti	4.79
Rinkite	AM81	Si,Ca,Ti,Fe	22.89

The complete analyses are listed in table (4) 2, and the REE contents, normalised in the customary manner to chondrite abundances (Sun et al 1979) are illustrated in figure 4.16. The analytical errors can become serious for the low abundances of small (heavy) REE, and the precision does in general deteriorate from La to Lu.

REE elements may enter a mineral if it has one or more large cation sites capable of taking trivalent ions. The resulting REE pattern is strongly dependent upon the sizes of those sites (Campbell and Gorton 1980). Typical REE patterns for zircon, for example, suggest two sites, one smaller than Lu and the other larger than La. Where the REE elements are substituted into two closely spaced sites, the resultant trends are flatter than normal, due to the combined effects of the two patterns. Apatite and sphene are examples of accessory phases with this type of pattern. Phases with a single site within the size range of the REE, such as pyrochlore, have a sharp peak centred at the atomic radius of the site. If the site is larger than the largest REE, a long and continuous LREE enrichment

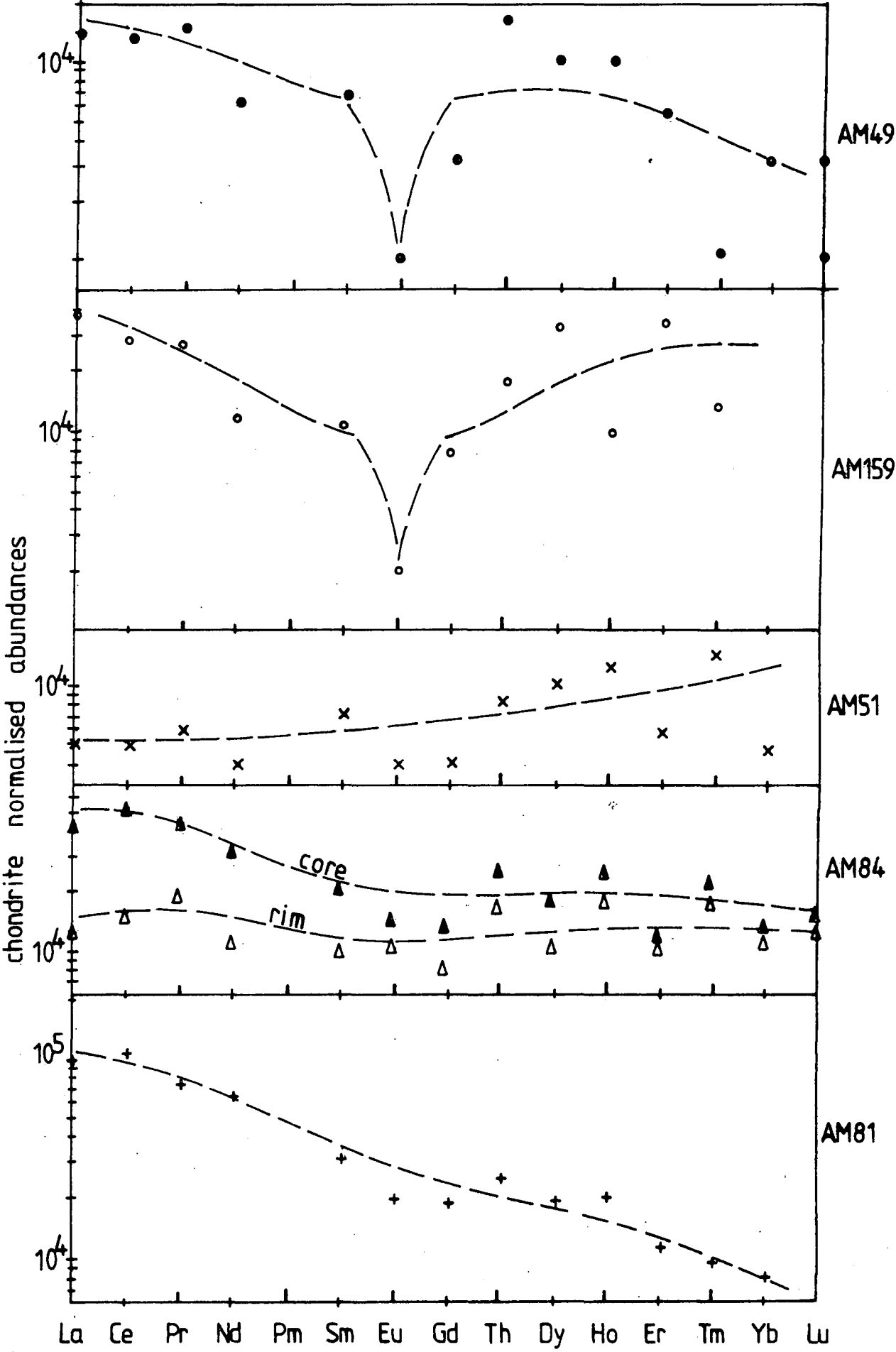


Fig. 4, 16

Table (4) 3. Caption

- (1) Mn-pectolite. Colourless interstitial, one prominent cleavage. Biax +ve. 2nd order biref. AM138, white lujavrite (SM6).
- (2) ?Melanite. Pale green euhedra, low biref. (cf:chlorite), no figure obtained. 63717, syenite (SM3). Some Fe almost certainly as Fe³.
- (3) (?)Pyrochlore. Dark yellow euhedral, isotropic. 63717, syenite (SM3).
- (4) Zircon. Core of euhedral crystal, usual optics. 63717, syenite (SM3).
- (5) Eudialyte. Core of euhedral phenocryst. Optical zonation, concentric anomalous biref. Y present in small amounts. AM164, dark lujavrite (SM6).
- (6) Sphene. Pale brown, high relief, interstitial. AM81, coarse-grained ne-syenite (SM5).
- (7) Sphene. Pale brown, high relief, small anhedral crystal. AM114, ne-microsyenite (HY).
- (8) Nb-rich lavenite. Colourless, moderate relief, low 1st order biref. Biax +ve. 63725, ne-syenite (SM4).
- (9) ?Lavenite/rinkite. Colourless, moderate relief, low 1st order biref to yellow. Interstitial. AM77, coarse-grained ne-syenite (SM5).
- (10) ?Lavenite/rinkite. Colourless, moderate relief, small anhedral crystal, 1st order biref. AM84, coarse-grained ne-syenite (SM5). From same section as analysis in Table (4) 2.

Notes:

Analysis (5) of eudialyte should be compared to AM49 and AM159, also of eudialyte, in Table (4) 2. Further analyses of REE-bearing phases, such as lavenite and rinkite are given in Table (4) 2.

Table (4) 3. Selected mineral analyses

	Mn-pct	Melan	Pyro	Zircon	Eud	Sphene	Sphene	Läv	?Läv/Rin	?Läv/Rin
	(1)	(2)	(3)	(4)	(5)	(6)	(7)	(8)	(9)	(10)
SiO ₂	55.95	34.86	0.12	32.29	49.29	29.42	30.82	30.24	31.71	32.85
TiO ₂	0.02	3.16	7.54	0.15	0.22	37.47	35.60	1.01	9.55	6.22
Al ₂ O ₃	0.11	3.07	0.14	0.05	0.36	0.64	1.93	0.08	1.62	0.21
FeO*	1.07	22.31	0.45	0.27	4.22	1.85	2.08	2.48	0.78	0.60
MnO	15.56	1.41	4.47	0.22	3.49	0.13	0.13	1.78	0.71	0.54
MgO	0.16	0.12	0.11	0.08	nd	0.19	0.13	0.26	0.11	0.03
CaO	16.44	32.08	14.34	0.04	8.53	27.83	26.96	26.33	30.54	28.02
Na ₂ O	8.82	0.30	8.12	0.05	12.48	0.84	0.69	8.40	2.16	7.60
K ₂ O	0.08	0.01	0.02	0.02	0.17	0.03	0.20	0.02	0.01	0.05
ZrO ₂	na	0.71	1.21	66.13	12.99	0.20	0.24	15.09	4.29	13.42
HfO ₂	na	na	na	1.03	na	na	na	na	na	na
Nb ₂ O ₃	na	na	57.30	na	1.61	0.79	na	11.90	3.13	2.10
Ce ₂ O ₃ ^a	na	na	1.50	na	1.54	na	na	na	3.95	1.13
Re ₂ O ₃ ^a	na	na	na	na	2.8	na	na	na	9.35	na
Total	98.20	98.04	95.32	100.33	97.70	99.40	98.75	97.58	98.15	92.77

Recalculations to n oxygens

Si	3.299	5.787	0.008	3.955	5.654	0.983	1.024
Ti	0.001	0.395	0.403	0.014	0.019	0.941	0.890
Al	0.007	0.601	0.011	0.007	0.048	0.025	0.076
Fe	0.053	3.092	0.027	0.028	0.404	0.052	0.058
Mn	0.777	0.198	0.269	0.022	0.339	0.004	0.004
Mg	0.014	0.030	0.011	0.014	0.000	0.009	0.004
Ca	1.039	5.706	1.093	0.005	1.049	0.996	0.960
Na	1.008	0.097	1.119	0.012	2.890	0.055	0.044
K	0.006	0.002	0.002	0.004	0.025	0.001	0.008
Zr		0.058	0.042	3.951	0.727	0.003	0.004
Hf				0.036			
Nb			1.976		0.095	0.014	
Ce ^a			0.039		0.066		
Re ^a					0.15		
n O	9.000	24.000	6.000	16.000	17.000	5.000	5.000

* total iron

^a total REE other than Ce.

na = not analysed

nd = not detected

GEOCHEMISTRY

5.1. Introduction

The display of major, minor and trace element abundances for any given set of rocks whose temporal relationships are understood can be very instructive. This is especially true of rocks formed by a suite of magmas which have been derived by the repeated withdrawal of liquids from some reservoir where successive crops of crystals have been removed. At each stage any given liquid may constitute a new reservoir, which may in turn fractionate to yield a new liquid. Every liquid may thus be related to an initial parental liquid and one might expect that each successively derived liquid fraction would be less voluminous than its predecessor. Thus, it is frequently possible to predict theoretical lines of descent for analyses of samples which represent liquid compositions. The variations in magma compositions may be further refined and modelled, where the chemistry and characteristics of the crystal phases responsible for the fractionation are known. Identification of these controlling phases should be supported by petrographic or field evidence and may sometimes be verified by, for example, melting experiments.

Variation diagrams of elements using SiO_2 as the ordinate are of little use, due to the restricted range of silica possessed by these syenitic rocks. Previous workers have used a "fractionation index" (FI) based on calculated normative mineralogy. This is essentially the "differentiation index" (DI) of Thornton and Tuttle (1960) with the addition of normative acmite, the latter becoming increasingly important with peralkalinity. Such indices should be treated with caution since, by virtue of their employment, one automatically assumes or at least infers that fractionation in the classical sense does occur. Thus, it is hardly surprising that when normative nepheline is plotted against FI, which itself includes normative nepheline, a positive correlation is achieved (eg: Chambers

1976; Stephenson 1976). Similarly an increase of any major element, which is normally related to a specific phase, must automatically be accompanied by an equal decrease in one or more compensating elements because the total remains 100 %. Thus an increase in the proportion of nepheline will necessarily coincide with corresponding changes in SiO_2 , Al_2O_3 , Na_2O and K_2O when plotted against FI, since it is from these very variations in oxide wt% that the norm has been calculated. Since the FI varies with iron oxidation ratio, a few samples from each unit were selected for Fe^3/Fe^2 determinations. Lastly, only where further evidence indicates should these samples be thought of as representing liquid compositions, since petrographic examination frequently reveals cumulus textures where none were obvious in the field.

Use of cumulus terminology

Throughout this chapter, as elsewhere in the thesis, the use of a cumulus terminology based on petrographic and field evidence has proved necessary and informative. Cumulus textures are usually associated with layered igneous rocks whose supposed origin by gravity settling of crystals through a less dense magma (Wager et al 1960; Wager and Brown 1968) has recently been disputed by McBirney and Noyes (1979) who favour an origin of in-situ crystallisation. Thus the term is used strictly in a textural context and is based on the definitions set out in Wager and Brown (1968) but does not here require that the mode of origin for cumulus textures be by gravitational accumulation of crystals alone. Their modes of origin are considered at greater length in Chapter 6.

Whole-rock samples for each syenite unit of the Motzfeldt Centre have been analysed by X-ray fluorescence for major, minor and trace elements. The analytical procedures, results and norms are tabulated in Appendix I. Sample density is indicated in Appendix I also.

Excluding xenoliths of supracrustal rocks, an estimated 90 % by volume of the Motzfeldt Centre consists

of nepheline syenites. Somewhat more basic larvikites and lardalites form the early parts of SM5, the last major unit north of the Flink's Dal fault. Some representative analyses of the newly defined unit SM6 and of the lavas preserved within the centre, are tabulated at the back of this chapter.

In the following sections, the data are presented as a series of x-y plots and other variation diagrams. These are referred to in the text, where salient features are described and their implications discussed. Samples thought to approximate to liquid compositions in SM2, 3 and 4 are circled by dots in these diagrams.

5.2. Units SM1, 2 and 3

By virtue of its outcrop, many of the samples of SM1 come from the outer part of an originally very large unit (c. 190 km² by area). Many of these samples are free of nepheline. This may in part be due to assimilation of silica rich material such as the country rock gneiss (Julianehåb Granite) or quartzites of the Eriksfjord Formation. Further causes are considered subsequently under section 5.2. for unit SM4.

The geochemical data suggest that units SM2 and SM3 are genetically related. Thus in figure 5,1 "P", a phonolite from SM2 and "B", a phonolite/microsyenite from SM3 show very similar characteristics. Their trace element ratios Ce/Y, Ce/La, Zr/Nb, and Zr/Y are also very similar. Both B and P are fine grained rocks and are thought to approximate to liquid compositions. Strictly speaking, they might have their respective phenocryst content (Fsp, Cpx, Ol, Ne) removed. Sample "A" in figure 5,1 is a fairly typical mafic cumulate from SM3 north of the Flink's Dal fault and could have been formed by accumulation of mafic minerals and feldspars from a liquid similar to P. Thus Sr versus Ba (fig. 5,1) reveals a slope between A and P and the origin consistent with removal of alkali feldspar, as predicted from the partition coefficient data of Larsen (1979). The relatively high proportion of mafic minerals in A (essentially Cpx, Mt, Amph)

Figure 5.1. Chemical variation of SM1, 2 and 3.

- A = cumulate from SM3, devoid of nepheline (63709)
- B = phonolite margin from SM2 (54142)
- C = phonolitic microsyenite from SM3, margin (54138).

The plot of Sr vs Ba shows nepheline and feldspar control lines, as predicted from the data of Larsen (1979). This diagram would suggest that extraction of feldspar from liquid P might yield a liquid of composition B. However, the degree of fractionation required is difficult to reconcile with the otherwise close similarities between B and P.

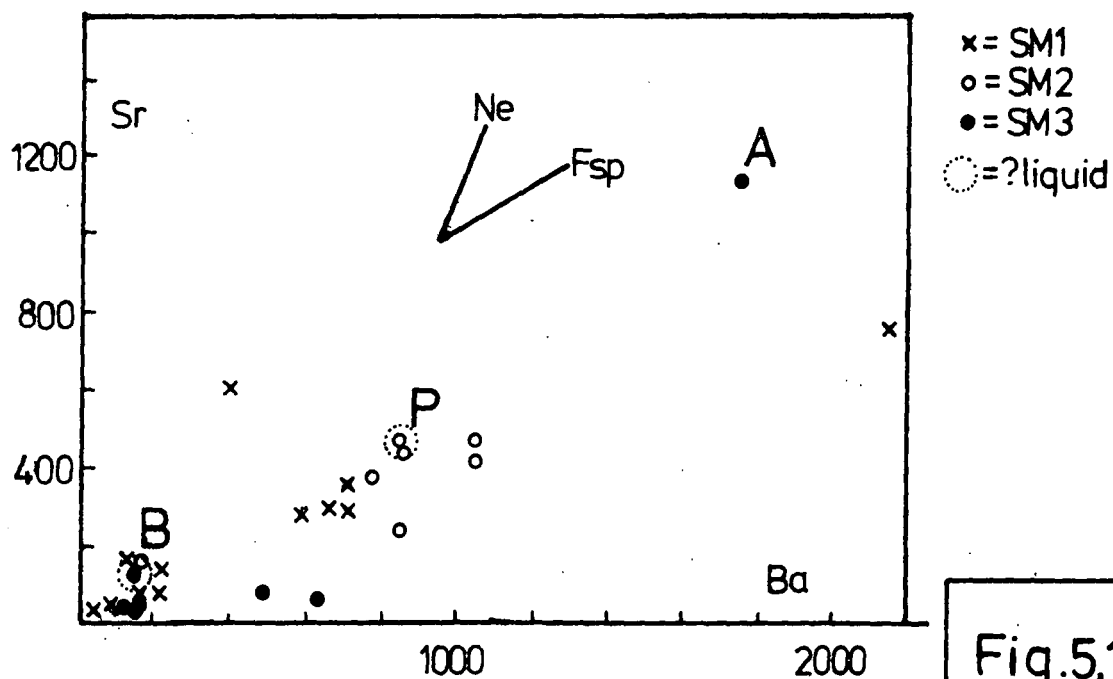
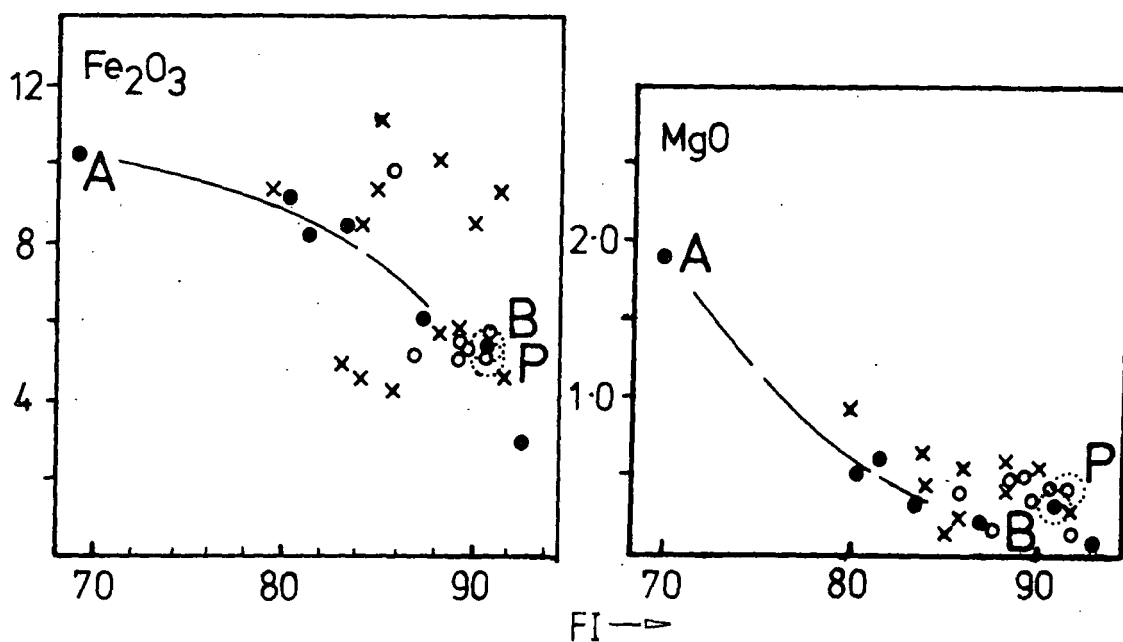
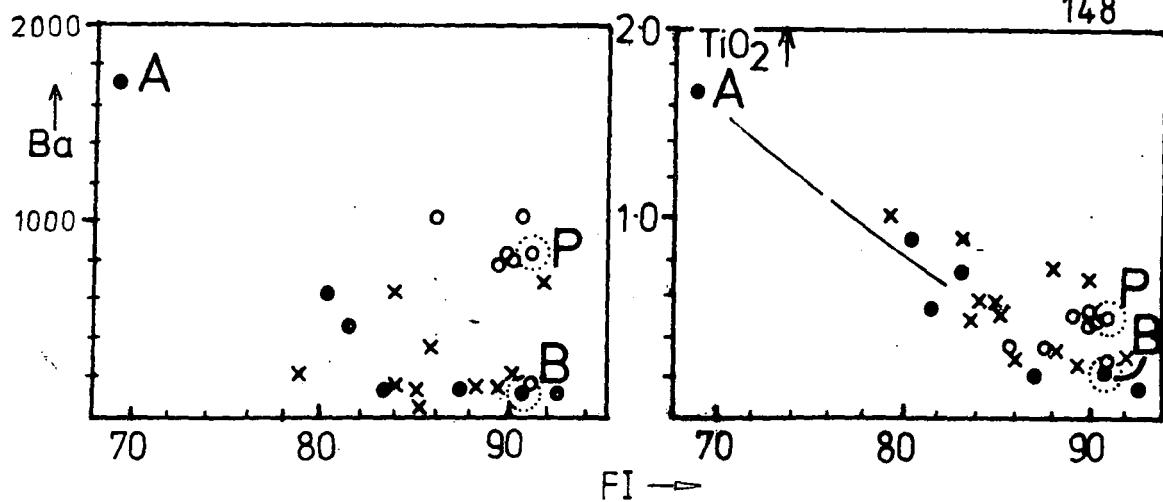
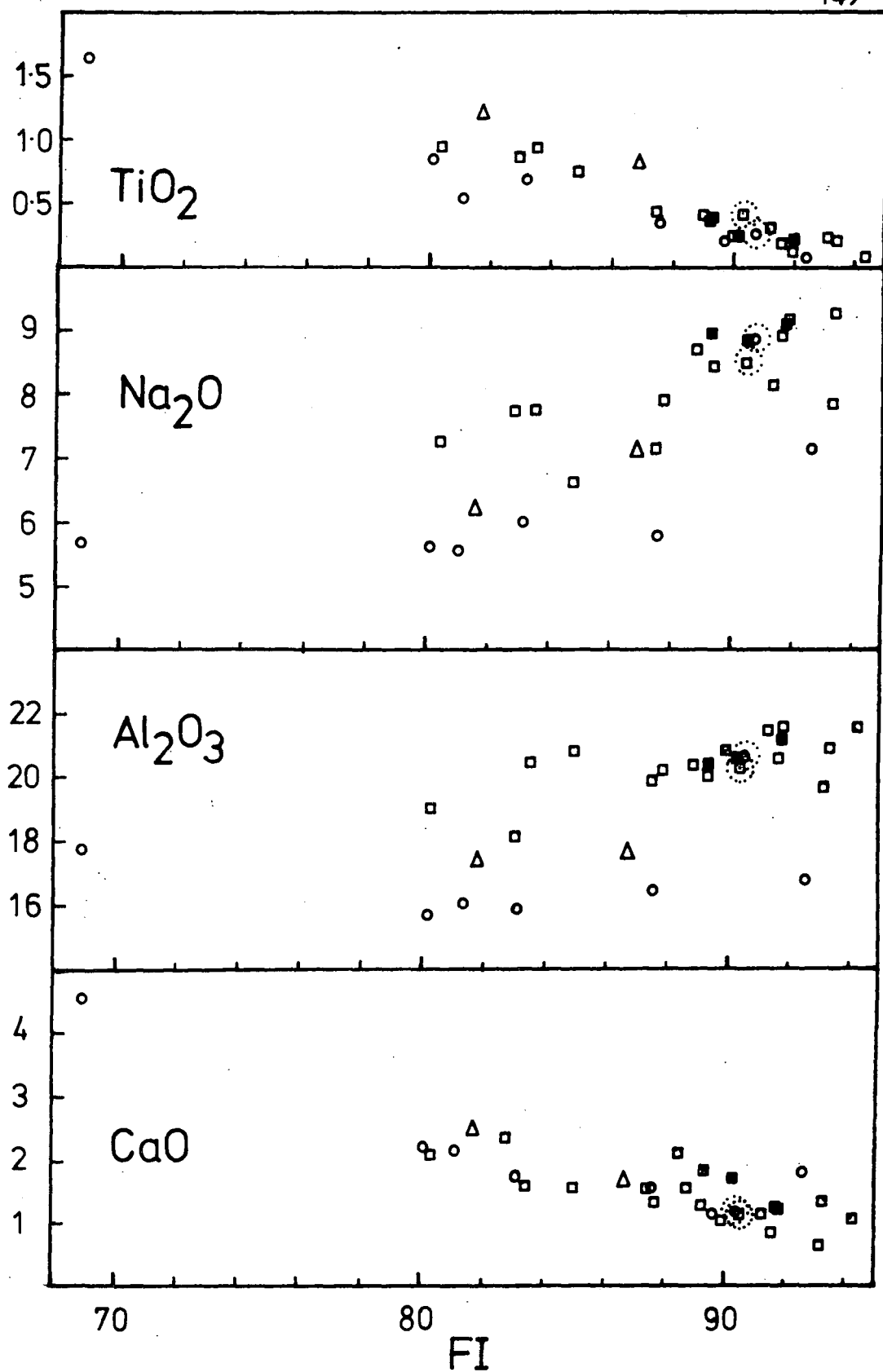


Fig.5,1



- = SM4
- = SM4 cutting N.Qôroq
- = SM3
- △ = structurally low SM4

Fig.5,2

causes the correspondingly low FI for its position in figure 5,1 .

It is interesting that the total amounts of Sr and Ba in B and P are quite different. This could be due to different origins of their respective feldspars and indeed, some of the unusual exsolution textures exhibited by phenocrysts in SM2 could be due to a xenocrystic origin. An open system magma chamber, as postulated by O'Hara (1977) might also explain some of these features.

5.3. Unit SM4

Diagrams of TiO_2 , Na_2O , Al_2O_3 and CaO versus FI (fig. 5,2) have been used to demonstrate the similarity between nepheline syenites cutting the east side of the North Qôroq Centre and unit SM4 to which they are thought to belong. In particular, these are compositionally very similar to nepheline-rich marginal variants of unit SM4 (see fig. 5,2). The average modal nepheline content of SM4 is around 20-25 %, in contrast to the nepheline-poor syenites from north of the Flink's Dal fault. However, porphyritic phonolites from both SM2 and SM3 in southeast Motzfeldt are also similar to marginal SM4. It seems that the immediate parental magmas to the three units SM2, 3 and 4 were all of phonolitic composition (see Table (5) 3).

In Flink's Dal, the syenites belonging to SM4 situated beneath the rafts of lavas often contain abundant euhedral nepheline, whereas cumulates upon raft-floors contain but small amounts of interstitial nepheline. Two samples of SM4 from structurally very low positions, close to the western shore of Motzfeldt Sø, are both relatively poor in nepheline and are rather mafic. There is a tendency for SM4 to become more mafic and nepheline poor with depth, although as seen in the Flink's Dal area, the variation of nepheline with height can be complex. Some possible causes for the presence or absence of nepheline from the liquidus are now considered.

(a) Pressure effects

Increased pressure in the system Ne-Ks-Qz enlarges

the field of feldspar relative to nepheline (eg: Gittins 1979). For liquid compositions which plot close to the phonolitic minimum in this system, relatively small increases in pressure could remove nepheline from the liquidus. Thus, a liquid plotting just on the trachytic side of the minimum at, for example, 5 kbars P_{H_2O} may suddenly find nepheline on the liquidus with a small drop in pressure (fig. 5,3). Perhaps the height of SM3 (c. 1.5 km minimum) is sufficient to cause the necessary pressure difference (taking 1.5 km = 0.5 kbars).

(b) Degrees of undercooling

Provided that the cumulus phases have similar crystallisation temperatures (negligible equilibrium melting intervals) and they have different rates of growth and nucleation, then their order of crystallisation from the liquid might be determined by the degree of undercooling. Such a process of oscillatory crystallisation in situ is preferred by Parsons (1979) for cyclic layering in the Klokken Intrusion. Since the degree of undercooling might be inversely related to P_{H_2O} and minerals of simpler crystal structure nucleate more readily during cooling (Wager 1959), nepheline should nucleate at lesser degrees of undercooling than feldspar. Assuming that volatiles would tend to accumulate at the roof of a chamber, or beneath a temporary roof such as a xenolithic raft, P_{H_2O} would be higher and the degree of undercooling^{perhaps} lessened. Such a system might be responsive to small variations in P_{H_2O} which would have no effect on phase boundaries in the system Ne-Ks-Qz. Thus nepheline might still crystallise first, in response to an increase in P_{H_2O} and reduced undercooling, since the corresponding increase in the field of feldspar (as in (a) above) would be trivial.

Because the variation in nepheline content in Flink's Dal occurs on a scale of about 100 m (or less), it is unlikely that variations in P_{total} are significant, although this appears to be the case in SM3. However, P_{H_2O} is quite likely to increase beneath the rafts and could give rise to the preferential crystallisation of nepheline in the manner outlined above. Furthermore, since phase boundaries

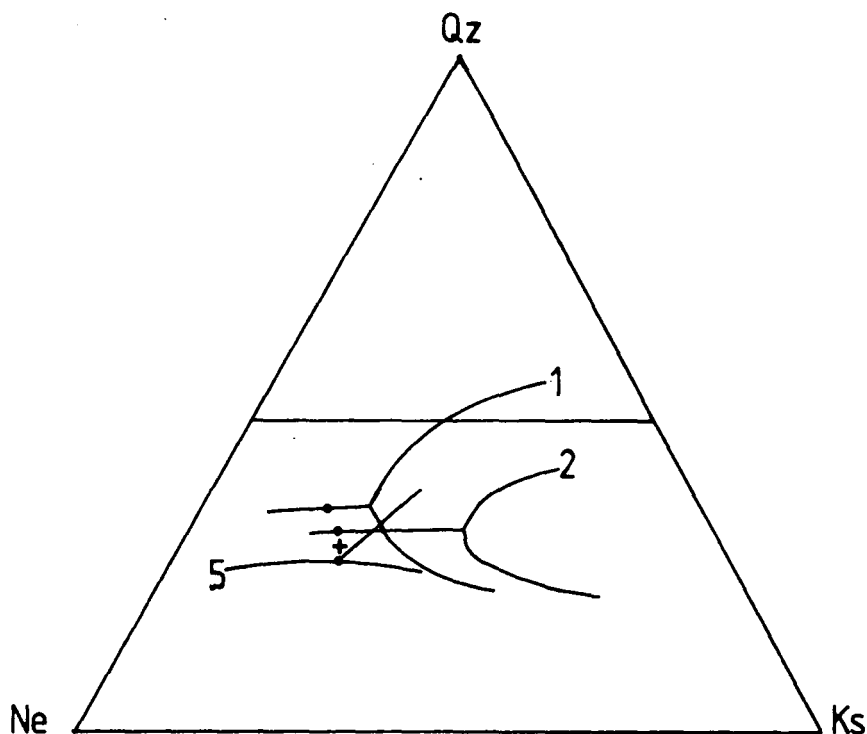


Figure. 5,3: pressure dependence of phases crystallising from a phonolitic melt.

—●—1
 —●—2
 —●—5

} phase boundaries at 1, 2 and 5 kbar
 P_{H_2O} respectively, showing minimum
 temperature positions, (after Gittins
 1979).

Decreasing pressure expands the field of nepheline, and nepheline may arrive on the liquidus of liquid "+" in the diagram for example, as pressure changes from 5 to 2 kbar. The increase in pressure with depth inside a magma chamber (ie: 1.5 km = 0.5 kbar) might be sufficient to depress nepheline from the liquidus of a phonolitic melt.

+ = phonolitic liquid

Figure 5.4.

(a) Fe_2O_3 vs FI is typical of the similar range of major elements exhibited by units SM4 and HY. Unit HY contains higher concentrations of incompatible elements.

(b) Sr vs Ba, indicating the overall more highly fractionated nature of unit HY. Feldspar control line is from the data of Larsen (1979) for comparison. Unit HY is also enriched in Rb and actually represents mixtures of a microsyenite with varying proportions of ne-syenite (eg: see p176).

(c) TiO_2 vs FI, for unit SM5 and SM5* - demonstrating the behaviour of a typical compatible element in this unit. Note the range of FI in SM5 compared with the majority of the Motzfeldt syenites, a result of their different immediate parental magma compositions (larvikitic parent to SM5, and phonolitic parent to SM2, 3 and 4).

- = SM4
- x = HY
- = SM5*
- = SM5 c = cumulate

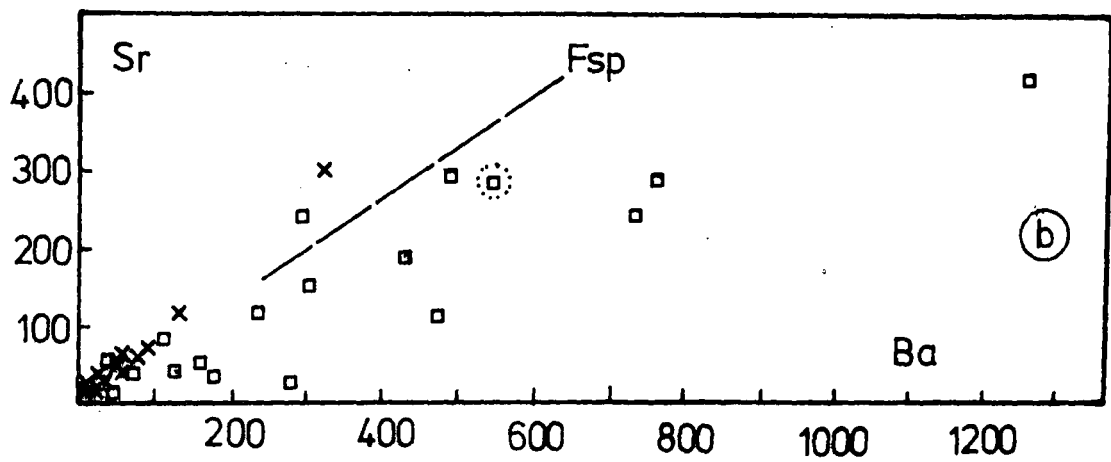
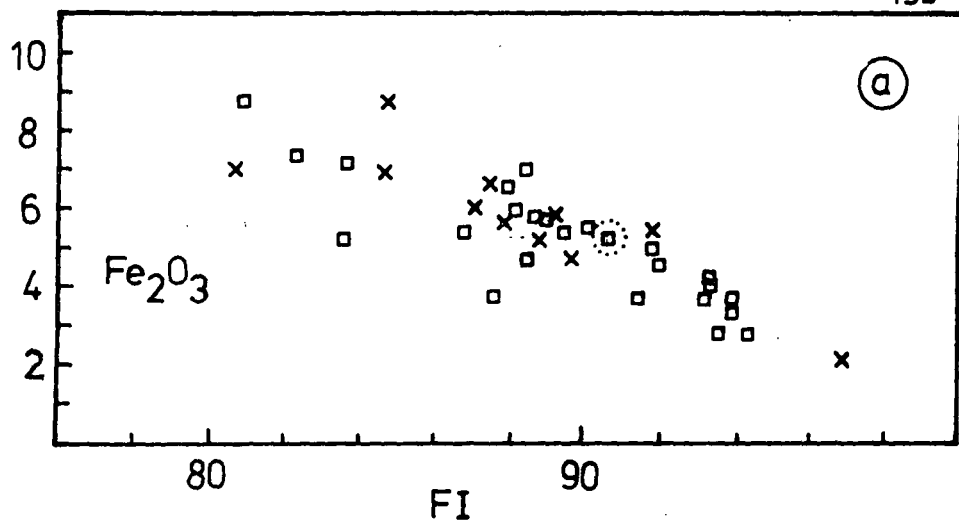
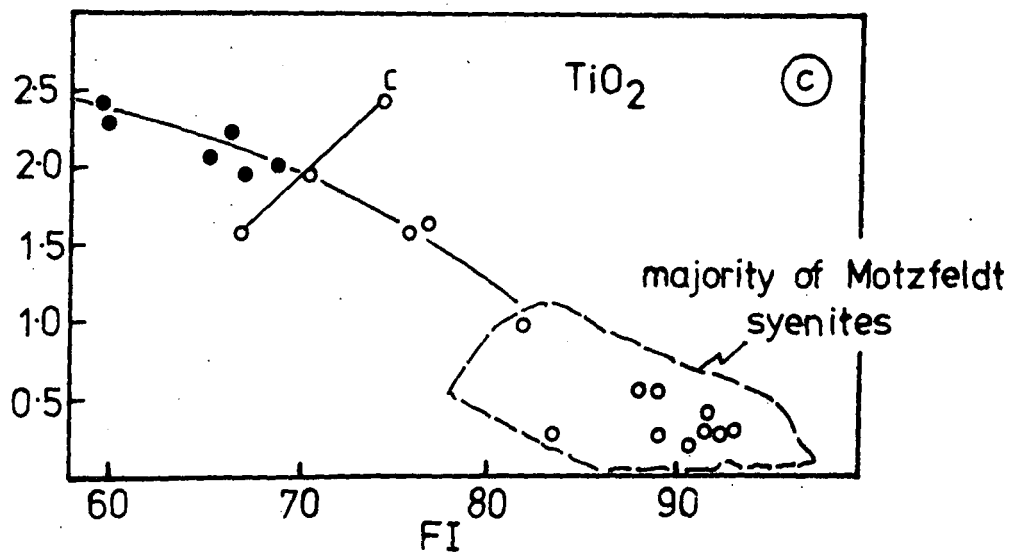


Fig.5,4



in the system Ne-Ks-Qz are apparently unaffected, then this might suggest fluctuation in P_{H_2O} on a scale of about 30 bars (if 3000 m = 1000 bars, then 100 m = 33 bars).

(c) Flotation of nepheline

Flotation of nepheline could account for the observed field relations in the Flink's Dal area. However, given the similarities in density between nepheline and a syenitic/phonolitic liquid, this might seem unreasonable. Certainly few of the convincing poikilitic textures visible in the naujites of Ilímaussaq (sodalite flotation cumulates) are seen in Motzfeldt. The incorporation of small amounts of water into the nepheline structure are unlikely to lower its density sufficiently.

(d) Modification to the liquid composition

The absence of nepheline from marginal syenites could be due to modification of the bulk liquid composition by the assimilation of siliceous material, such as country rock gneiss or quartzite. As Chambers (1976) points out, this need not be massive assimilation, provided that the liquid is already of near trachytic composition. He also suggests that addition of meteoric water could cause silica enrichment in the residual liquids, by preferential crystallisation of OH-bearing minerals undersaturated in silica. Alternatively, the loss of alkalis on a large scale, similar to that described for a phonolite dyke from the Redekammen district by Larsen and Steenfelt (1974) could depress the abundance of nepheline in favour of feldspar.

5.4. The Heterogenous Syenite-unit HY

Unit HY is notable in the field for its banded or layered appearance and its confusing and variable intrusive relations to SM4. In thin section there is evidence for flow deformation of syenites in various stages of digestion in microsyenite.

In terms of major elements, HY is similar to SM4 (eg: fig 5,4 (a)). However, trace elements such as Sr and Ba, whose partition coefficients predict strong compatibility

with feldspar, show a highly fractionated character, with much lower values of Sr and Ba in HY than in SM4 (fig. 5,4 (b)). Unit HY is enriched in Rb, the only element to behave consistently as an incompatible element in the later stages of fractionation in the Motzfeldt Centre.

Several features of HY are suggestive of the mode of origin of the even more fractionated unit SM6, the lujavrites. Indeed, one sample of HY bears a strong resemblance to the white lujavrites, consisting almost entirely of aegirine, two feldspars and nepheline, but lacking in eudialyte and the corresponding enrichment in Nb, Zr and Re_2O_3 . The origins of HY will be further considered in section 5.10.B.

5.5. Unit SM5

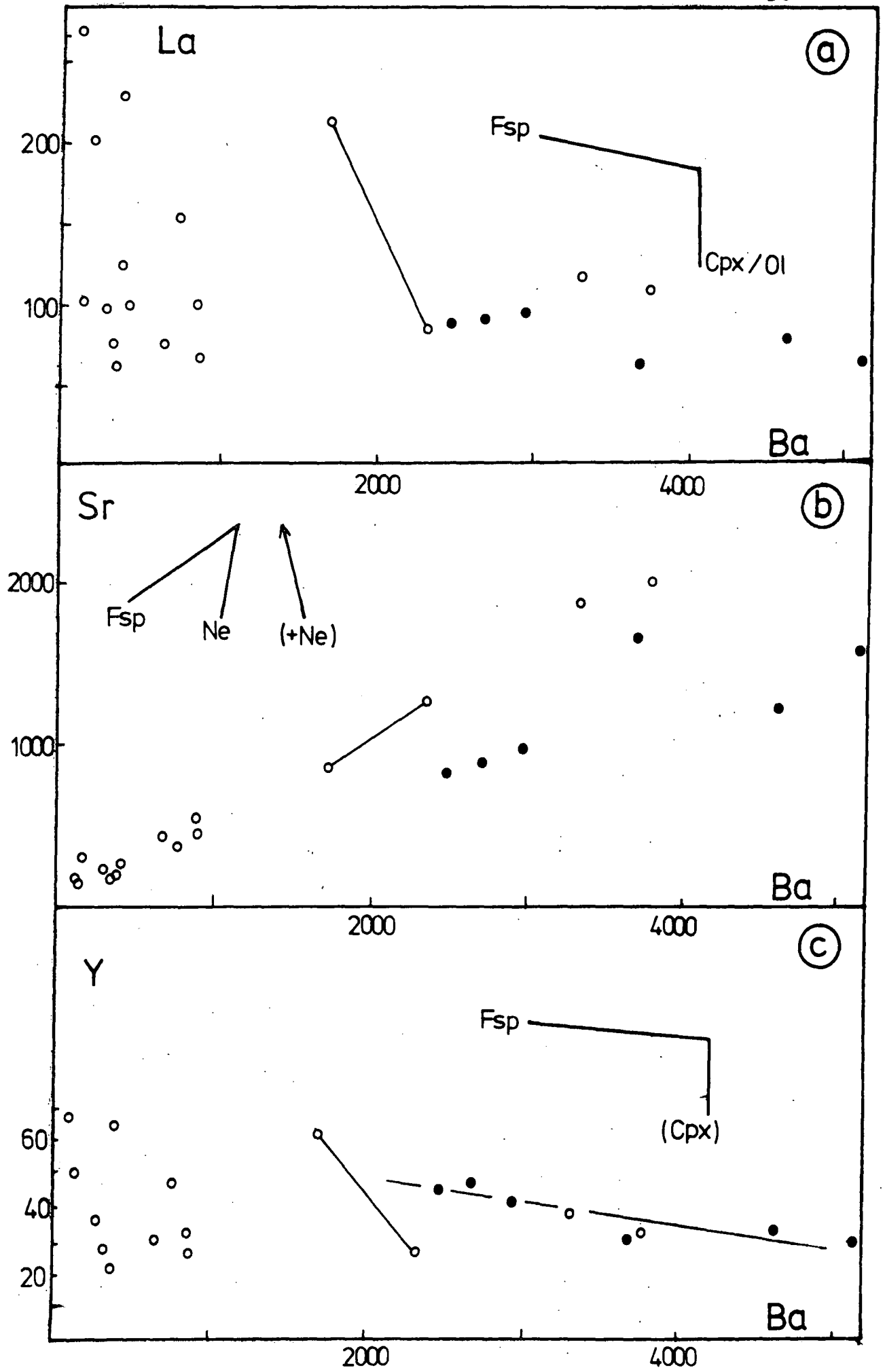
TiO_2 versus FI displays the behaviour of a typical compatible element in SM5 (fig. 5,4 (c)). From the most basic larvikites in the partial ring dyke in western Central Motzfeldt (SM5*), TiO_2 is removed by relatively high temperature crystallisation of ilmeno-magnetite. In later nepheline syenites, with lower liquidus temperatures, the amount of TiO_2 in silicate minerals becomes increasingly important, with sphene becoming a common accessory phase.

Plots of Y, Sr and La versus Ba (fig. 5,5) compare favourably with theoretical trends for feldspar fractionation predicted from the data of Larsen (1979). Unit SM5* shows a slightly lower Sr/Ba ratio than SM5, which is difficult to reconcile with the presence of plagioclase xenocrysts in SM5*, since this should increase Sr/Ba. In real terms, this probably represents the higher nepheline contents found in SM5, as nepheline has approximately a three fold preference for Sr over Ba (Larsen 1979). Simple feldspar fractionation can not account for the variable values of Y and La in the more evolved syenites, where Ba is low. This coincides with similar variations in Zr and Ce and presumably corresponds to crystallisation of minerals rich in these particular elements, such as eudialyte, rinkite, sphene and l  venite. A few euhedral crystals of eudialyte are found in the most evolved syenites of SM5.

Figure. 5,5. Trace element variation in unit SM5.

Phase control lines are after the partition coefficient data of Larsen (1979). Much of the variation in SM5 could be attributed to extraction of alkali feldspar (feldspar fractionation). The unpredictable variation in Y and La at low levels of Ba (in rocks with high values of FI) are though to be due to the sporadic proportions of accessory and minor phases rich in these elements.

- = SM5*
- = SM5 (tie line to a mafic segregation).



Unit SM5 (with SM5*) is the only unit at Motzfeldt to exhibit features reminiscent of fractionation from a basic parent, such as larvikite of augite syenite. In this respect, SM5 bears great similarities to rock suites from the South Qôroq Centre (Stephenson 1976) and the Igdlérfigssalik Centre (Powell 1976), yet SM5 proceeds to and is dominated by, far more evolved nepheline rich syenite which may contain eudialyte. That it is the last major intrusion of syenite north of the Flink's Dal fault, being cut only by the alkali gabbro dyke, may also be significant.

5.6. Summary of the variation between units

The combination of SiO_2 and FI (fig. 5,6) are indicative of the major differences existing between several units of the Motzfeldt Centre. Increasing amounts of feldspar will tend to increase SiO_2 , whereas increasing nepheline content will cause a decrease in SiO_2 , yet both will increase FI.

(i) Syenites of SM1 above the dashed line in figure 5,6 (a) are neither quartz nor nepheline bearing, though have up to about 5 % quartz in their norms.

(ii) Samples of SM3 above the dashed line in figure 5,6 (a) are all located north of the Flink's Dal fault and often show cumulus textures, with cumulus magnetite, pyroxene, feldspar, apatite and zircon.

(iii) The marginal rocks of SM2, 3 and 4 which possibly represent liquid compositions, are ornamented with a circle of dots in figure 5,6. Ideally these should have their phenocryst content, consisting of feldspar, nepheline, pyroxene and some olivine, removed.

(iv) Unit SM5 displays an inflexion in SiO_2 at around FI = 65 (SM5*) and again at around FI = 84 (SM5) (fig. 5,6 (c)). This coincides with the increasing importance of nepheline in the norm and is especially characteristic of fractionating augite syenite magmas from other centres in the Igalliko Complex. At Motzfeldt, the trend of increasing nepheline content in SM5, is accompanied by changing habit of the nepheline (see

Figure 5.6. Diagrams of SiO_2 vs FI to illustrate the general similarities and differences between the different SM- units.

FI= normative (Ab + Or + Ne + Ac)

Ab = Albite, Or = Orthoclase.

Samples above the dashed line in (a) are devoid of nepheline.

(a) Samples of SM1 may be either ne-bearing or ne-free. All samples of SM3 devoid of nepheline are from N of the Flink's Dal fault, show cumulate textures and are thought to be from a deep level. The positions of SM6 are shown for comparison.

(b) Samples of SM4, all ne-bearing. A sample representative of a possible liquid (AM7) is indicated by a circle of dots. Most of the variation could be explained by accumulations of different proportions of the major phases crystallised from this liquid (see fig.5,14: p177).

(c) Variations in SM5 (∇) and SM5* (\blacktriangledown) - showing a curved relationship between SiO_2 and FI, similar to fractionating augite syenite magmas from North Qoroq (Chambers, 1976).

(d) Summary loci of the different units.

x = SM1

\blacktriangledown = SM5*

o = SM2

∇ = SM5

• = SM3

Δ = SM6

□ = SM4

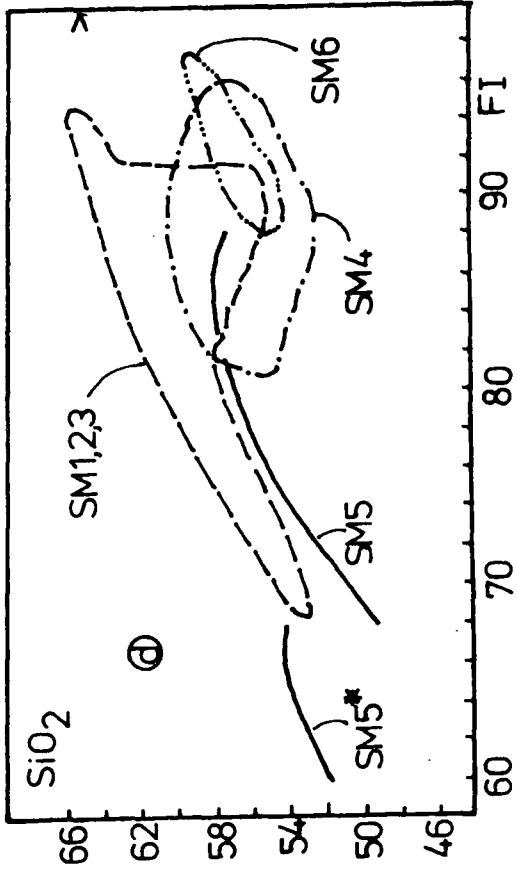
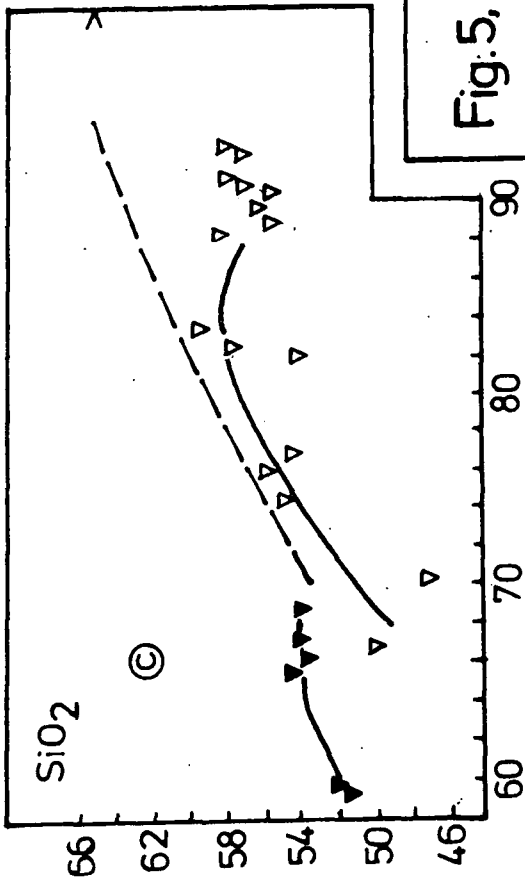
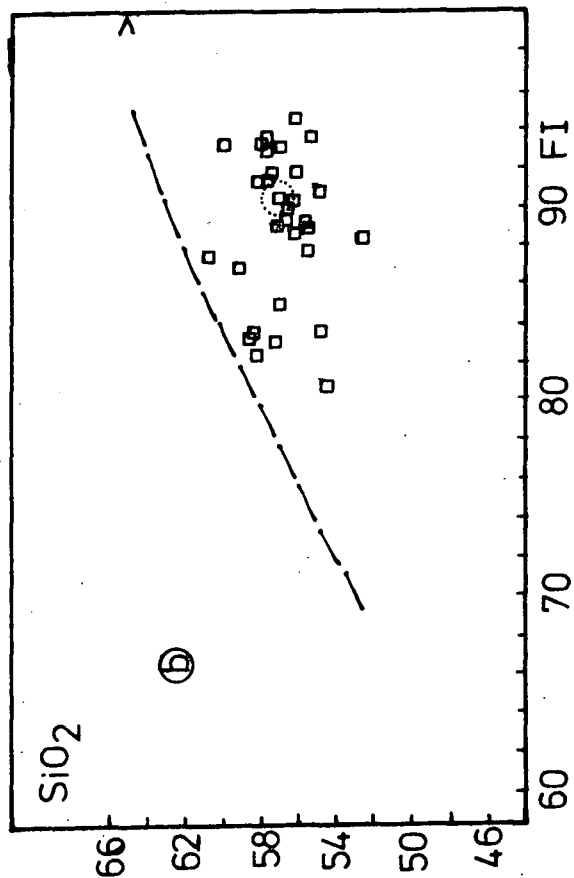
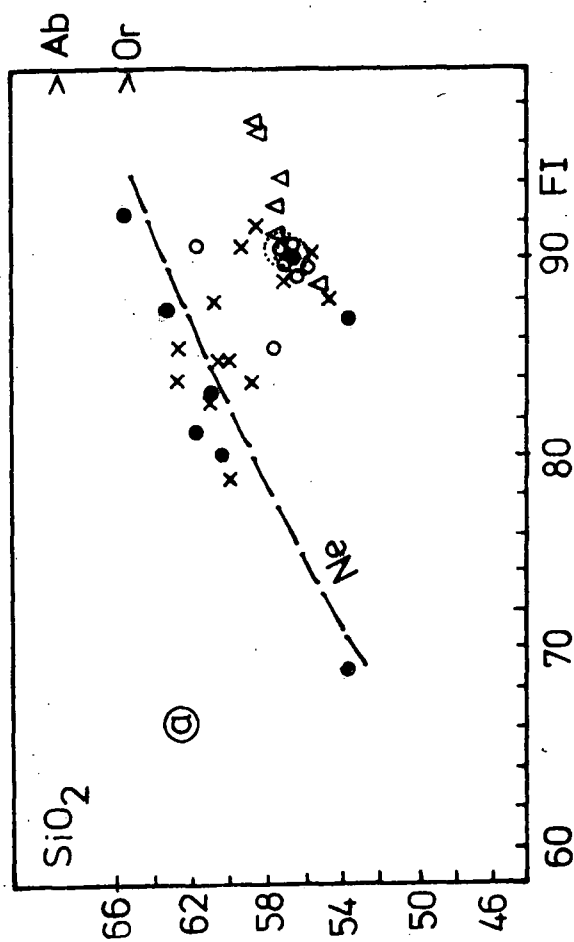
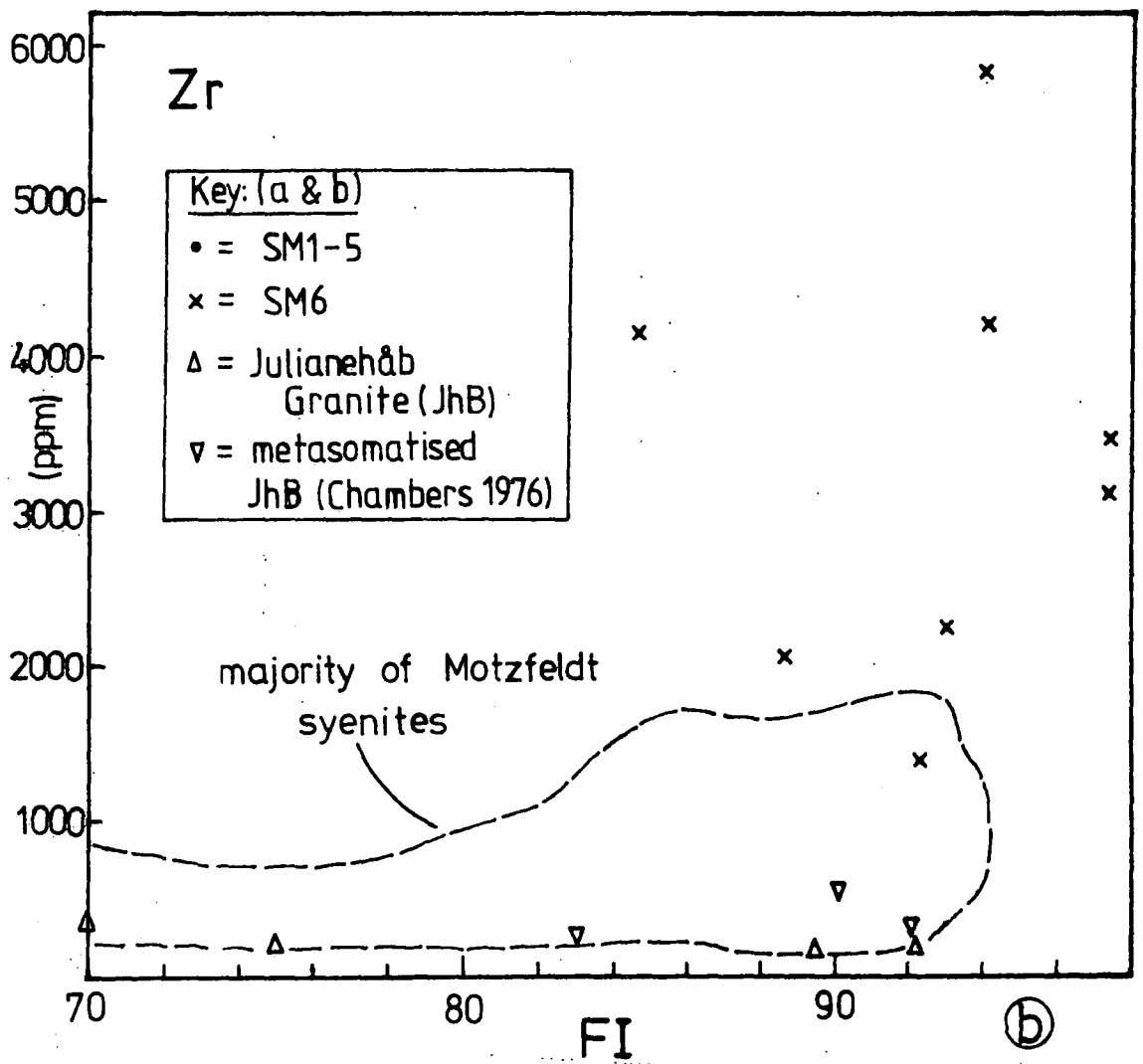
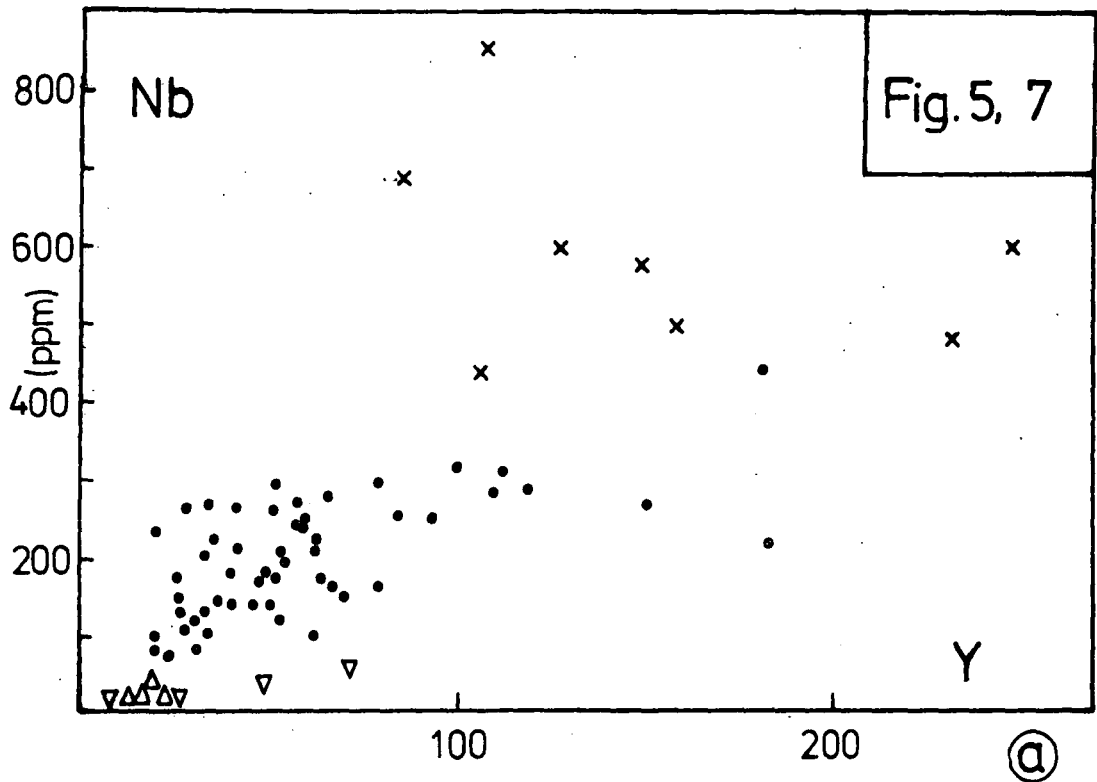


Fig. 5.6

Zr vs FI and Nb vs Y (fig. 5,7 (a & b))



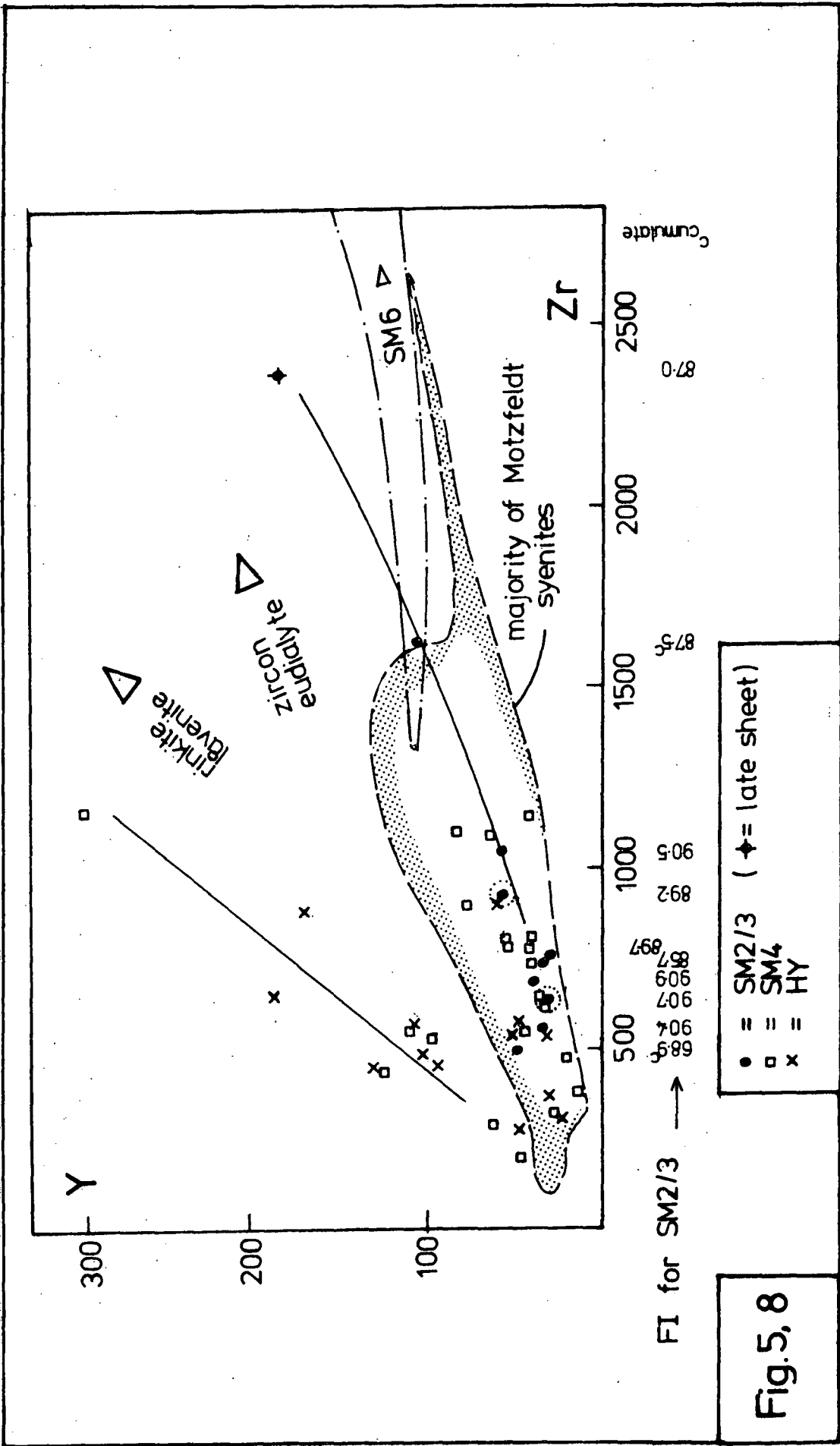


Fig. 5.8

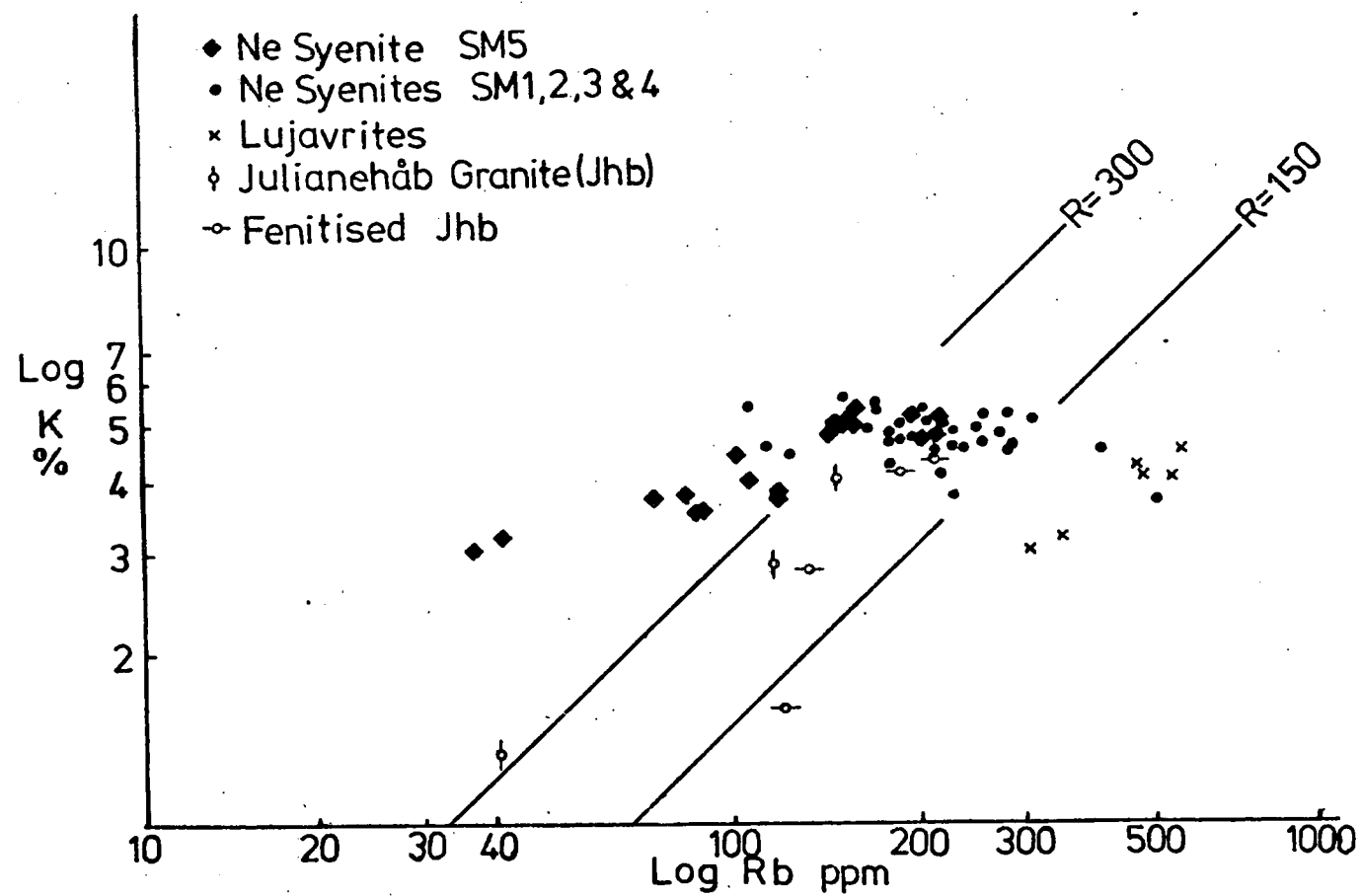


Fig.5,9

1, and Rb is just incompatible ($D_{Rb} = 0.4$, Larsen 1979). As K/Na increases in the fractionating feldspars, the K in the liquid becomes buffered, whilst Rb continues to increase. Thus K/Rb must decrease in late stage liquids.

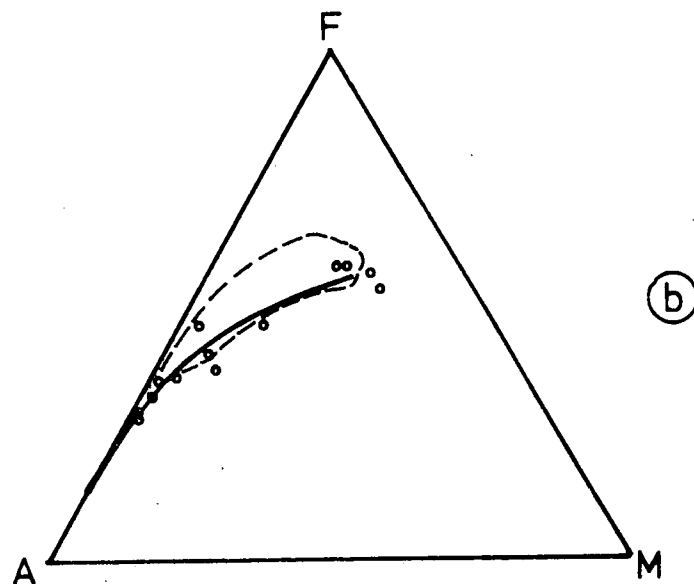
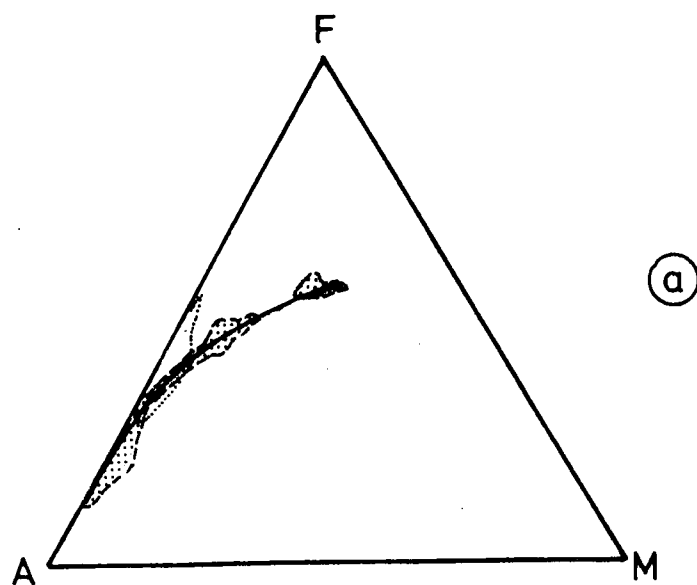
Excluding the more basic members of SM5, it is remarkable that Rb in the nepheline syenites maintains a fairly uniform value of around 150-200 ppm, only showing enrichment in the much more evolved samples such as SM6, where Rb is around 300-600 ppm. Rb is generally incompatible with mafic silicates other than biotite, for which it shows a two-fold preference over feldspar (Taylor 1965). The levels of Rb in the majority of the Motzfeldt syenites appear to be buffered, probably by the presence of small amounts of biotite. Where biotite becomes more common, as in HY, Rb increases. Since biotite is not present in unit SM6, the relatively high amounts of Rb must presumably be present in feldspar and nepheline, thereby reflecting a substantial increase in the partition coefficients for Rb in these phases. The same situation seems to occur in extreme granitic differentiates (Emeleus pers.comm.1980).

5.7. Triangular variation diagrams

Figure 5,10 (a) shows the whole rock analyses in terms of $A = Na_2O + K_2O$, $M = MgO$ and $F = FeO$. The trend is similar to, for example, the alkali basalt-trachyte/phonolite trend from St.Helena (Carmichael et al 1974 p.389). The position of 24 dykes which cut the Motzfeldt Centre has also been included.

12 samples from the lavas preserved as rafts within the centre and from the two basaltic flows near the base of the local succession, are compared to the main AFM trend in figure 5,10 (b). The position of the Ilímaussaq Volcanic Member (IVM) based on the data of Larsen (1977) is also indicated. In general, the Motzfeldt lavas are a little less rich in iron and are more alkalic (ie: more fractionated) which is in agreement with their trace elements and petrography.

The diagram $(Na + K) - Fe - Mg$ (fig. 5,10 (c)) has been included for comparison with the typical trend for



A = $\text{Na}_2\text{O} + \text{K}_2\text{O}$, F = FeO, M = MgO, (ox wt%)




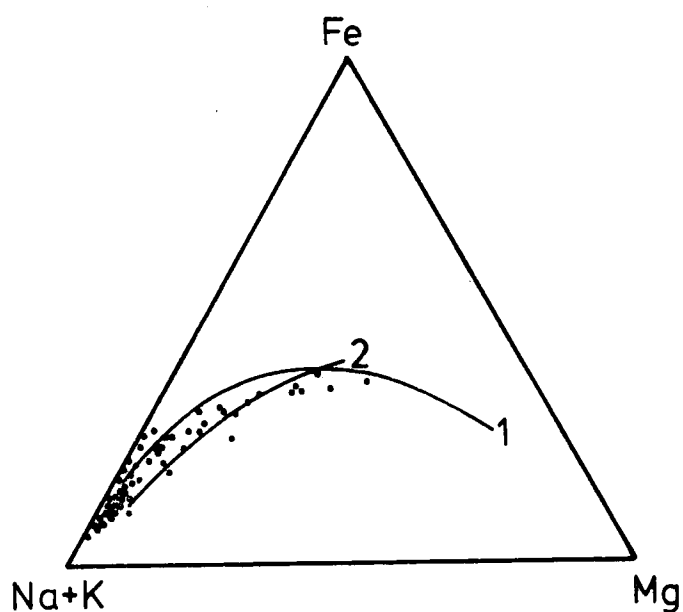
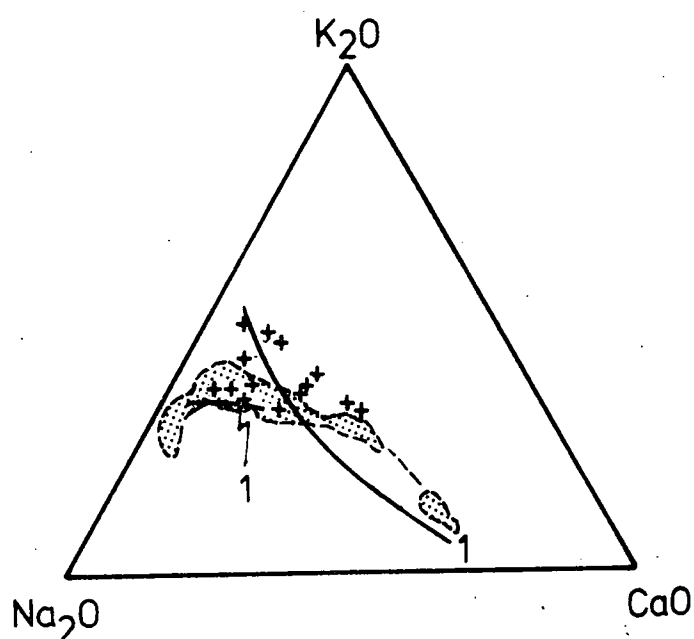
- (a)  = loci of majority of Motzfeldt intrusives
  = locus of Mid-Gardar dykes
 (b)  = locus of IVM (data Larsen 1977)
 • = lavas from Motzfeldt
 — = Motzfeldt trend

Fig.5,10



(c)



(d)

- 1 = Gardar trend (Watt 1966)
 2 = Oslo Province (Watt 1966 source Brøgger 1933)
 • = syenite (+alkali gabbro) data, Motzfeldt
 (shaded area) = loci of Motzfeldt intrusive units (all •'s above)
 + = xenoliths (lavas)

Fig. 5.10

the Gardar province as presented by Watt (1966). The Motzfeldt trend is, predictably, very similar, but lacks the most basic members rich in Mg. The trend from the Oslo province, as compiled by Watt (1966) from the original data of Broegger (1933) has also been added for comparison.

Superimposed upon the general trend for the Motzfeldt Centre in the system $\text{Na}_2\text{O} - \text{K}_2\text{O} - \text{CaO}$, are analyses from the freshest lava xenoliths (fig. 5,10 (d)). These come almost exclusively from unit SM4, where they are particularly plentiful and often massive. It is noticeable that these plot consistently to the K-rich side of the trend, which can at least in part be attributed to a relatively high proportion of mica, resulting from the hydrous breakdown of original mafic minerals accompanied by K-metasomatism.

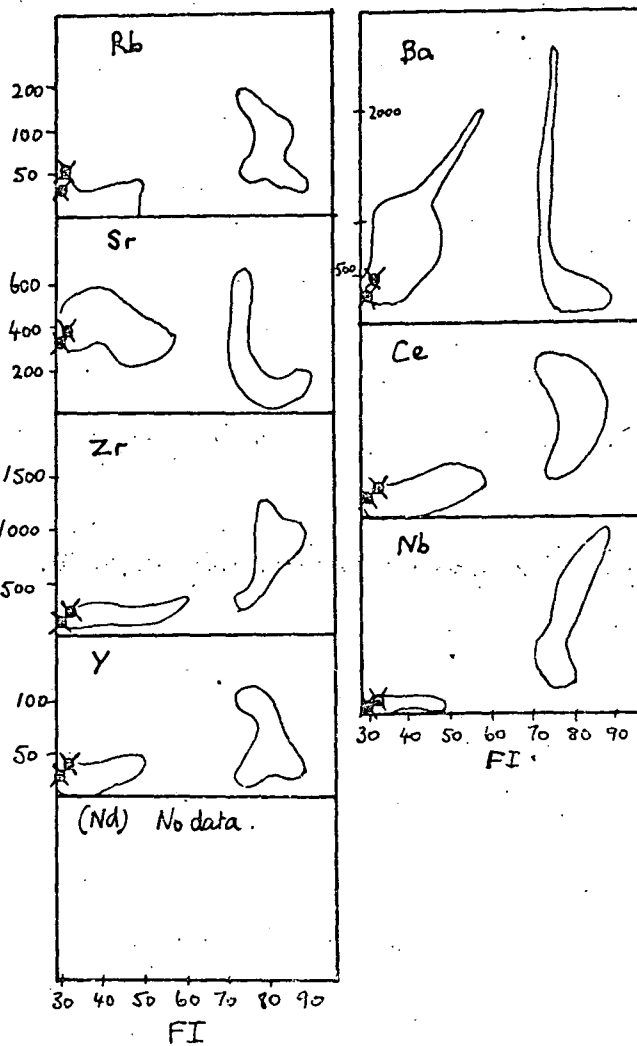
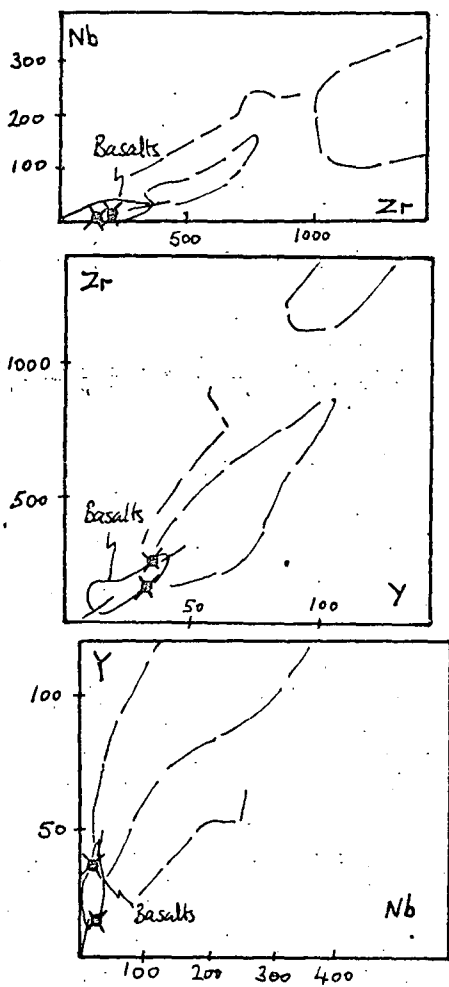
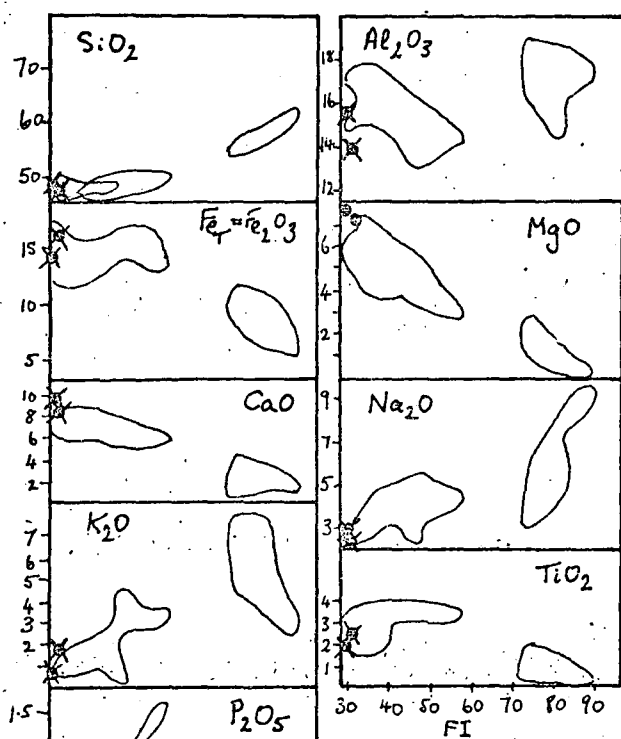
5.8. Lavas from the Motzfeldt Centre

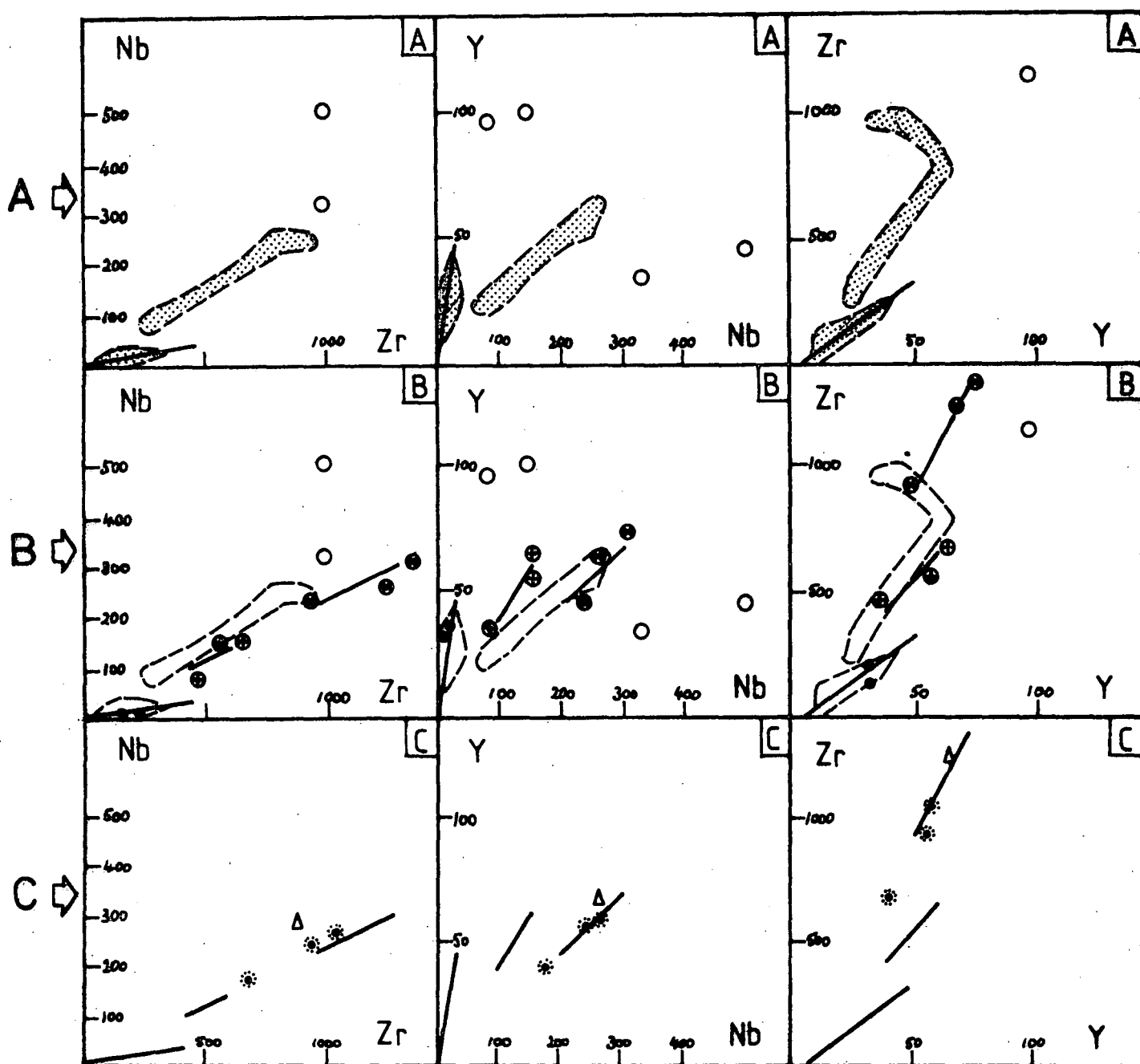
5.8.A. The local stratigraphic base

Two samples (63736, 63758) from basalt flows which immediately overlie the unconformable base of the Eriksfjord Formation at c. 1400 m in southwest Central Motzfeldt, are directly comparable to the lowermost members of the Ilímaussaq Volcanic Member (IVM) from the Narssaq peninsula. A series of diagrams redrawn from the work of Larsen (1977) are shown in figure 5,11 with these two unusually fresh samples superimposed. Major, minor and trace elements all show excellent correlation, suggesting that the Motzfeldt succession may start at a level almost equivalent to the base of the IVM. In practice, this may be just below the actual base of the IVM, in order to allow for up to 600 m of sandstones and assorted sedimentary rocks locally preserved around the Motzfeldt Centre (see Chapter 2) which are not found in the IVM, but which do occur below it.

5.8.B. Representative analyses and comparisons

The xenoliths and rafts of lavas found within the Motzfeldt Centre have suffered varying degrees of alteration. About 12 samples taken from the larger rafts are sufficiently fresh to warrant particular mention (Table (5) 2) and to





KEY

KEY	
IVM*	A
	= locus of IVM ○ = data point IVM = basalt trend IVM
Motzfeldt Lavas	B
	= locus of IVM ○ = data point IVM • = Motzfeldt basalts ⊙ = Motzfeldt trachytes (trachyandesites/trachytes) ● = Motzfeldt phonolites (incl: trachyphonolite)
Intrusive "phonolites"	C
	= Motzfeldt lava trends ⊙ = phonolites SM2/3 Δ = phonolite SM4
*data from J. Larsen (1977)	

Fig.5.12

serve as justification for the classification used in Chapter 2. Table (5) 2 presents seven of these lavas and compares them with two lavas from the IVM (Larsen 1977) and the average phonolite of Nockolds (1954). By using the bivariate trace element diagrams in figure 5,12, the lavas are then compared to the published trends of the IVM and to the intrusive phonolitic margins from units SM2, 3 and 4 in the Motzfeldt Centre. Thus figure 5,12 shows trace element plots of Nb versus Zr, Y versus Nb and Zr versus Y, for the IVM (Larsen 1977), the Motzfeldt lavas (Table (5) 2) and the intrusive phonolitic margins to units SM2, 3 and 4 (Table (5) 3). By comparing the three suites of diagrams in figure 5,12 (a, b and c) a number of points emerge.

1. The Motzfeldt lavas have been simplified into the three groups "basalts", "trachytes" and "phonolites" (fig. 5,12 (b)). The trachytes and phonolites are all from within the centre, whilst the basalts are from the local base to the succession, just outside the Motzfeldt Centre. Certain features of the trachytes and phonolites are similar to the fractionated lavas from the IVM, and the basalts conform nicely to the early (basaltic) trend of the IVM.

2. Assuming that the ratios between incompatible elements should remain constant with fractionation (eg: Weaver et al 1972; Ferrara and Treuill 1975), then the fractionated lavas preserved within the centre as rafts can not have been derived from the basalts, since their ratios are different. Larsen (1977) concluded that the fractionated lavas from the upper IVM were unrelated to the basic lavas in the lower IVM on this basis.

3. Comparing figure 5,12 (b) with 5,12 (c) reveals a close correlation between the phonolite magmas of SM2/3 and the phonolite lavas. This lends substantial support for derivation of the trachyphonolite and phonolite lavas from similar trachyte/phonolite magmas which cooled at depth to give the nepheline syenites as units SM2 and SM3. The lavas must have been derived from somewhat earlier magmas than those which actually produced SM2, 3 and 4.

4. There is a distinct similarity between samples of Motzfeldt lavas and intrusive phonolites, and the fractionated lavas of the IVM, in that Nb/Zr is the same and both Nb/Y and Zr/Y have increased with increasing fractionation (ie: from basalt through trachyte to phonolite).

5. The ratios Nb/Y and Zr/Y for the Motzfeldt lavas (fig 5,12 (b)) are discrete and constant for each of (a) basalts, (b) trachytes and (c) phonolites. The ratios increase in the order (a) (b) (c) for one of perhaps two plausible reasons;- Either they represent three separate magmatic events, derived from different parental magmas or they are the products of an open fractionating system, related to the same parental magma. Similar variations in incompatible ratios have been predicted by O'Hara (1977) for a periodically tapped and replenished magma chamber undergoing continuous fractionation.

6. Larsen (1977) states of the IVM that .."the thickness of the basaltic units generally increases towards the north and east indicating that the eruption sites should be sought in these directions ie: in the fjord Sermilik and the eastern part of the fjord Tunugdliarfik." The Igaliko Complex and the Motzfeldt Centre in particular, was apparently the source for at least part of the IVM. Perhaps the abundance of fractionated types, such as phonolites at Motzfeldt, and their comparative absence from Narssaq, is a function of distance from source and/or erosion from the top of the pile.

Lastly, it is difficult to estimate the original thickness of the lavas at Motzfeldt since correlation between sequences preserved around the centre has not proved possible. Nor has it been possible to correlate between the major rafts of lavas separated by the Flink's Dal fault, although this in itself may be significant. However, the visible rafts north of the Flink's Dal fault are individually up to about 300 m thick, whilst the rafts preserved in Flink's Dal itself, south of the fault, stack one above the other to a total thickness of about (?) 3-400 m.

5.9. Unit SM6: Analyses and comparisons

The lujavrites represent the most fractionated magma within the Motzfeldt Centre and were the last major intrusive event south of the Flink's Dal fault, except perhaps for the alkali gabbro dyke. The lujavrites are fine grained eudialyte-nepheline syenites of peralkaline character displaying prominent banding, which is often contorted and reminiscent of flow banding, in the field. Variations in the proportions of their constituent minerals gives rise to banding of melanocratic and leucocratic lujavrites on scales from centimetres to 10's of metres. Representative analyses are presented in Table (5) 1, where they are compared to lujavrites from the Ilímaussaq Intrusion and the Kola Peninsula. Samples collected in 1979 from the western end of the unit are as yet unanalysed. The latter are generally more mafic than those given and are petrographically very similar to porphyritic- and aegirine-lujavrites described from the Kola Peninsula (Vlasov et al 1966). Green lujavrite is indistinguishable from the rock of the same name at Ilímaussaq, although SM6 is not usually as iron rich or as poor in aluminium as the black lujavrites (eg: Gerasimovsky and Kusnetsova 1967) from that intrusion. Instead, SM6 corresponds more closely to white kakortokite and the "average kakortokite" of Ilímaussaq (Ferguson 1970). Thus it appears that "average kakortokite" -type magma can exist in its own right, perhaps as the extreme product of fractionating agpaitic phonolitic magma. A dyke of micro-kakortokite with almost identical trace elements to the "average kakortokite" and to SM6, has been examined by Larsen and Steenfelt (1974), who point out the probable cogenetic origin of this dyke and the agpaitic magma which produced the layered kakortokites of the nearby Ilímaussaq Intrusion. However, this micro-kakortokite is considerably richer in iron and poorer in aluminium than SM6 (eg: 42474 of Larsen and Steenfelt 1974). This difference could partly be due to alkali loss from SM6, in a similar manner to that described by Larsen and Steenfelt for different facies of the micro-kakortokite dyke, which could in turn result in partial loss of REE's

TABLE (5) 1. Lujavrites of SM6 compared.

	MOTZFELDT				ILIMAUSSAQ			LOVOZERO	
	46261	AM139	AM137	AM138	W.K.	B.L.	G.L.	P.L.	A.L.
SiO ₂	56.97	54.04	55.69	55.65	52.22	52.89	53.12	54.65	57.41
TiO ₂	0.02	0.37	0.16	0.14	0.28	0.35	0.28	0.41	0.50
Al ₂ O ₃	18.72	16.68	19.47	19.48	17.24	14.59	15.96	17.41	20.85
Fe ₂ O ₃	7.42	10.25	5.03	5.05	5.89	6.30	9.15	6.64	3.03
FeO	1.39	1.48	1.26	1.22	3.79	6.77	1.32	0.76	0.88
MnO	0.17	0.37	0.27	0.21	0.22	0.41	0.22	0.56	0.16
MgO	trace	0.48	0.03	0.03	0.23	0.54	0.20	trace	0.48
CaO	0.75	0.99	0.92	0.90	1.80	0.39	1.80	1.10	0.46
Na ₂ O	10.55	10.92	9.40	10.10	10.60	10.72	11.20	9.14	7.07
K ₂ O	3.96	3.58	5.15	4.95	4.38	3.28	3.35	6.56	6.70
H ₂ O	0.06	0.94	2.51	2.24	2.14	2.52	3.15	2.48	1.92
P ₂ O ₅	0.02	0.04	0.11	0.03	0.02	0.41	0.03	-	0.03
Total	100.03	100.14	100.00	100.00	100.12*	99.39*	100.14*	99.71	99.49
Trace elements					M.K.			W.K.=Av. White Kakortokite (Ferguson 1970)	
Rb	478	608	482	484	220		167	B.L.=Av. Black Lujavrite (Gerasimovsky and Kusnetsova 1967)	
Sr	26	50	73	39	148	81	132	G.L.=Av. Green Lujavrite (Ferguson 1970)	
Ba	40	190	250	273	226	10	176	P.L.=Porph. Lujavrite (Vlasov et al 1966)	
Ce	992	883	876	744		900		A.L.=Aegirine Lujavrite (Vlasov et al 1966)	
Y	251	86	108	106		365		M.K.=Microkakortokite (Larsen & Steenfelt 1974)	
La	404	319	354	286	335	453	327		
Nb	600	680	850	434	274	1100	189		
Zr	5970	2450	1310	2263	7139	4800	8243		
U	14	35	54	25		20			
Th	70	37	245	23					

*includes F and Cl in total (not listed here).

and incompatible elements. The overall difference is probably too great to be satisfactorily explained by this means.

The lujavrites from Motzfeldt lack the abundance of arfvedsonitic amphibole, so characteristic of similar rocks from the Ilímaussaq Intrusion, and are in this respect very similar to certain lujavrites from Lovozero.

5.10. Normative mineralogy

5.10.A. The Residua system

Almost all of the Motzfeldt syenites have normative (Ab+Or+Ne) in excess of 80 % and can thus reasonably be represented in the system Ne-Ks-Qz (Bowen 1937). The larvikitic ring dyke and lardalitic margin of SM5 contain relatively high amounts of CaO and MgO, and are not so accurately represented by this "Residua" system. Furthermore, many of the syenites are peralkaline and lie off the plane of the diagram in the Al-poor section of the larger system $\text{Al}_2\text{O}_3\text{-Na}_2\text{O-K}_2\text{O-SiO}_2$.

Whole rock compositions are plotted in the system Ne-Ks-Qz in figure 5,13 where the ternary minimum at $P_{\text{H}_2\text{O}} = 2$ kbars is also given (Taylor and MacKenzie 1975), as are the nepheline isotherms after Hamilton (1961). It should be emphasised that the experimentally determined minima in this system refer to conditions of water saturation ($P_{\text{H}_2\text{O}} = P_{\text{total}}$), a situation that is rarely achieved in natural magmas, except perhaps at the very late stages of crystallisation. Thus $P_{\text{H}_2\text{O}}$ represents the minimum value of P_{total} .

(a) Units SM1 and SM3: Trachytic compositions.

Much of SM1 and all of SM3 north of the Flink's Dal fault contains little, if any, nepheline. These samples plot just on the quartz-side of the Ab-Or join (see fig. 5,13) yet the quartz predicted from the norms has not been found in petrographic examinations. Since the trachytic rocks of SM3 are often mafic, and essentially cumulates (Cpx,Mt,Ap,Fsp,Zircon) they are not representative of liquid compositions. Limited evidence, namely Sr and Ba

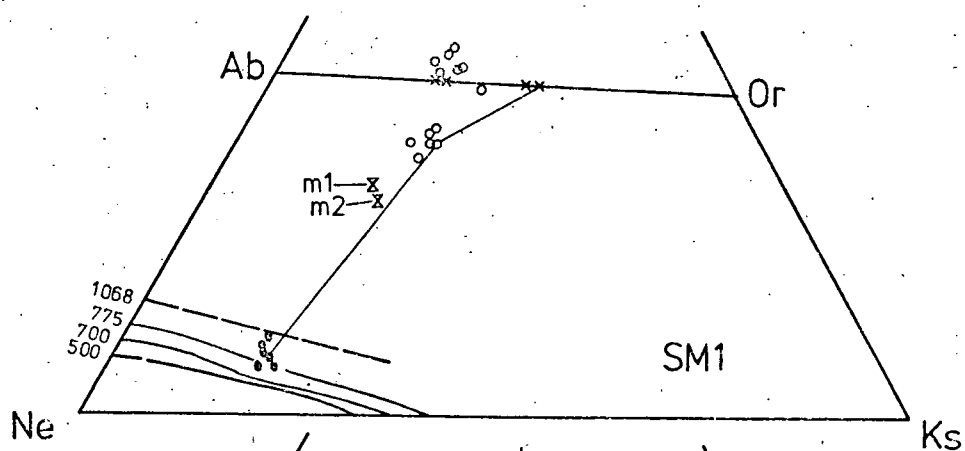
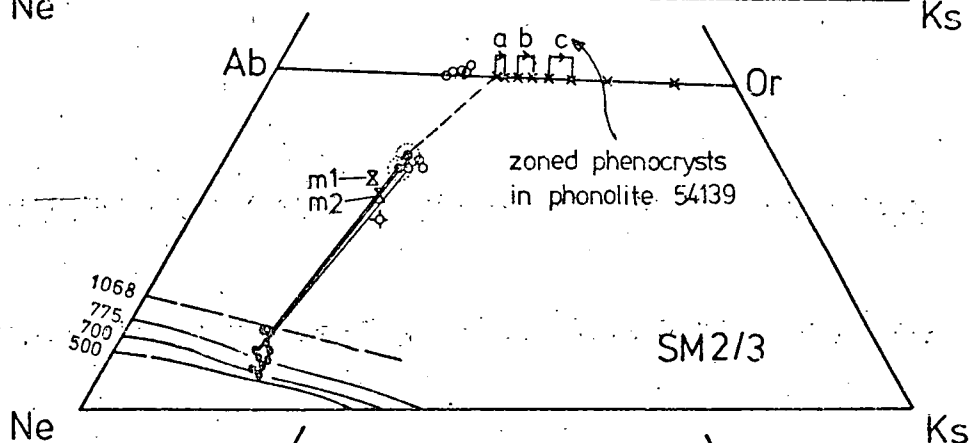
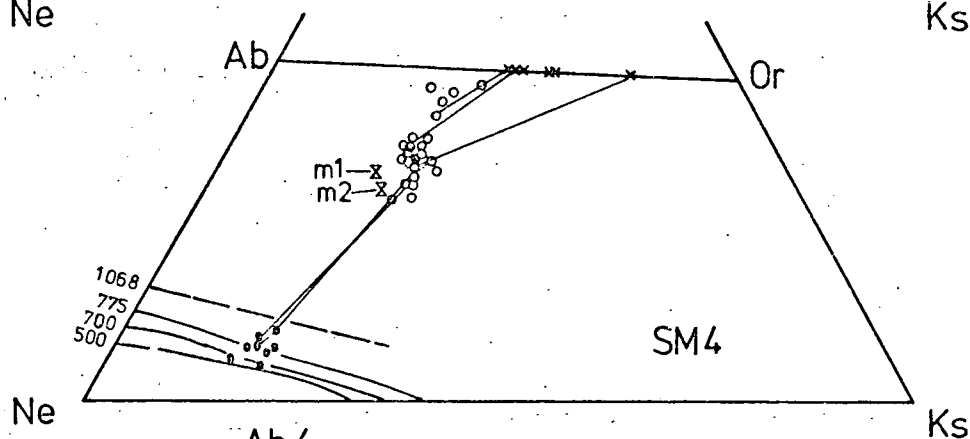


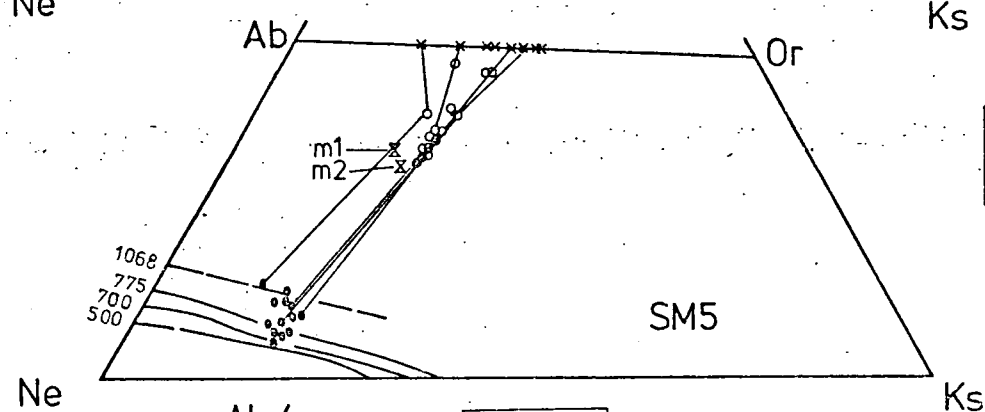
Fig. 5,13



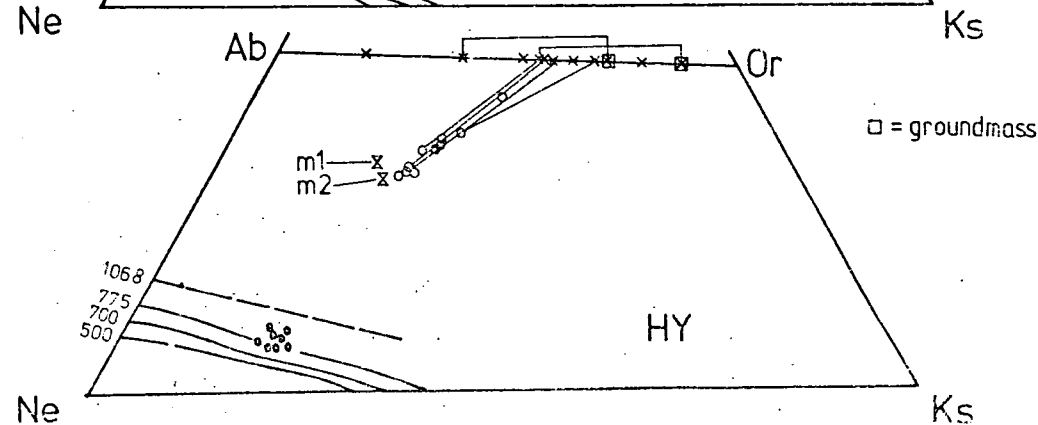
- = Whole rock
- ⊙ = ? liquid
- × = feldspar
- = nepheline
- ◇ = late sheet



m1 and m2 are ternary minima at 1 and 2 kbar P_{H_2O} respectively



nepheline isotherms are in °C



□ = groundmass

data, suggest that nepheline might have crystallised out from SM3 but is not present in the cumulates north of Flink's Dal fault. The explanation of siliceous SM1 may be more complex, since nepheline rich syenites do occur in a few localities close to the margins of SM1. There is evidence that SM1 was initially undersaturated at the time of intrusion, such as a "chill" of fine grained nepheline syenite in N.E.Motzfeldt (58377). It appears likely that its composition was modified by the interaction with quartz rich country rock. This need not apply just to unit SM1 since wherever a syenite abuts gneiss, the syenite tends to be poor in nepheline. Furthermore, the abundance of quartz in the gneiss sometimes drops noticeably as the syenites are approached, as for example in Flink's Dal, suggesting that the process occurs both ways. Studies of the metasomatised gneisses around the North Qôroq Centre (Chambers 1976) have revealed an increase in Na content of the mafic phases coupled with increased Na/K in the feldspars, and a rather more diffuse K-enrichment at greater distances from the centre (c. 1-200 m). Evidence against gneiss being the source of silica may also be found in Flink's Dal, where 100 m scale rafts of gneiss immediately adjacent to the outer contact of the centre are apparently little altered by their host syenite, although they are recrystallised somewhat. An alternative source of silica could be the more porous sandstones and quartzites of the Eriksfjord Formation, since apparently none are preserved within the centre, although they are seen at its edges. Further explanations for the lack of nepheline are considered in section 5.3. of this chapter. Perhaps the most likely explanation is the view of Chambers (1976) who believes that meteoric water played a crucial role in determining the level of silica saturation in the syenites of the North Qôroq Centre.

The presence of quartz in the norms must be due to the assignment of Fe/Mg cations to hypothetical silica poor olivines, rather than to the comparatively silica rich amphiboles, so characteristic of these rocks.

(b) Unit SM4

Bearing in mind the large volume and complex relationships seen within SM4, between xenolithic lavas and HY in Central Motzfeldt, it is quite possible that more than one liquid composition could have evolved separately during the cooling history of this unit. This appears to be the case in Flink's Dal (see Chapter 3) and may account for some of the scatter in figure 5,13. SM4 contains quite frequent cumulates which do not necessarily represent liquid compositions, and whose significance in the residua system should be carefully evaluated before attempting to extrapolate lines of liquid descent (see section 5.10.B.).

(c) Unit SM5

This unit appears to fractionate from larvikite (SM5*) through lardalite to nepheline syenite, the latter comprising about 80-90 % of the unit. This unit in particular, demonstrates a distinct similarity in its style of fractionation to that observed in other of the Igaliko centres.

5.10.B. The Residua system and phase tie-lines

Provided that the rock represents a liquid composition, tie-lines constructed between the rock and the coexisting feldspar will give the initial direction in which the residual liquid moves, as feldspar crystallisation continues. In practice, an array of tie-lines may define a set of conjugation lines from which fractionation curves can be constructed. In this way, for example, alkaline lavas from Mount Suswa in Kenya (Nash et al 1969) have been related to feldspar fractionation and compare favourably with experimentally determined trends for the synthetic system Ne-Ks-Qz obtained by Hamilton and MacKenzie (1965).

The positions of the minima in natural systems may deviate from the synthetic Ne-Ks-Qz for several reasons;- (1) Magmas containing an anorthite (An) component may be displaced towards the Ks-Qz join (Carmichael 1964: Gittins 1979): (2) For peralkaline magmas where $(Na+K)/Al > 1$,

the minimum may be displaced towards the Ne-Qz join: (3)
Where $P_{H_2O} < P_{total}$ the minimum may be displaced towards the Ne-Ks join.

A system which possesses, or develops one or more of the above characteristics will have rather more complex trends than might otherwise have been expected. Thus, a displacement of the liquid lines of descent to the K-rich side of the experimental system and concave towards Ne-Qz are shown by the lavas of Mount Suswa (Nash et al 1969) and the South Qôroq Centre (Stephenson 1976).

(a) Phonolitic "chills"

The phonolite from SM2 may contain phenocrysts of feldspar whose bulk composition varies. Sample 54139 from SM2 is indicated in figure 5,13 where each of three analysed phenocrysts show outward zonation towards K-enrichment. The compositions of the phenocrysts have not been subtracted from that of the rock, although their abundance is roughly similar to both the groundmass and the Norm. These rocks are just peralkaline and for that reason perhaps a little displaced towards the Ne-Qz boundary.

(b) SM4 and cumulates

There is evidence in SM4 and elsewhere in the Motzfeldt Centre for nepheline rich and nepheline poor cumulates. Feldspar cumulates which form from a phonolitic liquid will vary in composition in relation to both the composition of the feldspar and the liquid. Figure 5,14 illustrates the likely fields of "early" feldspar cumulates and "late" feldspar cumulates formed from increasingly K-rich feldspar. The K-enrichment shown by progressively more fractionated rocks may be at least in part due to crystallisation of nepheline, causing K/Na to increase in the residual liquid. It is clear that cumulates which do not represent liquid compositions, will extend the apparent range of compositions. Since nepheline changes its composition comparatively little with fractionation or decreasing temperature, nepheline rich cumulates should plot between the composition of their parental liquid and

that of nepheline. An example of a nepheline cumulate from beneath a raft in the vicinity of Flink's Dal, is indicated on figure 5,14.

(c) Unit HY, mixing and partial melting

Field evidence and petrographic examination suggests that HY consists essentially of nepheline microsyenite intimately associated with variable amounts of relic nepheline syenite. The deceptively simple trend in the system Ne-Ks-Qz (fig. 5,13) could be explained by mixing of rather 'late' formed feldspar cumulates (relic nepheline syenite) with new phonolitic magma (nepheline microsyenite). Any partial melts derived from the relic syenites will tend to be minimum temperature compositions and thus form near to the ternary minimum in the system Ne-Ks-Qz at the appropriate pressure. HY appears to form a fairly tight trend between K (and Rb) rich syenite and compositions very close to the ternary minimum at $P_{H_2O} = 2$ kbars. This is really a line of mixing, induced by varying proportions of minimum temperature partial melts, apparently formed in situ, and relic syenite. The need for an additional phonolitic liquid (ie: not the partial melt itself) arises from the need for a heat source and the field evidence which suggests that SM4 was this source.

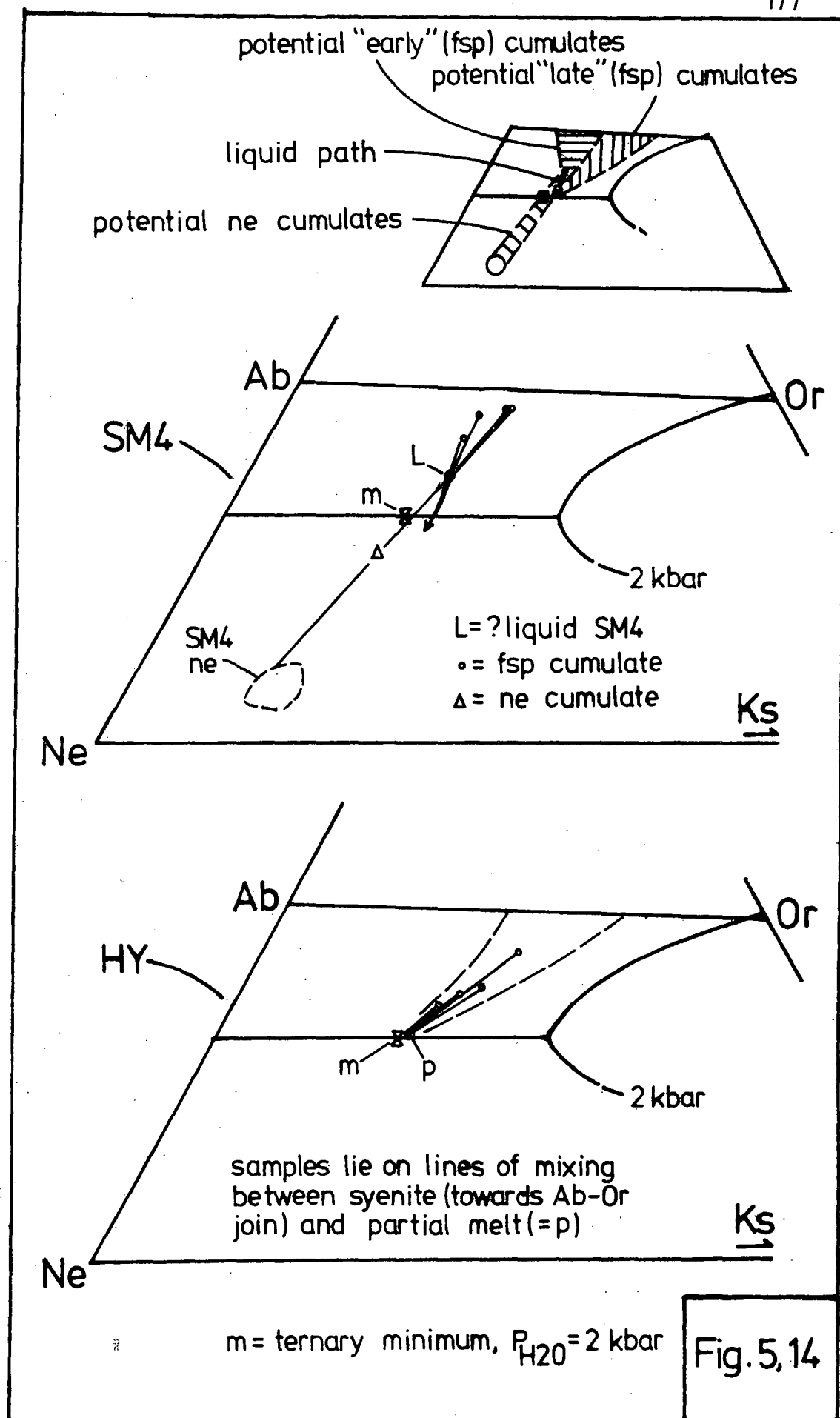
The common presence of sodalite and cancrinite suggests that the pressure of 2 kbar P_{H_2O} might well be a minimum, since significant amounts of fluorine and CO_2 were also present. The occasional presence of two separate feldspars may further suggest proximity to the phonolite minimum at pressures greater than 2 kbars.

Despite the abundance of nepheline, the microsyenite is sometimes composed predominantly of very K-rich feldspar (c. Or_{80}) and it is perhaps possible that some Na has been lost from these rocks.

5.11. Liquid lines of descent

5.11.A. Summary

A summary of the liquid lines of descent, deduced from the above discussion, is presented for the system



Ne-Ks-Qz in figure 5,15. It should be borne in mind that the trends of SM5 and to a lesser extent SM1, lie somewhat out of the plane of the diagram since they contain some An. The latter parts to most of the trends are similarly affected because they become peralkaline.

5.11.B. Unit SM6 and the system Al_2O_3 - Na_2O - Fe_2O_3 - SiO_2 .

Figure 5,16 illustrates part of the system Al_2O_3 - Na_2O - Fe_2O_3 - SiO_2 projected from the silica apex onto the plane Na_2O - Fe_2O_3 - Al_2O_3 . "E" is the experimentally determined ijolitic minimum at 1 atmosphere pressure (Bailey and Schairer 1966) while "E*" represents the amended ijolitic minimum postulated by Engell (1973) when applied to the agpaitic rocks from Ilímaussaq. Larsen attributed this shift as being due to CaO contents in the natural liquids and subsequent enlargement of the pyroxene stability field as predicted by Nolan (1966).

The locus of samples from a microkakortokite dyke suffering alkali loss as reported by Larsen and Steenfelt (1974) is indicated in figure 5,16. The more alkali rich of the latter plot in the "oxide" field, yet actually bear aenigmatite and are free of oxide. Similarly, lujavrites from Motzfeldt are also oxide free and appear to converge on the most alkaline microkakortokite from this dyke. The phase relations appear to be displaced in the natural, relative to the synthetic system (see fig. 5,16) in agreement with Larsen and Steenfelt (1974) who suggest that lowering $f\text{O}_2$ and the presence of other components such as halogens and water, might be important. Perhaps the most important factor here would be pressure, and essentially $P_{\text{H}_2\text{O}}$, since the experimental system was investigated at atmospheric pressure whereas the lujavrites at Motzfeldt probably crystallised at pressures of at least 2 kbars.

Samples of green lujavrite which are occasionally found at Motzfeldt, have not been analysed, but may plot close to the apparent minimum ("A" in fig. 5,16). The position of "average green lujavrite" from Ilímaussaq (Ferguson 1970) is indicated in figure 5,16 for comparison.

The lujavrites may represent a natural compositional

E = ijolite point, P=1atm, from
Bailey & Schairer (1966)

E' = suggested ijolite point for
natural system; Engell (1973)

A = suggested ijolite point for
Motzfeldt?

● = lujavrites, SM6

× = av. green luvavrite from
Ilímaussaq (Ferguson 1970)

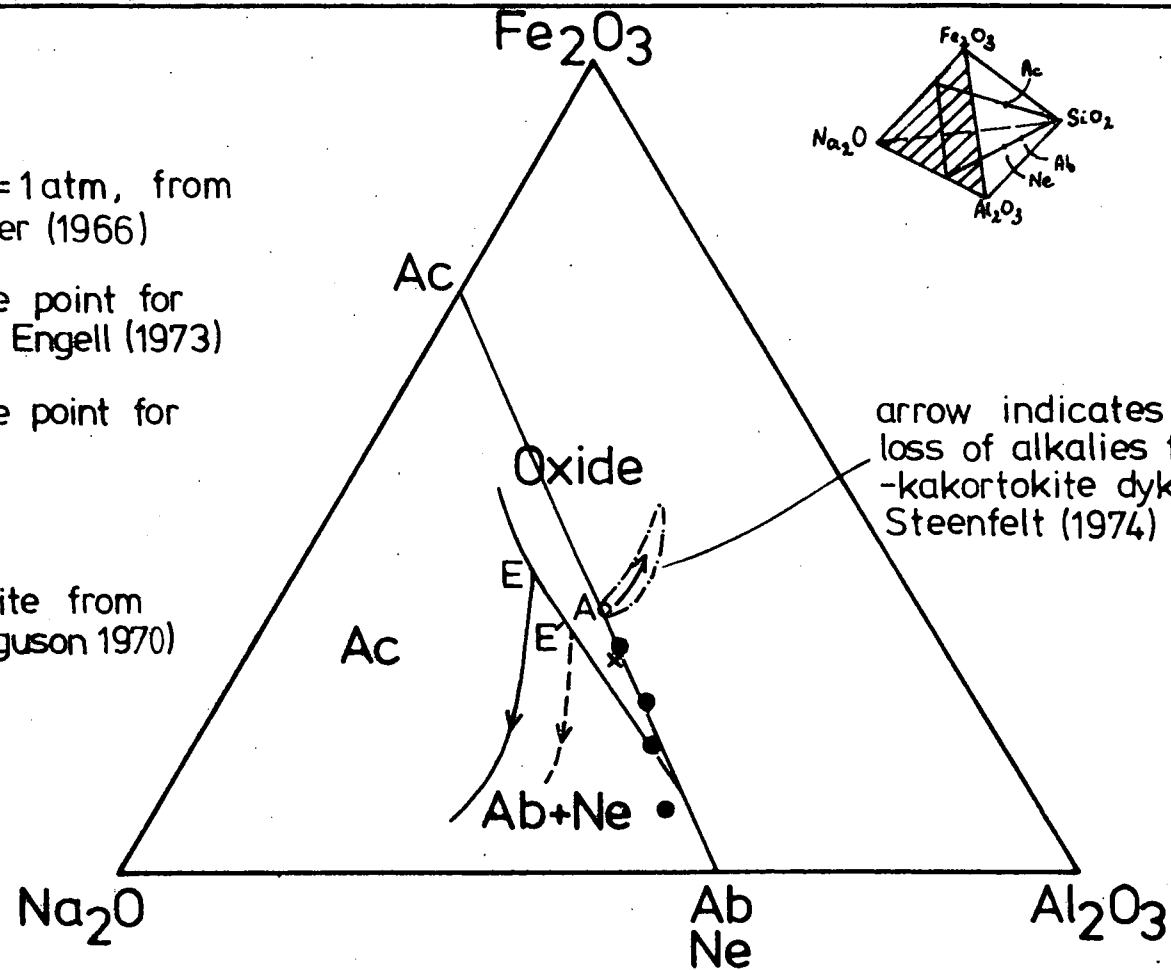


Fig. 5.16

goal for fractionating peralkaline syenitic magma (Bailey and Schairer 1966, p.156) however, a liquid of ijolitic composition ("E") in the synthetic system investigated by Bailey and Schairer (1966) could also form by partial melting of a slightly undersaturated acmite syenite.

Key to Table (5) 2. Lavas.

- 1. = basalt flow (63758)
- (2.) = trachyandesite; Larsen analysis no: 12
- 3. = trachyandesite (AM18)
- 4. = trachyandesite (54126)
- (5.) = trachyte; Larsen analysis no: 5
- 6. = trachyte (59639)
- 7. = trachyphonolite (AM24)
- 8. = trachyphonolite (AM25/I)
- (9.) = average phonolite; Nockolds 1954
- 10. = phonolite (AM32)

References:

J.G.Larsen 1977

S.R.Nockolds 1954

Sketch location of Motzfeldt lavas



Supracrustals, the Eriksfjord Formation:



Country rock, mostly Julianehåb Granite.

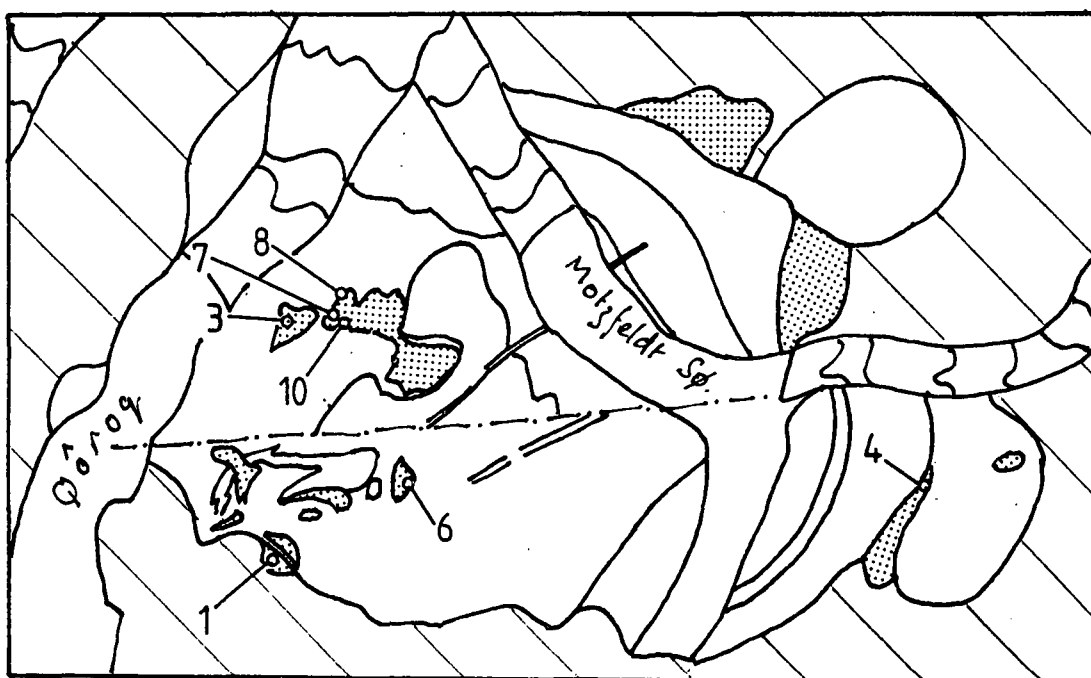


TABLE (5) 2. Lavas from the Motzfeldt Centre (compared).

	1. Basalt	(2.) Tr/And	3. Tr/And	4. Tr/And	(5.) Tr	6. Tr	7. Tr/Phon	8. Tr/Phon	(9.) Phon.Av	10. Phon
SiO ₂	47.84	55.40	54.00	56.58	58.50	57.05	58.23	58.38	56.90	56.71
TiO ₂	1.90	1.75	1.69	1.55	0.78	1.08	0.37	0.65	0.59	0.29
Al ₂ O ₃	15.61	16.43	19.75	16.17	16.41	16.65	20.29	19.03	20.17	20.86
Fe ₂ O ₃ *	14.26	8.26	6.03	9.40	9.01	10.48	5.63	7.37	4.31	5.92
MnO	0.18	0.14	0.24	0.20	0.20	0.32	0.27	0.34	0.19	0.25
MgO	7.65	1.72	2.24	1.93	0.64	0.79	0.30	0.89	0.58	0.26
CaO	9.09	3.44	2.74	3.33	1.79	3.22	1.94	2.01	1.88	1.21
Na ₂ O	2.99	5.62	5.87	4.88	5.78	5.36	5.44	6.46	8.72	8.34
K ₂ O	0.64	4.85	4.15	5.36	5.98	4.78	6.35	4.30	5.42	5.46
P ₂ O ₅	0.61	0.62	0.71	0.58	0.15	0.33	0.09	0.18	0.17	0.06
Total	100.77	98.9 ^a	97.42	99.98	99.9 ^a	100.06	98.91	99.61	99.87 ^a	99.36

Trace elements (ppm)

Rb	41	106	123	195	174	91	212	163		215
Sr	347	623	1981	402	106	133	482	655		69
Ba	254	2578	3018	2982	336	367	93	995		70
Y	34	26	56	35	63	67	47	75		65
Ce	51	102	232		307	354	359	478		503
La	19		158	67		135	143	222		182
Nb	9	97	152	85	248	156	241	310		263
Zr	137	285	562	468	664	648	918	1339		1235
U	3		5	2		4	8	6		12
Th	19		18	2		23	17	23		21

*total iron

Tr = trachyte, Tr/And = trachyandesite, Tr/Phon = trachyphonolite, Phon = phonolite

^aincludes l.o.i.

TABLE (5) 3. Intrusive phonolites (with one lava).

	SM2 54139	SM2 54142	SM3 54138	SM4 AM7	Lava AM32
SiO ₂	56.27	56.63	56.57	56.82	56.71
TiO ₂	0.49	0.49	0.25	0.39	0.29
Al ₂ O ₃	20.60	20.16	20.66	20.39	20.86
Fe ₂ O ₃ *	5.15	5.58	5.33	5.32	5.92
MnO	0.21	0.23	0.25	0.25	0.25
MgO	0.44	0.52	0.33	0.35	0.26
CaO	1.21	1.34	1.12	1.24	1.21
Na ₂ O	8.84	8.49	9.08	8.49	8.34
K ₂ O	5.91	5.73	5.64	5.92	5.46
P ₂ O ₅	0.18	0.19	0.07	0.16	0.06
Total	99.30	99.36	99.30	99.33	99.36
Na/(Na+K)	0.69	0.69	0.71	0.69	0.70
(Na+K)/Al	1.02	1.00	1.02	1.00	0.94
FI	90.7	89.2	90.5	90.5	87.5
<u>Trace elements (ppm)</u>					
Rb	188	194	231	216	216
Sr	466	388	153	284	69
Ba	834	762	139	546	70
Y	40	57	58	77	65
Ce	282	347	385	449	503
La	125	149	162	173	182
Nb	178	241	267	281	263
Zr	690	924	1045	895	1235
U	3	6	11	6	12
Th	14	30	35	23	21

*total iron as Fe₂O₃.

CONCLUSIONS AND PETROGENESIS

Introduction

This chapter essentially reiterates the major conclusions reached in this study and indicates how they effect the proposed petrogenetic scheme for the Motzfeldt Centre. A short review of the principal theories governing the origins of layered igneous rocks is given and the evolution of the centre is viewed in the light of the principle magma compositions intruded and their relationships to an earlier sequence of lavas. The centre is then considered in perspective of the Gardar province as a whole and features are compared to the Kenya Rift in East Africa. Finally, the likely sources and methods of generation of the magmas are assessed and plausible reasons for the degree of saturation with respect to silica are summarised.

6.1.A. Evolution at the current exposure level

The major syenite units SM1, 2, 4 and 5 of the Motzfeldt Centre, are rounded in plan and have outward sloping margins which show no signs of brecciation or crushing. It seems that they were emplaced permissively by a combination of block-stopping and ring fracture (Emeleus and Harry 1970). Units SM3 and SM5* are partial ring dykes with apparently very steep contacts.

In view of the large volumes of nepheline syenite found in units SM2, 3 and 4 and the absence of any basic marginal types, it seems likely that the parental magmas to these units were initially of similar composition to the average bulk composition of each unit. This is substantiated by the presence of phonolitic margins to SM2 and SM4. Unit SM3 in S.E.Motzfeldt is a nepheline microsyenite of almost identical composition to the latter two phonolites (see Chapter 5, Table 3). These phonolites contain euhedral phenocrysts of feldspar, nepheline, pyroxene and possibly olivine, whilst in

addition SM3 bears several phenocrysts of amphibole.

The Motzfeldt Centre is deeply dissected by valleys and glaciers, exposing a vertical sequence of nearly 2 km of intrusive rocks. Any movement which has occurred on the Flink's Dal fault will effectively increase this stratigraphic height. Deep levels of SM3 north of this fault are composed of syenites apparently devoid of nepheline but rich in mafic minerals. Here, sub-horizontal layers rich in mafic minerals (px, mt, zircon, amph) may alternate with less mafic layers on a 10 cm scale. Samples of SM4 from the lowest structural levels are notably poorer in nepheline and richer in mafic minerals than samples from structurally higher positions. In Flink's Dal, syenites beneath large rafts of lavas are often leucocratic and particularly rich in euhedral nepheline. Immediately above these rafts may be found several 10 cm scale layers of mafic syenite and laminated syenite both impoverished in nepheline and lying in a sub-horizontal attitude which parallels the topography of the underlying raft. Elsewhere in SM4 one or two mafic bands may be traced for up to 2-300 metres. In these layered rocks and commonly throughout the Motzfeldt Centre, petrographic textures bear a strong resemblance to cumulus textures described by Wager and Brown (1968). Far better layering is present in the Igdlarfigssalik Centre (Emeleus and Harry 1970; Powell 1976) and is found in other intrusive centres throughout the Gardar province.

Classically, such textures and layering would be attributed to the gravity accumulation described by Wager et al (1960) and Wager and Brown (1968), wherein successions of minerals have settled out through a less dense magma to form layers of cumulates. According to the model proposed by Wager (1963) for the Skaergaard Intrusion, crystals nucleated under the roof, grew as they were carried across the top and down the sides of the chamber and settled out as the current moved across the floor. Subsequent work by Irvine (1970) on heat transfer, further quantified many of the processes

which may take place during the formation of cumulates by gravity settling in a cooling igneous intrusion. The formation of layered igneous intrusions such as Skaergaard by gravity accumulation from a convecting magma chamber received strong support from the identification of demonstrably sedimentary structures formed by the magmatic currents.

However, inverted way up criteria, inverted graded bedding and inverted cryptic layering recently described in syenites from the Klokken Intrusion by Parsons (1979) have placed considerable strain upon the theory of gravitational accumulation. Parsons (1979) advocates a process of oscillatory crystallisation ~~in-situ~~ for these unusual layered rocks. Several previous workers have appealed to a similar process ~~and~~ in situ crystallisation, where layering can not easily be attributed to gravitational processes.

Recent fluid dynamic experiments and revised considerations of the physical properties of magmas and their cumulus minerals by McBirney and Noyes (1979) have provided an alternative explanation for all of the cumulus textures and types of layering described from the Skaergaard Intrusion (Wager 1963; Wager and Brown 1968). Thus McBirney and Noyes (1979) would now totally abandon the concept of crystal settling in favour of one of in situ crystallisation for the Skaergaard Intrusion. In their model, layering is produced in response to differential rates of thermal and chemical diffusion such that crystals that nucleated and grew, were trapped by an increasingly rigid zone that advanced more rapidly than the crystals sank or floated. Furthermore, they suggest that intermittent layering is due to gravitational stratification of the liquid and ascribe cyclic layering to oscillatory processes of nucleation and crystal growth.

In view of the current controversy surrounding the origins of layered igneous rocks, no single process can be advocated for the formation of the cumulus features observed in the Motzfeldt Centre. The settling

displayed by the rafts of lavas in Flink's Dal must suggest that similarly dense crystals might also have settled out from the same magma to form the small layered sequences seen upon these rafts. However, the mafic layers alternate with layers rich in flattened tabular feldspars preferentially aligned with their short axis at right angles to the layering. It is difficult to envisage alkali feldspar sinking through a magma of syenite or nepheline syenite composition since their densities might even suggest the converse.

Volumetrically, much of the Motzfeldt Centre is now represented by unit SM4. This unit measures approximately 18 x 12 km in area and was intruded as a magma of phonolitic composition from which its bulk composition has been comparatively little changed. The vertical extent of this unit is at least 1.7 km and possibly considerably more. SM4 has undergone some modification by local accumulation of phases as outlined above, which in the Flink's Dal area has been influenced by the disposition of the rafts of lavas. In this area, as possibly elsewhere, SM4 consists of more than one intrusion. Units SM2 and SM3 were also emplaced as liquids of phonolitic composition, and subsequent absence of nepheline from SM3 north of the Flink's Dal fault may be due to variation in P_{total} .

The silica saturated composition of much of the outer syenite, SM1, may be due to interaction with siliceous country rock. A similar "silica enrichment" has been noted in the North Qôroq Centre (Chambers 1976), where this could be due to the interaction of the magma with meteoric water. This would result in a tendency for fO_2 to increase, which would lead to preferential crystallisation of oxides over olivine resulting in increasing silica enrichment of the residual liquid (Morse 1968). Similarly the preferential crystallisation of OH-bearing phases such as biotite or amphibole, which are both relatively undersaturated (Macdonald 1974) would result in an oversaturated liquid trend. An increase in P_{H_2O} would also lower the temperature of the thermal divide

in the system Ne-Ks-Qz (Morse 1968; Chambers 1976) which would make it easier for a liquid of trachytic composition to be driven across, if already well above the liquidus temperature.

Estimates of the initial temperatures of the marginal phonolites at the time of their emplacement, based on the olivine/clinopyroxene geothermometer of Powell and Powell (1977) yield values of 980-1000 °C (see Chapter 4, geothermometry). Feldspar appears to have been a high temperature, early crystallising phase throughout the cooling history of SM4 (as for most other units). Preferential removal of feldspar from an undersaturated liquid will tend to drive the composition of the residual liquid towards further undersaturation. Using thermodynamic studies of mineral equilibria, Powell (1978) has demonstrated that initial high temperature phases crystallised from alkaline magmas of the Igdlarfigssalik Centre, continued to re-equilibrate with each other to varying degrees with falling temperature. A similar range in temperatures may be expected for unit SM5 of the Motzfeldt Centre, which bears strong similarities to the augite syenite related magmas of the other Igaliko centres. In SM5, nepheline and alkali feldspar continued to re-equilibrate to about 650 °C (see Chapter 4) while, based on the comparable data of Powell (1978) exsolution in Fe-Ti oxides probably continued to below 600 °C. Since the melting interval (liquidus-solidus) appears to be directly proportional to the peralkalinity of the melt (Piotrowski and Edgar 1970; Sood and Edgar 1970; Edgar and Parker 1974) an even greater temperature interval, during which phases continued to re-equilibrate, may have existed in the more evolved and peralkaline syenites of the Motzfeldt Centre. The volatile rich lujavrites of SM6 are just such an example.

6.1.B. Evolution of the lujavrites

There are two major sequences of crystallisation in the lujavrites. In the white lujavrites, feldspar crystallised early, followed by clinopyroxene or nepheline

and eudialyte is mainly interstitial. In the dark lujavrites, nepheline and eudialyte are phenocryst phases, whilst flow aligned groundmass laths consist of clinopyroxene and two separate feldspars. The experiments of Sood and Edgar (1970) suggest a melting interval for lujavrite from 880 to 430 °C at 1 kbar P_{H_2O} . However, their observed order of nucleation of phases (Fsp-Cpx-Ne-Eud/Amph) does not agree well with the petrographic description of a similar lujavrite given by Sørensen (1962, Ne/Sod-Fsp/Eud-Amph).

One further prominent feature of the dark lujavrites is that banding on a 1-5 cm scale parallel to their contacts, is expressed not only in the different proportions of the constituent minerals, but also by different sizes of nepheline euhedra. There is no predictable variation with distance from the margin, although the actual contact zones are usually finer grained. Whilst one may invoke a process of differential flow to account for these features, it seems more likely that they were caused by variation in the rates of crystal nucleation and growth. This may have been induced by different degrees of undercooling in a magma which may have suffered minor fluctuations in volatile content. In this way a rather passive but penetrative body of dark lujavrite could form bands without recourse to the comparatively vigorous flow mechanisms required for flow differentiation. Returning to the experimental results of Sood and Edgar (1970), it is possible that feldspar is the first phase to appear on the liquidus instead of nepheline because the degree of undercooling differed from that found in the natural system. It is interesting that the order of crystallisation observed by Sood and Edgar is very similar to that seen in the white lujavrites (Fsp-Cpx-Ne-Eud).

Increasing P_{H_2O} should expand the field of feldspar in the system Ne-Ks-Qz yet it should also decrease the amount of undercooling (Parsons 1979) which might favour crystallisation of nepheline. This apparent

dilemma may be resolved by assuming that these two phases (Fsp, Ne) have no equilibrium melting interval, in which case small variations in P_{H_2O} might be critical in determining nucleation and growth rates by effecting the amount of undercooling. Small variations in P_{H_2O} would have comparatively small effects on the phase boundaries in the system Ne-Ks-Qz, which is not strictly representative of the lujavrites in any case.

The lujavrites conform, more or less, to a minimum temperature "ijolite" composition in the system $Na_2O-Fe_2O_3-Al_2O_3-SiO_2-(H_2O)$ (Bailey and Schairer 1966). Thus the lujavrites apparently represent the consolidation of a liquid whose composition approximates to the bulk composition of the lujavrites and which may be the natural goal for fractionating peralkaline syenitic magma (Bailey and Schairer 1966, p.156). Deviations from the experimental system are probably due to differences in P_{H_2O} and the addition, as in most natural systems, of several other components including for example calcium which will expand the field of pyroxene (acmite) and halides (see Chapter 5, 10.B.).

The disposition of the lujavrites at Motzfeldt is broadly reminiscent of their more iron rich and aluminium deficient counterparts at Ilímaussaq (Ferguson 1964). They appear to form a sort of sandwich horizon and are situated beneath rafts of lavas, which may in the simplest sense have acted as a volatile trap. This magma presumably formed in response to the repeated intrusion and fractionation of undersaturated syenite and although not seen in the adjacent North Qôroq Centre, the presence of a similar magma is strongly inferred from the work of Chambers (1976). As Bailey and Schairer point out (1966), partial melting of an undersaturated acmite-bearing syenite would also lead to a liquid of ijolitic (~lujavritic) composition.

6.2. Partial melting of existing syenites

The relationship between HY and SM4 in Central Motzfeldt is complicated (see Chapter 2) but it appears that HY is a large remnant of nepheline syenite which

has undergone varying amounts of re-melting in situ. HY is rich in volatile constituents and has a variable though often peralkaline bulk composition. HY varies from little altered nepheline syenite to nepheline microsyenite bearing relics of nepheline syenite. The microsyenite is so intimately related on all scales that it is believed to have formed in situ. HY is fairly enriched in residual elements such as Ce and Y which are often present as rinkite-type minerals. Recrystallised syenites from the North Qôroq Centre exhibit an identical enrichment in rinkite (Chambers 1976). When plotted in the system Ne-Ks-Qz samples from HY form a fairly well defined line of mixing between relatively K-rich syenite and the experimentally determined minimum in the same system at a pressure of $P_{H_2O} = 2$ kbars. Field evidence suggests that SM4 just postdates HY and was presumably the source of heat for the re-melting. From the often very K-rich nature of HY it is possible that some Na has been lost.

Further evidence for the partial melting in situ of nepheline syenites comes from unit SM5 which has been remobilised over a distance of a few metres by the alkali gabbro dyke, and from the zone up to 1 km wide of the South Qôroq Centre recrystallised and in places remobilised by the younger Igdlérfigssalik Centre (Stephenson 1976). Stephenson reports of the recrystallised zone (1976) that the major elements are largely unaffected but the same rocks are consistently depleted in residual trace elements. He also reports that the Na/K ratios are depleted in the feldspars and Na is increased in the pyroxenes. Stephenson further concludes that the physical conditions pertaining during this recrystallisation involved increased fO_2 ($> FMQ$ buffer) combined with a CO_2 -bearing aqueous solution.

A natural extension of this same process comes from consideration of the stoped blocks of syenite which have resulted from the repeated and localised intrusions of magma in the Motzfeldt Centre. Estimates of cover at the time of formation of the centre based upon normative

mineralogy and crude minimum estimates of lava sequences, suggest that a pressure of $P_{\text{total}} (P_{\text{H}_2\text{O}}) = 2 \text{ kbars}$ is reasonable for the conditions under which the majority of the syenites crystallised. The deeply dissected topography enables a minimum chamber height to be placed at 1.7 km. By nature of the overlap of successive intrusions and, assuming the block-stopping process to apply, it becomes apparent that early formed syenites will be displaced downwards a considerable distance into the crust. Assuming that the first major unit, SM1, was emplaced at a depth of 6 km and by taking a chamber height of 3 km, SM1 can be displaced downwards by the equivalent height of each subsequent intrusion (SM1 is overlapped by SM2, 4 and 5) with the result that a considerable volume of SM1 must attain a depth of around 15-18 km below the Early Gardar landsurface. Ambient temperatures at these depths in a rift zone might be around 5-600 °C (see Chapter 3) which alone might cause partial melting of a minimum temperature composition, just such as nepheline syenite. In this way the two processes of fractionation and partial melting would have as their goal a minimum temperature composition at the relevant pressure, rich in residual elements.

6.3. Association of the Motzfeldt Centre with an earlier sequence of lavas

Rafts up to 5 km long and often in excess of 100 m thickness preserved within the Motzfeldt Centre are formed of lavas. The Motzfeldt lavas, whose base corresponds closely to the base of the Ilímaussaq Volcanic Member (see Chapter 5) apparently represent an upward extension to the currently preserved Eriksfjord Formation. Fresh samples of phonolitic lavas from the lavas are compositionally very similar to the phonolitic margins of units SM2, 3 and 4 and have several identical incompatible element ratios (see Chapter 5, 7.B.). It seems highly probable that these phonolitic lavas were derived from similar, though somewhat earlier phonolitic magmas to those which cooled at depth to give the nepheline syenites.

The lavas can be roughly divided into basalts, trachytes and phonolites in which case it can be seen that each "group" has a discrete set of incompatible element ratios. This suggests that the lava groups are not related to the same source by any simple form of fractionation and on this basis, Larsen (1977) concluded that the upper fractionated lavas of the Ilímaussaq Volcanic Member were unrelated to the lower basalts. However, O'Hara's open system (1977) provides one mechanism whereby these lavas could have been derived from the same source magma. In this situation (O'Hara 1977; O'Hara and Mathews 1980) a magma chamber undergoing continuous fractionation is periodically replenished with new batches of parental magma, possibly coincident with removal from the chamber of the more fractionated magma to produce lavas at the surface. This system of volcanic plumbing could lead to significant variations in the ratios of two incompatible elements between different erupted steady state lavas. In O'Hara's model the magma chamber advances upwards in front of a thickening pile of cumulates, and the volumes of magma added to or tapped from the chamber may be small in comparison to the size of the chamber. This process is akin to "zone refining" in that residual elements are enriched and may well apply to the recycled syenites considered in section 6.2. above. There is ample evidence at Motzfeldt that lavas were being incorporated into the magma chambers and according to O'Hara (1977) this might lead to even more peculiar characteristics.

6.4. Magma compositions

Any postulated source for the magmas which formed the Motzfeldt Centre, should not be considered in isolation, since there is apparently a clear genetic relationship between the phonolitic lavas now preserved as rafts and the nepheline syenites. This tends to confirm the implications of Larsen (1977) and the suggestion of Upton and Blundell (1978) that the lavas of the Eriksfjord Formation were erupted shortly before

the emplacement of the North Qôroq and Motzfeldt central complexes and that the petrogenesis of the intrusions and lavas is closely related. The lavas at Motzfeldt seem to have constituted an upward extension to the currently known Eriksfjord Formation (for review see Emeleus and Upton 1976), and their base correlates well with the base of the Ilímaussaq Volcanic Member (IVM). Many of the lavas from the Motzfeldt Centre are more fractionated than those described from the IVM by Larsen (1977) and contain, for example, frequent nepheline phenocrysts. Estimates of P_{total} derived from the normative mineralogy suggest a value of 2 kbars, which would correspond to a cover of around 6 km at the time of emplacement of the Motzfeldt Centre. A maximum pressure of $P_{\text{H}_2\text{O}} = 3$ kbars would not contradict the feldspar mineralogy (see Chapter 4). It seems likely that most of this cover could be attributed to a thick succession of trachytic and phonolitic lavas. This would imply that the 3500 m of the Eriksfjord Formation preserved between Sermilik and Tunugdliarfik fjords might represent perhaps as little as one third of the original succession.

From an occurrence of prehnite and pumpellyite on Ilímaussaq, Larsen (1977) affirms his opinion that the lavas on the Narssaq peninsula were subject to "low" pressure metamorphism. However, the experimentally deduced stability limits for this assemblage (see Chapter 3) favour a pressure in excess of 2.5 kbars, which would lend support to an original succession 2 or 3 times that currently observed. Beneath the 740-1300 m of the IVM on the Narssaq peninsula, the Eriksfjord Formation is composed of 2300 m of continental sandstone, a few conglomerates, alkaline ultramafic and carbonatitic volcanics, basalt lavas and sills (Poulsen 1964; Stewart 1964, 1970).

Within the whole Eriksfjord Formation it is estimated that hawaiites and basalts make up 70 %, more differentiated basic lavas 7 % and trachytes 23 % of the lava pile (Larsen 1977). If an additional 6 km of predominantly trachytic and phonolitic lavas were combined with the existing succession, then the frequency

distribution would be redressed (then about 25% basalts) strongly in favour of the areal distribution of intrusive rocks, where gabbros and dolerites comprise about 13 % (Watt 1966).

In general, the intrusive units of the Motzfeldt Centre become increasingly basic with time, in the order nepheline syenite (phonolite)-larvikite-alkali gabbro. Thus in summary, the phonolites have been modified primarily due to the combined processes of fractionation in situ and re-melting caused by multiple intrusion, which may both have converged on a similar minimum temperature residual peralkaline melt of lujavritic composition. Of lesser volume, the larvikites of SM5 pass rapidly into nepheline syenites which may bear eudialyte where they are highly fractionated. Feldspar fractionation appears to have been the primary cause of increasing undersaturation in SM5. Finally, a 200m wide alkali gabbro dyke bearing xenocrysts of plagioclase near its margins, intruded the centre but is not found outside.

The increasing basicity of successive intrusions with time has been recorded from other centres in the Gardar, such as Kûngnât (Upton 1960) and South Qôroq (Stephenson 1973). Irrespective of any volume considerations, this must signify the presence of basic magmas at depth towards the end of formation of each intrusive centre. Increasing basicity could perhaps be ascribed to a progressive partial melting event or to the tapping off from successively deeper levels within a stratified magma chamber (Stephenson 1973). The South Qôroq, Igdlérfigssalik and North Qôroq centres of the Igaliko Complex are thought to have been derived from alkali olivine basalt via liquids of augite syenite composition (Stephenson 1973, 1976; Powell 1976; Chambers 1976). Many workers in the Gardar advocate immediate parental liquids of augite syenite composition, from which the more salic rocks were derived by fractionation either in situ or at relatively shallow depth (Sørensen 1966; Bridgwater and Harry 1968; Upton 1971, 1974;

Engell 1973; Gill 1972) although an independent origin has not been excluded (Sørensen 1966).

Both the Motzfeldt and the North Qôroq centres are cut by small breccia plugs very rich in carbonates. One 200 m wide oval plug from Motzfeldt bears relic melilite and is in many ways very similar to the carbonatitic and ultramafic volcanic activity recorded from the early part of the Eriksfjord Formation at Qagssiarssuk (Stewart 1970). The alkaline ultramafic/carbonatitic activity, which also occurs at Grønnedal-Ika in the northwest of the province (Emeleus 1964) is apparently confined to the Early Gardar "1300 ma event" of Upton and Blundell (1978).

6.5. Comparison with the Kenya Rift

The Gardar igneous province appears to be the remains of Proterozoic rifting in which three phases of stretching and magmatism occurred (Emeleus and Upton 1976). The association of alkaline igneous rocks, abundant faulting and the presence of sediment-lava piles that clearly accumulated in a block-faulted environment has long suggested the idea of continental rift structures, comparable to those of East Africa, being associated with the evolution of the Gardar province. The fairly recent discovery of an axial gravity "high" of some 300 g.u. amplitude (Blundell 1978) elongated ENE-WSW is very similar to the axial "high" in the Kenya Rift (Fairhead 1976). This anomaly is interpreted in terms of a basic mass underlying a late Gardar rift, some 50 km long (ENE-WSW) and 25 km wide (Blundell 1978) intruding the crust to at least 10 km below present day sea level and surfacing as gabbroic rocks in the region of Narssaq-Tugtutoq.

6.6. Evidence for a mantle source region

Rb-Sr work by Blaxland et al (1978) has shown that the Motzfeldt Centre formed at around 1310 ma and had an initial $\text{Sr}^{87}/\text{Sr}^{86}$ ratio of 0.7024. They recorded a

low initial $\text{Sr}^{87}/\text{Sr}^{86}$ ratio (0.702-0.704) for most of the major syenites in the Gardar province and concluded that this is consistent with an origin from primitive mantle source regions, allowing little, if any, assimilation of sialic crustal rocks. Similarly low initial Sr ratios are taken by other workers as evidence for a mantle source region (eg Wright 1971). Strongly agpaitic magmatism may be associated with rather higher ratios, as for example at Norra Karr where initial $\text{Sr}^{87}/\text{Sr}^{86}$ is around 0.707 (Blaxland 1977) and at Ilímaussaq where initial $\text{Sr}^{87}/\text{Sr}^{86}$ is around 0.710 (Blaxland et al 1978). Blaxland et al (1976) attribute this to selective radiogenic enrichment in Sr^{87} , although Carmichael et al (1974 p.507) are reluctant to accept any Sr isotope evidence as proof of a mantle source.

Striking features of the alkaline salic lavas from the Kenya Rift are their huge volume and uniformity, with comparatively trivial amounts of associated basic lavas. Thus, sequences of phonolites up to 9 km thick are apparently devoid of xenoliths (Lippard pers.comm. 1980) as are the mildly peralkaline trachytes and phonolites of Mount Suswa (Nash et al 1969). However, boulders of rather mafic silica-saturated syenites enriched in Fe, Na and lanthanides, but not in Rb and Zr, have recently been described from a few Kenyan trachyte volcanoes (Jones 1979). Furthermore, the mineral eucolite, the calcic equivalent to the zirconium phase eudialyte, has been reported in pyroclastics from the carbonatitic environs of Oldoinyo Lengai in Tanzania (Dawson and Firsch 1971) and olivine nodules are known to exist in trachytes from the Jos plateau of Nigeria (Wright 1969). That felsic magmas may in fact develop at mantle depths is also suggested by the occurrence of kaersutitic amphibole and the occasional presence of spinel-lherzolite xenoliths in phonolites and trachytes (Wright 1971).

The association of the alkaline salic magmas with alkaline ultramafic and carbonatitic rocks, suggests that igneous activity was occurring, at least in the early stages of the Gardar period, to a deep level.

It is generally accepted that carbonatites are magmatic and may have a deep level origin similar to that of kimberlites and nephelinites (Carmichael et al 1974). It has been shown that hydrous alkaline ultrabasic silicate-carbonate magma splits with falling temperature into two immiscible fractions (Koster van Groos and Wyllie 1968; Wyllie 1977). One fraction ultimately crystallises as nephelinite or ijolite and the other as carbonatite. Experimental work by Mysen and Boettcher (1975) has shown that such magma would be in equilibrium with garnet lherzolite under conditions of low a_{H_2O} and high a_{CO_2} at depths of 125 to 175 km.

6.7. Derivation of the primary magmas

6.7.A. Partial melting

In view of the excess volume of salic volcanics over associated basic magmas in continental rift systems, and the features outlined above which indicate a mantle origin, some authors would attribute the formation of salic magmas by direct partial melting of the lower crust or mantle (Bailey 1970, 1974; Bailey and Schairer 1966; Wright 1971). Bailey (1974) envisages a mechanism in which local warping and fracturing of lithosphere in an uplifted region leads to a reduction in pressure and outgassing of volatiles, which in turn initiate localised and distinctive periods of volcanism. In his model, partial melting would be induced by the introduction of volatiles into the lower crust thereby reducing the melting range of the rocks and providing a heat-transfer medium. An origin for the salic magmas by partial melting has also been considered for the Oslo region (Barth 1954) and has not been ruled out for the Gardar province (Sørensen 1966).

The formation of such magmas would require very small degrees of partial melting (<c. 5%) of mantle materials, or alternatively slightly greater degrees of a pre-existing more fractionated source material (such as basanite) in the lower part of the crust. In the first instance, studies of the natural melting of

spinel-lherzolite by Maaloe and Printzlau (1979) suggest that small degrees of partial melt would not be able to separate out from their host and suggest that the minimum degree of partial melting required for the host to become permeable to the melt, is around 10-20 %. Such degrees of partial melting from typical mantle materials would result in basic liquids. It would be interesting to quantify the possible effects which a volatile flux would have on liberating the liquids formed at low degrees of partial melt. The formation of salic magmas by partial melting of more fractionated basic material at the base of the crust, must require this material to be extensive, which in turn leads one to question its particular origin.

6.7.B. Fractional crystallisation

High level feldspar fractionation of trachytic magmas to yield more undersaturated liquids of phonolitic *composition* has been advocated by many workers as an origin for the phonolites of the Kenya Rift (eg: Nash et al 1969; Lippard 1973; Griffiths and Gibson 1980). Fractionation of augite syenite type liquids either in situ or inferred at relatively shallow depths, has been widely advocated for many of the central complexes in the Gardar province (eg: Ilímaussaq, Ferguson 1964, 1970; South Qôroq, Stephenson 1973, 1976; Igdlérfigssalik, Powell 1976; North Qôroq, Chambers 1976). Recently, Upton and Thomas (1979) have demonstrated that fractional crystallisation of transitional olivine basalt magma gave rise to the gabbro-syenite suite of giant dykes in the Narssaq-Tugtutôq area. Experimental work by Upton (1971) has shown that the suite is compositionally related by low pressure (<10 kbars) olivine-plagioclase fractionation, preceded by deeper level pyroxene and possibly garnet fractionation. The aforementioned dykes are the highest level representatives of a larger basic complex responsible for the extensive linear gravity "high" in the Tugtutôq-Narssaq area (Blundell 1978; Upton and Blundell 1978) which must speak strongly for an extensive body of basic

magma having underlain much of the Gardar province.

The frequent occurrence of feldspathic inclusions in basic rocks (especially "Big Feldspar Dykes") throughout the Gardar province has prompted the opinion of Bridgwater (1967) and Bridgwater and Harry (1968) that a layer of anorthosites was formed by top accumulation of feldspar in a basic magma at depth, underlying the Gardar province. The precise concordance of $\text{Sr}^{87}/\text{Sr}^{86}$ ratios between xenolithic anorthosites and their host gabbro from the Narssaq area, lead Patchett et al (1976) to advocate a genetically related origin and to express a preference for models of differentiation of Gardar magmas involving plagioclase fractionation. However, experimental work by Upton (1971) on similar anorthosites and host gabbro concluded that the anorthosites could not have been produced from their host gabbro, since at no pressure did the latter have plagioclase on the liquidus. This has been confirmed by further geochemical work in which Upton and Thomas (1980) conclude that the anorthosites are not related to their host gabbro by crystal fractionation, suggesting instead separate batches of primary magma for their respective origins.

In view of the above evidence and in particular the gravity "high" associated with the Gardar province, it seems likely that large quantities of primary basic liquids were formed in the mantle, ~~these then~~ gave rise to salic derivatives by fractionation and liquids of augite syenite composition. Partial melting may have been locally important, as in the Motzfeldt Centre where repeated intrusion involved stopping of earlier units.

6.8. Saturation with respect to silica

Earlier workers in the Gardar province have noted a correlation between undersaturated igneous centres and major strike-slip faults. Chambers (1976) considers such crustal structures to permit a relatively rapid ascent of comparatively dry nepheline-normative alkali magmas, which continue to fractionate to more undersaturated residual liquids. Conversely, the leisurely ascent of

similar magmas into coherent crust away from strong faulting may lead to silica enrichment via the dual process of assimilation of siliceous country rock and incorporation of meteoric water. Increasing water content would favour the crystallisation of hydrous phases such as amphibole and biotite. Both of these phases are relatively silica-poor which may promote a build up of silica in the residual liquids (Macdonald 1974). As Carmichael et al (1974) point out, the assimilation of large amounts of country rock is difficult to reconcile with the strongly curved nature of typical variation diagrams.

Other mechanisms for determining oversaturated or undersaturated trends have been ascribed to feldspar compositions, since this mineral is the most abundant in most of the alkali salic rocks. Thus, for example, a deficiency in silica such as solid solution of nepheline in larvikitic feldspar might initiate an oversaturated trend (Macdonald 1974) and substitution of Fe^3 for Al in feldspar might drive a liquid of trachytic composition towards an undersaturated trend (Bailey and Schairer 1966).

6.9. Assimilation

The effects of assimilation of xenolithic lavas in the Motzfeldt Centre, does not appear to have seriously altered the bulk compositions of the major syenite units concerned. The xenolithic lavas show evidence for varying degrees of metamorphism and metasomatism ranging from mild amphibolitisation and recrystallisation to very occasional hornfelses. By contrast, the Tertiary nepheline syenites of the Borgtinderne Intrusion in east Greenland (Brown et al 1978) appear to have been extensively modified by the incorporation of country rock basalt lavas, producing a suite of hybrid syenites. The major element variation in these hybrids is essentially linear, as one might expect for compositions which lie on lines of mixing and some syenite hybrids exhibit polygonal granoblastic textures. Two fundamental differences between the Motzfeldt Centre

and the Borgtinderne Intrusion are the much greater volume of nepheline syenites and the closer compositional relationships between the intrusive magmas and the lavas incorporated as xenoliths in the Motzfeldt Centre.

There is much evidence to suggest that the xenolithic lavas at Motzfeldt were ^{water}saturated, or certainly water-bearing, at the time of their incorporation (see sections 3.7. and 3.10). It would be comforting to possess an array of δD values to support this contention. By contrast, a limited number of δD analyses from the Borgtinderne Intrusion (Brown et al 1978) suggest similarity to the Lilloise Intrusion (Brown 1973), with δD values of around -65 to -70‰, and have persuaded Brown et al (1978) to conclude that in the Borgtinderne Intrusion, incorporation of country rock xenolithic material was not a major mechanism of incorporation of meteoric water.

GEOCHEMISTRY

I.1. X-ray fluorescence techniquesI.1.A. Sample preparation

Rock samples weighing in general 0.5 to 1kg were roughly halved using a hydraulic splitter. At this stage any material likely to cause contamination was removed, such as weathered edges, veins etc. The large fragments were then passed through a 2" x 6" Jaw Crusher and the resulting gravel halved once, twice or three times to arrive at the required 100-200gram. This final unsorted fraction was then ground to a uniform fine powder using a Tema Laboratory Disc Mill, with tungsten carbide grinding barrels. All parts of the apparatus were meticulously cleaned between samples.

The powders were then pressed into briquettes using a hydraulic press operating at about 5tons/sq.inch and a few drops of "Mowiol" as a binder. Finally these prepared pellets were correctly labelled and run on the Phillips PW1212 automatic spectrometer using an automatic sample loader with 12 x 9 sample capacity (Torrens Industries TE-108).

I.1.B. Major element analysis

The nine major elements Si, Al, Fe(total), Mg, Ca, Na, K, Ti and P were determined using a Cr target and an evacuated X-ray path. Mn was determined separately using a W target. A pre-determined number of counts were then accumulated over time (t) on a monitor and three successive samples counted over the same time interval (t). By analysing this monitor with each subsequent set of 3 samples, any irregularity in the count rate (such as drift) can be detected.

The standards used included international standards and standards of similar composition to the unknowns. The latter were originally provided by Dr.B.G.J.Upton and the geochemical laboratory of Grønlands Geologiske Undersøgelse

(GGU) and have been used by earlier workers on Gardar alkaline rocks at the University of Durham (eg:Chambers 1976; Stephenson 1973). The complete list of standards used is given in Table (I) 1.

Particular attention has been payed to the final production of analyses. The correction procedure described by Holland and Brindle (1966) and Reeves (1971) has received criticism in previous years, notably from Gill (1972) who concluded that "normalisation" of the analyses to 100% for producing realistic analyses, is not entirely satisfactory. Further workers (Gill 1972; Stephenson 1973; Chambers 1976) have obtained analyses by direct comparison with standards of similar composition to the unknowns, and used empirical corrections where necessary (usually for high iron samples). In general, the use of direct comparison methods yielded widely varying totals for the Motzfeldt samples and the method of Holland and Brindle (1966) was found to reproduce standards very well. Thus, the "normalised" values have been used as a basis for the analyses. However, in a broadly similar manner to the above workers, it was found necessary to apply an empirical correction to standards with high iron contents, and a smaller correction to the normalised alumina values. This procedure then reproduced standards in the range of interest very well, and the international standards well. Adjustment to the iron value (requiring an increase in total iron at higher levels) was though to be due to the lack of a dead time correction in the original batch of data (R.Hardy pers.comm.1978).

I.1.C. Trace element analysis

The 11 trace elements, Ba, Nb, Zr, Y, Sr, Rb, U, Th, Pb, Ce, and La were analysed under conditions very similar to those above, using the identical briquettes. The analytical data were then converted to concentrations in ppm by the programme TRATIO developed by Gill (1972). Very briefly, this programme compares the count rate of peak/background and uses scattered (back-scattered) radiation as an

internal standard to compensate for mass absorption and matrix effects. The nominal detection limit is also calculated and presented with the upper limit as determined by the standards for each element, which are given below;

<u>Element</u>	<u>Detection limit (ppm)</u>	<u>Upper limit of standards (ppm)</u>
Ba	8	5000
Nb	3	250
Zr	3	5000
Y	3	500
Sr	3	1100
Rb	3	1000
U	8	2700
Th	6	1100
Ce	3	
La	3	280

Synthetic spiked glasses prepared by Pilkington Research Laboratory (Lathom, England) for use in lunar investigations at the University of Durham were used for most of the elements. These standards are in two sets to avoid interelement interferences as much as possible. International standards were used exclusively where interferences were too great in the Pilkington standards (Pb, Th) or where the element was not present (La).

Internal consistency and reproducibility for all of the trace elements were extremely good. Further details of the operating conditions and associated hardware can be found in Reeves (1971).

I.2. Iron oxidation state

FeO determinations were performed on very fresh samples selected from each of the major units, and the analytical methods follow the approach of previous workers. Here, a known weight of sample powder is dissolved in HF acid in the presence of ammonium metavanadate. Any vanadic ion remaining in solution, unreduced, is titrated against standardised ammonium sulphate solution to determine its quantity, and the subsequent amount of FeO can be calculated as a percentage of the starting powder.

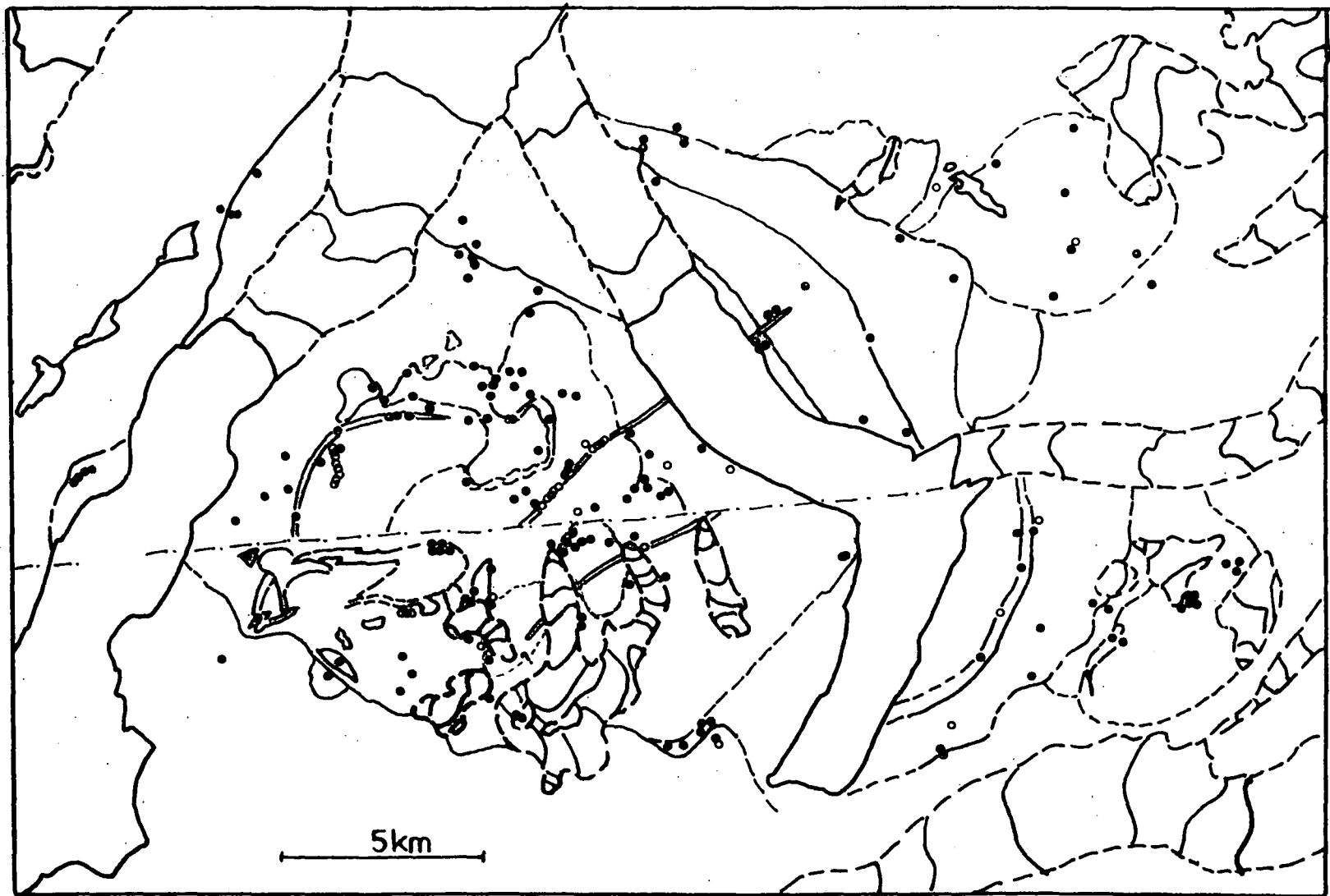


Figure I,1: XRF sample density

- SM units & satellites
- dykes -(not all reported)

Table (I) 1. List of standards used for major element analysis of rocks from the Motzfeldt Centre.

<u>Standard</u>	<u>Rock species</u>	<u>Locality</u>	<u>Reference</u>
30684	syenogabbro	Hviddal, Tugtutôq	Watt 1966
40452	gabbro	Giant Dyke, Tugtutôq	Watt "
40551	gabbro	Krydssø Syenogabbro	Watt "
50272	quartz syenite	Unit 5, Tugtutôq	Watt "
50345	microsyenite	Unit 1, Tugtutôq	Watt "
BCR-1		international*	*
GSP-1		"	
G-1		"	
W-1		"	
BR		"	
GH		"	
GA		"	
SY-1		"	
BOB-1		"	

*international standards references: Flanagan (1969, 1973) U.S.Geol.Survey.

Table (I) 2. Sample collection data . Page numbers refer to field diaries. CHE = C.H.Emeleus
WTH = W.T.Harry
APJ = A.P.Jones

1961

46268	-	59	CHE,p.56	Camp,Lower Flink's Dal
46260	-	68	CHE,p.57-58	" " " "

1962

58001	-	64	CHE,p.1-25	Camp,N of west end of Flink's Dal.
58065	-	117	CHE,p.25-39	Camp,by lake at ENE end of Flink's Dal .
59601	-	642	WTH,p.1-7	Camp,as CHE above.

1963

58352	-	395	CHE,p.14-21	Camp,960m alt. N of Motzfeldt SØ.
58396	-	400	CHE,p.21-26	Camp,on N shore of Motzfeldt SØ
63701	-	724	CHE, " "	" " " "
63725	-	759	CHE,p.26-31	Camp,valley N of Giesecke's Dal, at c. 1230m alt.
63760	-	780	CHE,p.32-35	Camp,north part of W.Motzfeldt
63787	-	802	CHE,p.48-49	Helicopter,NE of Motzfeldt SØ.
54122	-	163	WTH,p.14-22	Camp,1160m alt. valley 1.5km NE of S end of Motzfeldt SØ.
54164	-	184	WTH,p.23-26	Camp,1180m alt. valley E end of Giesecke's Dal.
54234	-	243	WTH,p.51-52	Helicopter,various (mostly E Motzfeldt).

1977

AM1	-	65	APJ	Camp,N of west end of Flink's Dal.
AM66	-	149	APJ	Camp,by lake at ENE end of Flink's Dal.

1979

AM150	-	174	APJ	Camp,Lower Flink's Dal.
-------	---	-----	-----	-------------------------

Fe³/Fe² determinations and some H₂O analyses.

Sample	Unit	wt%H ₂ O	FeO* _{total}	Fe ³ /Fe _{total}
46261	SM6	0.06	7.57	0.80
46268	SM6	1.87	8.98	0.86
54181	SM2	0.58	4.49	0.21
58378	SM1	0.78	3.72	0.61
58400	SM3	0.50	8.25	0.28
63720	SM3	0.57	7.68	0.30
63760	SM1	0.36	5.85	0.47
AM39b	SM5	0.86	12.56	0.02
AM48	SM4	0.93	5.38	0.28
AM49	SM4	0.63	3.89	0.30
AM52	SM4	0.39	4.11	0.34
AM54	SM5*	0.74	9.46	0.00
AM82	SM5	0.47	3.35	0.13
AM85	SM5	1.12	4.38	0.15
AM114	HY	1.25	4.27	0.35
AM117	HY	0.74	7.94	0.52
AM119	HY	1.08	4.70	0.38
AM134	HY	1.30	1.89	0.54
AM137	SM6	2.51	5.95	0.76
AM138	SM6	2.24	6.13	0.78
AM139	SM6	0.94	11.36	0.85

*ie: total iron expressed as FeO

I.3. H₂O Determination

H₂O determinations were carried out on those samples which had been set aside for FeO determinations. In simple terms, the samples of powder were inserted in a combustion tube which was heated. The resulting H₂O vapour was then removed with a flow of nitrogen, the H₂O was absorbed and the quantity determined gravimetrically. Water released at temperatures below 100 °C (H₂O⁺) and in excess of 100 °C (H₂O⁻) were not distinguished, since the temperatures used were around 400 °C.

I.4. Sample locations and collection

The sample locations are indicated visually on a sketch map of the Motzfeldt Centre, in figure (I),1.

The samples used in this study were collected by C.H.Emeleus and W.T.Harry on behalf of the Greenland Geological Survey (Grønlands Geologiske Undersøgelse=GGU) and by the author. Details of the sample collections are listed in table (I) 2. The samples collected by the author are distinguished by the prefix AM-, in contrast to the 6-figure identifiers of GGU samples.

I.5. Additional analyses

A few samples containing trace elements outside of the range covered by the XRF at Durham University, were re-analysed at the Research Laboratories, Risø in Denmark, a facility kindly provided by GGU. The agreement between the latter analyses and those obtained at Durham is very good, although higher estimates of Zr for the lujavrites of SM6 are indicated by the results from Risø. These are included for comparison in the following data tables.

I.6. Data tables

The following data tables present whole rock analyses in oxide wt% and trace element data for the same samples in ppm. Tables of the calculated Norms with their oxidation ratios are to be found at the rear of this appendix.

Unit SM1

	AM4	AM7	58007	63703	63704	63714	63775	63776	54132	54141	54161	58363	58377
SiO ₂	56.51	56.82	58.27	60.98	59.88	60.06	59.12	59.81	58.47	55.14	62.64	60.63	57.59
Al ₂ O ₃	20.51	20.39	20.14	16.55	15.75	14.51	14.32	15.78	19.75	19.38	15.70	15.56	20.15
Fe ₂ O ₃	5.62	5.32	4.54	4.96	9.40	11.06	9.29	9.27	4.60	8.54	8.48	10.17	5.69
MgO	0.60	0.35	0.29	0.67	0.23	0.17	1.60	0.93	0.48	0.56	0.16	0.44	0.36
CaO	1.45	1.24	1.10	4.32	2.27	2.03	3.81	1.26	1.34	1.73	0.85	1.26	1.24
Na ₂ O	8.06	8.49	8.00	5.58	6.46	6.75	6.23	5.68	7.45	7.19	5.94	5.87	8.26
K ₂ O	5.94	5.92	6.28	6.27	5.06	4.54	4.43	5.43	6.41	6.04	5.17	4.92	5.53
TiO ₂	0.36	0.39	0.31	0.88	0.58	0.54	0.53	1.03	0.52	0.70	0.60	0.78	0.26
MnO	0.18	0.25	0.17	0.19	0.29	0.33	0.29	0.25	0.16	0.29	0.30	0.33	0.21
P ₂ O ₅	0.11	0.16	0.16	0.24	0.08	0.07	0.47	0.11	0.13	0.15	0.08	0.12	0.08
Total	99.34	99.33	99.26	100.64	100.00	100.06	100.06	99.55	99.31	99.72	99.92	100.08	99.37

Trace elements in ppm

Ba	568	546	708	2142	91	53	703	219	639	214	161	114	133
Nb	205	281	176	73	463	438	266	435	210	114	313	252	259
Zr	870	895	634	290	2392	2302	840	1362	999	554	1424	1000	985
Y	33	77	30	24	147	182	151	107	32	30	100	94	51
Sr	280	284	284	769	51	30	372	81	295	152	61	26	179
Rb	227	216	251	107	363	233	518	326	177	191	184	222	247
U	6	6	3	4	26	19	17	17	9	6	15	11	6
Th	16	23	15	1	54	45	60	51	18	17	42	37	5
Pb	10	22	19	23	43	31	25	10	59		32	16	0
Ce	210	449	213	24	980	1136	1442	1034	188	289	1148	743	315
La	96	173	110	56	391	420	587	403	90	103	513	395	131

Unit SM1

Unit SM2

Unit SM3

	58378	63760	54139	54142	54170	54174	54181	54182	54184	54138	54157
SiO ₂	62.43	63.69	56.27	56.63	57.01	56.70	57.52	56.88	61.81	56.57	53.62
Al ₂ O ₃	16.98	16.48	20.60	20.16	20.08	19.90	20.22	20.62	19.10	20.66	20.10
Fe ₂ O ₃	4.13	6.49	5.15	5.58	5.07	5.09	5.98	5.43	5.77	5.33	5.18
MgO	0.57	0.08	0.44	0.52	0.44	0.50	0.40	0.38	0.14	0.33	0.20
CaO	3.10	0.57	1.21	1.34	1.36	1.83	1.45	1.44	0.25	1.12	3.11
Na ₂ O	5.92	6.41	8.84	8.49	8.48	8.50	8.57	8.81	7.60	9.08	11.15
K ₂ O	5.56	5.50	5.91	5.73	6.00	6.14	5.89	5.83	4.64	5.64	5.28
TiO ₂	0.31	0.22	0.49	0.49	0.48	0.47	0.37	0.46	0.29	0.25	0.20
MnO	0.14	0.21	0.21	0.23	0.22	0.25	0.19	0.23	0.17	0.25	0.23
P ₂ O ₅	0.26	0.02	0.18	0.19	0.17	0.19	0.15	0.21	0.03	0.07	0.26
Total	99.40	99.67	99.30	99.36	99.31	99.57	100.74	100.29	99.80	99.30	99.33

Trace elements in ppm

Ba	396	155	834	762	1045	841	1040	837	147	139	199
Nb	152	1589	178	241	160	153	149	131	154	267	439
Zr	960	668	690	924	562	601	762	744	644	1045	2356
Y	70	58	40	57	35	81	30	34	34	58	187
Sr	604	71	466	388	479	450	411	279	146	153	158
Rb	220	422	188	194	171	169	251	229	229	231	299
U	31	113	3	6	8	6	10	6	6	11	19
Th	63	30	14	30	17	26	6	11	17	35	20
Pb	35	58	7	17		36	28	25	12	32	22
Ce	461	477	282	347	221	583	140	248	237	385	1234
La	321	191	125	149	112	265	77	111	93	162	461

Unit SM3

	58399	58400	63709	63717	63720	63721b	63721c
SiO2	60.86	60.27	53.80	65.28	61.05	63.08	40.86
Al2O3	16.02	15.65	16.81	16.89	15.91	16.36	6.21
Fe2O3	8.26	9.16	10.19	2.91	8.52	6.03	35.0
MgO	0.61	0.53	1.91	0.08	0.34	0.17	1.18
CaO	2.15	2.20	4.60	1.88	1.75	1.58	9.91
Na2O	5.52	5.57	5.61	7.24	6.00	5.78	2.15
K2O	5.56	5.24	4.36	5.30	5.29	6.04	1.99
TiO2	0.53	0.89	1.63	0.13	0.70	0.36	2.65
MnO	0.21	0.31	0.26	0.11	0.25	0.18	1.10
P2O5	0.16	0.17	0.83	0.03	0.09	0.05	0.16
Total	99.88	99.99	100.00	99.85	99.90	99.63	101.21

Unit SM4/Qôroq

	AQM1	AQM2	AQM3	AQM4
	56.44	56.12	54.82	55.26
	20.74	21.25	21.39	20.40
	4.75	4.67	4.92	5.71
	0.13	0.09	0.16	0.18
	1.79	1.25	1.38	1.91
	8.84	9.10	9.97	8.95
	6.32	6.32	6.21	6.29
	0.24	0.21	0.16	0.36
	0.14	0.15	0.18	0.23
	0.09	0.05	0.04	0.08
Total	99.48	99.21	99.23	99.37

Trace elements in ppm

Ba	476	618	1740	113	158	147	98	113	28	179	91
Nb	211	192	140	1199	171	161	286	169	284	38	188
Zr	480	581	483	n%	632	1610	914	427	546	407	567
Y	64	61	46	235	49	80	120	135	110	35	108
Sr	90	73	1153	46	31	32	20	78	37	94	83
Rb	216	192	192	229	209	291	82	219	260	221	220
U	3	3		137	3	16	5		7	3	2
Th	32	19	7	60	8	20	35	14	30	14	24
Pb	40	35	28	54	15	6		12	14	19	27
Ce	532	394	236	769	464	606	1310	586	651	321	767
La	222	167	121	293	173	240	475	191	214	157	279

Unit SM4

	AM45	AM48	AM49	AM52	AM56	AM65	AM68	AM143	54241	54242	58026	58028	58039
SiO ₂	60.93	55.66	60.05	57.64	57.96	56.27	56.76	58.04	59.47	58.20	58.52	58.03	54.77
Al ₂ O ₃	19.91	20.38	19.70	20.57	20.54	21.55	20.02	20.90	17.96	17.51	20.52	21.45	18.99
Fe ₂ O ₃	3.91	5.97	4.32	4.56	5.08	2.96	5.64	2.86	5.53	7.44	5.34	3.37	8.80
MgO	0.18	0.24	0.03	0.14	0.15	0.04	0.51	0.02	0.33	0.44	0.49	0.06	0.87
CaO	1.58	1.63	0.65	1.26	0.81	1.12	1.29	1.42	1.73	2.51	1.58	0.81	2.14
Na ₂ O	7.10	8.73	7.84	9.20	8.88	10.50	8.35	9.25	5.91	6.28	5.62	9.16	7.35
K ₂ O	5.20	6.02	6.28	5.58	5.48	6.24	6.05	6.23	6.65	5.57	6.41	5.93	5.46
TiO ₂	0.23	0.39	0.23	0.12	0.21	0.09	0.40	0.20	0.75	1.23	0.43	0.10	0.91
MnO	0.11	0.24	0.09	0.14	0.13	0.17	0.20	0.10	0.20	0.22	0.22	0.13	0.30
P ₂ O ₅	0.08	0.13	0.07	0.03	0.05	0.07	0.14	0.04	0.16	0.31	0.18	0.04	0.25
Total	99.23	99.39	99.26	99.24	99.29	99.01	99.36	99.06	98.69	99.71	99.31	99.08	99.84

Trace elements in ppm

Ba	1254	189	277	201	166	57	298	37	433	736	433	107	1254
Nb	267	295	101	122	139	117	227	520	65	99	163	196	267
Zr	809	846	610	797	531	519	895	1133	194	289	547	795	808
Y	42	79	34	54	35	98	34	299	47	62	44	54	42
Sr	413	59	29	59	54	65	242	23	191	238	497	25	413
Rb	232	234	326	267	297	280	243	299	152	114	193	258	232
U	6	8	3	3	3	4	8			0	5		6
Th	16	14	4	5	9	34	10	21	2	19	14	10	16
Pb	13	26	7	17	22	24	22	11	20	31	15	31	13
Ce	294	423	196	159	184	635	274	1513	351	459	323	320	294
La	130	157	96	61	75	255	110	423	140	179	128	118	130

Unit SM4

	58066	58080	59603	63725	63728	63729	63730	63731	63742	63743	63746	63753	63754
SiO ₂	54.85	55.89	56.25	57.24	58.04	56.43	57.33	58.64	55.10	55.50	55.83	52.07	57.02
Al ₂ O ₃	19.30	20.36	19.23	21.08	20.83	20.86	20.78	18.09	20.65	22.22	20.22	22.27	20.35
Fe ₂ O ₃	7.26	5.83	5.77	4.11	3.79	5.71	5.67	6.08	6.68	3.81	6.66	7.27	6.08
MgO	0.93	0.46	0.27	0.09	0.14	0.15	0.37	0.56	0.13	0.06	0.28	0.27	0.23
CaO	2.18	1.45	2.22	0.88	0.90	1.09	1.61	2.86	1.20	1.06	1.53	1.34	1.23
Na ₂ O	7.72	8.91	8.56	8.68	8.52	8.79	6.64	6.46	9.50	10.24	8.40	10.62	8.44
K ₂ O	5.57	5.77	6.40	6.75	6.49	5.83	6.41	5.56	5.77	5.92	5.97	4.95	5.62
TiO ₂	0.88	0.37	0.33	0.18	0.27	0.23	0.28	0.85	0.18	0.10	0.30	0.33	0.21
MnO	0.28	0.21	0.30	0.14	0.13	0.20	0.18	0.19	0.22	0.12	0.22	0.21	0.15
P ₂ O ₅	0.62	0.12	0.11	0.03	0.03	0.05	0.07	0.24	0.02	0.04	0.06	0.08	0.04
Total	99.59	99.37	99.44	99.18	99.14	99.34	99.34	99.53	99.45	99.07	99.47	99.41	99.37

Trace elements in ppm

Ba	898	487	280	73	33	35	55	2387	135	66	43	33	477
Nb	177	280	214	115	254	244	208	140	237	80	250	215	78
Zr	748	1189	637		1195	952	746	633	868	466	944	733	371
Y	52	66	184		85	60	54	51	20	22	60	41	15
Sr	472	295	188	41	34	29	211	968	42	33	59	16	113
Rb	185	227	210	229	291	287	266	125	204	238	272	270	262
U	4	8	1	3	6	7	5	2	17	9	6	7	4
Th	19	28	45	9	16	40		16	13	13	21	12	22
Pb		9	44	35	15	18	38	24	30		7	3	1
Ce	437	309	1291	262	265	397	371	163	138	143	352	314	81
La	195	135	532	108	81	169	149	136	60	58	124	109	46

Unit SM5

	AM38	AM39	AM39b	AM40	AM43	AM77	AM82	AM85	AM86	AM87	AM88	AM91	AM92
SiO ₂	55.95	54.45	49.73	54.18	53.82	55.77	57.93	58.05	56.65	56.57	58.42	55.27	55.98
Al ₂ O ₃	17.97	18.32	16.14	18.44	19.13	20.78	20.66	19.61	20.77	21.06	20.53	22.04	20.25
Fe ₂ O ₃	7.44	9.72	13.57	7.73	8.09	5.36	3.72	4.86	3.37	3.86	3.77	4.01	5.67
MgO	1.21	1.06	2.43	1.70	0.86	0.37	0.30	0.51	0.24	0.57	0.32	0.60	0.14
CaO	3.43	2.43	4.15	3.22	2.44	1.40	0.92	1.59	1.85	1.38	1.16	1.15	1.67
Na ₂ O	6.00	6.03	5.99	7.22	7.83	8.76	8.74	7.67	9.68	9.00	8.13	9.58	9.13
K ₂ O	4.67	4.77	4.51	4.63	5.70	5.98	6.28	6.00	5.99	5.99	6.19	5.74	5.96
TiO ₂	1.58	2.49	1.58	1.65	0.96	0.58	0.34	0.58	0.21	0.43	0.29	0.43	0.27
MnO	0.21	0.26	0.51	0.21	0.26	0.17	0.14	0.21	0.25	0.15	0.19	0.14	0.23
P ₂ O ₅	1.20	0.34	1.43	0.71	0.58	0.15	0.13	0.26	0.10	0.13	0.15	0.14	0.07
Total	99.66	99.87	100.04	99.69	99.67	99.32	99.16	99.34	99.11	99.14	99.15	99.10	99.37

Trace elements in ppm

Ba	3766	2326	1702	3320	748	297	878	859	104	339	117	660	111
Nb	82	175	224	145	243	224	154	123	62	135	134	166	162
Zr	288	580	783	500	811	893	707	484	339	480	642	612	591
Y	32	26	62	38	47	36	26	32	78	27	34	30	67
Sr	1992	1249	841	1857	342	210	428	537	153	162	97	418	149
Rb	84	108	122	122	208	222	201	153	155	161	159	173	237
U	2	2	2	1	8	4	4	5		3	4	3	
Th	3	9	14	13	10	20	17	7	74	13	9	22	17
Pb	14	29	34	5	11	12	27	22	31	15	18	33	32
Ce	65	77	490	120	394	237	129	203	659	171	233	175	497
La	108	85	214	119	153	97	67	99	269	75	90	75	201

Unit SM5

	AM107	AM108	AM109	AM110	AM111	AM112	58025	58072
SiO ₂	59.51	56.27	58.83	57.24	57.76	59.83	46.73	57.28
Al ₂ O ₃	19.50	21.33	20.22	20.22	21.02	19.39	18.27	21.33
Fe ₂ O ₃	3.86	5.96	4.63	4.77	5.83	4.83	12.85	3.25
MgO	1.05	0.78	0.68	0.44	0.28	0.20	1.69	0.41
CaO	1.05	2.82	1.10	1.03	1.70	2.37	4.39	1.10
Na ₂ O	6.23	6.08	6.55	9.11	5.95	5.79	8.77	8.96
K ₂ O	6.82	4.93	6.36	5.80	6.07	6.38	3.94	6.22
TiO ₂	0.66	0.87	0.57	0.34	0.40	0.27	1.96	0.30
MnO	0.19	0.15	0.19	0.20	0.22	0.22	0.39	0.12
P ₂ O ₅	0.35	0.14	0.16	0.14	0.11	0.07	1.19	0.11
Total	99.22	99.33	99.29	99.29	99.34	99.35	100.18	99.08

Unit SM5*

	AM29	AM54	AM55	58036
	54.22	53.44	53.92	51.10
	17.25	15.77	16.57	15.82
	8.92	10.50	9.95	12.07
	2.04	1.73	1.50	2.72
	4.92	5.26	4.70	5.65
	4.47	5.24	5.89	4.38
	4.54	4.34	4.37	3.92
	2.07	2.26	2.05	2.47
	0.18	0.25	0.25	0.29
	1.24	1.30	0.82	1.86
Total	99.85	100.09	100.02	100.28

Trace elements in ppm

Ba	317	1198	514	433	140	394	381	370	3698	2685	2472	4618
Nb	184	133	194	271	178	171	334	100	68	102	122	46
Zr	518	463	633	1324	779	608	786	399	267	448	592	176
Y	38	24	34	37	50	65	64	21	30	47	45	33
Sr	137	969	416	241	277	243	225	174	1655	872	812	1219
Rb	226	141	205	222	198	161	138	149	75	87	89	41
U	8	6		11	7	3	5	10	3	2		3
Th	12	14	17	10	19	12	13	3	3	10	10	1
Pb	4	16	25	17	23	20	8	15	8	23	30	2
Ce	212	120	245	226	272	303	641	126		112	111	
La	85	82	100	99	105	123	229	60	62	90	89	77

Unit SM5*

Unit HY

	58037	58062	AM98	AM99	AM114	AM115	AM116	AM117	AM118	AM119	AM120	AM121
SiO ₂	51.87	53.87	56.08	56.78	57.17	55.20	56.64	52.77	55.77	56.10	55.35	57.67
Al ₂ O ₃	15.96	16.51	20.20	16.86	20.66	20.55	22.43	20.39	21.00	21.47	21.19	18.36
Fe ₂ O ₃	10.59	11.19	5.21	8.34	4.74	6.72	2.97	8.81	5.47	5.22	5.81	7.09
MgO	2.50	1.41	0.09	0.78	0.25	0.10	0.03	0.17	0.08	0.12	0.13	0.44
CaO	6.40	4.25	1.99	3.01	1.42	1.75	0.51	2.02	1.06	1.31	1.43	2.79
Na ₂ O	4.53	4.85	9.39	6.30	8.28	8.56	9.92	8.89	9.19	8.37	9.07	5.31
K ₂ O	3.70	4.56	5.88	6.19	6.14	6.10	6.28	5.91	6.36	6.20	5.90	7.05
TiO ₂	2.30	1.95	0.19	1.02	0.33	0.25	0.05	0.35	0.14	0.24	0.21	0.55
MnO	0.25	0.30	0.23	0.32	0.18	0.19	0.09	0.29	0.22	0.16	0.19	0.26
P ₂ O ₅	2.01	1.24	0.08	0.23	0.09	0.03	0.05	0.07	0.02	0.06	0.07	0.11
Total	100.11	100.13	99.34	99.83	99.26	99.45	98.97	99.67	99.31	99.25	99.35	99.63

Trace elements in ppm

Ba	15143	2949	54	769	133	34	43	43	58	98	77	318
Nb	42	98	128	223	197	203	160	328	213	207	141	198
Zr	180	359	585	877	666	700	574	835	901	540	530	487
Y	29	41	109	169	64	45	48	92	60	53	32	103
Sr	1601	965	42	284	111	20	24	21	51	67	61	293
Rb	37	102	230	160	177	289	313	262	278	200	213	201
U	7				1	9	5	1	5	2	1	2
Th	10	4	37	44	21	5	7	15	17	12	10	28
Pb		1	19	7	19	23	17	32	27	16	17	26
Ce		95	746	588	417	330	291	596	327	376	304	722
La	63	93	258	235	157	102	119	181	128	139	130	286

Unit HY

Unit SM6

	AM123	AM123b	AM134	AM137	AM138	AM139	AM140	AM141	46261	46265	46268
SiO2	56.03	55.91	57.03	57.43	56.92	54.90	58.67	58.56	56.97	55.98	57.11
Al2O3	20.54	20.15	22.40	19.94	19.92	16.91	21.51	21.84	18.72	20.67	19.25
Fe2O3	6.02	7.02	2.10	6.60	6.55	12.01	2.59	2.57	8.40	9.16	9.97
MgO	0.21	0.24	0.02	0.03	0.04	0.48	0.18	0.01	0.00	0.12	0.03
CaO	1.71	1.81	0.42	0.94	0.50	1.00	0.35	0.39	0.75	2.11	0.99
Na2O	7.75	7.08	10.59	9.64	10.33	11.02	10.81	10.50	10.55	7.16	6.96
K2O	6.53	6.63	6.24	5.28	5.10	3.61	4.90	5.45	3.96	3.98	5.23
TiO2	0.36	0.39	0.00	0.16	0.14	0.37	0.07	0.06	0.02	0.18	0.04
MnO	0.17	0.22	0.08	0.28	0.21	0.37	0.30	0.31	0.17	0.32	0.25
P2O5	0.08	0.08	0.01	0.11	0.03	0.04	0.03	0.03	0.02	0.02	0.03
Total	99.40	99.53	98.89	100.41	99.74	100.71	99.41	99.72	99.56	99.70	99.86

Trace elements in ppm

Ba	44	17	63	250	273	190	263	274	40	71	56
Nb	211	235	36	688	434	608	595	492	478	923	470
Zr	306	362	280	1040	2263	2005	2449	2972	4230	1644	4128
Y	23	30	49	108	106	86	127	159	251	234	230
Sr	22	25	54	73	39	50	56	57	26	244	149
Rb	179	190	294	482	484	313	542	562	357	198	476
U		1	4	54	25	35	37	24	14	6	16
Th	6		21	245	23	37	79	122	70	32	15
Pb	11	30	25	57	28	51	58	107	48	13	31
Ce	278	322	362	876	744	883	676	817	992	1516	870
La	93	106	159	354	286	319	294	337	404	693	358

Riso

Nb	850	680	690	600
Zr	1310	2450	3040	5970

Alkali Gabbro

	AM93	AM113	AM127	58078	58083	58105	58116	58117	59602	59631	63727	63779
SiO ₂	47.11	47.01	45.61	47.32	52.12	45.21	47.02	53.66	48.38	48.34	53.07	41.61
Al ₂ O ₃	16.46	16.50	16.40	13.23	16.08	13.79	16.36	20.15	18.64	18.10	15.72	12.85
Fe ₂ O ₃	13.30	13.83	14.82	15.96	9.66	16.32	13.84	5.86	11.47	11.59	11.71	15.76
MgO	4.07	4.20	4.51	4.88	3.03	7.28	5.31	1.13	3.52	3.74	2.15	5.44
CaO	8.16	7.96	8.25	7.59	4.77	7.92	7.54	10.45	9.15	9.06	4.26	11.26
Na ₂ O	4.39	3.98	3.91	3.88	4.82	3.20	3.85	4.95	3.99	3.99	4.21	3.08
K ₂ O	1.95	1.94	1.83	2.73	4.58	2.18	1.99	1.64	1.36	1.51	5.35	1.29
TiO ₂	2.83	2.77	3.16	3.04	2.92	3.38	2.83	1.32	2.28	2.54	2.20	3.94
MnO	0.16	0.16	0.17	0.19	0.26	0.18	0.17	0.04	0.12	0.13	0.29	0.16
P ₂ O ₅	1.91	1.74	1.84	1.96	1.76	1.32	1.49	0.20	1.10	1.27	1.26	4.79

Total 100.34 100.09 100.50 100.78 100.00 100.78 100.40 99.40 100.01 100.27 100.22 100.18

Trace elements in ppm

Ba	1703	1685	1513	1692	4948	1360	1628	1012	1317	1352	2285	926
Nb	26	30	25	44	93	36	31	3	19	20	87	18
Zr	148	152	131	196	267	193	141	33	92	96	305	85
Y	32	28	25	36	36	28	26		16	19	42	39
Sr	1021	1013	1018	822	2821	932	1068	1966	1433	1436	730	810
Rb	26	21	22	48	69	42	26	20	15	14	88	23
U		3	2	1		8			7	3	1	
Th	10	3	9		8		5		3	1	4	3
Pb	31	12	10	10	14	14	19	12	13	15	45	
Ce	38	43	43	114	29	61	30		15	18	167	96
La	43	51	39	65	111	47	39	6	27	31	97	40

Unit EM

	54234	54239	54240	63787	63788	63789	63793	63795
SiO ₂	62.00	61.62	61.41	61.41	60.94	61.08	61.39	61.97
Al ₂ O ₃	15.89	15.87	15.41	15.19	15.63	15.20	15.31	16.04
Fe ₂ O ₃	9.12	8.91	9.98	10.25	10.38	10.37	9.91	8.50
MgO	0.23	0.14	0.16	0.13	0.15	0.17	0.19	0.13
CaO	0.63	1.10	1.11	1.08	0.77	1.21	1.15	0.99
Na ₂ O	5.90	6.67	5.76	6.52	6.55	6.40	6.09	7.04
K ₂ O	5.19	4.74	5.10	4.67	4.71	4.65	5.00	4.48
TiO ₂	0.63	0.61	0.82	0.55	0.65	0.67	0.65	0.47
MnO	0.31	0.22	0.23	0.27	0.21	0.30	0.32	0.23
P ₂ O ₅	0.07	0.06	0.08	0.05	0.11	0.09	0.08	0.06

Total 99.97 99.94 100.06 100.12 100.10 100.14 100.09 99.91

Unit NM1/2

	58352	58367	58368	58369
	61.59	59.94	59.39	58.77
	18.51	18.27	18.63	19.45
	4.64	5.34	5.71	5.47
	0.28	0.44	0.23	0.36
	1.74	2.58	1.55	1.25
	6.51	6.43	7.24	7.32
	5.88	5.58	6.00	6.17
	0.45	0.58	0.27	0.35
	0.12	0.13	0.16	0.16
	0.12	0.17	0.07	0.10

99.84 99.46 99.25 99.40

Trace elements in ppm

Ba	116	90	88	83	189	138	108	72	982	1059	79	239
Nb	208	285	268	387	434	404	256	305	92	120	86	202
Zr	944	1765	1053	1961	2233	2063	985	1489	384	417	323	623
Y	76	111	89	167	157	161	111	140	22	26	19	33
Sr	25	17	27	16	25	29	23	24	515	714	35	119
Rb	200	282	212	311	193	281	228	256	129	128	164	157
U	8	10	11	17	24	17	7	15	2	3	1	5
Th	22	20	38	44	54	62	40	31	10	10	11	13
Pb	47	29	32	42	76	70	75	44	18		23	20
Ce	554	612	864	1107	1144	1193	872	855	136	141	161	217
La	275	282	402	491	479	529	532	371	80	80	63	96

Unit NM1/2			Basalts			Xenoliths					
	58370	58373	63736	63744	63758	AM6b	AM18	AM24	AM25	AM25b	AM32
SiO ₂	59.44	58.23	47.26	56.78	47.84	55.67	54.00	58.23	58.38	58.25	56.71
Al ₂ O ₃	18.68	19.29	13.92	19.15	15.61	20.74	19.75	20.29	19.03	19.22	20.86
Fe ₂ O ₃	5.44	6.48	16.53	8.00	14.26	5.24	6.03	5.63	7.37	7.38	5.92
MgO	0.43	0.23	7.32	0.15	7.65	0.12	2.24	0.30	0.89	0.86	0.26
CaO	2.28	1.33	8.09	1.60	9.09	1.14	2.74	1.94	2.01	1.82	1.21
Na ₂ O	6.88	8.02	2.27	7.84	2.99	10.49	5.87	5.44	6.46	6.18	8.34
K ₂ O	5.79	5.65	1.79	5.47	0.61	5.44	4.15	6.35	4.30	4.66	5.46
TiO ₂	0.59	0.35	2.36	0.30	1.90	0.17	1.69	0.37	0.65	0.69	0.29
MnO	0.15	0.20	0.17	0.28	0.18	0.25	0.24	0.27	0.34	0.34	0.25
P ₂ O ₅	0.16	0.10	0.61	0.07	0.02	0.03	0.71	0.09	0.18	0.20	0.06
Total	99.84	99.88	100.32	99.64	100.15	99.29	97.42	98.91	99.61	99.60	99.36
Trace elements in ppm											
Ba	882	182	494	127	254	120	3018	93	995	998	70
Nb	195	128	11	327	9	306	152	241	310	312	263
Zr	656	580	223	1572	137	2615	562	918	1339	1328	1235
Y	39	54	34	110	34	113	56	47	75	77	65
Sr	473	51	352	32	347	140	1981	482	655	720	69
Rb	151	159	56	219	41	295	123	212	163	185	215
U	9	5	9	13	3	22	5	8	6	8	12
Th	17	1	1	31	19	56	18	17	23	21	21
Pb	24	2	23	28		24	21	36	46	22	18
Ce	230	359	71	621	51	617	232	359	478	476	503
La	118	134	33	234	19	249	158	143	222	219	182

Xenoliths

JHb Granite

	AM37a	AM41	AM42	AM58	54126	54127	59639	58006	58007b	46260	54159	54167
SiO ₂	49.35	58.58	57.79	58.97	56.58	57.15	57.05	48.02	51.06	66.73	70.36	69.20
Al ₂ O ₃	14.84	19.53	19.62	19.99	16.17	20.31	16.65	14.93	16.69	14.05	14.74	14.05
Fe ₂ O ₃	12.81	7.53	5.93	6.39	9.40	6.48	10.48	13.43	10.91	4.53	2.58	3.16
MgO	3.58	0.55	0.46	0.41	1.93	0.32	0.79	3.94	2.34	1.04	0.52	0.99
CaO	5.28	0.88	1.49	1.55	3.33	1.37	3.22	4.97	3.64	3.08	1.20	2.33
Na ₂ O	4.75	5.49	6.92	5.20	4.88	7.66	5.36	5.12	6.17	7.83	4.72	5.04
K ₂ O	4.76	6.21	6.27	6.18	5.36	5.65	4.78	5.14	5.83	1.57	4.85	4.14
TiO ₂	2.70	0.46	0.48	0.43	1.55	0.21	1.08	2.89	1.99	0.31	0.29	0.36
MnO	0.28	0.34	0.22	0.28	0.20	0.24	0.32	0.27	0.30	0.31	0.05	0.05
P ₂ O ₅	1.62	0.05	0.27	0.06	0.58	0.04	0.33	1.76	1.16	0.16	0.10	0.17
Total	99.97	99.62	99.45	99.46	99.98	99.43	100.06	100.47	100.09	99.61	99.41	99.49

Trace elements in ppm

Ba	3273	55	540	95	2982	42	367	2849	3019	1134	1183	1175
Nb	88	433	211	263	85	306	156	102	186	923	11	10
Zr	332	1780	774	1199	468	1001	648	485	973	1644	139	126
Y	38	76	48	44	35	59	67	57	54	240	16	17
Sr	1940	45	184	97	402	43	133	1109	1317	577	590	618
Rb	103	286	252	202	195	223	91	272	262	40	148	96
U	3	11	2	12	2	13	4	1	8	58	1	2
Th	2	30	10	22	2	36	23	15	12	205	11	20
Pb	8	32	20	23	41	45	34	19	13	40	56	16
Ce	169	564	340	401	3	492	354	150	230			11
La	122	231	137	142	67	200	135	109	141		21	45

JHb Granite

	58395	63705	63774
SiO2	61.06	58.73	60.29
Al2O3	15.03	15.43	16.61
Fe2O3	6.87	7.07	5.57
MgO	2.79	3.29	1.78
CaO	4.41	4.66	4.43
Na2O	3.77	5.58	6.48
K2O	4.63	3.41	3.38
TiO2	0.73	0.99	0.62
MnO	0.10	0.10	0.10
P2O5	0.40	0.48	0.31
Total	99.79	99.74	99.57

Trace elements in ppm

Ba	1353	1283	1293
Nb	11	34	9
Zr	231	368	194
Y	22	21	17
Sr	831	1006	872
Rb	130	117	134
U	5	15	9
Th	9	50	2
Pb	52	43	33
Ce	53	121	10
La	52	79	44

NORMS FOR MOTZFELDT UNIT SM1 1980.

FE3/FE2 = 1.8.

NORMAL .. R.C.O.GILL

SUMMARY NORM TABLE

	AM4	(SM4) AM7	58007	63703	63704	63705	63707	63707	63714	63760	63775	63776
QUARTZ	0.0	0.0	0.0	0.0	0.2	2.5	0.0	3.4	1.5	4.3	0.2	3.1
ORTHOCLASE	35.4	35.3	37.5	36.9	30.0	20.3	10.6	18.7	26.9	32.7	26.2	32.3
ALBITE	33.6	34.9	37.6	44.6	53.0	47.5	12.8	31.1	49.5	54.5	49.1	48.5
ANORTHITE	2.3	0.0	0.5	1.6	0.0	7.0	0.0	8.4	0.0	0.0	0.0	1.5
NEPHELINE	19.1	20.4	16.6	1.3	0.0	0.0	14.8	0.0	0.0	0.0	0.0	0.0
ACMITE	0.0	0.0	0.0	0.0	1.6	0.0	8.0	0.0	6.9	0.1	3.3	0.0
DIOPSIDE	3.4	2.8	2.2	3.6	3.4	10.2	19.1	12.1	6.6	2.0	11.3	3.1
WOLLASTONITE	0.0	0.7	0.5	5.7	2.8	0.0	5.5	0.0	0.9	0.2	0.5	0.0
HYPERSTHENE	0.0	0.0	0.0	0.0	0.0	3.5	0.0	0.7	0.0	0.0	0.0	0.9
OLIVINE	0.2	0.0	0.0	0.0	0.0	0.0	0.0	0.0	0.0	0.0	0.0	0.0
MAGNETITE	5.1	4.8	4.1	3.5	7.6	5.3	12.9	11.7	6.5	5.8	6.7	8.2
HEMATITE	0.0	0.0	0.0	0.6	0.0	0.7	1.8	3.8	0.0	0.0	0.0	0.2
ILMENITE	0.7	0.7	0.6	1.7	1.1	1.9	9.2	6.8	1.0	0.4	1.0	2.0
APATITE	0.3	0.4	0.4	0.6	0.2	1.1	5.3	3.4	0.2	0.0	1.1	0.3
DIFF. INDEX	88.1	90.5	91.7	82.8	83.2	70.2	38.2	53.2	78.0	91.5	75.5	83.9
NA/(NA+K)	0.67	0.69	0.66	0.57	0.66	0.71	0.83	0.64	0.69	0.64	0.68	0.61
(NA+K)/AL	0.96	1.00	0.99	0.96	1.02	0.83	1.18	0.76	1.10	1.00	1.05	0.96
F3/(F2+F3)	0.62	0.62	0.62	0.62	0.62	0.62	0.62	0.62	0.62	0.62	0.62	0.62

NORMS FOR MOTZFELDT UNIT SM1 1980. FE3/FE2 = 1.8.

NORMCAL .. R.C.D.GILL

SUMMARY NORM TABLE

	54132	54141	54161	58363	58377	58378
QUARTZ	0.0	0.0	6.8	5.2	0.0	2.1
ORTHOCLASE	38.2	35.9	30.7	29.2	33.0	33.1
ALBITE	37.8	32.5	50.5	49.8	39.7	50.5
ANORTHITE	1.5	2.8	0.9	1.6	1.6	3.4
NEPHELINE	13.9	15.5	0.0	0.0	16.7	0.0
DIOPSIDE	2.6	3.8	2.0	3.2	3.2	3.5
WOLLASTONITE	0.4	0.0	0.2	0.0	0.1	2.5
HYPERSTHENE	0.0	0.0	0.0	0.1	0.0	0.0
MAGNETITE	4.1	7.7	7.6	9.1	5.1	3.7
HEMATITE	0.0	0.0	0.0	0.0	0.0	0.0
ILMENITE	1.0	1.3	1.1	1.5	0.5	0.6
APATITE	0.3	0.4	0.2	0.3	0.2	0.6
DIFF. INDEX	90.0	84.0	88.0	84.2	89.3	85.7
NA/(NA+K)	0.64	0.64	0.64	0.64	0.69	0.62
(NA+K)/AL	0.97	0.95	0.98	0.96	0.97	0.93
F3/(F2+F3)	0.62	0.62	0.62	0.62	0.62	0.62

NORMS FOR MOTZFELDT UNIT SM2 1980. $FE3/FE2 = 1.10$

NORMCAL .. R.C.D.GILL

SUMMARY NORM TABLE

	54139	54142	54170	54174	54181	54182	54184	63730	63731	63742
CORUNDUM	0.0	0.0	0.0	0.0	0.0	0.0	1.2	0.2	0.0	0.0
ORTHOCLASE	35.3	34.2	35.8	36.5	33.4	34.4	27.6	38.2	33.1	34.4
ALBITE	30.2	34.4	32.0	27.1	30.9	31.9	61.9	35.0	43.4	22.3
ANORTHITE	0.0	0.0	0.0	0.0	0.0	0.0	1.0	7.6	4.0	0.0
NEPHELINE	23.6	20.6	20.9	22.5	20.2	22.6	1.5	11.8	6.3	28.4
ACMITE	1.6	0.0	1.7	3.3	1.1	0.8	0.0	0.0	0.0	5.6
DIOPSIDE	4.1	4.6	4.8	6.7	5.2	4.9	0.0	0.0	5.9	5.2
WOLLASTONITE	0.0	0.0	0.0	0.0	0.0	0.0	0.0	0.0	0.7	0.0
OLIVINE	0.9	0.7	0.7	0.5	1.8	0.5	2.0	2.4	0.0	1.6
MAGNETITE	3.0	4.0	2.9	2.0	6.4	3.5	4.2	4.1	4.4	2.1
ILMENITE	0.9	0.9	0.9	0.9	0.7	0.9	0.6	0.5	1.6	0.3
APATITE	0.4	0.5	0.4	0.5	0.3	0.5	0.1	0.2	0.6	0.0
DIFF. INDEX	89.1	89.2	88.7	86.1	84.6	88.9	90.9	85.0	82.8	85.1
NA/(NA+K)	0.69	0.69	0.68	0.68	0.69	0.70	0.71	0.61	0.64	0.71
(NA+K)/AL	1.02	1.00	1.02	1.04	1.01	1.01	0.92	0.86	0.92	1.06
F3/(F2+F3)	0.50	0.50	0.50	0.50	0.50	0.50	0.50	0.50	0.50	0.50

NORMS FOR MOTZFELDT UNIT SM3 1980. FE3/FE2 = 0.60.

NORMAL .. R.C.D.GILL

SUMMARY NORM TABLE

	54138	54157	58399	58400	63709	63717	63720	63721	63721
QUARTZ	0.0	0.0	1.2	1.6	0.0	0.5	0.7	2.3	0.0
ORTHOCLASE	33.7	31.5	33.1	31.2	25.9	31.4	31.5	36.0	11.9
ALBITE	30.8	13.7	47.0	47.4	37.4	57.6	51.1	49.3	14.9
ANORTHITE	0.0	0.0	2.5	2.2	7.9	0.0	0.9	0.9	1.4
NEPHELINE	24.3	33.0	0.0	0.0	5.6	0.0	0.0	0.0	1.9
ACMITE	1.7	5.3	0.0	0.0	0.0	3.0	0.0	0.0	0.0
SOD METASIL	0.0	3.4	0.0	0.0	0.0	0.1	0.0	0.0	0.0
DIOPSIDE	4.5	11.8	6.2	6.6	8.0	6.3	6.4	5.9	41.4
WOLLASTONITE	0.0	0.2	0.0	0.0	0.0	0.8	0.0	0.0	0.0
HYPERSTHENE	0.0	0.0	4.4	4.2	0.0	0.0	3.5	1.8	0.0
OLIVINE	2.5	0.0	0.0	0.0	4.9	0.0	0.0	0.0	5.1
MAGNETITE	1.9	0.0	4.2	4.7	5.2	0.0	4.4	3.1	18.0
ILMENITE	0.5	0.4	1.0	1.7	3.1	0.2	1.3	0.7	5.1
APATITE	0.2	0.6	0.4	0.4	2.0	0.1	0.2	0.1	0.4
DIFF. INDEX	88.8	78.3	81.3	80.1	68.9	89.4	83.3	87.5	28.7
NA/(NA+K)	0.71	0.76	0.60	0.62	0.66	0.67	0.63	0.59	0.62
(NA+K)/AL	1.02	1.20	0.94	0.95	0.83	1.04	0.98	0.98	0.92
F3/(F2+F3)	0.35	0.35	0.35	0.35	0.35	0.35	0.35	0.35	0.35

NORMS FOR MOTZFELDT UNIT SM4 1980.

FE3/FE2 = 0.66 .

NORMALCAL ... P.C.D.GILL

SUMMARY NORM TABLE

	AQM1	AQM2	AQM3	AQM4	AM45	AM48	AM49	AM52	AM56	AM65	AM68	(SM5) AM89
ORTHOCLASE	37.7	37.8	37.1	37.5	31.0	35.9	37.5	33.3	32.7	37.3	36.1	37.0
ALBITE	23.4	23.7	15.0	18.1	51.5	25.3	42.4	32.5	38.9	21.7	30.9	36.3
ANORTHITE	0.0	0.0	1.0	0.0	7.2	0.0	0.0	0.0	0.0	0.0	0.0	1.3
NEPHELINE	26.4	27.3	32.7	29.4	5.0	25.3	13.4	23.3	20.1	30.0	21.2	18.0
ACMITE	2.9	2.6	5.4	5.2	0.0	2.3	0.0	2.8	0.0	3.2	1.1	0.0
SOD METASIL	0.0	0.0	0.7	0.0	0.0	0.0	0.0	0.0	0.0	2.1	0.0	0.0
DIOPSIDE	7.4	5.3	5.9	8.0	0.2	6.4	2.5	5.4	3.3	4.6	4.9	3.1
OLIVINE	0.5	1.2	2.0	1.4	2.3	1.6	1.3	1.3	1.8	0.7	2.3	1.4
MAGNETITE	1.1	1.3	0.0	0.5	0.1	2.1	2.4	1.1	2.8	0.0	2.5	2.1
ILMENITE	0.5	0.4	1.3	0.7	0.4	0.7	0.4	0.2	0.4	0.2	0.8	0.6
APATITE	0.2	0.1	0.1	0.2	0.2	0.3	0.2	0.1	0.1	0.2	0.3	0.4
DIFF. INDEX	87.4	89.2	85.7	84.1	87.5	86.5	93.2	89.1	91.7	89.0	88.2	91.3
NA/(NA+K)	0.68	0.69	0.71	0.68	0.67	0.69	0.65	0.71	0.71	0.72	0.68	0.67
(NA+K)/AL	1.03	1.03	1.09	1.06	0.87	1.02	1.00	1.03	1.00	1.11	1.01	0.98
FE3/(FE2+FE3)	0.37	0.37	0.37	0.37	0.37	0.37	0.37	0.37	0.37	0.37	0.37	0.37

NORMS FOR MOTZFELDT UNIT SM4 1980.

FE3/FE2 = 0.66 .

NORMCAL ... R.C.D.GILL

SUMMARY NORM TABLE

	AM143	54241	54242	58026	58027	58028	58039	58066	58080	59603	59627	63725
CORUNDUM	0.0	0.0	0.0	1.9	0.0	0.0	0.0	0.0	0.0	0.0	4.1	0.0
ORTHOCASE	37.2	40.0	33.2	38.3	33.8	35.4	32.5	33.2	34.4	38.2	37.0	40.3
ALBITE	28.5	41.8	43.5	41.9	39.3	34.6	32.3	31.9	27.3	19.5	15.4	25.9
ANORTHITE	0.0	2.9	3.2	5.7	4.5	0.0	3.2	1.6	0.0	0.0	17.9	0.0
NEPHELINE	24.5	4.9	5.4	3.3	15.3	23.6	16.0	18.4	24.9	24.0	0.0	24.8
ACMITE	3.1	0.0	0.0	0.0	0.0	0.2	0.0	0.0	2.5	6.3	0.0	2.3
SOD METASIL	0.5	0.0	0.0	0.0	0.0	0.0	0.0	0.0	0.0	0.5	0.0	0.0
DIOPSIDE	5.5	4.1	6.3	0.0	0.6	3.4	5.0	4.4	5.6	9.1	0.0	3.7
WOLLASTONITE	0.3	0.0	0.0	0.0	0.0	0.0	0.0	0.0	0.0	0.0	0.0	0.0
HYPERSTHENE	0.0	0.0	0.0	0.0	0.0	0.0	0.0	0.0	0.0	0.0	4.9	0.0
OLIVINE	0.0	1.5	1.3	3.7	3.0	0.7	3.9	3.4	2.3	1.5	11.6	1.5
MAGNETITE	0.0	3.0	4.0	2.9	2.7	1.8	4.8	4.0	1.9	0.0	7.9	1.1
ILMENITE	0.4	1.4	2.4	0.8	0.5	0.2	1.7	1.7	0.7	0.6	0.9	0.3
APATITE	0.1	0.4	0.7	0.4	0.2	0.1	0.6	1.5	0.3	0.3	0.4	0.1
DIFF. INDEX	90.2	86.7	82.1	83.5	88.4	93.7	80.8	83.5	86.7	81.7	52.4	91.0
NA/(NA+K)	0.69	0.57	0.63	0.57	0.68	0.70	0.67	0.68	0.70	0.67	0.31	0.66
(NA+K)/AL	1.05	0.94	0.93	0.79	0.92	1.00	0.94	0.97	1.03	1.09	0.48	1.02
F3/(F2+F3)	0.37	0.37	0.37	0.37	0.37	0.37	0.37	0.37	0.37	0.37	0.37	0.37

NORMS FOR MOTZFELDT UNIT SMA 1930.

FE3/FE2 = 0.66 .

NORMAL .. R.C.O.GILL

SUMMARY NORM TABLE

	63728	63729	63743	63746	63753	63754
ORTHOCLASE	39.8	34.8	35.4	35.6	29.6	33.6
ALBITE	31.5	31.6	29.8	28.6	18.4	35.2
ANORTHITE	0.0	0.2	0.0	0.0	0.0	1.1
NEPHELINE	21.8	23.6	33.3	23.2	37.6	20.0
ACMITE	1.0	0.0	4.2	0.3	2.6	0.0
SOD METASIL	0.0	0.0	0.2	0.0	0.0	0.0
DIOPSIDE	3.8	4.3	4.5	6.3	5.4	4.2
OLIVINE	0.9	1.3	1.4	1.7	2.9	2.1
MAGNETITE	1.6	3.1	0.0	3.5	2.7	3.3
ILMENITE	0.5	0.4	1.2	0.6	1.6	0.4
APATITE	0.1	0.1	0.1	0.1	0.2	0.1
DIFF. INDEX	92.1	90.0	89.5	87.4	85.6	88.8
NA/(NA+K)	0.67	0.70	0.72	0.68	0.77	0.70
(NA+K)/AL	1.01	1.00	1.05	1.00	1.03	0.98
F3/(F2+F3)	0.37	0.37	0.37	0.37	0.37	0.37

NORMS FOR MOTZFELDT UNIT SM5* (Larvikite) 1980. FE3/FE2 = 0.05.

NORMCAL .. R.C.O.GILL

SUMMARY NORM TABLE

	AM29	AM54	AM55	58036	58037	58062
ORTHOCLASE	27.1	25.9	26.1	23.3	22.0	27.2
ALBITE	38.2	35.2	33.8	34.5	36.8	38.2
ANORTHITE	13.7	6.7	5.9	12.0	12.4	9.9
NEPHELINE	0.0	5.1	8.9	1.5	1.0	1.7
DIOPSIDE	2.3	9.4	10.5	3.4	5.4	2.8
HYPERSTHENE	0.5	0.0	0.0	0.0	0.0	0.0
OLIVINE	10.7	9.5	8.3	15.3	12.5	12.8
MAGNETITE	0.6	0.7	0.6	0.8	0.7	0.7
ILMENITE	4.0	4.3	3.9	4.7	4.4	3.7
APATITE	3.0	3.1	2.0	4.4	4.8	3.0
DIFF. INDEX	65.3	66.2	68.8	59.4	59.8	67.1
NA/(NA+K)	0.60	0.65	0.67	0.63	0.65	0.62
(NA+K)/AL	0.71	0.84	0.87	0.72	0.72	0.78
F3/(F2+F3)	0.04	0.04	0.04	0.04	0.04	0.04

NORMS FOR MOTZFELDT UNIT SM5,1980. FE3/FE2 = 0.30.

NORMCAL .. R.C.O.GILL

SUMMARY NORM TABLE

	AM38	AM39	AM39B	AM40	AM43	AM77	AM82	AM85	AM86	AM87	AM91	AM92
ORTHOCLASE	27.8	28.4	26.9	27.6	34.0	35.7	37.5	35.8	35.8	35.8	34.3	35.6
ALBITE	44.6	39.4	26.2	34.4	25.6	27.2	30.7	36.5	24.6	27.8	26.0	23.2
ANORTHITE	8.4	8.9	3.9	4.3	0.2	0.0	0.0	1.4	0.0	0.0	0.2	0.0
NEPHELINE	3.6	6.5	13.5	14.8	22.3	25.6	22.5	15.7	26.9	26.0	30.4	26.3
ACMITE	0.0	0.0	0.0	0.0	0.0	0.5	2.3	0.0	2.1	1.0	0.0	3.5
SOD METASIL	0.0	0.0	0.0	0.0	0.0	0.0	0.0	0.0	1.4	0.0	0.0	0.5
DIOPSIDE	0.7	0.9	6.4	6.0	7.0	5.3	3.3	4.2	7.5	5.2	4.0	7.0
OLIVINE	6.6	7.2	12.5	5.7	5.0	2.9	2.8	3.1	0.9	2.3	2.7	3.1
MAGNETITE	2.3	3.0	4.2	2.4	2.5	1.4	0.0	1.5	0.0	0.7	1.3	0.0
ILMENITE	3.0	4.8	3.0	3.2	1.8	1.1	0.7	1.1	0.4	0.8	0.8	0.5
APATITE	2.9	0.8	3.4	1.7	1.4	0.4	0.3	0.6	0.2	0.3	0.3	0.2
DIFF. INDEX	76.0	74.4	66.6	76.7	82.0	88.5	90.7	88.1	87.4	89.7	90.7	85.1
NA/(NA+K)	0.66	0.66	0.67	0.70	0.68	0.69	0.68	0.66	0.71	0.70	0.72	0.70
(NA+K)/AL	0.83	0.82	0.91	0.92	1.00	1.00	1.02	0.97	1.08	1.01	1.00	1.06
F3/(F2+F3)	0.21	0.21	0.21	0.21	0.21	0.21	0.21	0.21	0.21	0.21	0.21	0.21

NORMS FOR MOTZFELDT UNIT SM5,1980. FE3/FE2 = 0.30.

NORMCAL .. R.C.O.GILL

SUMMARY NORM TABLE

	AM110	AM111	AM112	58025	58072
CORUNDUM	0.0	1.9	0.0	0.0	0.0
ORTHOCLASE	34.6	36.3	38.1	23.5	37.2
ALBITE	30.4	39.7	40.3	12.1	29.3
ANORTHITE	0.0	7.8	8.2	0.0	0.0
NEPHELINE	22.8	6.1	5.0	32.8	25.3
ACMITE	3.0	0.0	0.0	1.9	0.7
SOD METASIL	0.5	0.0	0.0	0.0	0.0
DIOPSIDE	3.7	0.0	2.9	12.1	4.1
OLIVINE	4.0	5.4	3.4	8.0	1.9
MAGNETITE	0.0	1.8	1.5	3.0	0.7
ILMENITE	0.7	0.8	0.5	3.8	0.6
APATITE	0.3	0.3	0.2	2.8	0.3
DIFF. INDEX	87.9	82.1	83.4	68.3	91.8
NA/(NA+K)	0.70	0.60	0.58	0.77	0.69
(NA+K)/AL	1.05	0.78	0.85	1.02	1.01
F3/(F2+F3)	0.21	0.21	0.21	0.21	0.21

NORMS FOR MOTZFELDT UNIT "HY" 1980. FE3/FE2 = 0.5.

NORMCAL .. R.C.O.GILL

SUMMARY NORM TABLE

	AM98	AM99	AM114	AM115	AM116	AM117	AM118	AM119	AM120	AM121	AM123	AM123
ORTHOCLASE	35.1	36.9	36.7	36.4	37.6	35.3	38.0	37.1	35.2	42.0	39.0	39.6
ALBITE	22.1	31.2	31.6	24.0	24.8	15.4	20.4	28.1	25.6	30.6	26.3	26.7
ANORTHITE	0.0	0.0	1.1	0.0	0.0	0.0	0.0	2.7	0.0	5.5	2.0	3.7
NEPHELINE	27.0	11.6	21.3	26.3	30.7	31.0	28.7	23.6	27.8	8.0	21.7	18.3
ACMITE	4.7	0.9	0.0	0.6	2.7	2.9	4.6	0.0	0.5	0.0	0.0	0.0
SOD METASIL	0.7	0.0	0.0	0.0	0.1	0.0	0.0	0.0	0.0	0.0	0.0	0.0
DIOPSIDE	8.4	11.6	4.7	7.6	2.0	8.5	4.6	3.0	5.9	6.7	5.3	4.3
OLIVINE	1.5	1.0	1.7	1.8	2.0	3.5	3.2	2.5	2.0	2.7	2.2	3.4
MAGNETITE	0.0	3.3	2.2	2.7	0.0	2.6	0.2	2.4	2.4	3.2	2.7	3.2
ILMENITE	0.4	2.0	0.6	0.5	0.1	2.7	0.3	0.5	0.4	1.1	0.7	0.7
APATITE	0.2	0.5	0.2	0.1	0.1	0.2	0.0	0.1	0.2	0.3	0.2	0.2
DIFF. INDEX	84.2	79.7	89.5	86.7	93.0	81.7	87.1	88.7	88.6	90.6	86.9	84.6
NA/(NA+K)	0.71	0.61	0.67	0.68	0.71	0.70	0.69	0.67	0.70	0.53	0.64	0.62
(NA+K)/AL	1.08	1.01	0.98	1.01	1.03	1.03	1.05	0.95	1.01	0.89	0.96	0.93
FE3/(FE2+FE3)	0.31	0.31	0.31	0.31	0.31	0.31	0.31	0.31	0.31	0.31	0.31	0.31

NORMS FOR MOTZFELDT UNIT "HY" 1980. $FE3/FE2 = 0.5$.

NORMAL .. R.C.O.GILL

SUMMARY NORM TABLE

	AM134	AM135	AM136
ORTHOCLASE	37.3	36.1	36.8
ALBITE	25.8	24.5	29.0
ANORTHITE	0.0	0.0	1.0
NEPHELINE	30.2	20.8	22.0
ACMITE	1.9	3.7	0.0
SOD METASIL	1.6	0.0	0.0
DIOPSIDE	1.8	9.4	5.7
OLIVINE	1.3	2.2	1.9
MAGNETITE	0.0	1.3	2.6
ILMENITE	0.0	1.4	0.7
APATITE	0.0	0.6	0.2
DIFF. INDEX	93.3	81.4	87.8
NA/(NA+K)	0.72	0.66	0.67
(NA+K)/AL	1.03	1.04	0.98
F3/(F2+F3)	0.31	0.31	0.31

NORMS FOR MOTZFELDT UNIT SM6 (LUJAVRITE) 1980. FE3/FE2 = 5.6

NORMCAL .. R.C.O.GILL

SUMMARY NORM TABLE

	(HY) AM134	AM137	AM138	AM139	AM140	AM141	46261	46265	46268
CORUNDUM	0.0	0.0	0.0	0.0	0.0	0.0	0.0	0.8	0.4
ORTHOCLASE	37.3	31.4	30.3	21.6	29.3	32.6	23.2	23.6	31.0
ALBITE	24.0	42.5	40.8	35.5	39.4	37.3	38.8	48.9	47.1
ANORTHITE	0.0	0.0	0.0	0.0	0.0	0.0	0.0	10.4	4.7
NEPHELINE	31.1	16.9	18.4	16.8	24.3	24.1	20.2	6.5	6.5
ACMITE	5.1	0.4	3.4	14.6	4.2	3.3	11.8	0.0	0.0
SOD METASIL	0.8	0.0	0.0	0.0	0.0	0.0	0.0	0.0	0.0
DIOPSIDE	1.5	0.2	0.2	2.6	1.3	0.7	0.3	0.0	0.0
WOLLASTONITE	0.1	1.6	0.9	0.6	0.0	0.4	1.4	0.0	0.0
OLIVINE	0.0	0.0	0.0	0.0	0.3	0.0	0.0	0.2	0.1
MAGNETITE	0.0	3.6	3.6	6.4	1.1	1.5	4.3	4.9	5.5
HEMATITE	0.0	2.9	2.1	1.0	0.0	0.0	0.0	4.3	4.5
ILMENITE	0.0	0.3	0.3	0.7	0.1	0.1	0.0	0.3	0.1
APATITE	0.0	0.3	0.1	0.1	0.1	0.1	0.0	0.0	0.1
DIFF. INDEX	92.4	90.8	89.5	73.9	93.0	93.9	82.2	79.0	84.6
NA/(NA+K)	0.72	0.71	0.73	0.80	0.76	0.74	0.80	0.73	0.67
(NA+K)/AL	1.08	1.00	1.04	1.19	1.04	1.03	1.14	0.78	0.89
F3/(F2+F3)	0.83	0.83	0.83	0.83	0.83	0.83	0.83	0.83	0.83

NORMS FOR MUTZFELDT ALKALI GABBRO 1980. FE3/FE2 = 0.1

NORMAL .. R.C.D.GILL

SUMMARY NORM TABLE

	AM93	AM113	AM127	58078	58083	58105	58116	58117	59602	59631	63727	63779
ORTHOCLASE	11.6	11.6	10.9	16.2	27.3	13.0	11.9	9.8	8.1	9.0	31.9	7.7
ALBITE	29.8	30.3	26.8	27.0	35.0	20.4	28.9	35.9	31.6	31.5	32.1	26.3
ANORTHITE	19.6	21.7	22.0	10.7	8.8	16.9	21.7	28.2	29.2	27.2	8.3	17.6
NEPHELINE	4.2	2.0	3.6	3.2	3.3	3.7	2.2	3.5	1.4	1.4	2.0	0.0
DIOPSIDE	7.2	5.7	6.0	12.0	2.9	11.5	5.2	18.3	7.9	8.1	4.1	6.0
WOLLASTONITE	0.0	0.0	0.0	0.0	0.0	0.0	0.0	0.6	0.0	0.0	0.0	0.0
HYPERSTHENE	0.0	0.0	0.0	0.0	0.0	0.0	0.0	0.0	0.0	0.0	0.0	4.3
OLIVINE	16.0	17.5	19.6	19.4	11.8	22.9	19.5	0.0	13.5	13.5	13.0	17.1
MAGNETITE	1.6	1.7	1.8	1.9	1.2	2.0	1.7	0.7	1.4	1.4	1.4	1.9
ILMENITE	5.4	5.3	5.0	5.8	5.6	6.5	5.4	2.5	4.4	4.9	4.2	7.6
APATITE	4.6	4.2	4.4	4.7	4.2	3.1	3.6	0.5	2.6	3.0	3.0	11.5
DIFF. INDEX	45.5	43.9	41.2	46.5	65.6	37.1	42.9	49.2	41.1	41.8	66.0	34.0
NA/(NA+K)	0.77	0.75	0.76	0.58	0.62	0.69	0.75	0.82	0.82	0.80	0.54	0.78
(NA+K)/AL	0.57	0.52	0.51	0.71	0.80	0.55	0.52	0.49	0.43	0.45	0.81	0.50
F3/(F2+F3)	0.08	0.08	0.08	0.08	0.08	0.08	0.08	0.08	0.08	0.08	0.08	0.08

NORMS FOR MOTZFELDT SATELLITES - NM1/2 1980. FE3/FE2 = 1.0

NORMCAL .. R.C.O.GILL

SUMMARY NORM TABLE

	58352	58367	58368	58369	58370	58373
ORTHOCLASE	34.9	33.2	35.8	36.8	34.4	33.5
ALBITE	50.2	46.5	42.4	40.0	42.9	40.0
ANORTHITE	3.9	4.5	0.6	2.0	3.0	0.0
NEPHELINE	2.8	4.5	10.6	12.2	8.4	15.2
ACMITE	0.0	0.0	0.0	0.0	0.0	0.1
DIOPSIDE	3.4	5.9	5.8	3.1	5.9	5.2
WOLLASTONITE	0.0	0.1	0.0	0.0	0.1	0.0
OLIVINE	0.5	0.0	0.1	1.3	0.0	0.6
MAGNETITE	3.2	3.7	4.0	3.8	3.8	4.4
ILMENITE	0.9	1.1	0.5	0.7	1.1	0.7
APATITE	0.3	0.4	0.2	0.2	0.4	0.2
DIFF. INDEX	87.8	84.3	88.8	89.0	85.7	88.8
NA/(NA+K)	0.63	0.64	0.65	0.64	0.64	0.68
(NA+K)/AL	0.92	0.91	0.99	0.96	0.94	1.00
FE3/(FE2+FE3)	0.47	0.47	0.47	0.47	0.47	0.47

NORMS FOR MOTZFELDT SATELLITES - EM 1980. FE3/FE2 = 1.0

NORMCAL .. R.C.O.GILL

SUMMARY NORM TABLE

	54234	54239	54240	63737	63788	63789	63793	63795
QUARTZ	4.8	1.9	5.1	2.6	2.1	2.8	3.6	1.2
ORTHOCASE	30.8	28.2	30.3	27.7	28.0	27.6	29.7	26.6
ALBITE	50.2	55.5	49.0	52.4	54.4	52.5	51.1	57.9
ANORTHITE	1.6	0.0	1.2	0.0	0.0	0.0	0.0	0.0
ACMITE	0.0	1.1	0.0	2.7	1.1	1.6	0.5	1.8
DIOPSIDE	1.0	4.5	3.4	4.5	2.7	4.8	4.6	4.0
HYPERSTHENE	4.0	2.0	2.5	3.3	3.6	2.8	2.5	2.5
MAGNETITE	6.3	5.6	6.9	5.7	6.6	6.3	6.6	5.0
ILMENITE	1.2	1.2	1.6	1.6	1.2	1.3	1.2	0.9
APATITE	0.2	0.1	0.2	0.1	0.3	0.2	0.2	0.1
DIFF. INDEX	85.8	85.5	84.3	82.7	84.5	82.9	84.4	85.7
NA/(NA+K)	0.63	0.68	0.63	0.58	0.68	0.68	0.65	0.70
(NA+K)/AL	0.96	1.01	0.97	1.04	1.02	1.02	1.01	1.02
F3/(F2+F3)	0.47	0.47	0.47	0.47	0.47	0.47	0.47	0.47

NORMS FOR MOTZFELDT XENOLITHS (ETC) 1980. FE3/FE2 = 0.5 .

NORMCAL .. R.C.O.GILL

SUMMARY NORM TABLE

	AM6B	AM18	AM24	AM25	AM25B	AM32	AM37A	AM41	AM42	AM58	AM122	54126
CORUNDUM	0.0	2.4	1.2	0.5	1.2	0.0	0.0	2.3	0.0	2.1	0.0	0.0
ORTHOCLASE	32.5	25.3	38.1	25.6	27.8	32.6	28.4	37.0	37.4	36.9	38.8	31.9
ALBITE	23.9	46.1	40.2	51.8	50.8	35.5	26.3	45.2	36.7	44.4	29.5	41.5
ANORTHITE	0.0	9.2	9.2	8.9	7.8	3.4	5.2	4.1	4.0	7.4	1.3	6.4
NEPHELINE	28.9	2.7	3.5	1.8	1.1	19.4	7.7	0.9	12.1	0.0	20.5	0.0
ACMITE	4.8	0.0	0.0	0.0	0.0	0.0	0.0	0.0	0.0	0.0	0.0	0.0
SOD METASIL	1.7	0.0	0.0	0.0	0.0	0.0	0.0	0.0	0.0	0.0	0.0	0.0
DIOPSIDE	4.9	0.0	0.0	0.0	0.0	2.0	8.7	0.0	1.5	0.0	4.1	5.3
HYPERSTHENE	0.0	0.0	0.0	0.0	0.0	0.0	0.0	0.0	0.0	1.6	0.0	0.1
OLIVINE	3.0	6.4	4.3	6.3	6.2	3.7	8.9	6.1	4.0	3.8	2.5	6.1
MAGNETITE	0.0	2.8	2.6	3.3	3.4	2.7	5.8	3.4	2.7	2.9	2.6	4.3
ILMENITE	0.3	3.3	0.7	1.2	1.3	0.6	5.2	0.9	0.0	0.8	0.5	3.0
APATITE	0.1	1.7	0.2	0.4	0.5	0.1	3.9	0.1	0.6	0.1	0.1	1.4
DIFF. INDEX	85.3	74.1	81.8	79.3	79.7	87.5	62.4	83.1	86.3	81.3	88.8	73.4
NA/(NA+K)	0.75	0.68	0.57	0.70	0.67	0.70	0.60	0.57	0.63	0.56	0.65	0.58
(NA+K)/AL	1.12	0.72	0.78	0.80	0.79	0.94	0.87	0.81	0.93	0.76	0.98	0.86
F3/(F2+F3)	0.31	0.31	0.31	0.31	0.31	0.31	0.31	0.31	0.31	0.31	0.31	0.31

NORMS FOR MOTZFELDT XENOLITHS (ETC) 1980. $FE3/FE2 = 0.5$

NORMCAL .. R.C.O.GILL

SUMMARY NORM TABLE

	54127	59639	58006	58007	dyke 58015
ORTHOCLASE	33.7	28.4	30.5	34.7	35.7
ALBITE	36.4	45.4	20.2	22.0	36.9
ANORTHITE	4.4	7.3	2.6	0.6	3.6
NEPHELINE	15.7	0.1	12.6	16.6	15.6
DIOPSIDE	1.9	5.7	8.7	8.3	2.4
OLIVINE	4.3	5.4	9.7	6.4	2.8
MAGNETITE	2.9	4.7	6.1	4.9	2.2
ILMENITE	0.4	2.1	5.5	3.8	0.7
APATITE	0.1	0.3	4.2	2.8	0.3
DIFF. INDEX	85.9	74.0	63.3	73.2	88.1
NA/(NA+K)	0.67	0.63	0.60	0.62	0.66
(NA+K)/AL	0.92	0.84	0.94	0.99	0.94
F3/(F2+F3)	0.31	0.31	0.31	0.31	0.31

NORMS FOR MOTZFELDT ERIKSFJ BASALTS 1980.

FE3/FE2 = 0.3

NORMCAL .. R.C.O.GILL

SUMMARY NORM TABLE

	63736	63744	63758
ORTHOCLASE	10.7	32.6	3.8
ALBITE	19.4	35.2	25.5
ANORTHITE	22.7	0.9	27.5
NEPHELINE	0.0	17.3	0.0
DIOPSIDE	11.3	5.9	14.6
HYPERSTHENE	15.8	0.0	6.6
OLIVINE	8.9	4.9	13.8
MAGNETITE	5.1	2.5	4.4
ILMENITE	4.5	0.6	3.6
APATITE	1.5	0.2	0.0
DIFF. INDEX	30.1	85.1	29.4
NA/(NA+K)	0.66	0.69	0.88
(NA+K)/AL	0.41	0.98	0.36
F3/(F2+F3)	0.21	0.21	0.21

NORMS FOR MOTZFELDT JHB-GRANITE 1980. $FE3/FE2 = 0.5$

NORMAL .. R.C.O.GILL

SUMMARY NORM TABLE

	46260	54159	54167	58395	63705	63774
QUARTZ	9.1	20.7	18.6	8.6	0.3	0.0
ORTHOCLASE	9.3	28.9	24.6	27.5	20.3	20.1
ALBITE	64.0	40.2	43.0	32.1	47.6	55.3
ANORTHITE	0.0	4.7	3.5	10.5	7.0	6.3
ACMITE	2.4	0.0	0.0	0.0	0.0	0.0
DIOPSIDE	12.1	0.5	5.8	7.3	10.6	11.4
HYPERSTHENE	1.3	3.0	1.9	8.5	7.9	1.0
OLIVINE	0.0	0.0	0.0	0.0	0.0	1.4
MAGNETITE	0.8	1.2	1.4	3.1	3.2	2.5
ILMENITE	0.6	0.6	0.7	1.4	1.9	1.2
APATITE	0.4	0.2	0.4	1.0	1.1	0.7
DIFF. INDEX	82.4	99.8	86.2	68.3	68.2	75.4
NA/(NA+K)	0.88	0.60	0.65	0.55	0.71	0.74
(NA+K)/AL	1.04	0.88	0.91	0.75	0.83	0.86
F3/(F2+F3)	0.31	0.31	0.31	0.31	0.31	0.31

APPENDIX II

MINERALOGY

II.1. Electron Probe Microanalysis

Mineral analyses were performed using a Cambridge Instrument Company 'Geoscan-Mk.II' electron microprobe analyser, at the University of Durham using methods similar to those described by Sweatman and Long (1969). Data was handled by an on-line Varian 620 L/100 computer. The programme TIM3 was written by A.Peckett (University of Durham) and performs a ZAF correction (Atomic number, Mass absorption and Fluorescence) on peak and background data for standards and sample. A revised version of this programme, TIM4 was used for the more recent analyses which allows greater flexibility for amending data and changing standards during analysis. The operating conditions and programme REE, also written by A.Peckett, are outlined in a subsequent section.

In general, 4 to 6 ten-second count accumulations were obtained for each peak and background position, and the average obtained for each element. The back scattered electrons are analysed by a wavelength dispersive system (WDS) using two spectrometers and the three analysing crystals, LiF, KAP and PET. The Geoscan was operated under a low vacuum usually with an accelerating voltage of 15Kv and a probe current of 40 nanoamps (nA). When focussed and held in one position, the beam produces a spot of 2-5 μm in diameter. The beam was sometimes defocussed for analyses of minerals which are prone to decomposition. Bulk compositions of exsolved perthitic alkali feldspars and other average compositions, were obtained by using a "line scan" whereby the beam oscillates rapidly along a 2-5 μm wide path for an infinitely variable distance from about 5 μm to 0.5cm.

The standard error for each element varies with concentration but is approximately as set out in the small table below;-

Table (II) 1. Electron probe operating conditions and standards.

<u>Z</u>	<u>Element</u>	<u>Line</u>	<u>Crystal</u>	<u>2θ (peak)</u>	<u>Standard</u>
11	Na	Ka	KAP	53°07'	jadeite (JD-1)
12	Mg	"	"	43°32'	MgO
13	Al	"	"	36°22'	jadeite or Al ₂ O ₃
14	Si	"	PET	109°08'	wollastonite (WO-2)
19	K	"	"	50°29'	alkali feldspar (AF-15)
20	Ca	"	LIF	113°09'	wollastonite (WO-2)
22	Ti	"	"	86°08'	TiO ₂
23	V	"	"	77°01'	V ₂ O ₅
25	Mn	"	"	63°15'	rhodonite
26	Fe	"	"	57°43'	Fe
28	Ni	"	"	48°39'	Ni
30	Zn	"	"	41°41'	Zn
39	Y	La	PET	126°58'	Y ₂ O ₃
40	Zr	"	"	87°55'	Zr
41	Nb	"	"	81°45'	Nb

Details of the analytical conditions for REE elements are given separately

<u>wt% oxide</u>	<u>relative error</u>
10-50	2%
1-10	about 5%
1	about 10%

Error in the major elements is primarily due to the interelement correction procedure and in the minor elements is usually due to counting statistics and estimation of background values. The operating conditions and the standards used are outlined in Table(II) 1.

II.2. Note on REE-mineral analysis.

The probe analysis of the rare earth elements is complicated by the plethora of spectral lines which make the measurement of background and the elimination of overlapping peaks rather difficult.

The analysing conditions used, entail an accelerating voltage of 20 kv, a probe current of 80 nA, and the LiF analysing crystal with a gas-flow proportional counter.

The procedure uses a calculated background based on the average atomic number of the mineral specimen, which in turn is based on the ratio of specimen current/probe current. The absolute backgrounds are determined by analysis of the three materials, SiO_2 , NaNbO_3 and SnO_2 , chosen to have no spectral lines in the region of interest and covering a wide range of \bar{Z} (atomic number). The background for the mineral specimen is interpolated by calculation from its measured specimen current.

C / The effect of overlapping peaks is partly mitigated by using collimating slits in front of the detector. The resolution is approximately 4' arc, or 5 eV, for the region of interest. Usually the analysis line for a particular rare-earth element is the $L\alpha_1$ line, but for three elements, Pr, Eu and Ho, these $L\alpha_1$ lines are completely overlapped by other rare-earth element lines and so the $L\beta_1$ lines are used for analysis. In spite of these steps, there is still some partial overlap on a few analysis lines, and so an interference matrix correction has been established

by experiment.

The probe analysis thus consists of measuring 14 RE elements in their standards and the three background materials are then analysed for all 14 REE. The analyst then measures the 14 REE in the mineral specimen and records the specimen current. The computer programme (written by Dr.A.Peckett, University of Durham) strips off calculated backgrounds and then, in an iterative procedure, removes the interferences. The results are presented as measured concentrations of REE.

This data is augmented by the measured concentrations of the major elements present and the conventional ZAF correction (see II.1.) is applied.

II.3. Pyroxene recalculation of end-members.

The steps in the procedure form one sequence of a choice of five options available in the computer programme PXPROG8 devised by Dr.A.Peckett, University of Durham. This option, number III, takes a probe analysis with all iron reported as FeO and computes the minimum amount of ferric iron to satisfy the formation of acmite and K-acmite, but does not generate $\text{CaFe}^3\text{AlSiO}_6$. In outline, the procedure begins by converting $\frac{\%}{100}$ weight percent oxide (analysis) to atomic proportions and then extracting from the numbers of atoms available, the amounts needed to form the pyroxene end-member molecules in the order stated below. The ferric/ferrous ratio, which is initially 0.0 for probe analyses, is adjusted at steps 1 and 10 in this sequence to remove any excess K and Na to form more K-acmite and acmite respectively. //

List of elements permitted in the programme.

Si, Ti, Al, Fe^3 , Fe^2 , Mn, Mg, Ca, Na, K, Zr, Hf, V, Cr, Y, Ni, Zn, Li, Nb, Ta, Sr, Ba.

These elements are partially grouped together such that: $\text{Zr} = \text{Zr} + \text{Hf}$; $\text{Nb} = \text{Nb} + \text{Ta}$; $\text{Ca} = \text{Ca} + \text{Ba} + \text{Sr}$;
 $\text{FM} = \text{Fe}^2 + \text{Mg}$.

Options

The full list of options available in the programme

is as follows:-

- I. Fe^3/Fe^2 is retained as in the original analysis.
- II. Fe^3/Fe^2 is allowed to change slightly and $\text{CaFe}^3\text{AlSiO}_6$ is allowed.
- III. Fe^3/Fe^2 is allowed to vary considerably and $\text{CaFe}^3\text{AlSiO}_6$ is not allowed.
- IV. As option II but Si is also allowed to vary, if necessary, to use up all the cations to form end-member molecules.
- V. As option III and allows Si to vary such that all of the cations are used up to form pyroxene end-member molecules.

List of End members, in the order calculated.

Note, pyroxene 20 is a linear combination of 25 and 26. Thus the combination 20+25 and 20+26 can exist, but never all three. Pyroxene 20 is retained since it is a commonly observed composition with a name. Similarly pyroxene 21 is linked to pyroxenes 25 and 27, and pyroxene 22 is linked to 24 and 25.

- | | | |
|--|--|--|
| 1. $\text{KFe}^3\text{Si}_2\text{O}_6$ | 2. NaZrSiAlO_6 | 3. NaTiAlSiO_6 |
| 4. $\text{NaZr}_{\frac{1}{2}}\text{FM}_{\frac{1}{2}}\text{Si}_2\text{O}_6$ | 5. $\text{NaTi}_{\frac{1}{2}}\text{FM}_{\frac{1}{2}}\text{Si}_2\text{O}_6$ | 6. $\text{NaNb}_{\frac{1}{3}}\text{FM}_{\frac{2}{3}}\text{Si}_2\text{O}_6$ |
| 7. NaYSi_2O_6 | 8. NaVSi_2O_6 | 9. $\text{NaCrSi}_2\text{O}_6$ |
| 10. $\text{NaFe}^3\text{Si}_2\text{O}_6$ | 11. $\text{NaAlSi}_2\text{O}_6$ | 12. $\text{LiAlSi}_2\text{O}_6$ |
| 13. $\text{CaZrAl}_2\text{O}_6$ | 14. $\text{CaTiAl}_2\text{O}_6$ | 15. CaYAlSiO_6 |
| 16. CaVAlSiO_6 | 17. CaCrSiAlO_6 | 18. $\text{CaFe}^3\text{SiAlO}_6$ |
| 19. CaAlSiAlO_6 | 20. $\text{CaZnSi}_2\text{O}_6$ | 21. $\text{CaMnSi}_2\text{O}_6$ |
| 22. $\text{CaFMSi}_2\text{O}_6$ | 23. FMAlSiAlO_6 | 24. $\text{FM}_2\text{Si}_2\text{O}_6$ |
| 25. $\text{Ca}_2\text{Si}_2\text{O}_6$ | 26. $\text{Zn}_2\text{Si}_2\text{O}_6$ | 27. $\text{Mn}_2\text{Si}_2\text{O}_6$ |
| 28. $\text{Ni}_2\text{Si}_2\text{O}_6$ | | |

Olivines

	58017 SM5	58017 SM5	58017 SM5	AM38 SM5	AM38 SM5	AM38 SM5	AM38 SM5	AM38 SM5	AM39b SM5	AM39b SM5
SiO2	31.32	32.06	32.24	33.40	31.54	31.34	31.62	32.63	31.40	30.22
TiO2	0.02	0.03	0.15	0.09	0.08	0.16	0.11	0.07	0.10	0.04
Al2O3	-	-	0.03	0.01	0.02	0.04	0.04	0.00	0.00	0.00
FeO	58.18	55.27	55.32	48.48	51.29	54.08	51.00	51.97	58.12	59.74
MnO	4.10	3.58	3.73	2.96	3.10	3.14	3.09	3.17	4.43	3.72
MgO	5.91	8.79	8.48	14.63	14.01	10.86	13.51	11.71	5.61	4.62
CaO	0.54	0.50	0.57	0.62	0.49	0.73	0.56	0.52	0.71	0.91
Na2O	-	-	0.05	0.04	0.05	0.41	0.03	0.05	0.07	0.10
K2O	-	-	-	-	-	-	-	-	-	0.06
Total	100.08	100.24	100.56	100.24	100.58	100.76	99.97	100.12	100.44	99.42
Cations to 4 oxygens										
Si	1.0087	1.0093	1.0118	1.0081	0.9689	0.9775	0.9765	1.0073	1.0088	0.9940
Ti	0.0006	0.0007	0.0034	0.0021	0.0019	0.0037	0.0026	0.0016	0.0024	0.0010
Al			0.0010	0.0004	0.0007	0.0014	0.0014	0.0001	0.0000	0.0000
Fe	1.5671	1.4551	1.4517	1.2237	1.3177	1.4108	1.3174	1.3417	1.5618	1.6432
Mn	0.1120	0.0954	0.0992	0.0757	0.0806	0.0829	0.0809	0.0830	0.1207	0.1037
Mg	0.2838	0.4126	0.3966	0.6583	0.6413	0.5049	0.6219	0.5389	0.2685	0.2263
Ca	0.0187	0.0169	0.0191	0.0201	0.0161	0.0244	0.0186	0.0171	0.0246	0.0322
Na			0.0028	0.0026	0.0032	0.0248	0.0016	0.0027	0.0041	0.0067
K										0.0027
Fe	79.84	74.12	74.54	62.51	64.61	70.59	65.20	68.33	80.05	83.15
Mg	14.46	21.01	20.36	33.62	31.44	25.26	30.78	27.44	13.76	11.56
Mn	5.71	4.86	5.09	3.87	3.95	4.15	4.01	4.23	6.19	5.29

Olivines

	AM39b SM5	AM39b SM5	AM40 SM5	AM40 SM5	AM40 SM5	AM29 SM5*	AM29 SM5*	AM29 SM5*	AM55 SM5*	AM55 SM5*
SiO2	31.09	30.95	31.75	32.07	31.04	32.92	32.96	32.64	31.73	31.37
TiO2	0.11	0.11	0.10	0.06	0.02	0.08	0.08	0.10	0.12	0.11
Al2O3	0.07	0.07	0.04	0.19	0.08	0.00	0.00	0.00	0.01	0.02
FeO	58.89	59.64	56.75	54.60	54.81	51.43	50.47	52.81	59.41	59.19
MnO	4.74	5.00	3.69	3.37	2.59	1.76	2.37	2.40	3.81	3.49
MgO	4.09	3.25	7.12	8.66	8.98	13.27	13.95	11.92	4.97	5.56
CaO	0.85	1.13	0.49	0.45	0.41	0.34	0.44	0.51	0.72	0.65
Na2O	0.12	0.12	0.10	0.13	0.16	0.08	0.00	0.00	0.00	0.08
Total	99.98	100.27	100.05	99.53	98.16	99.90	100.27	100.38	100.77	100.47
Cations to 4 oxygens										
Si ⁺	1.0121	1.0108	1.0115	1.0134	0.9987	1.0075	1.0025	0.9893	1.0175	1.0083
Ti	0.0027	0.0026	0.0024	0.0014	0.0004	0.0019	0.0019	0.0024	0.0029	0.0027
Al	0.0027	0.0027	0.0016	0.0069	0.0031	0.0001	0.0000	0.0000	0.0005	0.0006
Fe	1.6034	1.6288	1.5120	1.4429	1.4751	1.3165	1.2838	1.3387	1.5931	1.5910
Mn	0.1308	0.1383	0.0996	0.0903	0.0707	0.0457	0.0610	0.0617	0.1035	0.0950
Mg	0.1986	0.1582	0.3382	0.4078	0.4307	0.6051	0.6321	0.5382	0.2373	0.2665
Ca	0.0296	0.0396	0.0167	0.0151	0.0141	0.0113	0.0142	0.0781	0.0246	0.0223
Na	0.0078	0.0079	0.0064	0.0080	0.0101	0.0048	0.0000	0.0000	0.0000	0.0047
Fe	83.04	84.61	77.55	74.34	74.63	66.92	64.94	69.06	82.38	81.40
Mg	10.29	8.22	17.34	21.01	21.79	30.75	31.97	27.76	12.27	13.65
Mn	6.77	7.17	5.11	4.65	3.58	2.32	3.09	3.18	5.35	4.87

Olivines

	AM55 SM5*	58036 SM5*	58036 SM5*	58037 SM5*	58037 SM5*	54139 SM2	AM149 alk gab	58358 dyke
SiO2	30.82	33.71	33.83	32.58	33.52	31.21	36.47	28.89
TiO2	0.11	0.13	0.11	0.02	0.09	0.08	0.06	0.08
Al2O3	0.00	0.00	0.00	0.00	0.02	0.07	0.03	0.07
FeO	60.71	46.50	48.33	50.21	47.95	51.05	32.08	65.67
MnO	3.76	1.97	2.21	2.01	2.11	4.70	0.56	3.04
MgO	4.50	17.25	15.99	15.04	16.49	10.33	30.64	1.67
CaO	0.76	0.59	0.32	0.41	0.30	0.77	0.37	0.59
Na2O	0.05	0.05	0.01	0.08	0.07	0.00	0.04	0.33
K2O	0.02	-	-	-	0.00	0.00	0.00	0.00
Total	100.74	100.20	100.79	100.36	100.56	98.24	100.25	100.34
Cations to 4 oxygens								
Si	1.0000	1.0021	1.0076	0.9886	1.0001	0.9942	0.9959	0.9715
Ti	0.0026	0.0029	0.0024	0.0005	0.0021	0.0019	0.0012	0.0019
Al	0.0000	0.0000	0.0000	0.0000	0.0005	0.0026	0.0009	0.0027
Fe	1.6469	1.1561	1.2039	1.2741	1.1965	1.3599	0.7325	1.8468
Mn	0.1030	0.0497	0.0557	0.0518	0.0534	0.1267	0.0130	0.0866
Mg	0.2176	0.7641	0.7097	0.6800	0.7331	0.4904	1.2470	0.0836
Ca	0.0265	0.0186	0.0104	0.0135	0.0097	0.0263	0.0110	0.0212
Na	0.0034	0.0028	0.0008	0.0049	0.0039	0.0000	0.0020	0.0217
K	0.0007				0.0001	0.0012	0.0000	0.0000
Fe	83.70	58.69	61.13	63.52	60.34	68.79	36.81	91.56
Mg	11.02	38.79	36.04	33.90	36.97	24.81	62.59	4.14
Mn	5.27	2.52	2.83	2.58	2.69	6.41	0.60	4.29

Pyroxenes

	AM6a SM1	54132 SM1	54163 SM1	54163 SM1	58007a SM1	58007a SM1	58080 SM1	63703 SM1	63703 SM1	63760 SM1
SiO2	51.89	51.15	51.28	50.68	49.57	50.37	50.69	50.31	50.73	52.33
TiO2	2.08	0.72	0.28	1.34	0.33	0.29	1.51	0.78	0.81	0.40
Al2O3	1.19	1.47	1.07	1.14	1.03	0.87	1.62	1.35	1.53	0.75
FeO	27.76	11.68	20.42	27.79	19.85	18.39	26.77	14.19	13.07	28.77
MnO	0.42	0.67	1.29	0.54	1.46	1.38	0.27	0.73	0.70	0.00
MgO	0.06	10.55	4.91	0.04	5.10	6.31	0.72	10.25	11.03	0.00
CaO	2.51	23.09	17.79	2.02	20.12	20.30	1.83	21.82	21.87	0.66
Na2O	11.86	1.04	2.80	12.54	2.05	1.87	12.28	0.57	0.50	13.74
K2O	0.00	0.02	0.05	0.00	0.01	0.02	0.05	0.00	0.00	0.00
ZrO2	0.15	0.05	0.04	0.41	0.12	0.11	0.25	0.02	0.04	0.22
Total	97.92	100.44	99.92	96.51	99.64	99.90	95.99	100.01	100.29	96.87

Cations to 6 oxygens

Si	2.1177	1.9444	2.0216	2.1133	1.9754	1.9838	2.1069	1.9366	1.9349	2.1669
Ti	0.0639	0.0207	0.0082	0.0421	0.0099	0.0087	0.0472	0.0224	0.0233	0.0125
Al	0.0572	0.0657	0.0496	0.0563	0.0484	0.0404	0.0795	0.0612	0.0690	0.0367
Fe	0.9474	0.3712	0.6734	0.9690	0.6617	0.6056	0.9305	0.4568	0.4169	0.9962
Mn	0.0144	0.0217	0.0430	0.0191	0.0493	0.0460	0.0095	0.0237	0.0226	0.0000
Mg	0.0038	0.5976	0.2882	0.0026	0.3027	0.3701	0.0443	0.5878	0.6269	0.0000
Ca	0.1100	0.9403	0.7515	0.0904	0.8589	0.8566	0.0817	0.9001	0.8937	0.0294
Na	0.9384	0.0765	0.2143	1.0137	0.1583	0.1427	0.9900	0.0426	0.0372	1.1033
K	0.0000	0.0008	0.0024	0.0000	0.0006	0.0009	0.0027	0.0000	0.0000	0.0000
Zr	0.0031	0.0009	0.0008	0.0084	0.0024	0.0022	0.0051	0.0003	0.0008	0.0044

Na	88.6	7.7	20.9	92.9	15.4	13.8	91.5	3.9	3.5	99.9
Fe2+Mn	11.0	32.5	51.0	6.9	55.2	50.5	4.4	41.2	37.9	0.1
Mg	0.4	59.9	28.1	0.2	29.4	35.7	4.1	54.8	58.6	0.0

End members in mole% (PXPROG8) *zr/px=NAZAL+FM-NAZ

Ac	82.8	1.0	16.2	89.1	10.6	9.9	85.2	0.0	0.0	
Di/Hed	7.6	88.6	70.1	1.3	77.9	78.6	5.8	84.0	83.4	
zr/px*	0.3	0.1	0.1	0.8	0.2	0.2	0.5	0.1	0.1	

Pyroxenes

	63760 SM1	63760 SM1	54139 SM2	54142 SM2	54138 SM3	54138 SM3	54138 SM3	58400 SM3	58400 SM3	63717 SM3
SiO2	51.02	51.35	51.64	49.67	51.18	50.33	50.00	48.52	50.25	51.58
TiO2	0.58	0.13	0.45	0.45	1.21	1.22	0.77	0.45	0.36	1.75
Al2O3	0.82	0.40	1.25	1.19	0.96	1.25	0.45	0.51	0.82	1.04
FeO	27.30	31.02	13.75	17.23	24.67	23.84	24.09	23.23	24.17	28.21
MnO	0.41	0.31	1.06	1.27	1.57	1.13	1.21	1.32	1.61	0.21
MgO	0.12	0.00	9.53	7.70	0.59	0.18	0.20	2.53	2.12	0.19
CaO	3.03	0.26	22.25	21.68	3.07	2.24	4.25	22.01	16.93	0.38
Na2O	12.30	13.16	1.08	1.14	12.24	12.16	10.00	1.62	3.49	12.98
K2O	0.03	0.18	0.03	0.03	0.00	0.00	0.00	0.03	0.01	0.00
ZrO2	0.92	-	-	-	3.56	4.60	6.96	0.24	0.53	0.27
Total	96.62	96.83	101.02	100.36	99.06	96.94	97.93	100.46	100.23	96.62
Cations to 6 oxygens										
Si	2.1214	2.1550	1.9573	1.9422	2.0839	2.0892	2.0594	1.9625	2.0198	2.1350
Ti	0.0181	0.0041	0.0129	0.0132	0.0372	0.0382	0.0204	0.0137	0.0108	0.0545
Al	0.0400	0.0196	0.0557	0.0549	0.0462	0.0611	0.0219	0.0243	0.0387	0.0509
Fe	0.9494	1.0888	0.4357	0.5636	0.8401	0.8276	0.8300	0.7858	0.8127	0.9767
Mn	0.0146	0.0111	0.0339	0.0420	0.0541	0.0396	0.0422	0.0452	0.0548	0.0072
Mg	0.0074	0.0000	0.5382	0.4487	0.0361	0.0112	0.0120	0.1525	0.1272	0.0119
Ca	0.1348	0.0116	0.9081	0.9086	0.1339	0.0998	0.1876	0.9539	0.7291	0.0170
Na	0.9960	1.0720	0.0791	0.0863	0.9662	0.9785	0.9257	0.1271	0.2719	1.0417
K	0.0008	0.0097	0.0014	0.0013	0.0000	0.0000	0.0025	0.0015	0.0006	0.0001
Zr	0.0182				0.0706	0.0930	0.1397	0.0047	0.0103	0.0054
Na	93.1	89.0	7.8	7.6	96.4	98.9	98.7	12.8	26.6	94.8
Fe2+Mn	6.1	11.0	39.2	52.8	0.0	0.0	0.0	71.9	60.9	4.1
Mg	0.6	0.0	52.9	39.6	3.6	1.1	1.3	15.3	12.5	1.1
End members in mole% *zr/px=NAZAL+FM-NAZ										
Ac			2.3		74.6	68.2	48.5	9.8		92.0
Di/Hed			86.3		1.6	0.0	14.3	79.8		0.6
zr/px*					9.9	15.1	25.3	0.5		0.5

Pyroxenes

	63721c SM3	AM7 SM4	AM7a SM4	AM7a SM4	AM7a SM4	AM7b SM4	AM7b SM4	AM7c SM4	AM7c SM4	AM45a SM4
SiO2	49.40	49.93	50.30	50.51	50.55	50.37	50.77	50.17	52.17	50.29
TiO2	0.04	1.68	0.50	0.89	3.19	2.20	0.37	0.39	2.92	0.32
Al2O3	0.40	1.07	0.95	1.50	1.48 ^x	1.37	1.30	1.23	1.52 ^x	2.45
FeO	26.89	27.53	15.34	25.35	27.53 ^x	28.65 ^x	13.40	14.79	26.57 ^x	13.04
MnO	1.24	1.02	1.31	4.02	0.97	0.54	0.98	1.05	1.12	0.77
MgO	1.63	0.44	8.24	3.69	0.56	0.19	9.05	8.48	0.63	9.09
CaO	18.05	2.79	22.46	1.40	2.89	3.02	21.90	21.61	2.98	21.62
Na2O	1.92	12.47	1.57	8.98	12.17	12.45	1.28	1.24	11.74	1.50
K2O	0.01	0.03	0.01	1.73	0.08	0.10	0.00	0.01	0.03	0.01
ZrO2	0.26	0.47	0.05	0.13	0.46	0.72	0.00	0.11	0.43	0.12
Total	99.84	97.44	100.72	98.19	99.88	99.61	99.02	99.08	100.11	99.21
Cations to 6 oxygens (^x all iron as Fe2O3)										
Si	2.0164	2.0749	1.9485	2.0681	1.9362	1.9420	1.9703	1.9614	1.9772	1.0436
Ti	0.0012	0.0526	0.0147	0.0274	0.0919	0.0638	0.0108	0.0113	0.0832	0.0092
Al	0.0192	0.0522	0.0433	0.0723	0.0669	0.0623	0.0594	0.0568	0.0679	0.1115
Fe	0.9178	0.9569	0.4968	0.8680	0.7953	0.8312	0.4350	0.4837	0.7578	0.4215
Mn	0.0430	0.0359	0.0429	0.1395	0.0315	0.0176	0.0321	0.0348	0.0360	0.0253
Mg	0.0992	0.0271	0.4759	0.2254	0.0320	0.0109	0.5232	0.4939	0.0356	0.5238
Ca	0.7895	0.1243	0.9323	0.0612	0.1186	0.1248	0.9106	0.9054	0.1210	0.8955
Na	0.1521	1.0051	0.1178	0.7126	0.9039	0.9307	0.0960	0.0941	0.8627	0.1122
K	0.0005	0.0015	0.0005	0.0902	0.0039	0.0049	0.0000	0.0004	0.0015	0.0005
Zr	0.0051	0.0096	0.0009	0.0027	0.0086	0.0135	0.0000	0.0022	0.0079	0.0022
Na	14.7	89.9	11.5	51.5	95.5	97.8	9.6	9.2	94.3	11.4
Fe2+Mn	75.7	7.7	42.2	32.2	1.1	1.1	38.1	42.5	1.8	35.2
Mg	9.6	2.4	46.3	16.3	3.4	1.1	52.3	48.3	3.9	53.4
End members in mole % *zr/px=NAZAL+FM-NAZ										
Ac	13.1	84.4								
Di/Hed	73.9	3.6								0.0
zr/px*	0.5	0.9								83.3
										0.2

Pyroxenes

	AM45 SM4	AM45 SM4	AM45 SM4	AM48 SM4	AM48 SM4	AM48 SM4	AM49 SM4	AM50 SM4	AM51 SM4	AM68 SM4
SiO2	49.07	48.95	47.34	49.07	49.33	48.99	49.95	50.00	51.26	51.73
TiO2	0.28	0.21	0.21	0.34	0.26	0.33	0.05	0.37	0.30	0.41
Al2O3	2.09	1.77	1.78	1.06	1.06	0.67	0.68	0.76	0.96	0.98
FeO	15.33	20.89	21.32	20.99	22.35	25.20	27.78	26.30	22.01	15.73
MnO	1.02	1.47	1.47	10.2	1.19	1.11	1.03	0.82	1.37	0.84
MgO	8.37	3.94	3.95	4.14	2.37	0.91	0.70	1.22	3.04	8.13
CaO	21.63	21.03	20.95	20.69	18.26	14.70	11.48	7.56	14.16	20.68
Na2O	1.39	1.42	1.43	1.33	3.21	5.32	6.96	9.19	4.68	1.30
K2O	0.01	0.01	0.01	0.03	0.05	0.01	0.01	0.00	0.00	0.01
ZrO2	0.20	0.33	0.33	0.17	0.15	0.53	0.45	0.44	0.37	0.07
Total	99.39	100.03	98.80	98.85	98.22	97.78	99.07	96.66	98.15	99.88
Cations to 6 oxygens										
Si	1.9226	1.9557	1.9286	1.9792	2.0134	2.0345	2.0555	2.0854	2.0664	1.9988
Ti	0.0082	0.0062	0.0063	0.0103	0.0079	0.0104	0.0015	0.0117	0.0092	0.0119
Al	0.0968	0.0834	0.0853	0.0505	0.0510	0.0329	0.0330	0.0374	0.0456	0.0447
Fe	0.5024	0.6978	0.7266	0.7079	0.7627	0.8750	0.9561	0.9174	0.7420	0.5082
Mn	0.0339	0.0499	0.0508	0.0348	0.0410	0.0392	0.0358	0.0291	0.0468	0.0275
Mg	0.4887	0.2345	0.2400	0.2491	0.1440	0.0565	0.0429	0.0759	0.1826	0.4680
Ca	0.9078	0.9004	0.9147	0.8939	0.7986	0.6543	0.5060	0.3377	0.6116	0.8563
Na	0.1054	0.1102	0.1130	0.1043	0.2543	0.4287	0.5553	0.7432	0.3656	0.0972
K	0.0005	0.0006	0.0007	0.0017	0.0027	0.0003	0.0003	0.0000	0.0002	0.0007
Zr	0.0038	0.0065	0.0066	0.0034	0.0029	0.0107	0.0090	0.0090	0.0073	0.0013
Na	10.2	11.1	11.0	10.4	26.1	42.3	51.0	67.8	36.3	9.6
Fe2+Mn	42.6	65.3	65.7	64.7	59.0	52.1	45.8	25.3	45.6	44.2
Mg	47.2	23.6	23.3	24.9	14.9	5.6	3.2	6.9	18.1	46.2
End members in mole% *zr/px=NAZAL+FM-NAZ										
Ac	0.8	2.8	2.6	5.3	19.8	37.9	49.0	65.9		5.3
Di/Hed	81.9	81.9	81.1	84.2	68.3	51.3	44.2	26.9		82.8
zr/px*	0.4	0.6	0.6	0.3	0.3	1.0	0.9	0.8		0.1

Pyroxene

	54241 SM4	54241 SM4	54242 SM4	54242 SM4	58039 SM4	58039 SM4	59603 SM4	59603 SM4	63725 SM4	63725 SM4
SiO ₂	49.60	51.15	49.80	50.12	49.17	49.08	48.37	50.31	49.40	49.85
TiO ₂	0.44	0.35	0.53	0.46	0.39	0.41	0.47	0.29	0.28	0.30
Al ₂ O ₃	1.23	0.85	1.43	1.34	1.22	1.31	1.94	1.00	0.77	0.78
FeO	19.36	20.22	19.11	20.41	18.96	21.02	18.12	25.49	25.91	25.07
MnO	1.39	1.33	1.24	1.36	0.90	0.96	0.89	0.54	1.17	1.32
MgO	5.66	4.80	5.18	4.96	6.05	5.11	6.09	1.34	0.95	1.43
CaO	20.35	19.28	21.96	20.48	21.73	21.16	22.69	14.03	13.00	15.12
Na ₂ O	1.42	2.61	1.30	1.33	0.84	0.97	1.22	5.78	6.25	5.19
K ₂ O	0.00	0.02	0.01	0.00	0.00	0.01	0.02	0.04	0.01	0.00
ZrO ₂	0.09	0.13	0.00	0.00	0.00	0.00	0.04	0.26	0.71	0.55
Total	99.53	100.74	100.56	100.45	99.26	100.03	99.86	99.07	98.46	99.61
Cations to 6 oxygens										
Si	1.9695	2.0080	1.9597	1.9767	1.9562	1.9537	1.9167	2.0466	2.0390	2.0277
Ti	0.0131	0.0104	0.0158	0.0135	0.0117	0.0123	0.0141	0.0088	0.0088	0.0092
Al	0.0577	0.0395	0.0663	0.0623	0.0572	0.0617	0.0907	0.0478	0.0373	0.0372
Fe	0.6428	0.6637	0.6291	0.6370	0.6308	0.6997	0.6006	0.8672	0.8946	0.8522
Mn	0.0469	0.0442	0.0414	0.0454	0.0302	0.0325	0.0298	0.0187	0.0410	0.0455
Mg	0.3347	0.2806	0.3035	0.2917	0.3588	0.3032	0.3597	0.0812	0.0587	0.0869
Ca	0.8658	0.8110	0.9259	0.8652	0.9263	0.9025	0.9634	0.6115	0.5753	0.6588
Na	0.1092	0.1983	0.0991	0.1013	0.0647	0.0746	0.0939	0.4556	0.5000	0.4094
K	0.0000	0.0011	0.0003	0.0000	0.0000	0.0006	0.0010	0.0019	0.0006	0.0000
Zr	0.0018	0.0024	0.0000	0.0000	0.0000	0.0000	0.0008	0.0051	0.0143	0.0110
Na	10.6	19.7	10.1	9.9	6.3	7.2	9.4	45.1	47.9	39.9
Fe ₂ +Mn	57.1	52.5	59.1	61.5	58.6	63.8	54.6	46.9	46.5	51.6
Mg	32.3	27.8	30.8	28.6	35.1	29.0	36.0	8.0	5.6	8.5
End members in mole% *zr/px=NAZAL+FM-NAZ										
Ac	5.0	15.6	3.2	3.9	0.7	1.3	0.3	39.1	43.9	35.6
Di/Hed	79.6	75.2	85.6	80.4	86.6	83.9	87.3	51.7	46.5	54.3
zr/px*	0.2	0.2	0.0	0.0	0.0	0.0	0.1	0.5	1.4	1.0

Pyroxenes

	63725 SM4	63729 SM4	63729 SM4	63731 SM4	63731 SM4	63731 SM4	63731 SM4	63746 SM4	63746 SM4	63754 SM4
SiO2	49.91	52.15	51.02	49.45	49.93	49.35	48.37	50.37	51.00	49.25
TiO2	0.29	0.60	0.58	0.72	0.76	0.94	0.25	0.35	0.37	0.13
Al2O3	0.73	0.82	0.82	2.72	1.66	2.09	0.67	0.82	0.77	0.79
FeO	25.32	26.80	27.30	17.46	12.78	11.90	22.08	27.36	26.93	23.90
MnO	1.41	0.44	0.41	0.82	0.69	0.65	1.49	0.81	0.76	1.32
MgO	1.32	0.20	0.12	7.79	9.81	10.15	3.74	0.34	0.42	2.25
CaO	14.60	2.33	3.03	18.33	23.34	23.39	21.07	6.72	7.03	14.36
Na2O	5.76	12.49	12.36	1.37	0.55	0.90	1.35	9.77	10.07	5.24
K2O	0.00	0.00	0.00	0.29	0.00	0.06	0.29	0.00	0.01	0.00
ZrO2	0.66	1.53	1.39	0.08	0.00	0.06	0.08	0.56	0.67	0.42
Total	100.00	97.37	97.02	99.03	99.52	99.50	99.37	97.11	98.03	97.66
Cations to 6 oxygens										
Si	2.0267	2.1454	2.1214	1.9400	1.9281	1.9044	1.9644	2.0984	2.1007	2.0320
Ti	0.0088	0.0186	0.0181	0.0213	0.0222	0.0274	0.0076	0.0111	0.0116	0.0040
Al	0.0352	0.0400	0.0400	0.1258	0.0755	0.0950	0.0320	0.0405	0.0373	0.0384
Fe	0.8598	0.9221	0.9494	0.5730	0.4126	0.3843	0.7499	0.9534	0.9276	0.8246
Mn	0.0486	0.0154	0.0146	0.0273	0.0226	0.0213	0.0511	0.0286	0.0264	0.0461
Mg	0.0799	0.0124	0.0074	0.4558	0.5646	0.5838	0.2264	0.0209	0.0258	0.1385
Ca	0.6352	0.1027	0.1348	0.7705	0.9658	0.9672	0.9169	0.3000	0.3104	0.6348
Na	0.4531	0.9963	0.9968	0.1041	0.0410	0.0676	0.1065	0.7891	0.8046	0.4188
K	0.0000	0.0000	0.0000	0.0145	0.0000	0.0031	0.0148	0.0001	0.0004	0.0001
Zr	0.0131	0.0307	0.0282	0.0015	0.0001	0.0011	0.0015	0.0113	0.0134	0.0084
Na	43.9	95.0	93.1	9.8	4.1	6.8	10.3	73.0	74.4	39.9
Fe2+Mn	48.4	3.8	6.2	47.5	39.7	34.6	67.9	25.1	23.3	47.0
Mg	7.7	1.2	0.7	42.7	56.2	58.6	21.8	1.9	2.3	13.1
End members in mole% *zr/px=NAZAL+FM-NAZ										
Ac	39.6	88.6	87.9	0.0	0.0	0.0	7.1	70.2	71.9	36.3
Di/Hed	49.4	0.3	0.6	71.1	89.7	88.4	82.5	21.2	17.5	55.4
zr/px*	1.2	3.0	2.6	0.2	0.0	0.1	0.2	1.1	1.3	0.8

Pyroxenes

	AM55 SM5*	58037 SM5*	58062 SM5*	AM38 SM5	AM39b SM5	AM39b SM5	AM40 SM5	AM40 SM5	AM43 SM5	AM77 SM5
SiO2	51.81	50.85	50.87	50.29	52.07	50.32	50.06	50.05	50.19	50.35
TiO2	0.89	1.06	1.19	0.77	1.06	0.76	0.87	1.18	0.75	0.66
Al2O3	1.78	1.90	1.88	2.00	2.09	1.26	2.08	1.99	1.19	1.03
FeO	13.20	11.25	11.96	12.43	11.09	11.93	10.54	11.19	12.91	14.84
MnO	0.55	0.56	0.62	0.67	0.64	0.66	0.51	0.63	0.80	0.87
MgO	10.22	11.73	10.73	10.30	11.37	9.24	11.38	11.11	10.14	9.41
CaO	21.59	22.39	21.77	23.43	21.07	23.90	22.04	22.24	23.71	22.34
Na2O	0.68	0.62	0.59	0.71	0.92	0.83	0.85	0.70	0.86	0.84
K2O	0.00	0.00	0.00	0.00	0.31	0.03	0.04	0.04	0.02	0.00
ZrO2	0.06	0.06	0.03	0.00	0.00	0.02	0.04	0.00	0.00	0.00
Total	100.79	100.44	99.62	100.60	100.62	98.94	98.42	99.13	100.57	100.34
Cations to 6 oxygens										
Si	1.9587	1.9225	1.9406	1.9173	1.9542	1.9509	1.9275	1.9205	1.9249	1.9435
Ti	0.0253	0.0303	0.0341	0.0221	0.0300	0.0223	0.0252	0.0339	0.0216	0.0192
Al	0.0796	0.0848	0.0846	0.0900	0.0926	0.0575	0.0947	0.0900	0.0537	0.0469
Fe	0.4173	0.3559	0.3814	0.3963	0.3480	0.3868	0.3393	0.3590	0.4140	0.4791
Mn	0.0175	0.0180	0.0200	0.0215	0.0203	0.0215	0.0165	0.0204	0.0258	0.0283
Mg	0.5761	0.6610	0.6098	0.5850	0.6362	0.5338	0.6533	0.6355	0.5797	0.5413
Ca	0.8746	0.9070	0.8897	0.9571	0.8473	0.9927	0.9095	0.9143	0.9743	0.9239
Na	0.0501	0.0456	0.0436	0.0527	0.0672	0.0623	0.0636	0.0524	0.0641	0.0631
K	0.0000	0.0000	0.0000	0.0000	0.0146	0.0014	0.0018	0.0018	0.0012	0.0000
Zr	0.0010	0.0012	0.0005	0.0000	0.0000	0.0003	0.0008	0.0000	0.0000	0.0000
Na	4.9	4.4	4.3	5.3	6.7	6.6	6.3	5.1	6.3	
Fe2+Mn	38.4	32.0	35.7	38.0	30.4	37.1	29.4	32.6	37.2	
Mg	56.7	63.6	60.0	56.7	62.9	56.3	64.3	62.3	56.5	
End members in mole% *zr/px=NAZAL+FM-NAZ										
Ac	0.0	0.0	0.0	0.0	0.0	0.0	0.0	0.0	1.0	
Di/Hed	84.2	84.7	84.5	85.7	80.9	88.9	85.1	85.2	89.8	
zr/px*	0.1	0.1	0.1	0.0	0.0	0.0	0.1	0.0	0.0	

Pyroxenes

	AM77 SM5	AM77 SM5	AM77 SM5	AM77 SM5	AM77 SM5	AM77 SM5	AM82 SM5	AM82 SM5	AM82 SM5	AM84 SM5
SiO2	50.14	51.16	50.95	51.74	51.70	50.34	51.35	51.61	51.72	50.95
TiO2	1.37	0.46	0.73	1.05	0.43	0.54	0.51	0.48	0.79	0.85
Al2O3	0.83	0.50	0.68	0.80	0.81	0.98	0.75	0.92	0.98	1.28
FeO	26.30	25.88	25.20	26.73	16.03	16.88	24.59	15.85	25.45	13.04
MnO	0.85	0.94	0.83	0.61	0.81	0.77	1.09	0.90	0.84	0.83
MgO	0.67	1.44	1.33	0.85	7.78	8.03	2.27	8.53	1.75	9.42
CaO	7.77	11.84	7.93	5.82	21.46	22.44	9.87	20.85	12.28	21.78
Na2O	9.56	6.75	8.87	10.50	0.89	1.00	7.96	1.09	6.38	0.91
K2O	0.02	0.01	0.01	0.00	0.00	0.00	0.00	0.00	0.02	0.00
ZrO2	1.47	1.54	1.45		0.13		0.60			0.06
Total	98.98	100.51	98.01	98.11	100.08	100.98	98.98	100.24	100.21	99.11
Cations to 6 oxygens										
Si	2.0526	2.0574	2.0868	2.1113	2.0000	1.9489	2.0744	1.9886	2.0645	1.9676
Ti	0.0422	0.0139	0.0226	0.0324	0.0125	0.0157	0.0155	0.0141	0.0237	0.0247
Al	0.0402	0.0236	0.0328	0.0383	0.0367	0.0450	0.0359	0.0417	0.0461	0.0581
Fe	0.9005	0.8703	0.8633	0.9121	0.5181	0.5464	0.8308	0.5107	0.8496	0.4212
Mn	0.0293	0.0320	0.0287	0.0211	0.0265	0.0253	0.0372	0.0294	0.0284	0.0272
Mg	0.0408	0.0861	0.0810	0.0519	0.4482	0.4632	0.1364	0.4900	0.1041	0.5422
Ca	0.3406	0.5100	0.3481	0.2546	0.8890	0.9307	0.4271	0.8610	0.5252	0.9012
Na	0.7590	0.5262	0.7041	0.8308	0.0664	0.0753	0.6221	0.0818	0.4938	0.0680
K	0.0012	0.0004	0.0004	0.0001	0.0002	0.0000	0.0000	0.0002	0.0009	0.0000
Zr	0.0294	0.0301	0.0289		0.0024		0.0112			0.0012
Na	72.3	50.6	67.5	77.8	6.6	7.2	58.4	7.9	45.9	6.8
Fe2+Mn	23.5	41.1	24.7	17.3	48.5	48.4	28.8	44.9	44.4	38.7
Mg	4.2	8.3	7.8	4.9	44.9	44.4	12.8	47.2	9.7	54.3
End members in mole% *zr/px=NAZAL+FM-NAZ										
Ac	61.2	44.6	61.1	75.1	3.0	2.9	56.1	3.9	43.7	1.0
Di/Hed	23.6	45.8	28.0	16.3	86.9	86.8	36.5	82.6	48.5	86.6
zr/px*	2.8	3.4	2.8		0.3		1.1			0.1

Pyroxenes

	AM85 SM5	AM85 SM5	AM88 SM5	AM110 SM5	AM110 SM5	AM111 SM5	AM111 SM5	AM111 SM5	AM111 SM5	AM111 SM5
SiO2	50.14	51.02	50.47	52.79	49.94	49.72	49.70	48.32	50.22	49.31
TiO2	0.50	0.40	0.31	1.13	0.54	0.49	0.37	0.00	0.23	0.57
Al2O3	1.11	1.25	1.11	3.16	0.87	1.62	1.47	0.77	0.70	1.68
FeO	21.69	15.84	16.72	26.22	22.04	20.15	22.03	25.38	23.61	20.86
MnO	1.71	1.18	1.38	0.16	1.21	0.90	1.14	1.25	1.37	1.01
MgO	3.31	8.12	6.97	0.21	3.37	5.13	3.27	1.69	2.45	4.75
CaO	17.77	21.32	20.28	0.05	18.56	20.53	19.21	14.66	14.56	20.77
Na2O	3.20	0.97	1.21	14.49	3.74	0.81	1.84	5.01	5.08	0.90
K2O	0.01	0.01	0.00	0.02	0.03	0.03	0.04	0.04	0.01	0.01
ZrO2			0.07	0.00	0.45	0.00	0.03	0.00	0.13	0.00
Total	99.45	100.10	98.53	98.22	100.75	99.38	99.08	97.12	98.35	99.87

Cations to 6 oxygens

Si	2.0100	1.9752	1.9935	2.1206	1.9885	1.9741	1.9982	2.0219	2.0465	1.9597
Ti	0.0152	0.0118	0.0093	0.0341	0.0163	0.0148	0.0112	0.0000	0.0069	0.0171
Al	0.0524	0.0570	0.0518	0.1498	0.0410	0.0760	0.0699	0.0380	0.0336	0.0789
Fe	0.7273	0.5127	0.5524	0.8810	0.7339	0.6691	0.7407	0.8880	0.8048	0.6931
Mn	0.0582	0.0386	0.0463	0.0054	0.0410	0.0302	0.0388	0.0442	0.0471	0.0339
Mg	0.1975	0.4683	0.4105	0.0126	0.1998	0.3036	0.1959	0.1057	0.1487	0.2814
Ca	0.7634	0.8844	0.8583	0.0023	0.7919	0.8733	0.8275	0.6572	0.6358	0.8845
Na	0.2489	0.0729	0.0925	1.1284	0.2889	0.0625	0.1431	0.4068	0.4017	0.0696
K	0.0005	0.0003	0.0000	0.0009	0.0014	0.0015	0.0019	0.0021	0.0003	0.0006
Zr			0.0014	0.0000	0.0087	0.0000	0.0005	0.0000	0.0026	0.0000

Na	24.7	7.1	9.1	98.2	30.0	6.2	14.5	37.7	36.9	6.9
Fe2+Mn	55.7	47.3	50.6	0.5	49.2	63.7	65.7	52.5	49.5	65.4
Mg	19.6	45.6	40.3	1.3	20.8	30.1	19.8	9.8	13.6	27.7

End members in mole% *zr/px=NAZAL+FM-NAZ

Ac	19.2	1.6	4.1	84.5	23.6	0.0	7.3	34.4	35.5	0.0
Di/Hed	68.9	83.1	80.8	0.0	65.3	85.0	78.2	57.2	56.5	83.0
zr/px*			0.1	0.0	0.8	0.0	0.1	0.0	0.3	0.0

Pyroxenes

	58017 SM5	58020 SM5	58025 SM5	58025 SM5	58066 SM5	AM98 HY	AM98 HY	AM114 HY	AM114 HY	AM114 HY
SiO2	51.80	50.78	50.55	51.27	50.89	51.20	52.23	50.20	51.30	48.66
TiO2	0.75	1.34	0.53	0.40	0.54	0.33	0.29	0.58	0.48	0.69
Al2O3	1.52	2.31	1.32	1.10	0.58	0.74	1.17	1.82	1.32	1.87
FeO	10.19	12.83	15.38	14.62	26.68	26.41	25.63	17.71	20.01	17.64
MnO	0.49	0.62	0.93	1.04	0.89	1.28	1.05	0.78	1.05	0.71
MgO	11.33	9.97	8.28	9.15	0.77	1.11	0.99	6.37	4.74	6.35
CaO	23.19	21.52	20.74	19.56	8.47	10.47	7.60	21.63	18.84	20.69
Na2O	0.80	0.90	1.47	1.42	9.13	7.42	8.57	0.81	2.75	1.89
K2O	0.00	0.00	0.00	0.06	0.00	0.00	0.06	0.01	0.02	0.19
ZrO2					1.85	0.20	0.20	0.09	0.11	0.13
Total	100.06	100.27	98.33	98.61	99.80	99.16	97.80	100.02	100.61	99.09
Cations to 6 oxygens										
Si	1.9564	1.9319	1.9711	1.9950	2.0692	2.0808	2.1251	1.9618	2.0076	1.9327
Ti	0.0212	0.0384	0.0155	0.0116	0.0166	0.0101	0.0090	0.0170	0.0141	0.0205
Al	0.0678	0.1035	0.0607	0.0505	0.0277	0.0355	0.0560	0.0841	0.0610	0.0883
Fe	0.3219	0.4082	0.5016	0.4757	0.9073	0.8974	0.8716	0.5787	0.6550	0.5862
Mn	0.0156	0.0200	0.0307	0.0341	0.0307	0.0440	0.0367	0.0259	0.0347	0.0238
Mg	0.6377	0.5652	0.4812	0.5308	0.0466	0.0674	0.0602	0.3712	0.2762	0.3762
Ca	0.9385	0.8773	0.8666	0.8156	0.3689	0.4557	0.3314	0.9058	0.7901	0.8925
Na	0.0584	0.0666	0.1111	0.1070	0.7199	0.5849	0.6758	0.0616	0.2083	0.1455
K	0.0000	0.0000	0.0000	0.0027	0.0000	0.0000	0.0031	0.0003	0.0007	0.0097
Zr					0.0367	0.0039	0.0040	0.0018	0.0022	0.0025
Na	6.0	7.1	10.9	10.2	68.2	54.8	65.3	6.3	21.1	14.5
Fe2+Mn	29.0	39.2	42.0	39.3	27.4	38.9	28.9	55.9	50.9	47.9
Mg	65.0	53.6	47.1	50.5	4.4	6.3	5.8	37.8	28.0	37.6
End members in mole% *zr/px=NAZAL+FM-NAZ										
Ac	0.0	0.0	1.5	0.0	60.3	52.7	60.9	0.0	17.3	5.4
Di/Hed	90.2	82.9	81.5	77.5	27.0	39.5	29.0	86.2	64.0	81.9
zr/px*					4.3	0.4	0.4	0.2	0.2	0.3

Pyroxenes

	AM119 HY	AM119 HY	AM121 HY	AM121 HY	AM122 HY	AM122 HY	AM123b HY	AM123b HY	AM123b HY	AM135 HY
SiO2	50.60	48.74	50.32	49.49	49.32	49.40	50.10	49.31	50.97	49.67
TiO2	0.38	0.30	0.33	0.45	0.38	0.53	0.18	0.29	0.69	0.66
Al2O3	0.80	0.76	0.80	0.73	1.04	1.88	0.86	0.87	2.21	1.81
FeO	25.92	25.95	23.93	25.13	25.76	18.75	23.46	23.43	15.53	15.18
MnO	1.21	1.34	1.01	1.27	1.08	0.82	1.32	1.22	0.76	0.54
MgO	0.84	0.92	2.34	1.50	1.90	5.84	2.07	2.16	7.82	8.73
CaO	14.44	18.26	15.80	17.60	16.83	20.51	18.99	19.77	21.11	22.05
Na2O	5.16	2.92	3.88	2.90	3.65	0.94	2.40	1.38	0.95	0.78
K2O	0.01	0.02	0.04	0.02	0.28	0.03	0.07	0.00	0.01	0.01
ZrO2	0.28	0.29	0.09	0.14	0.21	0.06	0.23	0.06	0.04	0.07
Total	99.62	99.49	98.54	99.21	100.45	98.75	99.69	98.50	100.09	99.49
Cations to 6 oxygens										
Si	2.0530	2.0008	2.0439	2.0189	1.9955	1.9635	2.0205	2.0123	1.9634	1.9334
Ti	0.0116	0.0093	0.0101	0.0137	0.0114	0.0159	0.0056	0.0090	0.0201	0.0193
Al	0.0383	0.0368	0.0384	0.0350	0.0498	0.0880	0.0408	0.0418	0.1004	0.0830
Fe	0.8794	0.8911	0.8128	0.8572	0.8717	0.6232	0.7914	0.7997	0.5003	0.4940
Mn	0.0417	0.0465	0.0348	0.0438	0.0371	0.0276	0.0451	0.0423	0.0247	0.0177
Mg	0.0506	0.0561	0.1417	0.0911	0.1143	0.3462	0.1244	0.1313	0.4487	0.5061
Ca	0.6277	0.8030	0.6878	0.7695	0.7293	0.8733	0.8208	0.8643	0.8713	0.9202
Na	0.4057	0.2323	0.3053	0.2297	0.2870	0.0723	0.1879	0.1096	0.0710	0.0587
K	0.0004	0.0009	0.0020	0.0008	0.0146	0.0013	0.0037	0.0001	0.0004	0.0006
Zr	0.0056	0.0057	0.0018	0.0027	0.0041	0.0011	0.0045	0.0012	0.0008	0.0013
Na	40.1	22.8	29.9	22.6	27.3	7.2	19.3	11.1	7.2	5.7
Fe2+Mn	54.9	71.6	56.2	68.4	61.8	58.3	68.1	75.5	47.0	44.8
Mg	5.0	5.5	13.9	9.0	10.9	34.5	12.6	13.4	45.8	49.4
End members in mole% *zr/px=NAZAL+FM-NAZ										
Ac	36.0	18.9	26.4	19.2	22.6	0.0	14.6	6.8	0.0	0.0
Di/Hed	55.0	72.6	64.6	71.6	65.8	82.8	76.0	82.7	83.1	86.1
zr/px*	0.5	0.6	0.2	0.3	0.4	0.1	0.5	0.1	0.1	0.1

Pyroxenes

	AM135 HY	AM135 HY	AM149 Alk gab	AM149 Alk gab	AM149 Alk gab	58352 NM1	58352 NM1	58352 NM1	AM159 SM6	46261 SM6
SiO2	50.68	49.84	49.79	51.38	51.28	50.60	49.71	47.44	52.12	51.61
TiO2	0.35	0.56	1.75	1.10	1.65	0.69	0.54	0.34	1.18	1.25
Al2O3	0.44	1.76	3.10	1.77	3.10	1.47	1.22	1.17	1.05	0.17
FeO	21.27	17.35	10.67	10.23	9.94	14.25	15.83	25.38	27.37	28.01
MnO	1.23	0.78	0.28	0.32	0.36	0.64	0.67	1.37	0.93	0.38
MgO	3.89	7.10	12.28	12.61	11.82	10.09	8.81	1.53	0.14	0.13
CaO	19.44	21.85	22.41	22.39	20.78	20.99	22.28	21.90	3.25	3.00
Na2O	2.79	0.93	0.63	0.45	0.84	0.57	0.46	0.90	11.92	12.25
K2O	0.00	0.00	0.00	0.00	0.02	0.00	0.00	0.00	0.09	0.03
ZrO2	0.09	0.08	0.03	0.00	0.00				0.78	0.39
Total	100.19	100.26	100.92	100.24	99.78	99.29	99.53	100.02	98.84	97.22
Cations to 6 oxygens										
Si	2.0147	1.9444	1.8696	1.9317	1.9249	1.9542	1.9411	1.9436	2.1184	2.1339
Ti	0.0105	0.0164	0.0494	0.0310	0.0465	0.0199	0.0158	0.0104	0.0360	0.0053
Al	0.0207	0.0811	0.1373	0.0786	0.1371	0.0668	0.0563	0.0565	0.0504	0.0610
Fe	0.7073	0.5661	0.3349	0.3215	0.3120	0.4604	0.5169	0.8696	0.9303	0.9686
Mn	0.0414	0.0259	0.0088	0.0102	0.0115	0.0209	0.0220	0.0475	0.0321	0.0134
Mg	0.2307	0.4129	0.6870	0.7063	0.6613	0.5805	0.5129	0.0934	0.0085	0.0078
Ca	0.8279	0.9134	0.9015	0.9020	0.8360	0.8686	0.9323	0.9614	0.1416	0.1328
Na	0.2151	0.0704	0.0456	0.0330	0.0608	0.0424	0.0352	0.0712	0.9396	0.9823
K	0.0000	0.0000	0.0000	0.0000	0.0008	0.0000	0.0000	0.0000	0.0047	0.0016
Zr	0.0018	0.0000	0.0006	0.0000	0.0000				0.0155	0.0079
Na	21.5	7.0	4.4	3.2	6.1	4.0	3.3	7.0	88.3	90.4
Fe2+Mn	55.5	52.2	29.2	29.0	27.1	41.6	48.1	83.8	10.9	8.9
Mg	23.0	40.8	66.4	67.8	66.7	54.5	48.6	9.2	0.8	0.7
End members in mole% *zr/px=NAZAL+FM-NAZ										
Ac	19.0	0.0	0.0	0.0	0.0					
Di/Hed	72.8	85.5	81.8	85.7	79.4					
zr/px*	0.2	0.2	0.1	0.0	0.0					

Amphiboles

	AM4 SM1	AM4 SM1	54132 SM1	54132 SM1	54163 SM1	58007a SM1	58080 SM1	58080 SM1	63703 SM1	63760 SM1
SiO2	43.88	50.37	43.26	42.86	43.17	45.45	44.59	44.72	39.83	48.01
TiO2	2.08	0.22	2.71	3.06	2.41	1.53	1.65	1.85	3.46	0.63
Al2O3	7.59	1.27	7.00	5.93	7.89	6.63	4.67	4.09	10.48	2.36
FeO	20.04	20.88	21.19	28.03	23.71	20.58	29.10	29.24	22.86	33.17
MnO	0.83	1.10	0.94	1.31	1.16	1.20	2.05	1.53	0.63	1.22
MgO	7.95	8.41	8.25	3.02	6.69	8.53	2.22	3.00	5.51	0.72
CaO	10.24	3.66	11.27	7.41	9.22	9.38	3.66	5.32	11.28	1.72
Na2O	3.64	7.34	3.33	5.23	3.03	3.65	6.91	5.51	2.74	7.24
K2O	1.55	2.07	1.31	1.61	1.18	1.46	1.73	1.70	1.63	1.46
ZrO2	0.26	0.06	0.29	0.40	0.06	0.10	0.30	0.24	0.28	0.18
Total	98.06	95.40	99.35	98.86	98.54	98.53	96.88	97.20	98.69	96.70
Cations to 23 oxygens										
Si	6.7176	7.8980	6.5673	6.8318	6.6930	6.9457	7.2569	7.2413	6.2184	7.8342
Ti	0.2395	0.0259	0.3094	0.3668	0.2810	0.1761	0.2020	0.2253	0.4060	0.0770
Al	1.3704	0.2349	1.2533	1.1148	1.4430	1.1956	0.8964	0.7811	1.9291	0.4536
Fe	2.5658	2.7381	2.6904	3.7366	3.0749	2.6306	3.9608	3.9598	2.9852	4.5267
Mn	0.1076	0.1461	0.1209	0.1769	0.1521	0.1557	0.2826	0.2099	0.0835	0.1692
Mg	1.8139	1.9653	1.8665	0.7174	1.5461	1.9422	0.5385	0.7240	1.2821	0.1760
Ca	1.6797	0.6183	1.8820	1.2656	1.5324	1.5366	0.6383	0.9230	1.8866	0.3012
Na	1.0805	2.2316	0.9802	1.6165	0.9101	1.0812	2.1806	1.7300	0.8291	2.2897
K	0.3027	0.4141	0.2537	0.3274	0.2342	0.2845	0.3592	0.3512	0.3255	0.3030
Zr	0.0194	0.0046	0.0215	0.0311	0.0048	0.0075	0.0238	0.0190	0.0213	0.0140
Na ^x	0.348	1.392	0.178	0.885	0.371	0.472	1.372	0.960	0.137	1.706
Al ^y	0.877	0.459	0.671	0.987	0.950	0.664	1.144	0.685	1.009	1.268
Al ^z	1.347	0.231	1.270	1.118	1.349	1.091	0.863	0.778	1.861	0.352
Name	PA	RI	ED	ED	PA	ED	MY	RI	PA	ECK

Amphiboles

	63775 SM1	54138 SM3	54138 SM3	54141 SM1	54141 SM1	54142 SM2	58400 SM3	63721b SM3	63721c SM3	AM7 SM4
SiO2	48.35	41.90	50.94	42.79	50.52	42.63	42.45	50.13	43.06	52.94
TiO2	0.94	2.06	0.25	2.00	1.56	2.06	2.66	0.60	2.54	0.65
Al2O3	2.72	7.00	1.08	5.30	6.23	6.26	5.88	0.98	5.06	1.05
FeO	31.80	25.37	24.87	28.66	22.80	20.77	29.06	34.29	30.50	23.74
MnO	1.24	1.08	2.39	1.53	2.39	1.21	1.63	0.59	0.92	2.83
MgO	1.59	5.05	5.61	2.71	0.51	8.17	2.51	1.10	2.67	3.96
CaO	1.04	9.42	1.98	6.58	0.29	9.60	8.27	0.75	8.39	1.79
Na2O	8.29	3.56	8.24	5.26	9.41	3.44	3.93	7.06	3.89	9.39
K2O	1.40	1.44	1.96 ^a	1.66	1.58	1.54	1.42	1.31	1.35	1.38
ZrO2	0.36	0.15*	0.23 ^a	0.29	0.18		0.17	0.07	0.14	0.23
Total	97.73	97.03	97.55	96.78	95.47	95.68	97.98	96.89	98.52	97.96
Cations to 23 oxygens										
Si	7.7580	6.7163	7.9485	6.9918	7.9058	6.7803	6.8132	7.9642	6.9292	8.1722
Ti	0.1134	0.2483	0.0293	0.2458	0.1836	0.2464	0.3195	0.0698	0.3076	0.0755
Al	0.5154	1.3233	0.1987	1.0214	1.1498	1.1743	1.1141	0.1838	0.9609	0.1912
Fe	4.2673	3.4010	3.2454	3.9164	2.9840	2.7628	4.0348	4.5565	4.1054	3.0649
Mn	0.1692	0.1466	0.3159	0.2118	0.3168	0.1630	0.2216	0.0796	0.1255	0.3700
Mg	0.3809	1.2064	1.3046	0.6599	0.1189	1.9366	0.6009	0.2606	0.6403	0.9111
Ca	0.1791	1.6179	0.3310	1.1520	0.0486	1.6361	1.4226	0.1283	1.4474	0.2961
Na	2.5780	1.1065	2.4931	1.6665	2.8857	1.0609	1.2230	2.1739	1.2129	2.8106
K	0.2858	0.2945	0.3902	0.3460	0.3154	0.3125	0.2915	0.2705	0.2765	0.2718
Zr	0.0284	0.0088	0.0160	0.0231	0.0137		0.0131	0.0058	0.0108	0.0173
Na ^x	1.824	0.387	1.678	0.653	1.954	0.272	0.599	1.875	0.505	1.706
Al ^y	1.249	0.683	1.077	0.534	1.404	0.630	0.794	1.516	0.636	0.681
Al ^z	0.379	1.302	0.193	1.103	0.493	1.170	1.068	0.175	0.959	0.001
Name	ECK	ED	ECK	ED	ECK	ED	ED	ECK	ED	ECK

* includes 0.15 Ce2O3

^a includes 0.1 Ce2O3

Amphiboles

	AM7 SM4	AM7 SM4	AM7a SM4	AM7c SM4	AM7c SM4	AM7 SM4	AM45 SM4	AM68 SM4	AM68 SM4	AM68 SM4
SiO2	44.87	43.83	44.37	42.75	48.87	49.24	38.40	42.28	43.58	43.39
TiO2	2.07	1.78	1.92	1.57	0.73	0.93	1.07	1.43	1.92	1.85
Al2O3	5.20	5.64	6.11	5.01	2.88	2.08	9.75	6.24	6.23	5.07
FeO	26.94	20.46	22.08	29.20	27.53	25.27	30.15	21.01	20.76	31.35
MnO	1.59	1.18	1.21	1.63	2.74	2.77	1.39	1.52	0.84	1.53
MgO	3.81	8.62	7.14	2.20	2.11	3.52	0.96	7.78	7.12	0.69
CaO	7.10	9.55	9.21	6.35	1.33	1.59	9.98	8.88	9.59	1.63
Na2O	4.54	4.05	3.67	5.52	8.65	8.52	3.01	4.38	3.73	8.28
K2O	1.45	1.36	1.54	1.55	1.60	1.57	1.26	1.47	1.44	1.55
ZrO2	0.21	0.12	0.11	0.23	0.09	0.15	0.17	0.24	0.26	0.75
Total	97.79	96.58	97.37	96.01	96.52	95.63	96.14	95.23	95.47	96.09
Cations to 23 oxygens										
Si	7.4395	7.1842	7.2392	7.3275	8.1825	8.2419	6.3974	6.7938	6.9214	7.2020
Ti	0.2576	0.2197	0.2358	0.2031	0.0922	0.1169	0.1341	0.1728	0.2293	0.2309
Al	1.0167	1.0912	1.1759	1.0199	0.5691	0.4108	1.9157	1.1825	1.1669	0.9925
Fe	3.7361	2.8043	3.0123	4.2118	3.8543	3.5368	4.2008	2.8234	2.7575	4.3518
Mn	0.2234	0.1633	0.1676	0.2376	0.3884	0.3921	0.1962	0.2069	0.1130	0.2152
Mg	0.9419	2.1059	1.7372	0.5650	0.5270	0.8803	0.2384	1.8632	1.6853	0.1707
Ca	1.2620	1.6782	1.6104	1.1727	0.2379	0.2851	1.7815	1.5289	1.6320	0.2899
Na	1.4581	1.2860	1.1602	1.8470	2.8094	2.7611	0.9723	1.3647	1.1487	2.6648
K	0.3072	0.2840	0.3208	0.3402	0.3409	0.3348	0.2678	0.3014	0.2918	0.3282
Zr	0.0173	0.0093	0.0090	0.0192	0.0071	0.0120	0.0138	0.0188	0.0201	0.0607
Na ^x	0.805	0.316	0.461	0.885	1.782	1.736	0.226	0.402	0.392	1.717
Al ^y	0.909	0.421	0.571	0.789	1.217	1.040	0.782	0.524	0.655	1.511
Al ^z	0.951	1.045	1.081	0.968	0.519	0.379	1.630	1.179	1.149	0.961
Name	ED	ED	ED	ED	ECK	ECK	PA	ED	ED	MY

Amphiboles

	54241 SM4	54242 SM4	58039 SM4	58066 SM4	58066 SM4	59603 SM4	63729 SM4	63731 SM4	63754 SM4	AM55 SM5*
SiO2	41.14	41.04	40.20	48.12	43.16	39.53	40.94	38.97	45.31	42.82
TiO2	2.35	2.10	2.66	1.87	2.50	1.78	2.10	3.69	0.67	2.95
Al2O3	8.08	7.64	9.50	3.20	6.76	7.00	7.91	10.44	5.10	10.94
FeO	26.43	27.02	22.29	29.00	20.11	30.80	27.50	21.83	28.75	18.98
MnO	1.42	1.22	0.82	1.65	0.92	1.31	0.98	0.74	1.69	0.47
MgO	3.82	3.69	6.32	3.20	8.12	1.39	3.28	5.01	3.36	6.66
CaO	8.75	9.58	10.75	1.62	10.14	7.57	9.68	11.56	6.13	9.78
Na2O	3.90	3.58	3.55	8.17	3.69	4.81	3.36	2.80	5.35	3.77
K2O	1.63	1.45	1.19	1.57	1.54	1.71	1.64	1.60	1.51	1.50
ZrO2	0.17	0.00	0.05	0.09	0.14	0.28	0.25	0.24	0.25	0.27
Total	97.69	97.32	97.33	98.49	97.08	96.18	97.64	96.87	98.12	98.15
Cations to 23 oxygens										
Si	6.5952	6.6219	6.3446	7.5868	6.7392	6.6268	6.6000	6.1961	7.2322	6.5224
Ti	0.2833	0.2548	0.3157	0.2217	0.2936	0.2244	0.2546	0.4415	0.0804	0.3378
Al	1.5277	1.4539	1.7683	0.5950	1.2449	1.3840	1.5039	1.9569	0.9601	1.9656
Fe	3.5435	3.6462	2.9421	3.8239	2.6261	4.3182	3.7077	2.9027	3.8379	2.4181
Mn	0.1928	0.1667	0.1096	0.2204	0.1217	0.1860	0.1338	0.0996	0.2285	0.0612
Mg	0.9127	0.8873	1.4865	0.7519	1.8896	0.3473	0.7880	1.1871	0.7993	1.5127
Ca	1.5030	1.6563	1.8179	0.2737	1.6965	1.3598	1.6721	1.9689	1.0484	1.5960
Na	1.2123	1.1201	1.0864	2.4977	1.1172	1.5635	1.0503	0.8641	1.6558	1.1147
K	0.3334	0.2985	0.2396	0.3158	0.3068	0.3657	0.3371	0.3240	0.3075	0.2907
Zr	0.0133	0.0000	0.0038	0.0069	0.0107	0.0229	0.0197	0.0185	0.0195	0.0202
Na ^x	0.520	0.363	0.216	1.731	0.308		0.354	0.073	0.969	0.411
Al ^y	1.040	0.851	1.029	1.238	0.599		0.938	1.011	0.916	0.951
Al ^z	1.504	1.436	1.734	0.533	1.241		1.479	1.914	0.885	1.509
Name	PA	PA	PA	ECK	ED		PA	PA	RI	PA

Amphiboles

	58062 SM5*	AM38 SM5	AM39b SM5	AM43 SM5	AM43 SM5	AM77 SM5	AM82 SM5	AM85 SM5	AM88 SM5	AM110 SM5
SiO2	42.69	41.61	42.08	46.48	44.44	43.37	43.40	44.05	41.76	44.90
TiO2	4.14	3.83	2.53	1.38	2.41	2.33	2.32	2.45	2.50	2.09
Al2O3	9.25	8.80	9.02	3.12	6.72	4.22	7.30	5.88	8.40	4.85
FeO	14.85	15.15	20.83	29.66	20.59	29.78	22.72	27.84	21.86	25.83
MnO	0.51	0.55	0.65	1.50	0.86	1.25	0.76	1.35	1.37	1.36
MgO	10.73	9.18	8.72	2.61	8.36	2.88	7.04	3.48	6.64	4.99
CaO	11.44	12.12	10.26	2.63	9.71	6.94	9.12	7.44	9.43	6.78
Na2O	2.75	3.44	2.97	7.70	3.42	4.90	4.32	5.03	3.43	5.48
K2O	1.41	1.53	1.50	1.38	1.37	1.71	1.26	1.37	1.35	1.43
ZrO2	0.09	0.02	0.08	0.29	0.00	0.12			0.21	0.09
Total	97.86	96.23	98.64	96.75	97.88	97.50	98.24	98.89	96.95	97.80
Cations to 23 oxygens										
Si	6.4293	6.4367	6.4610	7.5302	6.8417	7.0564	6.2198	6.9621	6.5484	7.1077
Ti	0.4692	0.4456	0.2921	0.1681	0.2790	0.2851	0.2501	0.2912	0.2948	0.2488
Al	1.6425	1.6055	1.6334	0.5961	1.2202	0.8098	1.2339	1.0961	1.5535	0.9055
Fe	1.8701	1.9600	2.6748	4.0187	2.6511	4.0523	2.7231	3.6799	2.8668	3.4197
Mn	0.0656	0.0721	0.0845	0.2058	0.1122	0.1723	0.0923	0.1807	0.1820	0.1824
Mg	2.4078	2.1164	1.9954	0.6302	1.9181	0.6983	1.5036	0.8197	1.5517	1.1772
Ca	1.8459	2.0089	1.6880	0.4566	1.6018	1.2099	1.4005	1.2600	1.5844	1.1500
Na	0.8019	1.0318	0.8842	2.4189	1.0209	1.5459	1.2005	1.5415	1.0429	1.6821
K	0.2718	0.3020	0.2938	0.2852	0.2691	0.3550	0.2304	0.2762	0.2701	0.2888
Zr	0.0065	0.0015	0.0060	0.0229	0.0000	0.0095			0.0161	0.0069
Na ^x	0.161		0.252	1.553	0.402	0.606	0.501	0.750	0.427	0.865
Al ^y	0.834		0.898	1.258	0.710	0.771	0.909	0.819	1.069	0.655
Al ^z	1.595		1.575	0.580	1.176	0.806	1.320	1.087	1.501	0.873
Name	PA		PA	ECK	ED	ED	PA	ED	PA	ED

Amphiboles

	AM111 SM5	58017 SM5	58020 SM5	58025 SM5	AM114a HY	AM119 HY	AM121 HY	AM121 HY	AM121 HY	AM122 HY
SiO2	40.53	44.09	45.02	43.83	41.92	40.02	38.75	41.36	40.96	43.39
TiO2	2.79	3.92	0.88	2.53	2.57	2.18	3.20	1.77	1.85	1.40
Al2O3	9.01	7.72	3.64	7.53	7.25	7.73	10.30	8.47	7.96	6.01
FeO	26.78	13.49	24.75	17.28	28.92	30.52	26.99	30.26	30.27	30.24
MnO	1.47	0.36	1.14	0.79	1.18	1.15	0.93	1.09	1.12	1.15
MgO	2.75	11.15	6.48	10.19	2.52	1.36	2.63	1.56	1.83	1.11
CaO	9.39	11.68	6.31	8.34	7.85	9.46	10.11	8.11	8.99	7.95
Na2O	3.03	3.17	6.13	3.45	4.37	3.43	3.20	3.92	3.63	4.24
K2O	1.70	1.32	1.44	1.49	1.66	1.71	1.61	1.79	1.71	1.79
ZrO2	0.06			0.00	0.20	0.21	0.10	0.13	0.10	0.18
Total	97.51	96.89	95.78	95.43	98.43	97.79	97.81	98.46	98.41	97.45
Cations to 23 oxygens										
Si	6.5152	6.6560	7.2541	6.7965	6.7254	6.5607	6.2378	6.6676	6.6289	7.0588
Ti	0.3373	0.4449	0.1064	0.2950	0.3101	0.2689	0.3874	0.2140	0.2252	0.1709
Al	1.7082	1.3741	0.6920	1.3771	1.3711	1.4950	1.9558	1.6107	1.5193	1.1533
Fe	3.6003	1.7030	3.3354	2.2409	3.8803	4.1843	3.6333	4.0796	4.0971	4.1143
Mn	0.2002	0.0457	0.1551	0.1038	0.1598	0.1602	0.1262	0.1491	0.1529	0.1583
Mg	0.6588	2.5087	1.5562	2.3549	0.6025	0.3331	0.6309	0.3754	0.4409	0.2696
Ca	1.6174	1.8891	1.0888	1.3857	1.3496	1.6626	1.7431	1.3999	1.5589	1.3861
Na	0.9444	0.9273	1.9145	1.0373	1.3588	1.0898	1.0018	1.2241	1.1398	1.3374
K	0.3486	0.2540	0.2966	0.02948	0.3393	0.3587	0.3298	0.3685	0.3535	0.3723
Zr	0.0047				0.0156	0.0169	0.0082	0.0102	0.0081	0.0139
Na ^x	0.376	0.121		0.441	0.673	0.345	0.298	0.552	0.468	0.644
Al ^y	0.910	0.500		0.766	1.194	0.731	1.187	0.896	0.944	0.734
Al ^z	1.460	1.366		1.201	1.348	1.466	1.907	1.360	1.487	1.095
Name	PA	ED		ED	PA	PA	PA	PA	PA	ED

Amphiboles

	AM123b HY	AM140 SM6	AM159 SM6	AM159 SM6	58352 NM1	58352 NM1	58352 NM1
SiO2	40.30	52.94	47.87	47.24	38.96	38.91	38.88
TiO2	1.72	0.66	1.16	0.85	3.59	3.38	3.23
Al2O3	8.42	1.17	2.76	3.13	9.72	9.98	10.06
FeO	30.20	19.33	30.55	31.08	25.14	25.61	25.89
MnO	1.12	2.64	3.33	3.05	0.68	0.68	0.73
MgO	1.48	7.11	0.72	0.56	3.78	3.69	2.79
CaO	8.85	0.23	1.01	1.41	11.20	10.55	10.57
Na2O	3.35	9.97	8.01	8.38	2.25	2.23	2.74
K2O	1.68	2.27	1.76	1.53	1.61	1.83	1.66
ZrO2	0.24	0.00	0.23	0.50			
Total	97.35	96.32	97.40	97.74	96.94	96.85	96.55

Cations to 23 oxygens

Si	6.5965	7.7338	7.7527	7.8843	6.2672	6.3008	6.3027
Ti	0.2122	0.0728	0.1412	0.1050	0.4348	0.4114	0.3941
Al	1.6250	0.2013	0.5278	0.6030	1.8448	1.9057	1.9234
Fe	4.1338	2.3613	4.1378	4.2498	3.3824	3.4685	3.5092
Mn	0.1546	0.3134	0.4575	0.4223	0.0933	0.0931	0.0999
Mg	0.3604	1.4979	0.1740	0.1372	0.9059	0.8898	0.6747
Ca	1.5519	0.0383	0.1760	0.2465	1.9308	1.8297	1.8362
Na	1.0622	2.7083	2.5155	2.6511	0.7027	0.7002	0.8603
K	0.3501	0.4063	0.3638	0.3194	0.3296	0.3861	0.3427
Zr	0.0192	0.0000	0.0178	0.0397			

Na ^x	0.454				0.083	0.183	0.192
Al ^y	0.853				0.929	1.258	1.002
Al ^z	1.432				1.777	1.746	1.792

Name	PA				PA	PA	PA
------	----	--	--	--	----	----	----

Biotites

	AM149 Alk.gab	AM54 SM5*	58037 SM5*	58062 SM5*	AM39b SM5	58400 SM3	63746 SM4	AM121 HY	AM98 HY	AM119 HY
SiO2	35.51	35.31	36.30	35.82	34.95	36.30	35.58	36.18	34.05	35.49
TiO2	6.19	6.17	6.80	7.38	5.04	4.42	3.21	3.00	2.11	3.03
Al2O3	13.61	12.01	13.20	12.23	12.01	10.68	10.44	11.45	9.48	10.56
FeO	22.16	23.46	17.42	22.32	25.19	32.51	31.24	31.11	36.03	33.73
MnO	0.31	0.40	0.18	0.60	0.53	0.96	2.15	0.86	2.03	1.07
MgO	8.91	7.50	12.54	8.15	8.22	4.00	2.81	3.26	1.88	1.22
CaO	0.09	0.00	0.10	0.09	0.15	0.12	0.03	0.15	0.08	0.04
Na2O	0.47	0.46	0.51	0.32	0.56	0.29	0.16	0.20	0.22	0.14
K2O	8.80	8.87	8.92	8.96	7.97	8.12	8.91	9.29	8.39	8.99
ZrO2	0.01	0.00	0.00	0.00	0.00	0.00	0.00	0.00	0.00	0.00
Total	96.07	94.18	96.04	95.28	94.61	97.41	94.54	95.49	94.27	94.26
Cations to 22 oxygens										
Si	5.4761	5.6132	5.4690	5.5758	5.5612	5.7996	5.9090	5.8957	5.8355	5.9574
Ti	0.7176	0.7381	0.7707	0.8636	0.6028	0.5313	0.4011	0.3673	0.2723	0.3819
Al	2.4751	2.2510	2.3602	2.2455	2.2530	2.0125	2.0449	2.2015	1.9164	2.0915
Fe	2.8582	3.1190	2.1954	2.9065	3.3526	4.3436	4.3387	4.2396	5.1643	4.7349
Mn	0.0405	0.0540	0.0224	0.0807	0.0712	0.1301	0.3031	0.1187	0.2954	0.1519
Mg	2.0486	1.7766	2.8162	1.8193	1.9498	0.9526	0.6953	0.7910	0.4811	0.3059
Ca	0.0153	0.0000	0.0157	0.0153	1.0256	0.0201	0.0057	0.0254	0.0149	0.0066
Na	0.1418	0.1432	0.1480	0.0980	0.1681	0.0902	0.0501	0.0623	0.0730	0.0451
K	1.7308	1.7993	1.7138	1.7799	1.6181	1.6557	1.8882	1.9319	1.8350	1.9248
Zr	0.0006	0.0000	0.0000	0.0000	0.0000	0.0000	0.0000	0.0000	0.0000	0.0000
Fe/(Fe+Mg)	0.582	0.637	0.438	0.606	0.632	0.820	0.862	0.843	0.915	0.939
(Ti+Al) ^{iv}	2.524	2.387	2.531	2.424	2.439	2.200	2.091	2.104	2.165	2.043
Al/(Al+Si)	0.311	0.286	0.311	0.287	0.288	0.258	0.257	0.272	0.247	0.260

Feldspars

	AM6a SM1	58007a SM1	63760 SM1*	63760 SM1*	63760 SM1	63775 SM1	63775 SM1*	54139 SM2	54139 SM2	54139 SM2
SiO2	67.80	66.63	69.52	65.28	68.82	65.79	69.16	64.98	67.53	67.14
Al2O3	18.67	19.06	18.96	18.41	18.54	18.22	19.04	18.60	19.05	19.11
FeO ^a	0.12	0.05	0.00	0.04	0.14	0.86	0.62	0.34		
CaO	0.00	0.17	0.00	0.01	0.02	0.49	0.08	0.12	0.00	0.00
Na2O	7.80	6.84	10.75	0.18	7.25	5.24	10.55	5.76	5.97	5.75
K2O	5.95	7.92	0.22	15.85	5.56	9.17	0.15	9.18	8.10	8.14
Total	100.34	100.67	99.45	99.77	100.33	99.77	99.59	98.98	100.65	100.14

Cations to 32 oxygens

Si	12.047	11.917	12.147	12.041	12.154	11.959	12.099	12.014	12.025	12.012
Al	3.913	4.020	3.906	4.005	3.862	3.906	3.929	3.987	4.000	4.033
Fe	0.017	0.006	0.000	0.005	0.020	0.129	0.090	0.051		
Ca	0.000	0.032	0.000	0.003	0.004	0.095	0.014	0.026	0.000	0.000
Na	2.688	2.372	3.642	0.064	2.481	1.849	3.578	2.064	2.060	1.996
K	1.349	1.807	0.050	3.730	1.252	2.126	0.033	2.166	1.839	1.857
Na	66.6	56.3	98.7	1.7	66.4	45.4	98.8	48.5	52.8	51.8
Ca	0.0	0.8	0.0	0.0	0.1	2.3	0.4	0.6	0.0	0.0
K	33.4	42.9	1.3	98.3	33.5	52.2	0.8	50.9	47.2	48.2

* spot analysis

^a includes up to 0.1 wt% TiO2

Feldspars

	54139 SM2	54139 SM2	54139 SM2	54139 SM2	54142 SM2*	54142 SM2*	54142 SM2	54181 SM2	54138 SM3	54138 SM3
SiO2	67.59	66.45	67.55	66.48	69.48	65.74	66.14	66.54	67.83	67.32
Al2O3	18.69	18.25	18.96	18.57	19.47	18.53	18.41	19.22	18.54	18.89
FeO									0.00	0.06
CaO	0.00	0.00	0.00	0.00	0.00	0.00	0.00	0.00	0.00	0.06
Na2O	4.68	4.17	5.62	5.04	11.40	1.46	3.28	5.35	7.24	7.18
K2O	9.87	10.87	8.33	9.27	0.75	14.42	12.45	9.03	6.04	6.75
Total	100.83	99.74	100.46	99.35	100.10	100.15	100.27	100.15	99.65	100.25

Cations to 32 oxygens

Si	11.945	12.071	12.049	12.046	12.029	12.029	12.028	11.960	12.164	12.005
Al	3.895	3.910	3.988	3.968	3.974	3.999	3.948	4.075	3.910	3.974
Fe									0.000	0.009
Ca	0.000	0.000	0.000	0.000	0.000	0.000	0.000	0.000	0.000	0.012
Na	1.605	1.468	1.943	1.770	3.826	0.516	1.156	1.865	2.516	2.481
K	2.225	2.518	1.897	2.142	0.164	3.368	2.888	2.072	1.382	1.536
Na	41.9	36.8	50.6	45.2	95.9	13.3	28.6	47.4	64.5	61.6
Ca	0.0	0.0	0.0	0.0	0.0	0.0	0.0	0.0	0.0	0.3
K	48.1	63.2	49.4	44.8	4.1	86.7	71.4	52.6	35.5	38.1

* spot analysis

Feldspars

	54157 SM3	58400 SM3	63721b SM3	AM7 SM4m	AM7 SM4c	AM7 SM4	AM7 SM4*	AM48 SM4	AM49 SM4	AM49 SM4
SiO2	64.30	67.07	66.57	66.62	65.30	66.77	65.06	64.48	65.67	65.93
TiO2	0.00	0.01	0.00	0.00	0.00	0.00	0.00	0.00	0.00	0.00
Al2O3	18.69	18.98	19.41	19.39	18.98	18.60	17.64	19.00	18.63	18.76
FeO	0.00	0.33	0.68	0.08	0.01			0.04	0.08	0.18
CaO	0.00	0.02	0.00	0.11	0.28	0.00	0.00	0.00	0.01	0.00
Na2O	3.18	7.13	6.83	4.60	5.50	4.16	5.97	2.68	5.70	6.14
K2O	12.63	6.76	7.58	10.14	9.04	9.93	7.40	12.31	8.66	8.31
Total	98.81	100.30	101.08	100.94	99.12	99.47	96.07*	98.50	98.76	99.31

Cations to 32 oxygens

Si	12.046	11.965	11.867	11.889	11.900	12.084	12.116	11.923	11.978	11.957
Ti	0.000	0.001	0.000	0.000	0.000	0.000	0.000	0.000	0.000	0.000
Al	4.090	3.993	4.080	4.082	4.079	3.971	3.874	4.143	4.009	4.013
Fe	0.000	0.044	0.101	0.013	0.002			0.006	0.012	0.027
Ca	0.000	0.004	0.000	0.021	0.056	0.000	0.000	0.000	0.003	0.000
Na	1.144	2.466	2.360	1.590	1.942	1.460	2.157	0.961	2.017	2.158
K	2.989	1.539	1.725	2.309	2.103	2.293	1.757	2.904	2.015	1.923
Na	27.7	61.5	57.8	40.7	47.4	38.9	55.1	24.9	50.0	52.9
Ca	0.0	0.1	0.0	0.0	1.4	0.0	0.0	0.0	0.1	0.0
K	72.3	38.4	42.2	59.3	51.3	61.1	44.9	75.1	49.9	47.1

m = margin phenocryst c = core

*altered

Feldspars

	58066 SM4	59603 SM4	63725 SM4	AM39b SM5	AM40 SM5	AM40 SM5	AM43 SM5	AM77 SM5	AM82 SM5	AM84 SM5*
SiO2	65.92	66.38	64.67	65.96	65.64	66.69	66.22	67.70	66.27	69.31
TiO2	0.00	0.00	0.00	0.00	0.03	0.03	0.00	0.00	0.00	0.00
Al2O3	19.00	18.95	19.38	19.46	19.55	19.84	18.46	18.44	18.65	19.44
FeO	0.00	0.02	0.10	0.13	0.01	0.01	0.06	0.00		0.48
CaO	0.00	0.00	0.00	0.11	0.67	0.80	0.01	0.14	0.08	0.00
Na2O	4.83	5.42	4.64	6.58	6.28	8.13	7.51	5.98	6.17	11.47
K2O	9.78	9.16	9.79	7.22	7.09	4.50	6.19	8.63	8.15	0.18
Total	99.53	99.93	98.59	99.47	99.27	100.03	98.46	100.89	99.32	100.95

Cations to 32 oxygens

Si	11.903	11.974	11.863	11.887	11.858	11.846	12.013	12.031	11.992	11.971
Ti	0.000	0.000	0.000	0.000	0.004	0.004	0.000	0.000	0.000	0.000
Al	4.046	4.032	4.191	4.136	4.165	4.156	3.950	3.916	3.983	3.959
Fe	0.000	0.003	0.016	0.019	0.002	0.002	0.010	0.000		0.066
Ca	0.000	0.000	0.000	0.022	0.131	0.153	0.002	0.027	0.016	0.000
Na	1.694	1.896	1.650	2.299	2.198	2.801	2.643	2.088	2.167	3.841
K	2.253	2.106	2.292	1.661	1.633	1.021	1.434	1.969	1.882	0.039
Na	42.9	47.4	41.9	57.7	55.5	70.5	64.8	50.9	53.3	99.0
Ca	0.0	0.0	0.0	0.6	3.3	3.9	0.1	0.6	0.4	0.0
K	57.1	52.6	58.1	41.7	41.2	25.7	35.1	48.4	46.3	1.0

* spot analysis

Feldspars

	AM85 SM5	AM110 SM5	58025 SM5	AM29 SM5*	AM29 SM5*	AM54 SM5*	AM55 SM5*	58037 SM5*(1)	58037 SM5*(2)	58037 SM5*(3)
SiO2	66.91	66.14	67.21	64.96	64.91	66.75	64.84	65.03	62.84	62.11
TiO2	0.00	0.00	0.00	0.00	0.00	0.00	0.00	0.15	0.06	0.03
Al2O3	19.00	18.83	18.47	20.02	19.77	19.41	20.90	19.69	23.64	23.03
FeO	0.08	0.07		0.00	0.00	0.09	0.00	0.11	0.11	0.18
CaO	0.00	0.00	0.21	1.09	1.03	0.63	2.19	1.41	5.52	4.97
Na2O	5.20	5.34	5.72	5.41	4.15	5.38	7.55	4.78	7.68	7.49
K2O	8.62	9.10	9.29	7.36	9.22	8.19	3.10	8.29	0.51	1.67
Total	99.82	99.48	100.90	98.83	99.08	100.45	98.59	99.44	100.36	99.49

Cations to 32 oxygens

Si	12.025	11.982	12.028	11.782	11.815	11.931	11.637	11.782	11.087	11.116
Ti	0.000	0.000	0.000	0.000	0.000	0.000	0.000	0.020	0.008	0.004
Al	4.028	4.023	3.899	4.282	4.245	4.092	4.424	4.207	4.919	4.860
Fe	0.012	0.011		0.000	0.000	0.013	0.000	0.016	0.016	0.027
Ca	0.000	0.000	0.041	0.212	0.201	0.122	0.424	0.274	1.044	0.953
Na	1.812	1.878	1.984	1.902	1.463	1.863	2.627	1.678	2.628	2.599
K	1.978	2.104	2.122	1.702	2.141	1.867	0.710	1.916	0.116	0.382
Na	47.7	47.2	47.8	49.8	38.4	48.4	69.9	43.38	69.4	66.1
Ca	0.3	0.0	1.0	5.6	5.3	3.1	11.2	7.09	27.5	24.2
K	52.0	52.8	51.2	44.6	56.3	48.5	18.9	49.54	3.1	9.7

(1) mantle of alkali feldspar to core of plagioclase (2). (3) plagioclase core.

Feldspars

	58062 SM5*	AM149 Alk.Gab ^a	AM98 HY	AM98 HY	AM116 HY	AM118 HY	AM119 HY(x)	AM119 HY(g)	AM121 HY	AM122 HY(g)
SiO2	66.54	53.30	66.95	65.83	66.01	66.23	66.45	65.74	66.35	65.27
TiO2	0.01	0.09	0.00	0.00	0.00	0.00	0.00	0.00	0.00	0.00
Al2O3	19.25	29.16	18.44	18.40	18.68	18.65	18.67	18.42	18.71	18.63
FeO	0.10	0.63	0.21	0.08			0.00		0.00	0.29
CaO	0.85	11.44	0.13	0.10	0.03	0.00	0.07	0.07	0.08	0.04
Na2O	7.41	4.66	9.14	4.76	5.30	3.33	6.71	3.23	3.55	2.27
K2O	4.87	0.51	3.19	10.01	9.22	12.13	6.97	12.32	11.73	13.53
Total	99.03	99.80	98.05	99.18	99.24	100.34	98.87	99.78	100.43	100.03
Si	11.933	9.688	12.054	12.011	11.994	12.013	12.016	12.012	12.008	11.962
Ti	0.001	0.013	0.000	0.000	0.000	0.000	0.000	0.000	0.000	0.000
Al	4.072	6.252	3.916	3.959	4.003	3.989	3.981	3.970	3.993	4.026
Fe	0.015	0.111	0.031	0.013			0.000		0.000	0.045
Ca	0.164	2.228	0.025	0.020	0.005	0.000	0.014	0.014	0.015	0.008
Na	2.578	1.644	3.191	1.684	1.868	1.172	2.354	1.143	1.247	0.807
K	1.114	0.119	0.732	2.331	2.137	2.806	1.609	2.873	2.709	3.163
Na	66.9	41.2	80.8	41.7	46.6	29.5	59.2	28.4	31.4	20.3
Ca	4.3	55.8	0.6	0.5	0.1	0.0	0.3	0.4	0.4	0.2
K	28.8	3.0	18.6	57.8	53.3	70.5	40.5	71.2	68.2	79.5

^aplagioclase xenocryst (6cm long)

(x)xenocryst

(g)groundmass lath

Feldspars

	AM122 HY(g)	AM122 HY	AM123b HY	AM135 HY(x)	46261 SM6	AM138 SM6	58027 lava
SiO2	65.55	66.46	67.39	67.11	66.86	64.79	64.97
TiO2	0.01	0.00	0.00	0.00	0.00	0.02	0.04
Al2O3	18.19	18.58	18.23	18.66	19.68	18.23	18.84
FeO	0.39	0.06	0.02	0.00	0.42	0.53	0.08
CaO	0.12	0.07	0.02	0.03	0.31	0.00	0.67
Na2O	1.15	4.91	4.44	4.54	11.13	0.48	4.74
K2O	15.03	10.05	10.42	9.63	0.11	15.87	9.44
Total	100.45	100.13	100.51	99.97	99.58	99.95	98.78

Cations to 32 oxygens

Si	12.023	12.009	12.114	12.077	11.997	12.033	11.898
Ti	0.001	0.000	0.000	0.000	0.000	0.003	0.005
Al	3.936	3.960	3.866	3.961	4.104	3.994	4.069
Fe	0.059	0.010	0.003	0.000	0.063	0.079	0.013
Ca	0.024	0.013	0.003	0.006	0.058	0.000	0.132
Na	0.411	1.720	1.546	1.584	3.815	0.173	1.682
K	3.518	2.317	2.390	2.211	0.025	3.761	2.207
Na	10.4	42.5	39.3	41.7	97.9	4.2	41.8
Ca	0.6	0.3	0.1	0.2	1.5	0.0	3.3
K	89.0	57.2	60.6	58.1	0.6	95.8	54.9

(g) groundmass lath

(x) xenocryst

Nephelines

	AM6a SM1	54132 SM1	54163 SM1	58007a SM1	54138 SM3	54157 SM3	54139 SM2	54139 SM2	54142 SM2(c)	54142 SM2(r)
SiO2	45.66	46.13	46.03	44.72	45.64	44.62	46.81	46.16	44.11	44.08
TiO2	0.00	0.00	0.00	0.05	0.02	0.00	0.02	0.00	0.00	0.00
Al2O3	33.25	32.38	32.59	33.60	33.88	32.56	31.91	32.37	32.30	32.26
FeO	0.49	0.41	0.50	0.22	0.17		0.76	0.94	0.66	1.03
CaO	0.00	0.06	0.00	0.00	0.06	0.00	0.00	0.00	0.00	0.00
Na2O	16.30	15.30	16.03	15.73	16.25	16.98	15.76	15.33	15.42	16.06
K2O	5.32	5.13	5.33	5.44	4.98	5.22	4.94	5.18	5.29	5.38
Total	101.03	99.39	100.48	99.76	101.01	99.44	100.19	99.98	97.78	98.81

Cations to 32 oxygens

Si	8.671	8.784	8.712	8.525	8.571	8.564	8.848	8.761	8.591	8.541
Ti	0.000	0.000	0.000	0.007	0.003	0.000	0.003	0.000	0.000	0.000
Al	7.393	7.272	7.275	7.555	7.505	7.379	7.113	7.245	7.421	7.373
Fe	0.078	0.065	0.079	0.035	0.026		0.121	0.126	0.115	0.176
Ca	0.000	0.012	0.000	0.000	0.013	0.000	0.000	0.000	0.000	0.000
Na	5.956	5.648	5.881	5.813	5.918	6.327	5.775	5.643	5.825	6.034
K	1.280	1.245	1.288	1.322	1.193	1.280	1.191	1.255	1.314	1.331
Qz	7.3	10.2	8.2	7.4	7.8	4.9	10.0	10.0	7.8	6.2
Ne	74.8	72.1	73.8	73.9	75.3	77.6	73.1	72.1	73.7	75.3
Ks	17.9	17.7	18.0	18.7	16.9	17.5	16.9	17.9	18.5	18.5

(c)core and (r)rim

Nephelines

	54142 SM2	54142 - SM2(c)	54142 SM2(r)	54142 - SM2(c)	54142 SM2(r)	AM7 SM4	AM48 - SM4(c)	AM48 SM4(r)	AM49 SM4	AM68 SM4
SiO2	44.48	44.17	44.75	46.36	44.45	45.60	45.79	45.38	43.93	45.43
TiO2	0.00	0.00	0.00	0.00	0.00	0.00	0.00	0.00	0.00	0.00
Al2O3	33.14	32.48	32.47	32.34	32.20	32.29	32.45	32.33	32.74	32.28
FeO	0.71	0.67	0.80	0.88	0.66		0.43	0.58	0.70	0.50
CaO	0.00	0.00	0.00	0.06	0.06	0.00	0.00	0.00	0.00	0.00
Na2O	15.94	16.73	16.64	16.01	16.16	16.60	15.37	16.15	15.83	15.65
K2O	5.54	5.44	5.36	5.14	5.44	5.01	5.37	5.03	5.35	5.45
Total	99.80	99.49	100.01	100.79	98.97	99.50	99.41	99.48	98.55	99.32

Cations to 32 oxygens

Si	8.513	8.510	8.566	8.749	8.589	8.706	8.739	8.680	8.513	8.703
Ti	0.000	0.000	0.000	0.000	0.000	0.000	0.000	0.000	0.000	0.000
Al	7.480	7.379	7.331	7.196	7.337	7.270	7.304	7.293	7.483	7.293
Fe	0.120	0.110	0.128	0.126	0.107		0.068	0.092	0.114	0.080
Ca	0.000	0.000	0.000	0.011	0.011	0.000	0.000	0.000	0.000	0.000
Na	5.916	6.248	6.176	5.859	6.056	6.147	5.687	5.991	5.948	5.814
K	1.353	1.338	1.308	1.238	1.341	1.219	1.307	1.228	1.323	1.333
Qz	6.6	4.8	5.6	8.8	6.3	7.0	9.3	7.7	6.6	8.3
Ne	74.4	76.9	76.3	73.8	75.2	76.2	72.2	75.2	74.9	73.1
Ks	19.0	18.3	18.1	17.4	18.5	16.8	18.5	17.1	18.5	18.6

(c)core and (r)rim

Nephelines

	54241 SM4	54241 SM4	54242 SM4	58039 SM4	58066 SM4	59603 SM4	63725 SM4	63746 SM4	AM55 SM5*	AM38 SM5
SiO2	44.96	45.26	47.04	44.54	46.00	44.62	43.49	45.31	46.16	47.90
TiO2	0.00	0.00	0.00	0.00	0.00	0.00	0.00	0.00	0.00	0.00
Al2O3	31.72	33.26	32.17	33.67	31.97	33.28	33.04	32.07	32.73	32.95
FeO	0.51	0.45	0.00	0.46	0.35	0.20	0.59	0.38		0.43
CaO	0.01	0.04	0.00	0.00	0.00	0.00	0.00	0.00	0.71	0.66
Na2O	16.35	16.03	16.05	17.15	16.17	15.64	16.53	16.49	15.68	15.77
K2O	5.40	5.81	5.26	4.22	4.92	5.76	5.63	4.71	4.57	2.83
Total	98.94	100.84	100.51	100.04	99.42	99.48	99.29	98.97	99.84	100.54

Cations to 32 oxygens

Si	8.680	8.569	8.860	8.467	8.780	8.545	8.407	8.699	8.735	8.899
Ti	0.000	0.000	0.000	0.000	0.000	0.000	0.000	0.000	0.000	0.000
Al	7.221	7.426	7.146	7.547	7.195	7.516	7.532	7.263	7.306	7.220
Fe	0.082	0.071	0.000	0.074	0.056	0.031	0.096	0.061		0.066
Ca	0.002	0.008	0.000	0.000	0.000	0.000	0.000	0.000	0.143	0.132
Na	6.119	5.883	5.861	6.320	5.984	5.806	6.197	6.139	5.755	5.680
K	1.329	1.404	1.263	1.024	1.198	1.406	1.399	1.154	1.103	0.670
Qz	6.4	6.7	9.2	5.9	8.4	7.1	4.3	7.4	8.5	12.6
Ne	75.4	73.7	73.3	79.7	74.9	73.2	76.6	76.6	72.5	74.2
Ks	18.2	19.6	17.6	14.4	16.7	19.7	19.1	16.0	15.5	9.8
								An	3.5	3.4

Nephelines

	AM38 SM5	AM43 SM5	AM77 SM5	AM77 SM5	AM81 SM5	AM82 SM5	AM82 SM5	AM82 SM5	AM84 SM5	AM111 SM5
SiO2	47.14	44.82	44.29	45.93	45.52	46.50	46.18	45.37	45.78	46.46
Al2O3	32.46	33.66	33.04	32.15	32.48	32.80	32.26	32.33	32.56	32.27
FeO	0.38	0.34	0.33	0.00	0.60	0.81	0.00	0.00	0.70	0.27
CaO	0.59	0.00	0.00	0.01	0.00	0.00	0.03	0.06	0.00	0.01
Na2O	15.30	15.21	16.59	16.22	15.94	15.42	16.37	16.56	16.71	15.73
K2O	3.90	5.59	5.28	5.46	4.86	4.86	5.19	5.28	5.23	5.76
Total	99.77	99.63	99.53	99.77	99.40	100.38	100.03	99.60	100.98	100.49

Cations to 32 oxygens

Si	8.874	8.548	8.499	8.752	8.693	8.767	8.763	8.672	8.648	8.788
Al	7.208	7.572	7.477	7.223	7.312	7.293	7.220	7.288	7.254	7.199
Fe	0.060	0.055	0.053	0.000	0.096	0.127	0.000	0.000	0.110	0.042
Ca	0.119	0.001	0.000	0.002	0.000	0.000	0.006	0.012	0.000	0.003
Na	5.584	5.624	6.174	5.993	5.902	5.637	6.022	6.138	6.122	5.769
K	0.937	1.360	1.293	1.327	1.832	1.169	1.257	1.286	1.261	1.389
Qz	11.5	8.5	5.4	7.7	8.6	10.7	7.8	6.5	6.6	8.5
Ne	72.0	72.1	76.7	76.5	74.7	72.6	74.9	75.8	76.0	72.1
Ks	13.6	19.4	17.9	15.8	16.7	16.7	17.3	17.7	17.4	19.3
(An)	2.9									

Nephelines

	58017 SM5	AM98 HY(1)	AM114 HY	AM116 HY	AM118 HY	AM119 HY(c)	- AM119 HY(r)	AM121 HY	AM122 HY	AM122 HY
SiO2	47.29	44.58	45.17	44.77	45.71	44.84	44.94	44.73	45.40	45.85
Al2O3	31.98	31.53	32.85	32.51	32.82	32.22	31.21	33.68	31.70	32.15
FeO	0.34	0.74	0.25			0.47	0.64		0.50	0.40
CaO	0.05	0.00	0.01	0.00	0.04	0.04	0.01	0.59	0.10	0.02
Na2O	17.19	15.45	16.24	16.27	16.01	15.92	16.21	14.67	15.83	16.63
K2O	5.02	5.36	5.93	5.56	5.54	5.64	5.05	5.26	5.46	5.13
Total	100.88	97.65	100.46	99.11	100.12	99.13	98.07	98.93	98.99	100.17

Cations to 32 oxygens

Si	8.831	8.701	8.593	8.611	8.676	8.634	8.738	8.557	8.739	8.717
Al	7.042	7.257	7.371	7.375	7.349	7.318	7.157	7.600	7.198	7.208
Fe	0.054	0.012	0.040			0.075	0.103		0.080	0.063
Ca	0.010	0.000	0.003	0.000	0.007	0.009	0.003	0.122	0.020	0.004
Na	5.862	5.848	5.991	6.067	5.892	5.944	6.112	5.445	5.910	6.129
K	1.196	1.335	1.440	1.365	1.342	1.385	1.253	1.283	1.341	1.243
Qz	7.3	8.1	6.1	6.2	7.6	6.8	7.2	10.1	7.8	7.0
Ne	76.4	73.3	74.1	75.0	73.7	74.0	75.6	71.2	73.6	75.9
Ks	16.3	18.6	19.8	18.8	18.7	19.2	17.2	18.7	18.6	17.0

Nephelines

	AM122 HY(c)	- AM122 HY(r)	AM123b HY	AM123b HY	AM123b HY	AM135 HY	AM138 SM6	AM138 SM6	AM138 SM6	AM138 SM6
SiO2	45.37	44.67	46.01	46.15	45.29	45.71	43.12	44.85	44.70	44.14
Al2O3	32.53	32.67	32.50	32.15	32.06	33.29	32.92	31.50	31.85	32.18
FeO	0.32	0.14	0.42	0.39	0.26	0.00	0.45	0.72	0.60	0.61
CaO	0.03	0.00	0.00	0.01	0.00	0.27	0.00	0.00	0.00	0.00
Na2O	16.02	15.81	15.79	15.69	16.17	15.53	16.03	16.07	16.08	15.87
K2O	5.57	6.18	5.22	5.87	5.51	5.42	6.96	6.71	7.02	7.10
Total	99.83	99.47	99.94	100.25	99.30	100.21	99.48	99.85	100.25	99.90

Cations to 32 oxygens

Si	8.654	8.585	8.737	8.766	8.694	8.649	8.367	8.645	8.594	8.523
Al	7.317	7.403	7.280	7.202	7.258	7.429	7.532	7.160	7.222	7.322
Fe	0.051	0.023	0.067	0.063	0.042	0.000	0.073	0.116	0.095	0.100
Ca	0.007	0.000	0.000	0.001	0.000	0.055	0.000	0.000	0.000	0.000
Na	5.924	5.890	5.814	5.779	6.018	5.697	6.031	6.005	5.995	5.971
K	1.355	1.515	1.265	1.422	1.350	1.308	1.722	1.651	1.721	1.752
Qz	7.2	6.2	8.8	8.2	6.9	8.8	3.2	5.0	4.5	4.1
Ne	73.9	72.9	73.4	72.0	74.5	72.6	73.4	72.7	72.4	72.3
Ks	18.9	20.9	17.8	19.8	18.6	18.6	23.4	22.2	23.1	23.6

(c)core and (r)rim

Nephelines

	AM159	58027
	SM6	lava
SiO2	46.00	45.83
Al2O3	31.49	32.23
FeO		0.24
CaO	0.00	0.06
Na2O	16.07	16.80
K2O	5.88	5.23
Total	99.44	100.40

Cations to 32 oxygens

Si	8.812	8.700
Al	7.116	7.215
Fe		0.038
Ca	0.001	0.013
Na	5.969	6.184
K	1.437	1.268
Qz	7.3	6.4
Ne	73.1	76.3
Ks	19.6	17.3

Aenigmatites

	AM7 SM4	58066 SM4	AM43 SM5	AM82 SM5
SiO ₂	38.19	39.06	36.52	38.34
TiO ₂	8.50	7.00	8.49	8.37
Al ₂ O ₃	1.59	1.63	3.26	2.56
FeO	40.51	40.12	40.50	40.24
MnO	2.72	2.35	1.75	1.93
MgO	0.46	0.39	0.49	0.82
CaO	0.49	0.85	2.29	1.42
Na ₂ O	7.07	6.61	6.20	6.35
K ₂ O	0.02	0.03	0.04	0.02
Total	99.55	98.05	99.55	100.05

Cations to 20 oxygens. Fe³/Fe² assuming stoichiometry

Si	5.6255	5.7864	5.3645	5.5562
Al	0.2751	0.2856	0.5656	0.4371
Fe ³	0.0998	0.0000	0.0699	0.0067
Fe ²	4.8923	4.9707	4.9117	4.8722
Ti	0.9414	0.7799	0.9380	0.2375
Mn	0.3399	0.2954	0.2177	0.1776
Ca	0.0000	0.0000	0.1850	0.0000
Ca	0.0774	0.1347	0.1751	0.2208
Na	2.0056	1.8992	1.7653	1.7839
K	0.0039	0.0060	0.0079	0.0032

REFERENCES

- Abbott, M.J., 1969: Petrology of the Nandewar volcano, N.S.W. Australia. *Contrib. Mineral. Petrol.* 20, 115-134.
- Anderson, E.M., 1942: The dynamics of faulting and dyke formation with applications to Britain. Edinburgh: Oliver and Boyd.
- Anderson, J.G., 1974: The geology of Alàngorssuaq, Northern Nunarssuit complex, South Greenland. Unpubl. PhD. Thesis, University of Aberdeen.
- Bachinski, S.W. and Muller, G., 1971: Experimental determinations of the microcline-low albite solvus. *J. Petrol.* 12, 329-356.
- Bailey, D.K., 1970: Volatile flux, heat focussing and the generation of magma. *Geol. J. Spec. Iss.* 2, 177-186.
- Bailey, D.K., 1974: Origin of alkaline magmas as a result of anatexis-crustal anatexis. In Sørensen, H. (ed), The Alkaline Rocks. 436-442. London: John Wiley and Sons.
- Bailey, D.K. and Schairer, J.F., 1966: The system $\text{Na}_2\text{O}-\text{Al}_2\text{O}_3-\text{Fe}_2\text{O}_3-\text{SiO}_2$ at 1 atmosphere, and the petrogenesis of alkaline rocks. *J. Petrol.* 7, 114-170.
- Barth, T.F.W., 1954: Studies on the igneous rock complex of the Oslo region 14: Provenance of the Oslo magmas. *Norske Vidensk. Akad. Oslo. Mat.-Naturv.* 4, 19pp
- Beaman, D.A. and Igasi, J.A., 1970: Electron probe micro-analysis techniques. *Anal. Chem.* 42, 1540-1557.
- Beddoe-Stephens, B., 1977: The petrology and geochemistry of the Rossland Volcanic Rocks, Southern British Columbia. Unpubl. PhD. Thesis, University of Durham,
- Berthelsen, A. and Noe-Nygaard, A., 1965: The Precambrian of Greenland. In Rankama, K. (ed), The Precambrian. 113-262. New York: Wiley.
- Blaxland, A.B., 1977: Agpaitic magmatism at Norra Kärr? Rb-Sr isotopic evidence. *Lithos* 10, 1-9.

- Blaxland, A.B., van Breeman O. and Steenfelt, A., 1976: Age and origin of agpaitic magmatism at Ilímaussaq, South Greenland: Rb-Sr study. *Lithos* 9, 31-38.
- Blaxland, A.B., van Breeman O., Emeleus, C.H. and Anderson, J.G., 1978: Age and origin of the major syenite centres in the Gardar province of South Greenland: Rb-Sr studies. *Bull. Geol. Soc. Am.* 89, 231-244.
- Blundell, D.J., 1978: A gravity survey across the Gardar Igneous Province, S.W. Greenland. *Quart. J. geol. Soc. Lond.* 135, 545-554.
- Bottinga, Y.A. and Weill, D.F., 1970: Densities of liquid silicate systems calculated from partial molar volumes of oxide components. *Am. J. Sci.* 269, 169-182.
- Bottinga, Y.A. and Weill, D.F., 1972: The viscosity of magmatic silicate liquids: A model for calculation. *Am. J. Sci.* 272, 438-475.
- Bowen, N.L. and Tuttle, O.F., 1950: The system $\text{NaAlSi}_3\text{O}_8$ - KAlSi_3O_8 - H_2O . *J. Geol.* 58, 489-511.
- Bridgwater, D., 1967: Feldspathic inclusions in the Gardar igneous rocks of south Greenland and their relevance to the formation of major anorthosites in the Canadian Shield. *Can. J. Earth. Sci.* 4, 995-1014.
- Bridgwater, D. and Harry, W.T., 1968: Anorthosite xenoliths and plagioclase megacrysts in Precambrian intrusions of South Greenland. *Meddr. Grønland* 185 (2), 1-66.
- Brown, G.M. and Vincent, E.A., 1963: Pyroxenes from the late stages of fractionation of the Skaergaard Intrusion, East Greenland. *J. Petrol.* 4, 175-197.
- Brown, P.E., 1973: A layered plutonic complex of alkali basalt parentage: the Lilloise Intrusion, east Greenland. *Quart. J. geol. Soc. Lond.* 129, 405-418.
- Brown, P.E., Brown, R.D., Chambers, A.D. and Soper, N.J., 1978: Fractionation and assimilation in the Borgtinderne Syenite, East Greenland. *Contrib. Mineral. Petrol.* 67, 25-34.

- Brøgger, W.C., 1933: Die Eruptivgesteine des Oslogebietes. VII. Die chemische zusammenetzung der Eruptivgesteine des Oslogebietes. Norske Vidensk. Akad. Oslo. Mat.-Naturv. 1933, 1.
- Cambell, I.H. and Borley, G.D., 1974: The geochemistry of pyroxenes from the lower layered series of the Jimberlana intrusion, Western Australia. Contrib. Mineral. Petrol. 47, 281-297.
- Cambell, I.H. and Gorton, M.P., 1980: Accessory phases and the generation of LREE-enriched basalts - a test for disequilibrium melting. Contrib. Mineral. Petrol. 72, 157-163.
- Carmichael, I.S.E., 1964: Natural liquids and the phonolite minimum. Geol. J. 4, 55-60.
- Carmichael, I.S.E., Turner, F.J. and Verhoogen, J., 1974: Igneous Petrology. New York: McGraw-Hill Inc.
- Cawthorn, R.G., 1976: Some chemical controls on igneous amphibole compositions. Geochim. cosmochim. Acta. 40, 1319-1328.
- Chambers, A.D., 1976: The petrology and mineralogy of the South Qôroq Centre, Igaliiko Complex, South Greenland. Unpubl. PhD. Thesis, University of Durham.
- Dawson, J.B. and Firsch, T., 1971: Eucolite from Oldoinyo Lengai, Tanzania. Lithos 4, 297-303.
- Deer, W.A., Howie, R.A. and Zussman, J., 1963: Rock-forming minerals, 4, framework silicates. 435pp. London: Longmans, Green and Co.
- Deer, W.A., Howie, R.A. and Zussman, J., 1978: Rock-forming minerals, 2A, single chain silicates. London: Longman Group Limited.
- Deer, W.A. and Wager, L.R., 1939: Olivine from the Skaergaard intrusion, Kangerdlugssuaq, East Greenland. Am. Miner. 24, 18-25.
- Downes, M.J., 1974: Sector and oscillatory zoning in calcic augites from Mt. Etna, Sicily. Contrib. Mineral. Petrol.

47, 187-196.

- Duncomb, P. and Jones, E.M., 1969: Electron probe micro-analysis: an easy to use computer program for correcting quantitative data. Company Report. Tube Investments Research Laboratories, Hinxton Hall, Nr. Saffron Walden, Essex, U.K.
- Edgar, A.D. and Parker, L.M., 1974: Comparison of melting relationships of some plutonic and volcanic peralkaline undersaturated rocks. *Lithos* 7, 263-273.
- Emeleus, C.H., 1964: The Grønnedal-Ika alkaline complex, South Greenland. *Meddr Grønland*. Bd. 172, (3) 75pp. (also *Bull. Grønlands geol. Unders.* 45, 75pp.)
- Emeleus, C.H. and Harry, W.T., 1970: The Igaliko Nepheline Syenite complex. General Description. *Meddr Grønland* 186, (3) (also *Bull. Grønlands geol. Unders.* 85) 115pp.
- Emeleus, C.H. and Upton, B.G.J., 1976: The Gardar period in southern Greenland. In Escher, A. and Watt, W.S. (eds), *The Geology of Greenland*. 153-181. Copenhagen: The Geological Survey of Greenland.
- Engell, J.E., 1973: A closed system crystal fractionation model for the agpaitic Ilímaussaq intrusion, South Greenland, with special reference to the lujavrites. *Bull. Geol. Soc. Denmark*. 22, 276-302.
- Ernst, W.G., 1962: Synthesis, stability relations and occurrence of riebeckite and riebeckite-arfvedsonite solid solutions. *J. Geol.* 70, 689-736.
- Ernst, W.G., 1968: Minerals, rocks and inorganic materials, 1, amphiboles. New York: Springer.
- Fairhead, J.D., 1976: The structure of the lithosphere beneath the Eastern Rift, East Africa, deduced from gravity studies. *Tectonophysics* 30, 269-298.
- Ferguson, J., 1964: Geology of the Ilímaussaq alkaline intrusion, South Greenland. *Meddr Grønland* 172, (4) (also *Bull. Grønlands geol. Unders.* 89) 193pp.

- Ferguson, J., 1970: The differentiation of agpaitic magmas: the Ilímaussaq Intrusion, South Greenland. *Can. Miner.* 10, 335-349.
- Fitton, J.G. and Gill, R.C.O., 1970: The oxidation of ferrous iron in rocks during mechanical grinding. *Geochim. cosmochim. Acta.* 34, 518-523.
- Flanagan, F.J., 1969: U.S. Geological Survey standards-II. First compilation of data for the new U.S.G.S. rocks. *Geochim. cosmochim. Acta.* 33, 81-120.
- Flanagan, F.J., 1973: 1972 values for international geochemical reference standards. *Geochim. cosmochim. Acta.* 37, 1184-1200.
- Flink, G., 1898: Berattelse om en mineralogisk resa i Syd-Gronland sommaren 1897. *Meddr Grønland.* 14, (2).
- Gerasimovsky, V.J. and Kusnetsova, S.Ya., 1967: On the petrochemistry of the Ilímaussaq Intrusion, South Greenland. *Geochem. Int.* 4, 236-246.
- Gibb, F.G., 1973: The zoned clinopyroxenes of the Shiant Isles Sill, Scotland. *J. Petrol.* 14, 203-229.
- Giesecke, K.L., 1910: Karl Ludwig Gieseckes mineralogisches Reisejournal Uber Gronland. *Meddr Grønland.* 35.
- Gill, R.C.O., 1972: The geochemistry of the Grønneidal-Ika alkaline complex, South Greenland. Unpubl. PhD. Thesis, University of Durham.
- Gittins, J., 1979: The feldspathoidal alkaline rocks. In Yoder, H.S.Jr. (ed), The Evolution of the Igneous Rocks: Fiftieth Anniversary Prospectives. Princeton University Press.
- Gomes, C de B., Moro, S.L. and Dutra, C.V., 1970: Pyroxenes from the alkaline rocks of Itipirapuã, São Paulo, Brazil. *Am. Miner.* 55, 224-230.
- Griffiths, P.S. and Gibson, I.L., 1980: The geology and petrology of the Hannington Trachyphonolite formation, Kenya Rift Valley. *Lithos* 13, 43-54.

- Hamilton, D.L., 1961: Nephelines as crystallisation temperature indicators. *J. Geol.* 69, 321-329.
- Hamilton, D.L. and MacKenzie, W.S., 1965: Phase equilibrium studies in the system $\text{NaAlSi}_3\text{O}_8$ - KAlSi_3O_8 - SiO_2 - H_2O . *Mineralog. Mag.* 34, 214-231.
- Helz, R.T., 1973: Phase relationships of basalts in their melting range at $P_{\text{H}_2\text{O}} = 5\text{kbar}$ as a function of oxygen fugacity: Part 1, mafic phases. *J. Petrol.* 14, 249-302.
- Hess, P.C., 1960: Stillwater igneous complex, Montana. *Geol. Soc. Am. Mem.* 80, 230pp.
- Hess, P.C., 1971: Polymer model of silicate melts. *Geochim. cosmochim. Acta.* 35, 289-306.
- Hodges, F.N. and Barker, D.S., 1973: Solid solution in aenigmatites. *Carn. Inst. Yr. Bk.* 72, 578-581.
- Holland, J.G. and Brindle, D.W., 1966: A self consistent mass absorption correction for silicate analysis by X-ray fluorescence analysis. *Spectrochim. Acta.* 22, 2083-
- Hollister, L.S. and Gancartz, A.J., 1971: Compositional sector-zoning in clinopyroxene from the Narce area, Italy. *Am. Miner.* 56, 959-979.
- Irvine, T.N., 1970: Heat transfer during solidification of layered intrusions. I, sheets and sills. *Can. J. Earth. Sci.* 7, 1031-1061.
- Jaeger, J.C., 1968: Cooling and solidification of igneous rocks. In Hess, H.H. (ed), Basalts Vol.2. 503-536. New York: Wiley.
- Jakes, P. and White, A.J.R., 1972: Hornblendes from calc-alkaline volcanic rocks of island arcs and continental margins. *Am. Miner.* 57, 887-902.
-
- Jones, A.P. and Peckett, A., (in press). Zirconium-bearing aegirines from the Motzfeldt Centre, South Greenland. *Contrib. Mineral. Petrol.*
- Jones, W.B., 1979: Syenite boulders associated with Kenyan trachyte volcanoes. *Lithos* 12, 89-97.
- Kelsey, C.H. and McKie, D., 1964: The unit cell of aenigmatite. *Mineralog. Mag.* 33, 986-1001.
- Kempe, D.R.C. and Deer, W.A., 1970: The mineralogy of the

- Kangerdlugssuaq alkaline intrusion, east Greenland.
Meddr Grønland. 190, (3) 95pp.
- Knight, J.L., 1976: The classification and interpretation of the amphiboles. Unpubl. PhD. Thesis, University of Durham.
- Koster van Groos, A.F. and Wyllie, P.J., 1968: Melting relationships in the system $\text{NaAlSi}_3\text{O}_8\text{-NaF-H}_2\text{O}$ to 4 kilobars pressure. J. Geol. 76, 50-70.
- Larsen, J.G., 1973: Petrochemical work on the Precambrian lavas, Eriksfjord Formation, south Greenland. Rapp. Grønlands geol. Unders. 55, 40-41
- Larsen, J.G., 1977: Petrology of the late lavas of the Eriksfjord Formation, Gardar Province, South Greenland. Bull. Grønlands geol. Unders. 125, 31pp.
- Larsen, L.M., 1976: Clinopyroxenes and coexisting mafic minerals from the alkaline Ilímaussaq intrusion, South Greenland. J. Petrol. 17, 258-290.
- Larsen, L.M., 1977: Aenigmatites from the Ilímaussaq intrusion, south Greenland: Geochemistry and petrological implications. Lithos 10, 257-270.
- Larsen, L.M., 1979: Distribution of REE and other trace elements between phenocrysts and peralkaline under-saturated magmas, exemplified by rocks from the Gardar igneous province, south Greenland. Lithos 12, 303-315.
- Larsen, L.M. and Steenfelt, A., 1974: Alkali loss and retention in an iron-rich peralkaline phonolite dyke from the Gardar province, south Greenland. Lithos 7, 81-90.
- Lawn, B.R. and Wilshaw, T.R., 1975: Fracture of brittle solids. (Cambridge Solid State Science Series). Cambridge University Press.
- Lerman, A., 1978: Geochemical processes water and sediment environments. New York: John Wiley and Sons.
- Lindsley, D.H., 1971: Synthesis and preliminary results on the synthesis of Aenigmatite. Carn. Inst. Yr. Bk. 69, 188-190.
- Liou, J.G., 1971: Synthesis and stability relations of prehnite, $\text{Ca}_2\text{Al}_2\text{Si}_3\text{O}_{10}(\text{OH})_2$. Am. Mineral. 56, 507-531.

- Lipman, P.W., 1971: Iron-titanium oxide phenocrysts in compositionally zoned ash-flow sheets from Southern Nevada. *J. Geol.* 79, 438-456.
- Lippard, S.J., 1973: The petrology of phonolites from the Kenya Rift. *Lithos* 6, 217-234.
- Maaløe, S. and Printzlau, I., 1979: Natural melting of spinel lherzolite. *J. Petrol.* 20, 727-741.
- Macdonald, R., 1974: The role of fractional crystallisation in the formation of the alkaline rocks. In Sørensen, H. (ed), The Alkaline Rocks. 442-459. London: John Wiley and Sons.
- Marsh, J.S., 1975: Aenigmatite stability in silica-undersaturated rocks. *Contrib. Mineral. Petrol.* 50, 135-144.
- McBirney, A.R. and Noyes, R.M., 1979: Crystallisation and layering of the Skaergaard Intrusion. *J. Petrol.* 20, 487-554.
- Mercier, J.C. and Carter, N.L., 1975: Pyroxene geotherms. *J. Geophys. Res.* 80, 3349-3362.
- Morse, S.A., 1969: Syenites. *Carn. Inst. Yr. Bk.* 67, 112-120.
- Mueller, R.F. and Saxena, S.K., 1977: Chemical Petrology. New York: Springer-Verlag Inc.
- Mysen, B.O. and Boettcher, A.L., 1975: Melting of hydrous mantle: II, Geochemistry of crystals and liquids formed by anatexis of mantle peridotite at high pressures and temperatures as a function of controlled activities of water, hydrogen and carbon dioxide. *J. Petrol.* 16, 549-593.
- Nash, W.P., Carmichael, I.S.E. and Johnson, R.W., 1969: The mineralogy and petrology of Mount Suswa, Kenya. *J. Petrol.* 10, 409-439.
- Nash, W.P. and Wilkinson, J.F.G., 1970: Shonkin Sag Laccolith Montana. 1, Mafic minerals and estimates of temperature, pressure, oxygen fugacity and silica activity. *Contrib. Mineral. Petrol.* 25, 241-269.
- Nicholls, J. and Carmichael, I.S.E., 1969: Peralkaline

- acid liquids: a petrological study. *Contrib. Mineral. Petrol.* 20, 268-294.
- Nockolds, S.R., 1954: Average chemical compositions of some igneous rocks. *Bull. Geol. Soc. Am.* 65, 1007-1032.
- O'Hara, M.J., 1977: Geochemical evolution during fractional crystallisation of a periodically refilled magma chamber. *Nature, Lond.* 266, 503-507.
- O'Hara, M.J. and Mathews, R.E., 1980: "Geochemical evolution in an advancing, periodically replenished, periodically tapped, continuously fractionated magma chamber." Unpubl. M/s delivered to Volcanic Studies Group at meeting of Geol. Soc. Lond. May 15-16 1980. (Glasgow).
- Parsons, I., 1965: The feldspathic syenites of the Loch Ailsh intrusion, Assynt, Scotland. *J. Petrol.* 6, 365-394.
- Parsons, I., 1978: Feldspars and fluids in cooling plutons. *Mineralog. Mag.* 42, 1-17.
- Parsons, I., 1979: The Klokken Gabbro-Syenite Complex, South Greenland: Cryptic variation and origin of inversely graded layering. *J. Petrol.* 20, 653-694.
- Patchett, P.J., Hutchinson, J., Blaxland, A.B. and Upton, B.G.J., 1976: Origin of anorthosites, gabbros and potassic ultramafic rocks from the Gardar Province, South Greenland: Sr isotopic ratio studies. *Bull. geol. Soc. Denmark.* 25, 79-84.
- Phillips, R., 1966: Amphibole compositional space. *Mineralog. Mag.* 35, 945-952.
- Phillips, R. and Layton, W., 1964: The calciferous and alkali amphiboles. *Mineralog. Mag.* 33, 1097-1109.
- Piotrowski, J.M. and Edgar, A.D., 1970: Melting relations of undersaturated alkaline rocks from South Greenland. *Meddr Grønland.* 181, (9) 62pp.
- Poldervaart, A. and Hess, H.H., 1951: Pyroxenes in the crystallisation of basaltic magma. *J. Geol.* 59, 472-489.
- Poulsen, V., 1964: The sandstones of the Precambrian.

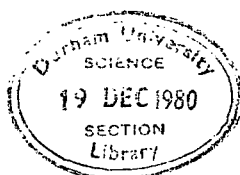
- Eriksfjord Formation in South Greenland. Rapp. Grønlands geol. Unders. 2, 16pp.
- Powell, M., 1976: Theoretical, geochemical and petrological study of the Igdlarfigssalik nepheline syenite intrusion, Greenland. Unpubl. PhD. Thesis, University of Leeds.
- Powell, M., 1978: The crystallisation history of the Igdlarfigssalik nepheline syenite intrusion, Greenland. Lithos 11, 99-120.
- Powell, M. and Powell, R., 1974: An olivine-clinopyroxene geothermometer. Contrib. Mineral. Petrol. 48, 249-263.
- Powell, M. and Powell, R., 1977: A nepheline-alkali feldspar geothermometer. Contrib. Mineral. Petrol. 62, 193-204.
- Reeves, M.J., 1971: Geochemistry and mineralogy of British Carboniferous seatearths from northern coalfields. Unpubl. PhD. Thesis, University of Durham.
- Roberts, J.L., 1970: The intrusion of magma into brittle rocks. In Newall and Rast (eds), Mechanisms of Igneous Intrusions. Geol. J. Spec. Iss. 2, 1970.
- Rowbotham, G., 1973: Hydrothermal synthesis and mineralogy of the alkali amphiboles. Unpubl. PhD. Thesis, University of Durham.
- Schairer, J.F. and Bowen, N.L., 1947: The system Anorthite-Leucite-Silica. Bull. Comm. Geol. Finland. 20, 67-87.
- Seitz, M.G., 1974: Promotion of kinetic disequilibrium of trace thorium. Carn. Inst. Yr. Bk. 73, 551-553.
- Shaw, H.R., 1964 : Theoretical solubility of H₂O in silicate melts: Quasicrystalline models. J. Geol. 72, 601-617.
- Shaw, H.R., 1972: Viscosities of magmatic silicate liquids: An empirical method of prediction. Am. J. Sci. 272, 870-893.
- Simkin, T. and Smith, J.V., 1970: Minor element distribution in olivine. J. Geol. 78, 304-325.
- Smith, J.V., 1974: Feldspar minerals, vols 1 & 2. Berlin, Heidelberg, New York: Springer Verlag.
- Smith, J.V. and Muir, I.D., 1958: The reaction sequence

- in larvikite feldspars. Zeit. Krist. 110, 11-20.
- Smith, P. and Parsons, I., 1974: The alkali feldspar solvus at 1 kilobar water-vapour pressure. Mineralog. Mag. 39, 747-767.
- Sood, M.K. and Edgar, A.D., 1970: Melting relations of understaturated alkaline rocks. Meddr Grønland. 181, (12) 41pp.
- Sørensen, H., 1962: On the occurrence of Steenstrupine in the Ilímaussaq Massif, Southwest Greenland. Meddr Grønland. 167, (1) (also Bull. Grønlands geol. Unders. 32) 125pp.
- Sørensen, H., 1966: On the magmatic evolution of the alkaline igneous province of South Greenland. Rapp. Grønlands geol. Unders. 7, 19pp.
- Sørensen, H., Hansen, J. and Bondesson, E., 1969: Preliminary account of the geology of the Kvanefield area of the Ilímaussaq intrusion, South Greenland. Rapp. Grønlands geol. Unders. 18, 40pp.
- Steenstrup, K.V.J. and Kornerup, A., 1881: Beretring om Expeditionen til Julianehaabs Distrikt; 1876. Meddr Grønland. 2, (1).
- Stephenson, D., 1972: Alkali clinopyroxenes from nepheline syenites of the South Qôroq Centre, South Greenland. Lithos 5, 187-201.
- Stephenson, D., 1973: The petrology and mineralogy of the South Qôroq Centre, Igaliiko Complex, South Greenland. Unpubl. PhD. Thesis, University of Durham.
- Stephenson, D., 1974: Mn and Ca enriched olivines from nepheline syenites of the South Qôroq Centre, south Greenland. Lithos 7, 35-41.
- Stephenson, D., 1976: The South Qôroq Centre nepheline syenites, South Greenland: Petrology, felsic mineralogy and petrogenesis. Bull. Grønlands geol. Unders. 118, 55pp.
- Stephenson, D., 1976b: A simple-shear model for the ductile deformation of high-level intrusions in South Greenland. J. Geol. 132, 307-318.

- Stewart, J.W., 1964: The earlier Gardar igneous rocks of the Ilímaussaq area, South Greenland. Unpubl. PhD. Thesis, University of Durham.
- Stewart, J.W., 1970: Precambrian alkaline-ultramafic/carbonatite volcanism at Qagssiarssuk, south Greenland. Bull. Grønlands geol. Unders. 84, 70pp.
- Stormer, J.C., 1973: Calcium zoning in olivine and its relationships to silica activity and pressure. Geochim. cosmochim. Acta. 37, 1815-1821.
- Sun, S.S., Nesbitt, R.W. and Sharaskin, A.V., 1979: Geochemical characteristics of mid-ocean ridge basalts. Earth Plan. Sci. Lett. 44, 119-138.
- Surdam, R.C., 1973: Low grade metamorphism of tuffaceous rocks in the Karmutsen Group, Vancouver Island, British Columbia. Bull. Geol. Soc. Am. 84, 1911-1925.
- Sweatman, T.R. and Long, J.V.P., 1969: Quantitative electron probe microanalysis of rock-forming minerals. J. Petrol. 10, 332-379.
- Taylor, D. and MacKenzie, W.S., 1975: A contribution to the pseudoleucite problem. Contrib. Mineral. Petrol. 49, 321-333.
- Thompson, A.B., 1971: P_{CO_2} in low grade metamorphism; zeolite, carbonate; clay mineral, prehnite relations in the system $CaO-Al_2O_3-SiO_2-CO_2-H_2O$. Contrib. Mineral. Petrol. 33, 145-161.
- Thornton, C.P. and Tuttle, O.F., 1960: Chemistry of igneous rocks: 1, Differentiation Index. Am. J. Sci. 258, 664-684.
- Tilley, C.E., 1954: Nepheline-alkali feldspar paragenesis. Am. J. Sci. 252, 67-75.
- Tyler, R.C. and King, B.C., 1967: The pyroxenes of the alkaline igneous complexes of eastern Uganda. Mineralog. Mag. 36, 5-22.
- Upton, B.G.J., 1960: The alkaline igneous complex of Kûngnât Fjeld, South Greenland. Meddr Grønland. 123, (4) 1-145.
- Upton, B.G.J., 1964: The geology of Tugtutôq and neighbouring

- islands, South Greenland. Bull. Grønlands geol. Unders. 27, (also Meddr Grønland 123, (4)) 145pp.
- Upton, B.G.J., 1971: Melting experiments on chilled gabbros and syenogabbros. Carn. Inst. Yr. Bk. 70, 112-118.
- Upton, B.G.J., 1974: The alkaline province of Southwest Greenland. In Sørensen, H. (ed), The Alkaline Rocks. 221-238. London: John Wiley and Sons.
- Upton, B.G.J. and Blundell, D.J., 1978: The Gardar Igneous Province; Evidence for Proterozoic continental rifting. In Neumann, E.R. and Ramberg, I.B. (eds), Petrology and Geochemistry of Continental Rifts. Dordrecht, Holland: Reidel Publishing Co.
- Upton, B.G.J. and Thomas, J.E., 1979: The Tugtutôq Younger Giant Dyke Complex, South Greenland: Fractional crystallisation of transitional olivine basalt magma. J. Petrol. 21, 167-198.
- Ussing, N.V., 1894: Mineralogisk-petrografiske Undersøgelser af Grønlandske Nefelinsyeniter og beslaegtede Bjaergarter. Anden del: De Kiselsyrefattige Hovedminerdlere. Meddr Grønland. 14, (1).
- Ussing, N.V., 1912: Geology of the country around Julianehåb, Greenland. Meddr Grønland. 38.
- Vlasov, K.A., Kuz'menko, M.V. and Eskova, E.M., 1966: The Lovozero Alkali Massif. Edinburgh and London: Oliver and Boyd.
- Wager, L.R., 1959: Differing powers of crystal nucleation as a factor producing diversity in layered igneous intrusion. Geol. Mag. 96, 75-80.
- Wager, L.R., 1963: The mechanism of adcumulus growth in the layered series of the Skaergaard intrusion. Mineralog. Soc. Am. Spec. Pap. 1, 1-19.
- Wager, L.R. and Brown, G.M., 1968: Layered Igneous Rocks. Edinburgh: Oliver and Boyd.
- Wager, L.R., Brown, G.M. and Wadsworth, W.J., 1960: Types

- of igneous cumulates. *J. Petrol.* 1, 73-85.
- Walton, B.J., 1965: Sannerutian appinitic rocks and Gardar dykes and diatremes, north of Narssarssuaq, South Greenland. *Meddr Grønland.* 179, (9).
- Wasserburg, G.J., 1957: The effects of H_2O in silicate systems. *J. Geol.* 65, 15-23.
- Watson, E.B., 1979: Zircon saturation in felsic liquids; Experimental results and applications to trace element geochemistry. *Contrib. Mineral. Petrol.* 70, 407-419.
- Watt, W.S., 1966: Chemical analyses from the Gardar Igneous Province, South Greenland. *Rapp. Grønlands geol. Unders.* 6, 92pp.
- Wegmann, C.E., 1938: Geological investigations in Southern Greenland: 1, On the structural divisions of Southern Greenland. *Meddr Grønland.* 113, (2).
- Widenfalk, L., 1973: Myrmekite-like intergrowths in larvikite feldspars. *Lithos* 5, 255-267.
- Wills, K., 1974: The geological history of Southern Dominica and plutonic nodules from the Lesser Antilles. Unpubl. PhD. Thesis, University of Durham.
- Wright, J.B., 1969: Olivine nodules in trachyte from the Jos Plateau, Nigeria. *Nature, Lond.* 223, 285-286.
- Wright, J.B., 1971: The phonolite-trachyte spectrum. *Lithos* 4, 1-5.
- Wyllie, P.J., 1977: Peridotite- H_2O - CO_2 , and carbonatitic liquids in the upper asthenosphere. *Nature, Lond.* 266, 45-47.
- Yoder, H.S., Stewart, D.B. and Smith, J.R., 1957: Ternary feldspars. *Carn. Inst. Yr. Bk.* 56, p206.
- Ødum, H., 1927: Geologiske Iagttagelser i landet Øst for Igaliko Fjord. *Meddr Grønland.* 74, (4).



THE MOTZFELDT CENTRE
THE IGALIKO COMPLEX, SOUTH GREENLAND
By A.P.Jones (see below)

SCALE 1:50,000

Syenites of Motzfeldt Centre

SM6	Lujavrites	Brown Syenite postdates SM4
HY	Heterogenous Syenite	Other Intrusives
SM5 w/ larvikitic types		EM
SM4		1 2 NM1 & 2
SM3		Microsyenite
SM2		Alkali Gabbro
SM1		

Syenites of North Qôroq Centre

nq

Supracrustal rocks

Basalts, agglomerates etc	Overprint where metasomatised by the syenites
Sediments, eg: quartzites	

Julianehåb Granite

Gneiss, granite etc

GEOLOGICAL SYMBOLS

Geological boundary broken where uncertain	Fault
18 Dip of bedding or flow banding	30 Igneous lamination w/ dip or vertical
30 Mafic banding w/ dip or vertical	80 Dip of contact

TOPOGRAPHICAL SYMBOLS

672 Height in metres
Glacier w/ 100 m contours

Modifications to the original map of Emeleus, C.H. and Harry, W.T. 1970 Meddr Grønland BD 186 NR.3 plate 4

1. Motzfeldt syenite SM4 cuts North Qoroq syenites; Chambers, A.D. & Jones, A.P.
2. Remapped. Jones, A.P.
3. Roof region unit Heterogenous Syenite. Jones, A.P.

